Integrability, Localisation and Bifurcation of an Elastic Conducting Rod in a Uniform Magnetic Field

David Sinden

Centre for Nonlinear Dynamics,

Department of Civil, Environmental & Geomatic Engineering,

University College London,
Gower Street,
London,
WC1E 6BT

March 20, 2009

Submitted to University College London in partial fulfillment
of the requirements for the degree of
Doctor of Philsophy,
2009.

'I, David Sinden, confirm that the work presented in this thesis is my own and has not been previously submitted to this or any other institution for any degree, diploma or other qualification. Where information has been derived from other sources, I confirm that this has been indicated in the thesis.'

Acknowledgements

Firstly I must thank my supervisor Gert van der Heijden for his insight, patience and enthusiasm. It has been a pleasure and an honour to work alongside. I would like to thank Dr Paul Greening and Dr Tristan Robinson for careful reading of the thesis and helpful comments.

This thesis represents the cumulation of many years of study. I hope to thank everyone who has contributed in any way and I apologise in advance to those I may have missed out. I would like to thank the contribution of my friends and colleagues at UCL - Jason, Tristan, Ali, Joe, Joao, Laurent, Ricky for the constant supply of crisps and Simon for fixing my computer and talking about football. The good friends I made while at Bath - David, Sioned, Spyros, Caroline, Vicky, Jackie and Nefeli. My friends from undergraduate days at Imperial - Mike, Tim, Dom and Alan. Friends from school and those met along the way - Phil, James, Paul, Lewis, Kate, Ryan, Doug, Sean, Sarah, Emma and Kirsty.

Lastly, I would like to thank all my family: Teta and Grandad, Colin and Gay, Stephen and Shani, Trevor, Lyn, Grandma (without her kindness and generosity this thesis would have never been finished) and Grandad and of course Mum, Dad, Graeme, Debra (and Nick) and Paul for all their support, patience, interest and love. This is both for and because of them.

Abstract

The classical problem of the buckling of an elastic rod in a magnetic field is investigated using modern techniques from dynamical systems theory. The Kirchhoff equations, which describe the static equilibrium equations of a geometrically exact rod under end tension and moment are extended by incorporating the evolution of a fixed external vector (in the direction of the magnetic field) that interacts with the rod via a Lorentz force. The static equilibrium equations (in body cordinates) are found to be noncanonical Hamiltonian equations. The Poisson bracket is generalised and the equilibrium equations found to sit, as the third member, in a family of rod equations in generalised magnetic fields. When the rod is linearly elastic, isotropic, inextensible and unshearable the equations are completely integrable and can be generated by a Lax pair.

The isotropic system is reduced using the Casimirs, via the Euler angles, to a four-dimensional canonical system with a first integral provided the magnetic field is not aligned with the force within the rod at any point as the system losses rank. An energy surface is specified, defining three-dimensional flows. Poincaré sections then show closed curves.

Through Mel'nikov analysis it is shown that for an extensible rod the presence of a magnetic field leads to the transverse intersection of the stable and unstable manifolds and the loss of complete integrability. Consequently, the system admits spatially chaotic solutions and a multiplicity of multimodal homoclinic solutions exist. Poincaré sections associated with the loss of integrability are displayed.

Homoclinic solutions are computed and post-buckling paths found using continutaion methods. The rods buckle in a Hamiltonian-Hopf bifurcation about a periodic solution. A codimension-two point, which describes a double Hamiltonian-Hopf bifurcation, determines whether straight rods buckle into localised configurations at either two critical values of the magnetic field, a single critical value or do not buckle at all. The codimension-two point is found to be an organising centre for primary and multimodal solutions.

Table of Contents

List of Figures

List of Tables

Chapter 1

Introduction

The problem of the configurations and buckling of elastic conducting wire in a magnetic field is a classical one in magnetoelasticity and is of both theoretical and practical interest. In this thesis the problem is investigated using modern techniques from dynamical systems theory.

It is well-known that a straight current-carrying wire held between pole faces of a magnet buckles into a coiled configuration at a critical current [110, §10.4.3]. A rigorous bifurcation analysis of this buckling problem (for a uniform magnetic field directed parallel to the undeformed wire) was developed in a series of papers by Wolfe. Wolfe first considered a nonlinearly-elastic string model for the wire, i.e., a perfectly flexible elastic line, and by studying the linearised eigenvalue problem about the trivial straight solution found that an infinite number of solution branches bifurcate from the trivial solution [104, 108], much like in the Euler elastica under compressive load. Wolfe constructed a potential energy function and derived a set of Euler-Lagrange equations in the classical manner. It was then shown that the equations can be solved exactly and that the non-trivial solutions are exact helices. In subsequent work Wolfe then modelled the wire as a rod [81, 106]. In addition to extension, a rod can undergo flexure, torsion and shear. For the case of welded boundary conditions it was found that in certain cases bifurcation occurs, again with an infinity of non-trivial equilibrium states.

Many technical devices such as motors, generators and transformers use elastic structures in magnetic fields [72] but recently the problem of a conducting rod in a magnetic

field has attracted interest as a model for electrodynamic space tethers [93, 100]. Electrodynamic tethers are long slender conducting cables that exploit the Earth's magnetic field to generate Lorentz forces through Faraday's law. The generated drag force could be used for maneuvering satellites when de-orbiting, eliminating the need for additional chemical fuel, thus reducing the weight of satellite and hence operational costs. The reduction in cost has been estimated at a billion dollars over ten years for the international space station alone [54]. Tethers are spun about their axis for gyroscopic stability and therefore must resist bending and twisting. Such tethers need to be described as an elastic rod rather than the traditional wire. Analysis of electrodynamic tethers has been performed using techniques from multibody system dynamics [93]. Geometric nonlinearities were found to have a stabilizing effect on the tether configurations. However, a drawback with the analysis was that elastic displacements in each substructure were assumed to be small, diminishing the stabilizing effect.

In this thesis a *geometrically exact* formulation is adopted using Cosserat theory. The static equilibrium equations of a rod under end force and moment, known as the Kirchhoff equations [2], are extended by incorporating a fixed external vector in the direction of the magnetic field that interacts with the rod via a Lorentz force. A geometrically exact formulation is naturally a noncanonical Hamiltonian formulation [83] and retains the symmetry properties of the physical system. The noncanonical Hamiltonian formulation allows deep insight into the system and allows a number of powerful methods to be applied; for example in the study of nonlinear stability [26, 84]; bifurcation theory [25, 30]; complete integrability [6, 56]; spatially chaotic solutions [33, 52] and in numerical analysis [24]. A principal advantage is the large body of work relating to finite-dimensional noncanonical Hamiltonian systems [6, 67].

If the rod is isotropic and without initial curvature, that is if the principal bending stiffness are equal, the Kirchhoff equations are completely integrable and all possible solutions can be expressed in closed form. Consequently, the Kirchhoff equations have been used to model a variety of physical systems. Examples include: the deformation of biological materials such as DNA [38, 80], climbing plants [44, 68], the visualisation of

hair [10], the spin dynamics of the superfluid ^{3}He [75] and an Heisenberg XY particle [31], the configurations of undersea cables [28], the motion of a body submerged in an ideal compressible fluid with coincident centres of gravity and bouyancy [50, 62, 63, 87]. The Kirchhoff equations are related to the (integrable) modified Korteweg-de Vries equation by the Hasimoto transform [47, 59] and through the Kirchhoff kinetic analogy to the vast canon of literature devoted to the motion of rigid bodies [67, 103].

Despite the Kirchhoff equations being static, mathematically they have the same structure as many problems in dynamics: arclength along the rod plays a role similar to that of time in a dynamical system such as the spinning top or a pendulum. The Kirchhoff kinetic analogy relates the *shape* of a deformed rod with the *motion* of a heavy spinning top [28, 57, 92]. In the same way the motion of the centre of gravity of a top and its spin prescribes the motion of the entire top so the position of the centreline of the rod and its rigidly transformed cross-section prescribes the configuration of a rod. For example, an initially straight rod whose principal moments of inertia are equal can be deformed via end forces and moments into a helix, corresponding to the periodic orbit of the spinning top. The analogy is not perfect however, as concepts such as shear, extensibility and nonlinear constitutive relationships have no physical interpretation in the context of rigid body dynamics[1]. More importantly, rod problems are typically boundary value problems, while problems in rigid body dynamics are initial value problems. However, if one is concerned with homoclinic solutions for arbitarily long rods then one effectively is dealing with a rigid body problem.

Homoclinic solutions represent localising buckling modes which are the physically preferred buckling configurations for long rods [53, 91] and thus are the natural configurations to study. Homoclinic orbits are organising centres for dynamics in their neighbourhood and their bifurcation structure, through the homoclinic tangle, leads to spatially chaotic solutions. In general systems homoclinic solutions to a hyperbolic fixed point are a codimension-one phenomena, however in Hamiltonian systems homoclinic solutions are a codimension-zero phenomena and hence are generic under perturbations [32]. While

[1] In many ways the rod model is more flexible than the rigid body model!

the localised buckling of rods under end loading has been investigated [21, 23, 92, 95, 98], the localised buckling of rods due to magnetic effects has yet to be investigated.

Previous analysis of localised solutions of Cosserat rods under end tension and moment has shown that neither shear and extensibility [23, 88] nor nonlinear constitutive relationships [3, 21] has any significant qualitative effect on the rod in terms of phase portraits or localised configurations. Indeed, in both cases the isotropic system is integrable. Other material properties such as anisotropy [70] and initial curvature [64] are shown through Mel'nikov analysis to lead to the loss of complete integrability and the emergence of spatial chaos and multimodal configurations. The resulting localised multmodal configurations and their bifurcation structure were investigated in [95] and [23] respectively. Nonlinear normal form analysis was performed on the buckling of anisotropic [98] and initially curved rods [68]. It was shown that a codimension-two point distinguishes between weakly anisotropic rods and strongly anisotropic rods. Weakly anisotropic rods buckle according to a subcritical Hamiltonian-Hopf bifurcation and strongly anisotropic rods buckle according to the Hamiltonian-pitchfork bifurcation [98].

In this thesis material properties are not the main focus of the investigation, instead the governing equations are extended to include the effect of the magnetic field. It is shown that the static equilibrium equations for a rod in a magnetic field sit in a family of non-canonical Hamiltonian systems. The first member of the family is the force-free rod (the Euler-Poinsot top), the Kirchhoff equation is the second member (the Lagrange top) and the third member is the rod in a magnetic field (the abstract 'Twisted Top' [90]). The fourth member of the family is a rod in a linearly varying magnetic field that depends on the configuration of the rod. A rod in a uniform magnetic field is the first member whose Poisson bracket is extended in a nontrivial, i.e., non-semidirect, manner.

When the rod is isotropic the system can be reduced to a four-dimensional canonical system with an additional integral. The reduction holds provided that the magnetic field is not aligned with the force in the rod at any point as the parameterised system loses rank [76]. From the reduction a modified version of Mel'nikov's method for perturbations which are applied to the Hamiltonian [52] is applied to show that a uniform magnetic

field is a perturbation which destroys integrability for extensible rods. The Mel'nikov analysis shows that the stable and unstable manifolds of the perturbed homoclinic orbit intersect transversely and there exists Smale horseshoes on the Poincaré sections of the homoclinic energy level [33, 86]. The loss of integrability is the classical result but it is the presence of horseshoes which is the more significant result: given the presence of horsehoes on the stable and unstable manifolds implies the existence of a multiplicity of multimodal homoclinic orbits [9].

The result is of interest as alone neither the presence of a magnetic field nor extensibility affect the integrability of a rod. However, when extensibility and the magnetic field are both considered to be perturbations of equal order the interaction of the combined perturbations destroys integrability. In the case where both effects are small higher order approximations to the Mel'nikov integral are required in order to show the loss of integrability. Higher order Mel'nikov integrals have been computed before in simple examples [42, 60, 65, 78] but it is believed that this is the first physical system in which the coupling between two integrable perturbations leads to the loss of integrability and spatially chaotic solutions.

Due to the effect of the magnetic field the trivial configuration, a straight twisted rod, is a periodic solution. Thus standard numerical methods for the computation and continuation of homoclinic solutions need to be adapted [8, 19]. The coupling between body and spatial frames has been seen in the context of rods constrained to lie in a plane [96] or on a cylinder [94, 97]. The underlying periodicity does not affect the codimension of the problem. Localised solutions are computed and their post-buckling paths followed using the continuation software AUTO97 [35].

The thesis is structured as follows, chapter 2 gives the theoretical background and outlines the analytical tools used in the thesis. Chapter 3 introduces geometrically exact rod theory. A family of equilibrium equations is formulated and identified with a family of noncanonical Hamiltonian systems. Crucially, every member of the family is completely integrable in the sense of Liouville [6] if the rod is linearly elastic, initially straight, isotropic, unshearable and inextensible. The subfamily can be generalised by a Lax pair.

Chapter 4 gives a description of the Kirchhoff rod. In chapter 5 the governing equation for a rod in a magnetic field is reduced using the Casimirs from a nine-dimensional non-canonical Hamiltonian system to a six-dimensional canonical system. Mel'nikov's method is then applied to an extensible rod in magnetic field, implying the existence of multimodal solutions. Chapter 6 then investigates the multiplicities of multimodal homoclinic orbits and their bifurcation structure. A codimension-two point is identified from the spectrum of the Floquet multipliers in the nondimensional body loading and end loading parameter plane which determines whether configuration with a single localisation may bifurcate at either two critical values of the magnetic field, one critical value, or do not bifurcate at all. The codimension-two point is a double Hamiltonian-Hopf bifurcation point and acts as an organising centre for the bifurcation set for primary and multimodal homoclinics. Finally, chapter 7 summarises the main results, discusses conclusions, limitations and directions for future research. The thesis concludes with two appendices; the appendix A introduces the Euler angles and the Euler parameters and appendix B outlines the standard numerical techniques to compute and continue homoclinic orbits in reversible dynamical systems to a hyperbolic fixed point and illustrates the method for the Kirchhoff rod.

Chapter 2

Hamiltonian Systems

The rigorous study of elasticity truly began in 1744 when Euler solved the problem of the equilibrium configurations of a thin extensible wire. Euler's insight was that the problem of finding the equilibrium configurations was equivalent to minimizing the sum of the squared curvatures for curves of fixed length [66, §263]. Thus the problem of the Elastica became a variational problem. Over 250 years afterwards, Novikov [75] eloquently writes

> "It is now scarcely a matter of dispute that dynamical systems describing real physical processes are, as a rule, Hamiltonian in one sense or another if the dissipation of energy can be disregarded. ... However the Hamiltonian formalism may turn out to be non-classical, that is it may not originate from a Lagrangian formalism as a result of a Legendre transform."

For many problems in nonlinear elasticity the static equilibrium equations are noncanonical Hamiltonian equations of the form

$$f' = \{f, \mathcal{H}\}$$

where f say is a component of the generalised stresses in the rod, i.e. a component of the force or moment say, $\mathcal{H}$ is the Hamiltonian function and $\{\cdot, \cdot\}$ is a Poisson bracket. As mentioned, the formulation allows for a vast array of analytical and numerical tools to be applied. In this chapter the analytical tools which are applied are introduced but for a more detailed description, see Arnol'd [6] or Olver [76].

2.1 Hamiltonian Systems with Symmetry

The geometrically exact rod formulation is naturally a noncanonical Hamiltonian formulation [83] and retains the symmetry properties of the physical system. The importance of the formulation is that each constituent effect, e.g. applied moment, applied force or body force is produced by a Poisson bracket. Thus the rod model is extended through extensions of the original bracket.

Definition 2.1.1. *Let $\mathcal{M}$ be a smooth m-dimensional manifold, then for any smooth real-valued functions f, g and h on $\mathcal{M}$, the Poisson bracket $\{\cdot,\cdot\}$ defines another smooth real-valued function on $\mathcal{M}$ with the following properties*

(i) Bilinearity: $\{\alpha f + \beta g, h\} = \alpha\{f,h\} + \beta\{g,h\}, \quad \forall\, \alpha, \beta \in \mathbb{R}$.

(ii) Skew-Symmetry: $\{f,g\} + \{g,f\} = 0$.

(iii) Jacobi's Identity: $\{f,\{g,h\}\} + \{h,\{f,g\}\} + \{g,\{h,f\}\} = 0$.

(iv) Leibniz's Rule: $\{f \circ g, h\} = g \circ \{f,h\} + f \circ \{g,h\}$.

If the manifold has a Poisson bracket then the manifold is called a Poisson manifold.

Although a Poisson manifold is not necessarily a symplectic manifold it is, however, foliated by collection of submanifolds which are symplectic.

Theorem 2.1.2 (Darboux's Theorem). *Let $\mathcal{M}$ be a smooth m-dimensional Poisson manifold of constant rank $2n \leq m$ everywhere. At each $\boldsymbol{x} \in \mathcal{M}$ there exist canonical local coordinates $(q,p,z) = (q_1,\ldots,q_n,p_1,\ldots,p_n,z_1,\ldots z_k)$, where $2n+k=m$, in terms of which the Poisson bracket takes the form*

$$\{f,g\}_{(q,p)} = \sum_{i=1}^{n} \left(\frac{\partial f}{\partial q_i}\frac{\partial g}{\partial p_i} - \frac{\partial f}{\partial p_i}\frac{\partial g}{\partial q_i} \right). \tag{2.1}$$

The Poisson bracket (2.1) *is called the canonical bracket.*

Proof of 2.1.2. See [76, §6.22]. □

Classically the Hamiltonian function is defined from the Legendre transform of the Lagrangian and is the total energy of the system. Hamilton's canonical equations are then

computed from the (canonical) bracket. In this thesis the static equilibria are derived and associated with a system of non-canonical Hamiltonian equations. For the precise forms of the governing equations and their structure see §3.

Definition 2.1.3. *Let $\mathcal{M}$ be an m-dimensional Poisson manifold and let $\mathcal{H}$ be a smooth function, $\mathcal{H}(q,p,z):\mathcal{M}\mapsto\mathbb{R}$. The Hamiltonian vector field is the unique, smooth vector field on $\mathcal{M}$ satisfying*

$$\frac{\mathrm{d}f}{\mathrm{d}t}=f'=\{f,\mathcal{H}\}$$

for every smooth function $f(q,p,z):\mathcal{M}\mapsto\mathbb{R}$. $\mathcal{H}$ is called the Hamiltonian and the governing equations are referred to as Hamilton's equations. When the bracket is the canonical bracket (2.1)*, the governing equations are referred to as Hamilton's canonical equations*

$$q'=\frac{\partial\mathcal{H}}{\partial p},\quad p'=-\frac{\partial\mathcal{H}}{\partial q}\quad \textit{and}\quad z'=0.$$

Definition 2.1.4. *A function, f, is a conserved quantity of a Hamiltonian system if it is constant for all solutions of the system. This is equivalent to being in involution with the Hamiltonian, i.e. $\{f,\mathcal{H}\}=0$. Functions which are conditionally dependent on the parameters of the system are called first integrals. Functions which are in involution with every function in the phase space are called Casimir functions. They too are conserved quantities since they are in involution with the Hamiltonian.*

Casimirs only exist in non-canonical formulations and in finite-dimensional Hamiltonian systems Casimirs can be found in systematic way [48]. In a sense first integrals are analytic, based on the form of the Hamiltonian, while Casimirs are geometric integrals, based on the structure of the Poisson manifold. In the context of rod theory

First integrals or nontrivial integrals, are conserved quantities which are dependent on the parameters of the system. In the context of rod theory the first integrals are dependent on the constitutive relations. The Hamiltonian and the integrals of Lagrange and Kovalevskaya, cf. (3.30) and (3.31) are examples of first integrals in rod theory. They are rare, often difficult to find and may not have an intuitive physical

meaning. In some case, such as the Chaplygin-Goryachev integral, cf. (3.32), they maybe dependent on the values of the Casimirs as well as the parameters of the system.

Casimirs or distinguished functions are integrals which are independent of the specific Hamiltonian function but are dependent on the equilibrium equations. Examples of Casimirs in rod theory are the conservation of the applied moment about the loading axis (3.29a) or the conservation of the magnitude of force force in the body (3.29b) for a rod under end force and torque. Casimirs may be expressed as functions of parameters, see (5.2a), but are not dependent on them.

Knowledge of the conserved quantities allows for the equations to be classified as integrable or nonintegrable. In the context of finite dimensional Hamiltonian systems complete integrability is well defined.

Definition 2.1.5. *An m-dimensional Hamiltonian system is said to be completely integrable in the sense of Liouville if it possesses k Casimirs and n first integrals where*

$$2n + k = m. \tag{2.2}$$

Additionally an m-dimensional system is superintegrable if $2n + k > m$, minimally superintegrable if it possesses $2n + k = m - 1$ integrals and maximally superintegrable if $2n + k = 2m - 1$.

The algebraic and geometric properties of integrability are given by the Arnol'd-Liouville theorem [6, pg. 272].

Theorem 2.1.6 (Arnol'd-Liouville Integrability). *Let an m-dimensional Hamiltonian vector field be completely integrable with k Casimirs and n first integrals. Then by theorem 2.1.2 the Casimirs induce a canonical Hamiltonian bracket on an n-dimensional reduced phase space with n integrals $I = (I_1, I_2, \ldots, I_n)$ in involution. Then*

(i) The level set of all integrals is a manifold $\mathcal{M}_I$ which is invariant under the phase flow with Hamiltonian function $\mathcal{H} = I_1$.

(ii) If the manifold $\mathcal{M}_I$ is compact and connected then it is diffeomorphic to the n-dimensional torus $\mathbb{T}^n = \{(\varphi_1, \varphi_2, \ldots, \varphi_n) \bmod 2\pi\}$.

(iii) The phase flow with Hamiltonian function determines a conditionally periodic motion on $\mathcal{M}_I$, i.e., in angular coordinates $\varphi_i' = \omega_i$ and $\omega_i = \omega_i(I)$.

(iv) The canonical equations can be integrated by quadratures.

Proof of 2.1.6. See [6, §10]. □

The existence of action-angle variables shows that a system is solvable by quadrature, although for practical purposes it is often an existence theorem only. However, integrability has dynamical consequences: the action-angle formulation creates a set of symplectic coordinates (I, φ) such that the actions I depend on the integrals and the angles φ are angular coordinates that flow linearly on the n-torus. Thus the Hamiltonian is a function of the actions only. Hence Hamilton's equations are

$$I' = -\frac{\partial \mathcal{H}}{\partial \varphi} \quad \text{and} \quad \varphi' = \frac{\partial \mathcal{H}}{\partial I}. \tag{2.3}$$

It follows that

$$I_i' = 0 \quad \text{and} \quad \varphi_i' = \omega_i \quad i = 1, \ldots, n \tag{2.4}$$

where ω_i are the frequencies of the motion on the torus and

$$I = I(h, p) \quad \text{such that} \quad I_i = \frac{1}{2\pi} \oint_{\gamma_i} p_i \, \mathrm{d}q_i \quad i = 1, \ldots, n$$

over cycles γ_i.

As mentioned in §1, if an Kirchhoff rod whose principal bending stiffnesses are equal then the governing equations are completely integrable. Thus all configurations can be expressed in closed form. However the independent integrals do not form a compact and smooth manifold, prohibiting the construction of global action-angle coordinates [29].

The main benefits of action-angle coordinates are that they allow insight into the bifurcation structure of a system and through perturbation analysis can shed light on the behaviour of nonintegrable systems nearby.

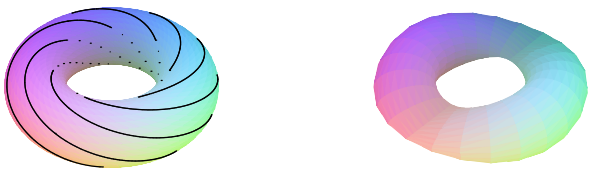

(a) (b)

Figure 2.1: All integrable systems can be described by action-angle variables which define motion on a torus, in this figure two degenerate cases are illustrated. Subfigure 2.1(a) gives a schematic illustration of closed resonant motion on a 2-torus which does not densely fill the surface of the torus. In this situation two of the angular frequencies will be in resonance. Subfigure 2.1(b) shows a pinched-torus which relates to systems which do not have global action-angle variable formations.

2.2 Mel'nikov's Theory

It is believed that most naturally occurring systems are nonintegrable [75], however many can be considered to be perturbations of integrable systems. As shall be demonstrated, for Cosserat rods some perturbations such as extensibility and a force due to a magnetic field do not destroy integrability, while others such as anisotropy and initial curvature do destroy integrability through the loss of a first integral. In this section a perturbation technique determining integrability called Mel'nikov's method is introduced and an instructive example presented. In this thesis the Mel'nikov integral needs to computed to second order so the Mel'nikov integral is derived in detail to first and second order.

The Mel'nikov integral [52, 69] is used to analyse a perturbation of a homoclinic orbit in an integrable Hamiltonian system, giving a measure of the distance between the unstable and stable manifolds of the perturbed homoclinic orbit, as is illustrated in figure 2.2. If the Mel'nikov integral has simple zeroes then the stable and unstable perturbed homoclinic manifolds intersect transversely. Devaney's theorem [33] states that if the perturbation yields a transverse intersection of the stable and unstable manifolds then the existence of an associated transverse homoclinic orbit allows, via the Smale-Birkhoff theorem, horseshoes on the Poincaré sections of the level sets defined by the

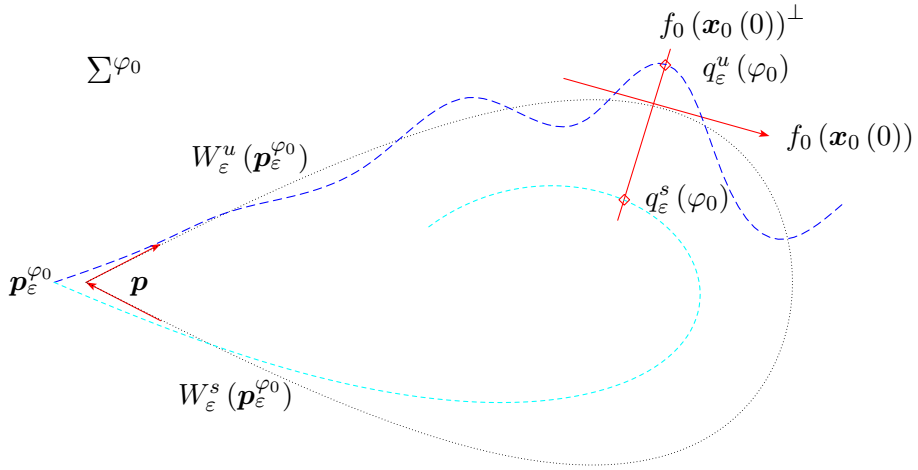

Figure 2.2: Schematic illustration of Mel'nikov's method on a Poincaré section Σ^{φ_0}. The Mel'nikov integral $\mathcal{M}(\varphi_0)$ measures the distance (red line) between approximations of the stable W_ε^s (cyan) and unstable manifolds W_ε^s (blue) of a homoclinic orbit $\boldsymbol{x}_0(\varphi)$ (dotted) at a point φ_0. Note that $\boldsymbol{p}$ is a fixed point but $\boldsymbol{p}_\varepsilon^{\varphi_0}$ is a periodic orbit with a fixed point on the Poincaré map Σ^{φ_0}.

homoclinic energy. In turn, the system is no longer integrable. Given the transversal intersection of the stable and unstable manifolds, configurations with arbitrarily high period which are embedded in an invariant Cantor set may then exist, implying the existence a multiplicity of multimodal homoclinic solutions [9] and [45, §2.4.1].

Let the perturbed system take the form

$$\mathcal{H}_\varepsilon(q,p,\varphi,I) = \mathcal{H}_0(q,p,I) + \varepsilon\mathcal{H}_1(q,p,\varphi,I) + \mathcal{O}\left(\varepsilon^2\right), \quad (q,p) \in \mathbb{R}^2. \tag{2.5}$$

In order for the analysis to hold when the perturbation of the Hamiltonian, two assumptions need to be satisfied:

(H1) The unperturbed Hamiltonian system $\mathcal{H}_0$ possesses a homoclinic orbit of the form

$$\boldsymbol{x}_0(s) = (q(s;h), p(s;h))$$

to a hyperbolic fixed point

$$\boldsymbol{p} = \boldsymbol{x}_0(0) = (q(0;h), p(0;h))$$

for each 'energy' level h in an interval $h \in J^h \subset \mathbb{R}$, where the interval J^h is the set of energy levels which admit homoclinic orbits. The homoclinic depends on the energy level via the action $I_h = I(h)$ corresponding to the homoclinic orbit.

(H2) For $h \in J^h$ and $\boldsymbol{x}_0$ the frequency

$$\omega_0 = \omega_0(\boldsymbol{x}_0, I_h) = \frac{\partial \mathcal{H}_0}{\partial I} \tag{2.6}$$

of the unperturbed system satisfies the condition $|\omega_0| \geq \delta > 0$ for some arbitrarily small $\delta \in \mathbb{R}^+$ and holds $\forall s \in (-\infty, +\infty)$. Thus

$$\varphi(s) = \varphi_0 + \int^s \omega_0(\bar{s})\, \mathrm{d}\bar{s} = \varphi_0 + \bar{\varphi}(s) \tag{2.7}$$

and

$$\lim_{s \to \pm\infty} \varphi(s) = \pm\infty. \tag{2.8}$$

By the first condition (H1), the unperturbed Hamiltonian may be inverted and solved for I_h. By the second condition (H2) φ can be treated as a 'time-like' variable.

The (constant) action I_h can be expanded in powers of the perturbation

$$I_h = I_h(q, p, \varphi) = I^{(0)} + \varepsilon I^{(1)} + \mathcal{O}\left(\varepsilon^2\right). \tag{2.9}$$

The derivative of the angle coordinate, i.e. the frequency on the torus, can be expanded for small ε

$$\begin{aligned} \varphi' = \frac{\partial \mathcal{H}_\varepsilon}{\partial I} &= \omega_\varepsilon \\ &= \omega_0 + \varepsilon \frac{\partial \mathcal{H}_1}{\partial I} + \mathcal{O}\left(\varepsilon^2\right). \end{aligned} \tag{2.10}$$

Since

$$\frac{\partial \mathcal{H}}{\partial p} = \frac{\mathrm{d}q}{\mathrm{d}\varphi}\frac{\mathrm{d}\varphi}{\mathrm{d}t} \quad \text{and} \quad \frac{\partial \mathcal{H}}{\partial q} = -\frac{\mathrm{d}p}{\mathrm{d}\varphi}\frac{\mathrm{d}\varphi}{\mathrm{d}t}, \tag{2.11}$$

then from (2.10) and (2.11) the following relationships hold

$$\frac{\mathrm{d}q}{\mathrm{d}\varphi} = \omega_\varepsilon^{-1}\frac{\partial \mathcal{H}_\varepsilon}{\partial p} \quad \text{and} \quad \frac{\mathrm{d}p}{\mathrm{d}\varphi} = -\omega_\varepsilon^{-1}\frac{\partial \mathcal{H}_\varepsilon}{\partial q}. \tag{2.12}$$

Given $h = \mathcal{H}_\varepsilon$ then implicit differentiation of $\mathcal{H}_\varepsilon\left(q, p, I\left(q, p, \varphi\right), \varphi\right)$ with respect to both canonical coordinates (q, p) at the homoclinic energy level yields

$$\frac{\partial \mathcal{H}_\varepsilon}{\partial q} + \omega_\varepsilon \frac{\partial I_h}{\partial q} = 0 \quad \text{and} \quad \frac{\partial \mathcal{H}_\varepsilon}{\partial p} + \omega_\varepsilon \frac{\partial I_h}{\partial p} = 0. \tag{2.13}$$

It follows from (2.12) and (2.13) that

$$\frac{\mathrm{d}q}{\mathrm{d}\varphi} = -\frac{\partial I_h}{\partial p} \quad \text{and} \quad \frac{\mathrm{d}p}{\mathrm{d}\varphi} = \frac{\partial I_h}{\partial q}. \tag{2.14}$$

The angle coordinate on the torus, φ, now plays the role of time in a new Hamiltonian system, where the Hamiltonian is played by the constant action, I_h. In order to find the terms in the expansion of I_h in (2.9) the Hamiltonian (2.5) is expanded along the homoclinic energy level

$$\begin{aligned} h &= \mathcal{H}_\varepsilon\left(q, p, \varphi, I^{(0)} + \varepsilon I^{(1)} + \mathcal{O}\left(\varepsilon^2\right)\right) \\ &= \mathcal{H}_0\left(q, p, I^{(0)} + \varepsilon I^{(1)} + \mathcal{O}\left(\varepsilon^2\right)\right) + \varepsilon \mathcal{H}_1\left(q, p, \varphi, I^{(0)} + \varepsilon I^{(1)} + \mathcal{O}\left(\varepsilon^2\right)\right) \\ &= \mathcal{H}_0\left(q, p, I^{(0)}\right) + \varepsilon I^{(1)} \omega_0\left(q, p, I^{(0)}\right) + \varepsilon \mathcal{H}_1\left(q, p, \varphi, I^{(0)}\right) + \mathcal{O}\left(\varepsilon^2\right). \end{aligned} \tag{2.15}$$

Comparing coefficients of ε for the expansions of the Hamiltonian (2.15) with the action (2.9) to first order yields

$$I^{(0)}\left(q, p\right) = \mathcal{H}_0^{-1}\left(q, p\right)\left(h\right), \tag{2.16a}$$

$$\begin{aligned} I^{(1)}\left(q, p, \varphi\right) &= -\frac{\mathcal{H}_1\left(q, p, \varphi, I^{(0)}\right)}{\omega_0\left(q, p, I^{(0)}\right)} \\ &= -\frac{\mathcal{H}_1\left(q, p, \varphi, \mathcal{H}_0^{-1}\left(q, p\right)\left(h\right)\right)}{\omega_0\left(q, p, \mathcal{H}_0^{-1}\left(q, p\right)\left(h\right)\right)}, \end{aligned} \tag{2.16b}$$

where $\mathcal{H}_0^{-1}\left(q, p\right)\left(h\right)$ denotes the inversion of $\mathcal{H}_0$ with respect to I at h. Hence Hamilton's equations are

$$\frac{\mathrm{d}q}{\mathrm{d}\varphi} = -\frac{\partial I^{(0)}}{\partial p} - \varepsilon \frac{\partial I^{(1)}}{\partial p} - \mathcal{O}\left(\varepsilon^2\right), \tag{2.17a}$$

$$\frac{\mathrm{d}p}{\mathrm{d}\varphi} = \frac{\partial I^{(0)}}{\partial q} + \varepsilon \frac{\partial I^{(1)}}{\partial q} + \mathcal{O}\left(\varepsilon^2\right). \tag{2.17b}$$

Using the expressions for $I^{(n)}$ derived in (2.16), a n^{th}-order approximation to the governing equations in terms of the unperturbed system can be calculated. The unperturbed

vector field is in fact a scaled version of the original problem, that is

$$\left(-\frac{\partial I^{(0)}}{\partial p}, \frac{\partial I^{(0)}}{\partial q}\right) = \frac{1}{\omega_0}\left(\frac{\partial \mathcal{H}_0}{\partial p}, -\frac{\partial \mathcal{H}_0}{\partial q}\right). \tag{2.18}$$

Thus, if the first condition (H1) is satisfied then the unperturbed vector field (2.17) has a hyperbolic fixed point.

For simplicity in the notation let $\boldsymbol{x} = (q, p)$ and let

$$f_i = \varepsilon^i \left(-\partial I_i/\partial p, \partial I_i/\partial q\right)^T.$$

For $u = (u_1, u_2)$ and $v = (v_1, v_2)$ the wedge product is defined as

$$u \wedge v = u_1 v_2 - v_1 u_2.$$

Let $Df_0(\boldsymbol{x})$ denote the Jacobian of f_0 evaluated at $\boldsymbol{x}$ and let $D^2 f_0 \boldsymbol{x}^2$ be shorthand for $\left(D\left(Df_0\boldsymbol{x}\right)\right)\boldsymbol{x}$. The Mel'nikov integral is now derived to first and second order.

Theorem 2.2.1. *Consider the 'time' dependent distance function*

$$\Delta_\varepsilon(\varphi, \varphi_0) = f_0\left(\boldsymbol{x}_0(\varphi - \varphi_0)\right) \wedge \left(\boldsymbol{x}_\varepsilon^u(\varphi, \varphi_0) - \boldsymbol{x}_\varepsilon^s(\varphi, \varphi_0)\right) \tag{2.19}$$

where $\boldsymbol{x}_\varepsilon^u$ and $\boldsymbol{x}_\varepsilon^s$ are the flows on the stable and unstable perturbed homoclinic manifolds of the form $\boldsymbol{x}_\varepsilon^u = \boldsymbol{x}_0 + \varepsilon \boldsymbol{x}_1^u + \mathcal{O}\left(\varepsilon^2\right)$ (see appendix §B.1 for more detail). The Mel'nikov function is defined as

$$\Delta_\varepsilon(\varphi_0) = \Delta_\varepsilon(\varphi_0, \varphi_0). \tag{2.20}$$

The Mel'nikov function can be expanded in powers of the perturbation

$$\Delta_\varepsilon(\varphi_0) = \varepsilon \mathcal{M}_h^{(1)}(\varphi_0) + \varepsilon^2 \mathcal{M}_h^{(2)}(\varphi_0) + \mathcal{O}\left(\varepsilon^3\right). \tag{2.21}$$

The first order Mel'nikov integral is given by

$$\mathcal{M}_h^{(1)}(\varphi_0) = \int_{-\infty}^{+\infty} f_0\left(\boldsymbol{x}_0(\varphi - \varphi_0)\right) \wedge f_1\left(\boldsymbol{x}_0(\varphi - \varphi_0), \varphi\right) \mathrm{d}\varphi \tag{2.22}$$

and the second order Mel'nikov integral is given by

$$\begin{aligned}\mathcal{M}_h^{(2)}(\varphi_0) = \frac{1}{2}\int_{\varphi_0}^{+\infty} f_0 \wedge D^2 f_0 \left(\boldsymbol{x}_1^s\right)^2 \,\mathrm{d}\varphi + \frac{1}{2}\int_{-\infty}^{\varphi_0} f_0 \wedge D^2 f_0 \left(\boldsymbol{x}_1^u\right)^2 \,\mathrm{d}\varphi \\ + \frac{1}{2}\int_{\varphi_0}^{+\infty} f_0 \wedge Df_1 \boldsymbol{x}_1^s \,\mathrm{d}\varphi + \frac{1}{2}\int_{-\infty}^{\varphi_0} f_0 \wedge Df_1 \boldsymbol{x}_1^u \,\mathrm{d}\varphi \\ + \int_{-\infty}^{+\infty} f_0\left(\boldsymbol{x}_0\left(\varphi-\varphi_0\right)\right) \wedge f_2\left(\boldsymbol{x}_0\left(\varphi-\varphi_0\right),\varphi\right) \,\mathrm{d}\varphi. \end{aligned} \tag{2.23}$$

Where $\boldsymbol{x}_1^{s,u}(\varphi,\varphi_0)$ *are the solutions to a variational equation [45]*

$$\frac{\mathrm{d}}{\mathrm{d}\varphi}\boldsymbol{x}_1^{s,u}(\varphi,\varphi_0) = Df_0\left(\boldsymbol{x}_0\left(\varphi-\varphi_0\right)\right)\boldsymbol{x}_1^{s,u}(\varphi,\varphi_0) + f_1\left(\boldsymbol{x}_0\left(\varphi-\varphi_0\right),\varphi\right) \tag{2.24}$$

subject to the two conditions that the first order approximations to the perturbed homoclinic orbits are bounded (2.25a) *and transverse* (2.25b) *to the flow of the unperturbed homoclinic orbits*

$$\lim_{\varphi\to\pm\infty} \left|\left\langle \boldsymbol{x}_1^{s,u}(\varphi_0,\varphi_0), f_0\left(\boldsymbol{x}_0\left(\varphi-\varphi_0\right)\right)\right\rangle\right| \leq K, \tag{2.25a}$$

$$\left\langle \boldsymbol{x}_1^{s,u}(\varphi_0,\varphi_0), f_0\left(\boldsymbol{x}_0\left(\varphi-\varphi_0\right)\right)\right\rangle = 0. \tag{2.25b}$$

The two conditions provide initial conditions so that the variational equation is well-posed and unique solutions can be found. If the Mel'nikov function has simple zeroes then the stable and unstable manifolds intersect transversally for the perturbed system. Conversely, if the Mel'nikov integral is bounded away from zero then the manifolds do not intersect and there are no transverse intersections.

The theorem is not new but is extended to include higher order approximations for the splitting of the stable and unstable manifolds.

Proof of 2.2.1. The distance function (2.19) is be decomposed into constituent parts, so to second order

$$\Delta_\varepsilon(\varphi,\varphi_0) = \Delta_{\varepsilon,1}^-(\varphi,\varphi_0) - \Delta_{\varepsilon,1}^+(\varphi,\varphi_0) + \Delta_{\varepsilon,2}^-(\varphi,\varphi_0) - \Delta_{\varepsilon,2}^+(\varphi,\varphi_0) + \mathcal{O}\left(\varepsilon^3\right) \tag{2.26}$$

where the stable part of the first order term is given by

$$\Delta_{\varepsilon,1}^+(\varphi,\varphi_0) = f_0\left(\boldsymbol{x}_0\left(\varphi-\varphi_0\right)\right) \wedge \boldsymbol{x}_1^s(\varphi,\varphi_0). \tag{2.27}$$

Similarly, the corresponding second order term is given by

$$\Delta^{+}_{\varepsilon,2}(\varphi,\varphi_0) = f_0(\boldsymbol{x}_0(\varphi-\varphi_0)) \wedge \boldsymbol{x}_2^s(\varphi,\varphi_0). \tag{2.28}$$

The derivative of the first order term is

$$\begin{aligned}\frac{\mathrm{d}}{\mathrm{d}\varphi}\Delta^{+}_{\varepsilon,1}(\varphi,\varphi_0) = {} & Df_0(\boldsymbol{x}_0(\varphi,\varphi_0))\, f_0(\boldsymbol{x}_0(\varphi-\varphi_0)) \wedge \boldsymbol{x}_1^s(\varphi,\varphi_0) \\ & + f_0(\boldsymbol{x}_0(\varphi-\varphi_0)) \wedge Df_0(\boldsymbol{x}_0(\varphi-\varphi_0))\, \boldsymbol{x}_1^s(\varphi,\varphi_0) \\ & + f_0(\boldsymbol{x}_0(\varphi-\varphi_0)) \wedge f_1(\boldsymbol{x}_0(\varphi-\varphi_0),\varphi),\end{aligned}$$

which can be expressed in a compact form as

$$\frac{\mathrm{d}}{\mathrm{d}\varphi}\Delta^{+}_{\varepsilon,1}(\varphi,\varphi_0) = \operatorname{trace}(Df_0)\,\Delta^{+}_{\varepsilon,1} + f_0(\boldsymbol{x}_0(\varphi-\varphi_0)) \wedge f_1(\boldsymbol{x}_0(\varphi-\varphi_0),\varphi).$$

By exploiting the fact that f_0 is a Hamiltonian vector field

$$\operatorname{trace}(Df_0) = \frac{\partial^2 I^{(0)}}{\partial p \partial q} - \frac{\partial^2 I^{(0)}}{\partial q \partial p} = 0.$$

Hence the trace of the Jacobian is zero, thus

$$\frac{\mathrm{d}}{\mathrm{d}\varphi}\Delta^{+}_{\varepsilon,1}(\varphi,\varphi_0) = f_0(\boldsymbol{x}_0(\varphi-\varphi_0)) \wedge f_1(\boldsymbol{x}_0(\varphi-\varphi_0),\varphi). \tag{2.29}$$

Integrating from φ_0 to $+\infty$ yields

$$\Delta^{+}_{\varepsilon,1}(+\infty,\varphi_0) - \Delta^{+}_{\varepsilon,1}(\varphi_0,\varphi_0) = \int_{\varphi_0}^{+\infty} f_0(\boldsymbol{x}_0(\varphi-\varphi_0)) \wedge f_1(\boldsymbol{x}_0(\varphi-\varphi_0),\varphi)\ \mathrm{d}\varphi$$

since

$$\Delta^{+}_{\varepsilon,1}(+\infty,\varphi_0) = \lim_{\varphi\to+\infty}\left[f_0(\boldsymbol{p}) \wedge f_1(\boldsymbol{p},+\infty)\right] = 0$$

because

$$\lim_{\varphi\to+\infty} f_0(\boldsymbol{p}) = \boldsymbol{0}.$$

Hence

$$\Delta^{+}_{\varepsilon,1}(\varphi_0,\varphi_0) = -\int_{\varphi_0}^{+\infty} f_0(\boldsymbol{x}_0(\varphi-\varphi_0)) \wedge f_1(\boldsymbol{x}_0(\varphi-\varphi_0),\varphi)\ \mathrm{d}\varphi. \tag{2.30}$$

Similarly for the unstable part, integrating from $-\infty$ up to φ_0

$$\Delta^{-}_{\varepsilon,1}(\varphi_0,\varphi_0) = \int_{-\infty}^{\varphi_0} f_0(\boldsymbol{x}_0(\varphi-\varphi_0)) \wedge f_1(\boldsymbol{x}_0(\varphi-\varphi_0),\varphi)\,\mathrm{d}\varphi. \tag{2.31}$$

Thus, the first order approximation is then

$$\Delta^{-}_{\varepsilon,1}(\varphi_0,\varphi_0) - \Delta^{+}_{\varepsilon,1}(\varphi_0,\varphi_0) = \int_{-\infty}^{+\infty} f_0(\boldsymbol{x}_0(\varphi-\varphi_0)) \wedge f_1(\boldsymbol{x}_0(\varphi-\varphi_0),\varphi)\,\mathrm{d}\varphi.$$

Now dealing with the second order results in a similar manner, the derivative is given by

$$\begin{aligned}\frac{\mathrm{d}}{\mathrm{d}\varphi}\Delta^{+}_{\varepsilon,2}(\varphi,\varphi_0) = {} & Df_0(\boldsymbol{x}_0(\varphi,\varphi_0))\, f_0(\boldsymbol{x}_0(\varphi-\varphi_0)) \wedge \boldsymbol{x}_2^s(\varphi,\varphi_0) \\ & + f_0(\boldsymbol{x}_0(\varphi-\varphi_0)) \wedge Df_0(\boldsymbol{x}_0(\varphi-\varphi_0))\,\boldsymbol{x}_2^s(\varphi,\varphi_0) \\ & + \frac{1}{2}\left(f_0(\boldsymbol{x}_0(\varphi-\varphi_0)) \wedge D^2 f_0(\boldsymbol{x}_0(\varphi-\varphi_0))\,(\boldsymbol{x}_1^s(\varphi,\varphi_0))^2\right) \\ & + \frac{1}{2}\left(f_0(\boldsymbol{x}_0(\varphi-\varphi_0)) \wedge Df_1(\boldsymbol{x}_0(\varphi-\varphi_0),\varphi)\,\boldsymbol{x}_1^s(\varphi,\varphi_0)\right) \\ & + f_0(\boldsymbol{x}_0(\varphi-\varphi_0)) \wedge f_2(\boldsymbol{x}_0(\varphi-\varphi_0),\varphi).\end{aligned}$$

Once again exploiting the fact that f_0 is a Hamiltonian vector field yields

$$\begin{aligned}\frac{\mathrm{d}}{\mathrm{d}\varphi}\Delta^{+}_{\varepsilon,2}(\varphi,\varphi_0) = {} & \frac{1}{2} f_0(\boldsymbol{x}_0(\varphi-\varphi_0)) \wedge D^2 f_0(\boldsymbol{x}_0(\varphi-\varphi_0))\,(\boldsymbol{x}_1^s(\varphi,\varphi_0))^2 \\ & + f_0(\boldsymbol{x}_0(\varphi-\varphi_0)) \wedge Df_1(\boldsymbol{x}_0(\varphi-\varphi_0),\varphi)\,\boldsymbol{x}_1^s(\varphi,\varphi_0) \\ & + f_0(\boldsymbol{x}_0(\varphi-\varphi_0)) \wedge f_2(\boldsymbol{x}_0(\varphi-\varphi_0),\varphi).\end{aligned} \tag{2.32}$$

On integrating and combining with the unstable part, to second order the Mel'nikov integral is given by the integral

$$\begin{aligned}\mathcal{M}_h^{(2)}(\varphi_0) = {} & \frac{1}{2}\int_{\varphi_0}^{+\infty} f_0(\boldsymbol{x}_0(\varphi-\varphi_0)) \wedge D^2 f_0(\boldsymbol{x}_0(\varphi-\varphi_0))\,(\boldsymbol{x}_1^s(\varphi,\varphi_0))^2\,\mathrm{d}\varphi \\ & + \frac{1}{2}\int_{-\infty}^{\varphi_0} f_0(\boldsymbol{x}_0(\varphi-\varphi_0)) \wedge D^2 f_0(\boldsymbol{x}_0(\varphi-\varphi_0))\,(\boldsymbol{x}_1^u(\varphi,\varphi_0))^2\,\mathrm{d}\varphi \\ & + \frac{1}{2}\int_{\varphi_0}^{+\infty} f_0(\boldsymbol{x}_0(\varphi-\varphi_0)) \wedge Df_1(\boldsymbol{x}_0(\varphi-\varphi_0),\varphi)\,\boldsymbol{x}_1^s(\varphi,\varphi_0)\,\mathrm{d}\varphi \\ & + \frac{1}{2}\int_{-\infty}^{\varphi_0} f_0(\boldsymbol{x}_0(\varphi-\varphi_0)) \wedge Df_1(\boldsymbol{x}_0(\varphi-\varphi_0),\varphi)\,\boldsymbol{x}_1^u(\varphi,\varphi_0)\,\mathrm{d}\varphi \\ & + \int_{-\infty}^{+\infty} f_0(\boldsymbol{x}_0(\varphi-\varphi_0)) \wedge f_2(\boldsymbol{x}_0(\varphi-\varphi_0),\varphi)\,\mathrm{d}\varphi\end{aligned} \tag{2.33}$$

where, it is shown in appendix §B.1 that $\boldsymbol{x}_1^{s,u}(\varphi, \varphi_0)$ is a unique solution to

$$\frac{\mathrm{d}}{\mathrm{d}\varphi}\boldsymbol{x}_1^{s,u}(\varphi, \varphi_0) = Df_0(\boldsymbol{x}_0(\varphi - \varphi_0))\,\boldsymbol{x}_1^{s,u}(\varphi, \varphi_0) + f_1(\boldsymbol{x}_0(\varphi - \varphi_0), \varphi) \tag{2.34}$$

when subject to the two conditions on transverse intersection of perturbed flows of the homoclinic with a Poincaré section and boundedness of solutions

$$\langle \boldsymbol{x}_1^{s,u}(\varphi_0, \varphi_0), f_0(\boldsymbol{x}_0(\varphi - \varphi_0))\rangle = 0, \tag{2.35a}$$

$$\lim_{\varphi \to \pm\infty} |\langle \boldsymbol{x}_1^{s,u}(\varphi_0, \varphi_0), f_0(\boldsymbol{x}_0(\varphi - \varphi_0))\rangle| \leq K \tag{2.35b}$$

for a constant $K > 0$. □

Corollary 2.2.2. *If the Mel'nikov integral has simple zeroes then the perturbed Hamiltonian system has no analytic first integrals in the neighbourhood of ε, hence is non-integrable.*

Proof of 2.2.2. See [45, §4.8.2] □

For first order approximations of the Mel'nikov integral it is not necessary to compute the perturbations of the action I_h and integrate with respect to φ as a more compact form can be used.

Lemma 2.2.3. *The first order Mel'nikov function can be written as*

$$\mathcal{M}_h^{(1)}(\varphi_0) = \int_{-\infty}^{+\infty} \left\{\mathcal{H}_0, \frac{\mathcal{H}_1}{\omega_0}\right\}_{(q,p)} \mathrm{d}s. \tag{2.36}$$

Proof of 2.2.3. Note that

$$f_0 \wedge f_1 = \frac{\partial I^{(0)}}{\partial q}\frac{\partial I^{(1)}}{\partial p} - \frac{\partial I^{(1)}}{\partial q}\frac{\partial I^{(0)}}{\partial p} = \left\{I^{(0)}, I^{(1)}\right\}_{(q,p)}.$$

The three relations

$$\frac{\partial I^{(0)}}{\partial q} = \frac{\partial I^{(0)}}{\partial \mathcal{H}_0}\frac{\partial \mathcal{H}_0}{\partial q} = -\frac{1}{\omega_0}\frac{\partial \mathcal{H}_0}{\partial q}, \quad \frac{\partial I^{(0)}}{\partial p} = -\frac{1}{\omega_0}\frac{\partial \mathcal{H}_0}{\partial p} \quad \text{and} \quad I^{(1)} = -\frac{\mathcal{H}_1}{\omega_0}$$

on substitution yield

$$\begin{aligned}\left\{I^{(0)}, I^{(1)}\right\}_{(q,p)} &= \frac{\partial I^{(0)}}{\partial q}\frac{\partial I^{(1)}}{\partial p} - \frac{\partial I^{(0)}}{\partial p}\frac{\partial I^{(1)}}{\partial q} \\ &= -\frac{1}{\omega_0}\frac{\partial \mathcal{H}_0}{\partial q}\frac{\partial}{\partial p}\left(\frac{\mathcal{H}_1}{\omega_0}\right) + \frac{1}{\omega_0}\frac{\partial \mathcal{H}_0}{\partial p}\frac{\partial}{\partial q}\left(-\frac{\mathcal{H}_1}{\omega_0}\right) \\ &= \frac{1}{\omega_0}\left\{\mathcal{H}_0, \frac{\mathcal{H}_1}{\omega_0}\right\}_{(q,p)}.\end{aligned}$$

From condition (H2) it follows that $\omega_0\,\mathrm{d}s = \mathrm{d}\varphi$, hence the lemma is proved. □

The second order the Mel'nikov integral can not be expressed in a similarly compact form. An example of both first and second order Mel'nikov method is given in the next section.

2.3 The construction of the Horseshoe map for Hamiltonian perturbation of a Hamiltonian system

The Smale-Birkhoff homoclinic theorem asserts the existence, near a transversal homoclinic point, of a zero-dimensional Cantor set on which some power of the map P_ε^N is homeomorphic to a Bernoulli shift on m-symbols. However caution should be exercised when drawing conclusions regarding transverse intersections. The C. Neumann top is an completely integrable system which has transverse intersections of its stable and unstable manifolds. However, despite possessing transverse intersections the system does not exhibit sensitive dependence on initial conditions or any other of the hallmarks of spatial chaos [33]. This is because the flow on the invariant set is not minimal and thus does not have necessary recurrence properties in the sense of [45, def. 5.2.3]. Without the explicit construction of the horseshoe maps on the Poincaré section of the perturbed firm conclusions of the dynamics cannot be inferred. To prove that a transverse homoclinic point can lead to spatial chaos is a long and involves process, for example see [45, §5] for more details. Here the basic idea is sketched and in each case where Mel'nikov's method is applied a horseshoe map will be constructed.

Firstly select an energy level h in the class energy levels J^h which admit homoclinic

orbits. Next define a Poincaré section as

$$P_{\varepsilon}^{\varphi_0} \,:\, \Sigma^{\varphi_0} \mapsto \Sigma^{\varphi_0}$$

associated with the periodically perturbed systems (2.5). For shorthand denote the map by P_{ε} and the global cross section as

$$\Sigma^{\varphi_0} = \{(q, p, \varphi) \,:\, \varphi = \varphi_0 \in [0, 2\pi]\}\,.$$

When $\varepsilon = 0$ the set P_{ε} is a fixed point. By the two hypotheses (H1) and (H2) when $\varepsilon = 0$ then the Poincaré map has an invariant manifold filled with a continuous family of nontransverse homoclinic orbits. The manifold has fixed points which do not intersect, hence for small ε the Poincaré map P_{ε} is topologically equivalent to P_0, since P_0 is structurally stable. Thus the Poincaré map P_{ε} has the structure identical to that of the unperturbed vector field in that the stable and unstable manifolds of the saddle of the Poincaré map are the same as the separatices emanating from the saddle for the vector field.

To construct the horseshoe map one takes a small region R, containing a transverse homoclinic point, partially bounded by pieces of the stable and unstable manifolds $W_{\varepsilon}^{s,u}\left(\boldsymbol{p}_{\varepsilon}^{\varphi_0}\right)$. Integers l_+ and l_- can be choosen so that the forward and backward images of the Poincaré map of the region r lie in the neighbourhood U of the saddle point $\boldsymbol{p}_{\varepsilon}$. The linearised Poincaré map $DP_{\varepsilon}\left(\boldsymbol{p}_{\varepsilon}\right)$ can then be used to approximate the motions in the neighbourhood of the saddle point. Moreover it can be shown that there is an integer N and two disjoint 'horizontal' stripes H_1 and $H_2 \subset P^{l_+}\left(R\right)$ whose images under the N^{th}-iterate of the Poincaré map are disjoint 'vertical' stripes V_1 and V_2. The map $P_{\varepsilon}^{N} \,:\, H_i \to V_i$ for $i = 1, 2$ is the horseshoe map.

In order to show hyperbolicity of the Cantor set Λ, it is necessary to find 'sector' bundles, i.e. collection of vector bundles for every point in the region R which are mapped onto themselves by the linearised Poincaré map. This implies that the choices of $l_{\pm}$ are related to ε since the angle between the tangent vectors of the manifold at a tranverse homoclinic point is $\mathcal{O}\left(\varepsilon\right)$ [51]. It has been shown that $\max\left(l_{\pm}\right) \sim \ln\left(1/\varepsilon\right)$ [33].

Theorem 2.3.1 (Smale-Birkhoff Homoclinic Theorem). *Let $f : \mathbb{R}^n \mapsto \mathbb{R}^n$ be a diffeomorphism such that $\boldsymbol{p}_\varepsilon^{\varphi_0}$ is a hyperbolic fixed point and there exists a point $\boldsymbol{q}$ at which there is a transversal intersection of the stable and unstable manifolds of the hyperbolic fixed point $W^{s,u}\left(p_\varepsilon^{\varphi_0}\right)$ with $\boldsymbol{p} \neq \boldsymbol{q}$. Then f has a hyperbolic invariant set Λ on which f is topologically equivalent to a subshift of finite type.*

Proof of 2.3.1. See [45, §5.3.5] □

Corollary 2.3.2. *Since $P_\varepsilon^N \| \Lambda$ possess a dense orbit of solution curves it follows that the perturbed system possess no new analytic integrals.*

2.3.1 An Example of the Second Order Mel'nikov Method: a Modified Duffing Oscillator

The celebrated harmonically forced Duffing oscillator was formulated to describe the hardening spring effect seen in mechanical oscillators and has been used to model a wide variety of systems. The Duffing oscillator is not the focus of this study and a modified version is used only as an example of higher order approximations to the Mel'nikov method. Further examples of when the first order approximation of the Mel'nikov integral may be zero are outlined in [42].

In [71, 73] the authors considered the buckling of a beam or plate in a magnetic field with only one mode of vibration, with a cubic damping. The authors state that experimental evidence suggests that vibrations primarily occur about the first mode. On performing a Galerkin-type approximation the system was reduced to a second order nonlinear ordinary differential equation

$$x'' = x - x^3 + \varepsilon\delta x' + \varepsilon\gamma\cos\left(\omega\left(t + t_0\right)\right), \tag{2.38}$$

where ε is a term of an order of magnitude less than the $\mathcal{O}(1)$ parameters δ, γ and ω. The dissipation due to friction, viscous damping due to air resistance and magnetic damping was modelled by a linear velocity dependent term of $\mathcal{O}(\varepsilon)$.

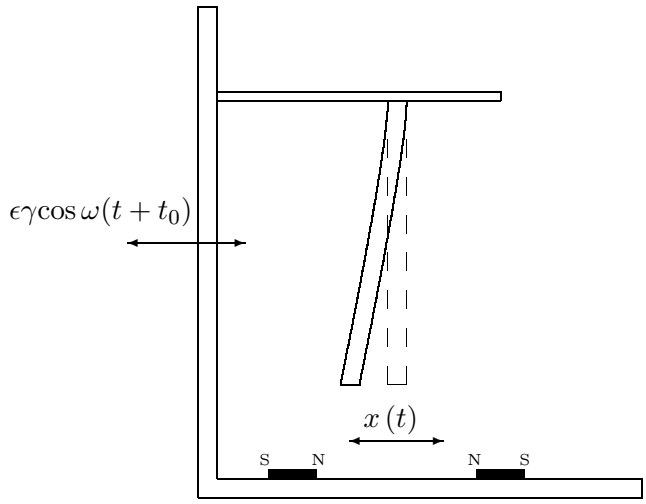

As a one-and-a-half-degrees of freedom system (2.38) is

$$x' = y, \tag{2.39a}$$

$$y' = x - x^3 - \varepsilon\delta y - \varepsilon^2\gamma\cos\theta, \tag{2.39b}$$

$$\theta' = \omega. \tag{2.39c}$$

In the notation of the previous section for $\boldsymbol{x} = (x, y)$ then $\boldsymbol{x}' = f_0(\boldsymbol{x}) + \varepsilon f_1(\boldsymbol{x}, t)$. The functions are given by

$$f_0 = \left(y, x - x^3\right)^T \quad \text{and} \quad f_1 = \left(0, -\delta y - \gamma\cos\theta\right)^T.$$

The unperturbed system is Hamiltonian with

$$\mathcal{H}(x, y) = \frac{1}{2}y^2 - \frac{1}{2}x^2\left(1 - \frac{1}{2}x^2\right). \tag{2.40}$$

The system has a pair of centres at $(\pm 1, 0)$, a hyperbolic saddle at $\boldsymbol{p} = (0, 0)$ and a pair of homoclinic orbits emananting from the saddle given by

$$x_0(t) = \pm\sqrt{2}\,\mathrm{sech}\,t \quad \text{and} \quad y_0(s) = \mp\sqrt{2}\,\mathrm{sech}\,t\tanh t. \tag{2.41}$$

Here the homoclinic orbit is taken to be $x_0 = \sqrt{2}\mathrm{sech}\,t$ and $y_0 = -\sqrt{2}\,\mathrm{sech}\,t\tanh t$.

The first order Mel'nikov integral is given by

$$\begin{aligned}\mathcal{M}_h^{(1)}(t_0) &= \int_{-\infty}^{+\infty} f_0(\boldsymbol{x}_0(t-t_0)) \wedge f_1(\boldsymbol{x}_0(t-t_0), t)\,\mathrm{d}t \\ &= \sqrt{2}\gamma \sin\omega t_0 \int_{-\infty}^{+\infty} \operatorname{sech} t \tanh t \sin\omega t\,\mathrm{d}t \\ &\quad - \sqrt{2}\gamma \cos\omega t_0 \int_{-\infty}^{+\infty} \operatorname{sech} t \tanh t \cos\omega t\,\mathrm{d}t \\ &\quad - 2\delta \int_{-\infty}^{+\infty} \operatorname{sech}^2 t \tanh^2 t\,\mathrm{d}t.\end{aligned}$$

The second term in the integral is odd and when integrated over a symmetric range is zero

$$-\sqrt{2}\gamma \cos\omega t_0 \int_{-\infty}^{+\infty} \operatorname{sech} t \tanh t \cos\omega t\,\mathrm{d}t = 0.$$

The third term can be evaluated as

$$-2\delta \int_{-\infty}^{+\infty} \operatorname{sech}^2 t \tanh^2 t\,\mathrm{d}t = -\frac{4}{3}\delta.$$

To evaluate the first integral it is necessary to use Cauchy's Residue theorem and evaluate the contour integral of the associated complex function $f(z) = e^{i\omega z} \operatorname{sech} z \tanh z$ where $z = u + iv$. The complex function has a singularity at $z = i\pi/2$ at which the residue is $\operatorname{Res}[f(z)] = i\omega e^{\pi\omega/2}$.

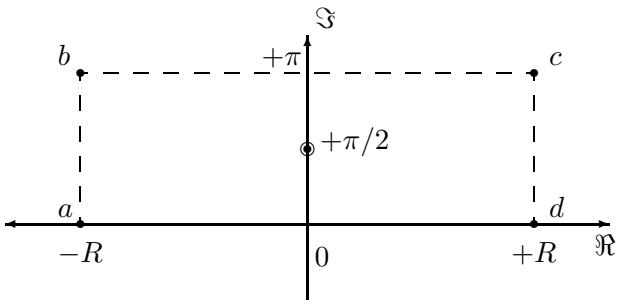

A rectangular contour with vertices at $a = (-R, 0)$, $b = (-R, \pi)$, $c = (R, \pi)$ and $d = (R, 0)$ is chosen as a suitable domain for (anticlockwise) integration. In the limit

of $R \to \infty$ the integrals of the contours parallel to the imaginary axis tend to zero. The integrals along the contours parallel to the real axis yield

$$\begin{aligned} 2\pi\omega e^{\pi\omega/2} &= \int_{-R}^{+R} \frac{e^{i\omega u}\sinh u}{\cosh^2 u}\,\mathrm{d}u + \int_{+R}^{-R} \frac{e^{i\omega(u+i\pi)}\sinh(u+i\pi)}{\cosh^2(u+i\pi)}\,\mathrm{d}u \\ &= (1+e^{\pi\omega})\int_{-R}^{+R} \frac{e^{i\omega u}\sinh u}{\cosh^2 u}\,\mathrm{d}u. \end{aligned}$$

Hence

$$\mathcal{M}_h^{(1)}(t_0) = -\frac{4\delta}{3} + \sqrt{2}\gamma\pi\omega\,\mathrm{sech}\left(\frac{\pi\omega}{2}\right)\sin\omega t_0. \tag{2.42}$$

Thus, in order for simple zeroes to occur

$$\frac{\gamma}{\delta} > \frac{4\cosh(\pi\omega/2)}{3\sqrt{2}\pi\omega}. \tag{2.43}$$

When the inequality becomes an equality the system has quadratic zeroes and (quadratic) homoclinic tangencies. Thus, there is a condition on the parameters independent of the perturbation necessary for transverse intersections of the stable and unstable homoclinic manifolds. When $\omega = 1$ and $\varepsilon\delta = 0.25$ then the analysis predicts homoclinic tangencies, to first order, occur at $\varepsilon\gamma = 0.188$ and numerical evidence puts the bifurcation value at about $\varepsilon\gamma = 0.190$ [45].

Now consider the system with two modifications: weak periodic forcing of $\mathcal{O}\left(\varepsilon^2\right)$ and quadratic damping

$$x'' = x - x^3 + \varepsilon\delta\left(x'\right)^2 + \varepsilon^2\gamma\cos(\omega t + t_0) \tag{2.44}$$

which as a system of first order equations is given by

$$x' = y, \tag{2.45a}$$

$$y' = x - x^3 - \varepsilon\delta y^2 - \varepsilon^2\gamma\cos\theta, \tag{2.45b}$$

$$\theta' = \omega. \tag{2.45c}$$

The vector fields now take the form

$$f_0 = \left(y, x - x^3\right)^T, \quad f_1 = \left(0, -\delta y^2\right)^T \quad \text{and} \quad f_2 = \left(0, -\gamma\cos\theta\right)^T. \tag{2.46}$$

Denote $\bar{f}_1 = -\delta y^2$ and $\bar{f}_2 = -\gamma \cos\theta$. The modification on the damping is somewhat unphysical, however quadratic damping has appeared as a mechanical analogue in field theory [55].

The first order Mel'nikov integral is

$$\begin{aligned}\mathcal{M}_h^{(1)}(t_0) &= \int_{-\infty}^{+\infty} f_0(\boldsymbol{x}_0(t-t_0)) \wedge f_1(\boldsymbol{x}_0(t-t_0), t)\, \mathrm{d}t \\ &= -\delta \int_{-\infty}^{+\infty} y_0^3(t-t_0)\, \mathrm{d}t \\ &= -2\sqrt{2}\delta \int_{-\infty}^{+\infty} \operatorname{sech}^3(t-t_0) \tanh^3(t-t_0)\, \mathrm{d}t \\ &= 0. \end{aligned} \tag{2.47}$$

Thus it is necessary to compute higher order terms. The first order variational equation is

$$\frac{\mathrm{d}}{\mathrm{d}s}\begin{pmatrix} x_1^{s,u} \\ y_1^{s,u} \end{pmatrix} = \begin{pmatrix} 0 & 1 \\ 1-3x_0^2 & 0 \end{pmatrix}\begin{pmatrix} x_1^{s,u} \\ y_1^{s,u} \end{pmatrix} + \begin{pmatrix} 0 \\ -\delta y_0^2 \end{pmatrix}.$$

A coupled pair of first order equations can be expressed as a second order system of the general form

$$\mathcal{L}[x] = x'' + P(t)\, x' + Q(t)\, x = \bar{f}_1(t)$$

where for this example

$$P(t) = 0, \quad Q(t) = 1 - 6\operatorname{sech}^2(t-t_0) \quad \text{and} \quad \bar{f}_1(t) = \delta \operatorname{sech}^2(t-t_0) \tanh^2(t-t_0).$$

As $P(t) = 0$ the first order perturbations $x_1^{s,u}$ and $y_1^{s,u}$ can be expressed by the linearly independent functions u_1 and u_2 which are derived from the Wronskian of the unperturbed inhomogeneous linear system $\mathcal{L}[x] = 0$. The unperturbed system can be expressed as $\mathcal{L}[x] = x'' - D\bar{f}_0(x_0(t)) = 0$. On differentiating it becomes $x_0''' = D\bar{f}_0(x_0(t))\, x_0'$ hence x_0' is a solution to the variational equation $y_0'' = D\bar{f}_0(x_0(t))\, y_0$ which is $\mathcal{L}[y] = 0$. Thus $x_0' = y_0 = u_1^{s,u}$. Thus, the first linearly independent solution is given by

$$u_1^{s,u}(t) = y_0 \tag{2.48a}$$

and by integrating the Wronskian

$$u_2^{s,u}\frac{\mathrm{d}}{\mathrm{d}t}u_1^{s,u} - u_1^{s,u}\frac{\mathrm{d}}{\mathrm{d}t}u_2^{s,u} = 1$$

the second solution is

$$u_2^{s,u}(t) = -u_1^{s,u}(t)\int^t \frac{1}{\left(u_1^{s,u}(\tau)\right)^2}\,\mathrm{d}\tau. \tag{2.48b}$$

Remark 2.3.3. *The problem of computing first order approximations to homoclinics is in fact equivalent to computing exponential dichotomies forwards and backwards in time on the intervals* $(-\infty, t_0]$ *and* $[t_0, +\infty)$ *respectively [77]. For detail on exponential dichotomies, please refer to §B.3.1. In §5 a robust numerical algorithm is presented to compute first order approximations to the perturbed stable and unstable manifolds.*

Thus, for the modified Duffing oscillator

$$u_1^{s,u}(t) = \sqrt{2}\,\mathrm{sech}\,t\tanh t, \tag{2.49a}$$

$$u_2^{s,u}(t) = -\sqrt{2}\,\mathrm{sech}\,t\left(\left(\cosh^2 t - 3\right)/4 + (3t/4)\tanh t\right). \tag{2.49b}$$

Note that $u_1 = u_1^s = u_1^u$ and $u_2 = u_2^s = u_2^u$ as the system is linearised about a homoclinic solution, rather than a hetroclinic solution. The derivatives of u_1 and u_2 are given by

$$\frac{\mathrm{d}}{\mathrm{d}t}u_1(t) = \sqrt{2}\,\mathrm{sech}\,t\left(1 - 2\tanh^2 t\right) \tag{2.50a}$$

$$\begin{aligned}\frac{\mathrm{d}}{\mathrm{d}t}u_2(t) = \frac{\sqrt{2}}{4}\,\mathrm{sech}\,t\Big(&\left(2\tanh^2 t - 1\right)\left(\coth t\left(\cosh^2 t - 3\right) + 3t\right)\\ &+ \tanh t\left(\coth^2 t\left(\cosh^2 t - 3\right) - 3\cosh^2 t\right)\Big).\end{aligned} \tag{2.50b}$$

Also note that both u_2 and its derivative become unbounded as $t \to \pm\infty$.

Following [60] the first order perturbations are given by

$$x_1^{s,u} = u_1\left(N_1^{s,u} + \int_{t_0}^t u_2(\tau)\,\bar{f}_1(\tau)\,\mathrm{d}\tau\right) + u_2\left(M_1^{s,u} - \int_{t_0}^t u_1(\tau)\,\bar{f}_1(\tau)\,\mathrm{d}\tau\right),$$

$$y_1^{s,u} = \frac{\mathrm{d}}{\mathrm{d}t}u_1\left(N_1^{s,u} + \int_{t_0}^t u_2(\tau)\,\bar{f}_1(\tau)\,\mathrm{d}\tau\right) + \frac{\mathrm{d}}{\mathrm{d}t}u_2\left(M_1^{s,u} - \int_{t_0}^t u_1(\tau)\,\bar{f}_1(\tau)\,\mathrm{d}\tau\right).$$

Although u_2 can become unbounded, see subfigure 2.3(b), the first term in the expressions for $x_1^{s,u}$ and $y_1^{s,u}$ reach periodic motion as $t \to \pm\infty$, see subfigures 2.3(e) and 2.3(f).

However the second term of the expressions for $x_1^{s,u}$ and $y_1^{s,u}$ must be set to zero through the constants of integration $M^{s,u}$.

The first integral in the first order perturbation is

$$\begin{aligned}\int_{t_0}^{t} u_2(\tau)\,\bar{f}_1(\tau)\,\mathrm{d}\tau = \delta\Big(&(t_0-t) + \left(e^{2t}-e^{2t_0}\right)(3(t+t_0)+4) + 3\left(e^{4t}+e^{4t_0}\right)(t-t_0)\\ &- 4\left(e^{4t}-e^{4t_0}\right) - 6\left(e^{6t}-e^{6t_0}\right)(t+t_0) - 9e^{2(t+t_0)}(t-t_0)\\ &+ 9e^{4(t+t_0)}(t-t_0) - e^{6(t+t_0)}(t-t_0)\\ &- 9(t+t_0)\,e^{2(t+t_0)}\left(e^{2t}-e^{2t_0}\right) + (4+3(t-t_0))\,e^{2(t+t_0)}\left(e^{4t}-e^{4t_0}\right)\\ &+ (4-3(t+t_0))\,e^{4(t+t_0)}\left(e^{2t}-e^{2t_0}\right)\Big) \Big/ \left(\left(e^{2t}+1\right)^3\left(e^{2t_0}+1\right)^3\right).\end{aligned}$$

The second integral is

$$\int_{t_0}^{t} u_1(\tau)\,\bar{f}_1(\tau)\,\mathrm{d}\tau = \frac{2}{3}\delta\left(\tanh^3 t - \tanh^3 t_0\right).$$

The constants of integration are

$$M_1^s(t_0) = \int_{t_0}^{+\infty} u_1(\tau)\,\bar{f}_1(\tau)\,\mathrm{d}\tau, \quad M_1^u(t_0) = \int_{t_0}^{-\infty} u_1(\tau)\,\bar{f}_1(\tau)\,\mathrm{d}\tau \tag{2.52a}$$

and

$$N_1^{s,u}(t_0) = -\,M_1^{s,u}(t_0)\left.\frac{u_1(t)\,u_2(t) + \dfrac{\mathrm{d}}{\mathrm{d}t}u_1(t)\,\dfrac{\mathrm{d}}{\mathrm{d}t}u_2(t)}{(u_1(t))^2 + \left(\dfrac{\mathrm{d}}{\mathrm{d}t}u_1(t)\right)^2}\right|_{t=t_0}. \tag{2.52b}$$

The constant of integration $M_1^{s,u}$ ensures that solutions are bounded and $N_1^{s,u}$ ensures that solutions are transverse to the unperturbed homoclinic orbit, satisfying (2.35). Hence, explicitly, the constants of integration are

$$\begin{aligned}M_1^s(t_0) &= \int_{t_0}^{+\infty} u_2(\tau)\,\bar{f}_1(\tau)\,\mathrm{d}\tau = \frac{2}{3}\delta\left(1-\tanh^3 t_0\right),\\ M_1^u(t_0) &= \int_{t_0}^{-\infty} u_2(\tau)\,\bar{f}_1(\tau)\,\mathrm{d}\tau = \frac{2}{3}\delta\left(1+\tanh^3 t_0\right)\end{aligned}$$

and

$$N_1^{s,u}(t_0) = M_1^{s,u}(t_0)\frac{\cosh t_0 \sinh t_0\left(12-7\cosh^2 t_0\right) + s_0\left(6\cosh^4 t_0 - 15\cosh^2 t_0 + 12\right)}{4\left(2\cosh^4 t_0 - 5\cosh^2 t_0 + 4\right)}.$$

It is important to note that the first order variational equation is always a second order linear inhomogeneous equation linearised about the homoclinic solution and thus is globally computable [45, pg 186] with exponential dichotomies on the intervals $[t_0, +\infty)$ and $(-\infty, t_0]$.

In figure 2.3 the evolutions of u_1, u_2 the homoclinic orbit x_0, y_0 and the first order perturbations $x_1^{s,u}$ and $y_1^{s,u}$ are displayed. As the inset plots in subfigures 2.3(e) and 2.3(f) show, at $t = t_0$ the first order approximations to the homoclinic orbits posses exponential dichotomies over half intervals $(-\infty, t_0]$ and $[t_0, +\infty)$ as $x_\varepsilon^u(t_0, t_0) \neq x_\varepsilon^s(t_0, t_0)$.

To second order the Mel'nikov integral is given by

$$\mathcal{M}_h^{(2)}(t_0) = \sqrt{2}\gamma\pi\omega\,\mathrm{sech}\left(\frac{\pi\omega}{2}\right)\sin\omega t_0 + \int_{t_0}^{+\infty} y_0(t)\left(2\,\delta\,y_0(t)\,y_1^s(t,t_0) + 6\,x_0(t)\,(x_1^s(t,t_0))^2\right)\mathrm{d}t$$
$$- \int_{-\infty}^{t_0} y_0(t)\left(2\,\delta\,y_0(t)\,y_1^u(t,t_0) + 6\,x_0(t)\,(x_1^u(t,t_0))^2\right)\mathrm{d}t. \tag{2.54}$$

Figure 2.4 displays the second order Mel'nikov integrals for a variety of parameter values. The integrals were computed numerically using the integrator `dop853.f`. Given that in all cases examined with $0 < \gamma,\ \delta < 1$ there are simple zeroes in the range, spatially chaotic solutions exist.

Note that the first term in the Mel'nikov integral is dependent on γ and the second and third terms are dependent on δ. Preliminary numerical evidence suggests that generically the Mel'nikov integral has simple zeroes for all $\gamma,\ \delta \sim \mathcal{O}(1)$.

Now having shown the existence of transverse homoclinic points in both cases all that remains to show spatially chaotic behaviour is to construct the Poincaré map which is conjugate to a Bernoulli shift. This can be achieved by following [73]. First construct the Poincaré section $P_\varepsilon : \Sigma^0 \mapsto \Sigma^0$ where Σ^0 is the cross-section $\Sigma^0 = \left\{(x, y, \theta) \in \mathbb{R}^2 \times S^1 \,:\, \theta = 0, 2\pi, \ldots\right\}$ for solutions x and y of the system (2.39).

As it is shown in [73] that the system (2.39) has a non-periodic strange attractor, by [15] the effect of sensitivity to initial conditions on the primary homoclinic solutions can be seen from the time series for the amplitude of the homoclinic orbit will show intermittent excursions away from zero in the form of a homoclinic solution

$$|x| = \frac{4\delta}{3} - \sqrt{2}\gamma\pi\omega\mathrm{sech}^2\left(\frac{\pi\omega}{2}(t + t_0)\right)$$

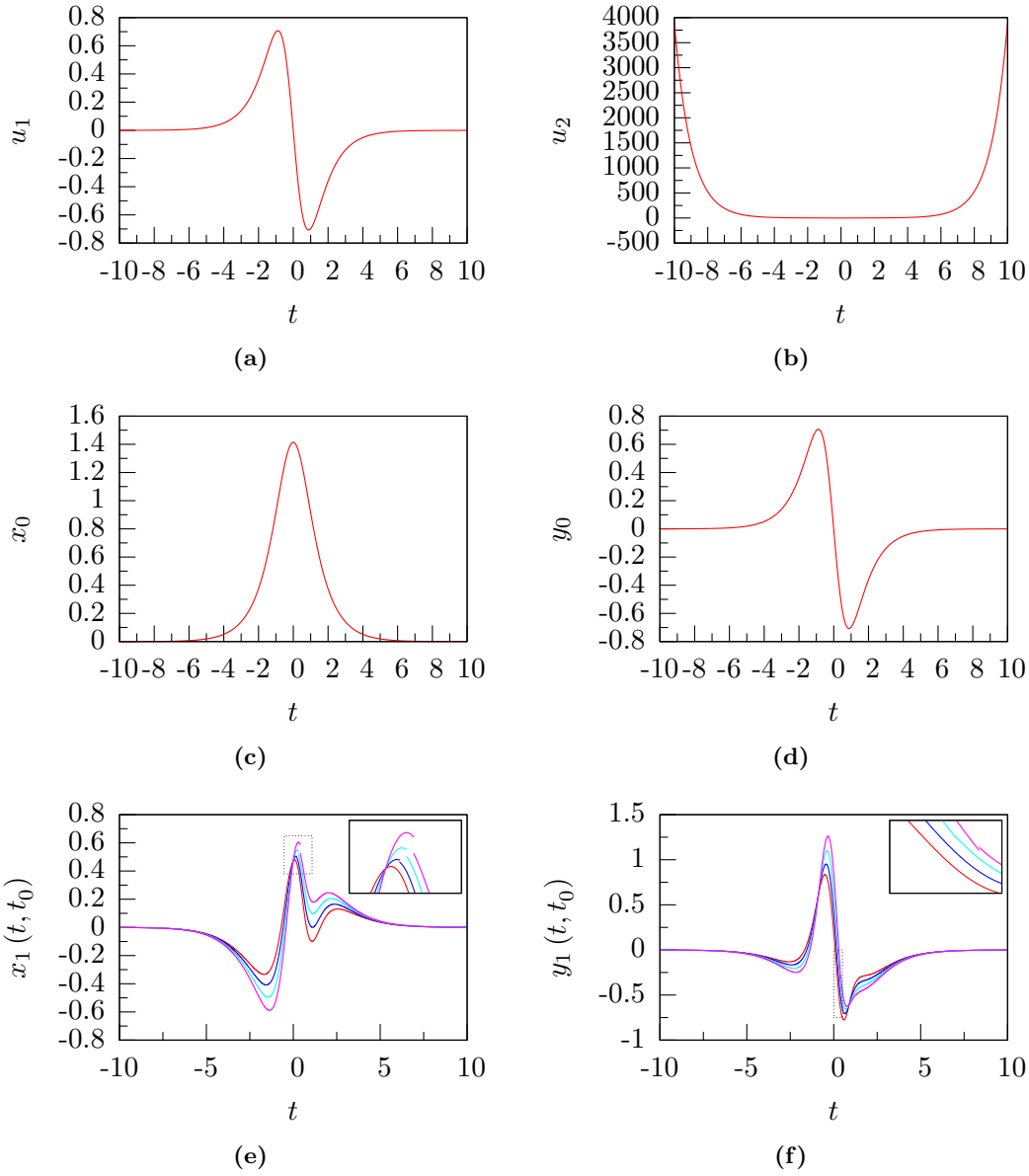

Figure 2.3: Components of the first order perturbations for homoclinic orbits for the modified Duffing oscillator over a suitable range. In these diagrams $\delta = 1$, $\omega = 1$ and $\gamma = 1$. The linearly independent solutions (2.49) to the inhomogeneous problem are displayed in subfigures 2.3(a) and 2.3(b). The homoclinic solutions (2.41) are displayed in subfigures 2.3(a) and 2.3(b). In subfigures 2.3(e) and 2.3(f) the first order approximations are computed for $t_0 = 0.1$ (red), 0.2 (blue), 0.3 (cyan) and 0.4 (magenta).

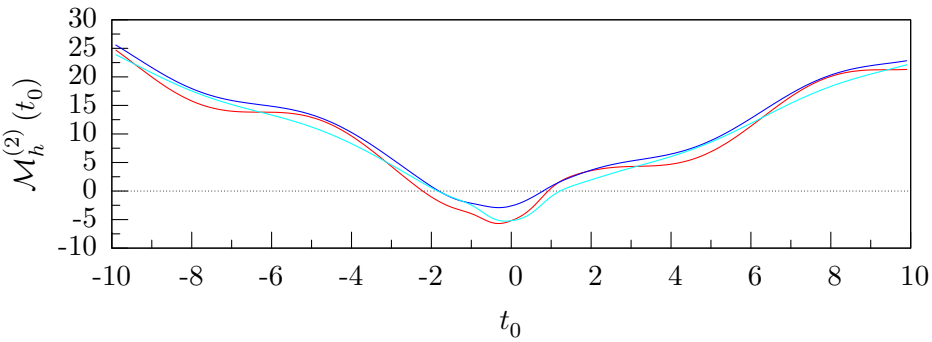

(a)

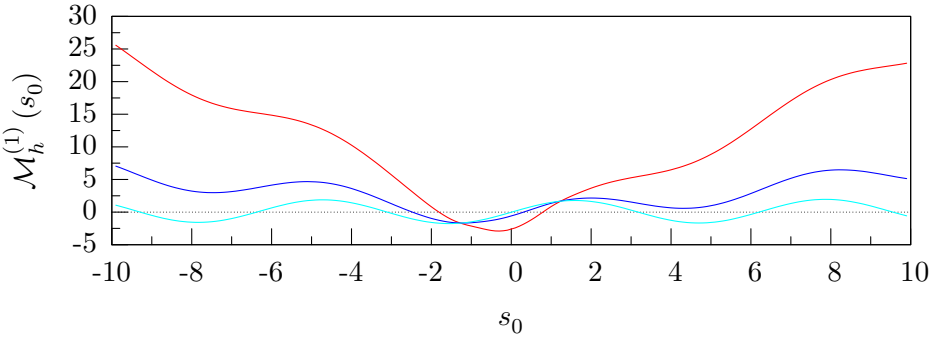

(b)

Figure 2.4: Second order Mel'nikov integral (2.54) for modified Duffing oscillator, showing the existence of simple zeroes and hence transverse intersections of the perturbed stable and unstable manifolds. In subfigure 2.4(a) $\delta = 1$ and $\gamma = 1.5$ (red), 1.0 (blue) 0.5 (cyan). In subfigure 2.4(b) $\gamma = 1$ and $\delta = 1.0$ (red), 0.5 (blue) and 0.1 (cyan). In both subfigures $\omega = 1$.

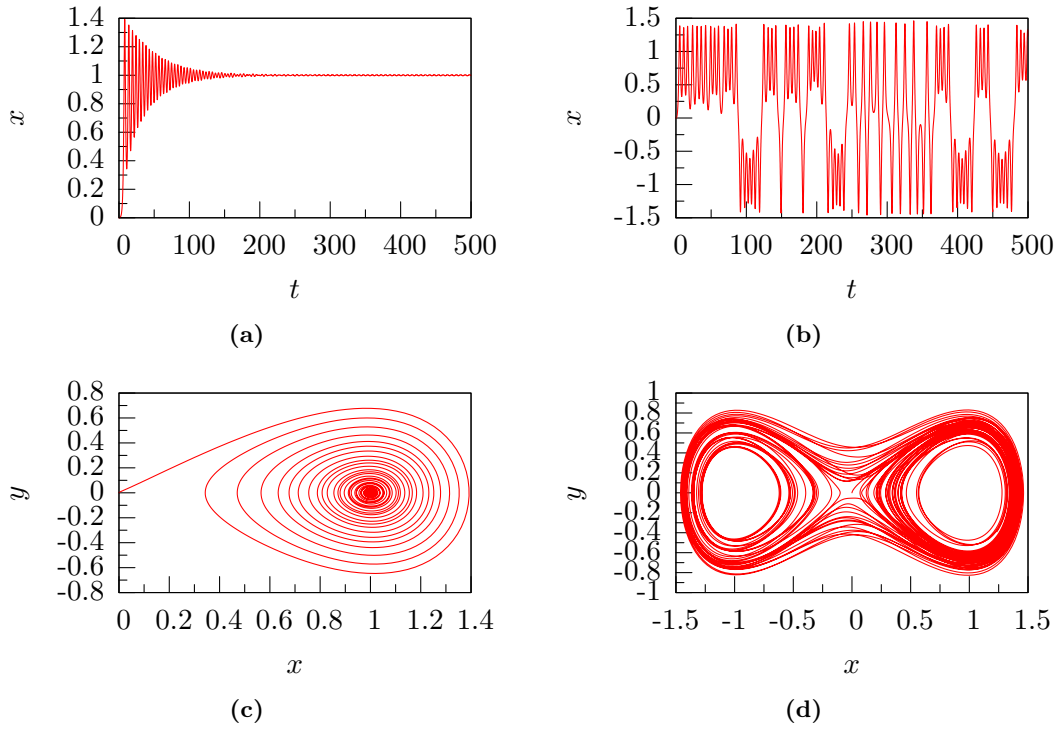

Figure 2.5: The trajectories and phase diagrams of a regular and irregular Duffing oscillator illustrating the qualatative difference in solutions once the Mel'nikov threshold has been passed. Subfigure 2.5(a) shows the motion of a beam which is heavily damped which deforms towards a magnet, so that the phase portrait in subfigure 2.5(c) shows the trajectory spiralling towards a stable fixed point. Once the Mel'nikov threshold has been passed, the motion may become chaotic as subfigures 2.5(b) and 2.5(d) illustrate. In this situation the tip of the beam oscillates wildly between the two magnets.

where t_0 is now indistinguishable from a random variable, because of the extreme sensitivity to initial conditions for this motion.

As the perturbation increases, it has been shown that the stable and unstable manifolds intersect giving rise to an infinite number of homoclinic points. An iterate of the Poincaré map of solutions which emanate from the saddle $P_\varepsilon^N(\boldsymbol{p})$ results in the horseshoe construction and a complicated invariant set of Cantor points Λ which is topologically conjugate to a Bernoulli shift.

There are two centres and a saddle in the unperturbed problem so that in the perturbed problem the beam moves irregularly between two states corresponding to oscillations about the magnets. The figure 2.5 shows the difference between 'regular' motion dominated damping term and irregular motion. Note that global stability of the unperturbed problem ensures that there are no orbits escaping to infinity.

Chapter 3

A Family of Cosserat Elastic Rods

In this chapter the system of equations which determine the configurations of a geometrically exact Cosserat rod under a class of (generalised) forces is introduced. The rod configurations are determined by the strains of the system. The strains are related to the stresses on the rod by a set of constitutive relations, which when hyperelastic allow a variational formulation. A family of balance equations, which are noncanonical Hamiltonian equations describe the stresses on the rod. For a thorough exposition of rod theory see [2].

3.1 Kinematic Equations

In this section the equations which define a Cosserat rod are introduced. A Cosserat rod is defined by a one-dimensional curve, called the centreline, along which a right-handed orthonormal triad, called the directors, are attached. The centreline describes the position of the rod while the directors describe the orientation of the cross section of the rod. The rod, $\boldsymbol{r}(s)$, is embedded in the spatial frame as the vector space spanned by the righthanded orthonormal triad of vectors $\{\boldsymbol{e}_1, \boldsymbol{e}_2, \boldsymbol{e}_3\}$. The body frame, also referred to as the director frame, is given by a local rod-centred right-handed orthonormal triad $\{\boldsymbol{d}_1(s), \boldsymbol{d}_2(s), \boldsymbol{d}_3(s)\}$. The director $\boldsymbol{d}_1$ lies in the normal cross section of the rod and under certain conditions, namely inextensibility and unshearability, $\boldsymbol{d}_2$ also lies in the cross section and $\boldsymbol{d}_3$ is tangent to the centreline as illustrated in figure 3.1. For clarity vectors in the spatial frame are denoted by the bold type $\boldsymbol{p}$ and components of the vector

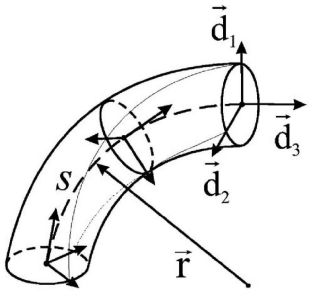

Figure 3.1: Schematic diagram of a Cosserat rod $\boldsymbol{r}(s)$ showing the orthonormality of the directors $\boldsymbol{d}_i(s)$ along the arclength s.

in the director frame form a 3-tuple denoted by the sans serif $\mathsf{p} = (\boldsymbol{p}\cdot\boldsymbol{d}_1, \boldsymbol{p}\cdot\boldsymbol{d}_2, \boldsymbol{p}\cdot\boldsymbol{d}_3)$.

By orthonormality, the directors satisfy

$$\boldsymbol{d}_i(s)\cdot\boldsymbol{d}_j(s) = \delta_{ij}, \qquad i=1,2,3 \quad j=1,2,3 \tag{3.1a}$$

$$\boldsymbol{d}_i(s)\times\boldsymbol{d}_j(s) = \varepsilon_{ijk}\boldsymbol{d}_k(s) \tag{3.1b}$$

where δ_{ij} is the Kronecker delta and ε_{ijk} is the standard Levi-Civita permutation symbol. The orthogonality of the directors shall be exploited throughout the rod models derived.

Let R be an element of the special orthogonal group, $SO(3)$, i.e. the group of rotations. The rotations can convert quantities from the spatial frame into the director frame, preserving their length and orientation. Thus

$$\boldsymbol{d}_i = R\boldsymbol{e}_i \quad \text{for} \quad i=1,2,3. \tag{3.2}$$

The Lie group $SO(3)$ consists of the set of all three-by-three skew-symmetric matrices with unit determinant. An element of the corresponding Lie algebra $\mathfrak{so}(3)$ may be related to an element of $\mathbb{R}^3$ through the "hat map" isomorphism [49] where

$$a = (a_1,a_2,a_3)^T \in \mathbb{R}^3 \quad \text{and} \quad \hat{a} = \begin{pmatrix} 0 & -a_3 & a_2 \\ a_3 & 0 & -a_1 \\ -a_2 & a_1 & 0 \end{pmatrix} \in \mathfrak{so}(3) \tag{3.3}$$

Equivalently the isomorphism is given by $\hat{a}b = a\times b$ for all $a,\, b\in\mathbb{R}^3$ and $\hat{a}\in\mathfrak{so}(3)$.

The evolution of the directors along the rod is found by differentiating equation (3.2)

with respect to the parameter s

$$\begin{aligned}\boldsymbol{d}_i' &= R'\boldsymbol{e}_i \\ &= R'R^{-1}\boldsymbol{d}_i \\ &= \hat{\boldsymbol{u}}\boldsymbol{d}_i \\ &= \boldsymbol{u}\times\boldsymbol{d}_i \end{aligned} \tag{3.4}$$

for $\hat{\boldsymbol{u}} := R'R^{-1} = R'R^T$. Using the dot product and the orthogonality of the directors, the components of the strain $\boldsymbol{u}$ are expressed as

$$u_i = \frac{1}{2}\varepsilon_{ijk}\boldsymbol{d}_j'\cdot\boldsymbol{d}_k. \tag{3.5}$$

The second set of strains $\boldsymbol{v}$, associated with shearing and extension are given by

$$\boldsymbol{v} = \boldsymbol{r}'. \tag{3.6}$$

The triples $\mathsf{u} = (u_1, u_2, u_3)$ and $\mathsf{v} = (v_1, v_2, v_3)$ are the generalised strains in the body. The projections onto the director frame $v_1 = \boldsymbol{v}\cdot\boldsymbol{d}_1$ and $v_2 = \boldsymbol{v}\cdot\boldsymbol{d}_2$ are associated with transverse shearing, while $v_3 = \boldsymbol{v}\cdot\boldsymbol{d}_3$ is extension if $v_3 > 1$ and compression if $v_3 < 1$. Likewise, $u_1 = \boldsymbol{u}\cdot\boldsymbol{d}_1$ and $u_2 = \boldsymbol{u}\cdot\boldsymbol{d}_2$ are associated with bending and $u_3 = \boldsymbol{u}\cdot\boldsymbol{d}_3$ is the twist in the body. Often the strain u_3 is referred to as the local twist and is denoted by τ. Since it is natural to assume that a rod cannot be compressed to zero length it is assumed

$$v_3 > 0.$$

If a rod is unshearable then

$$v_1 = \boldsymbol{v}\cdot\boldsymbol{d}_1 = 0 \quad \text{and} \quad v_2 = \boldsymbol{v}\cdot\boldsymbol{d}_2 = 0.$$

If a rod is inextensible

$$\left|\boldsymbol{r}'\right| = 1.$$

Thus, the centreline of an unshearable and inextensible rod is determined by the single condition

$$\boldsymbol{r}' = \boldsymbol{d}_3 \tag{3.7}$$

and the parameter s can now be interpreted as the arc-length of the rod.

3.2 Constitutive Relationships

Having formulated the configurations of a Cosserat rod in terms of the strains $\boldsymbol{u}$ and $\boldsymbol{v}$, in this section the relationship between the stresses and the strains are introduced.

If the rod is hyperelastic then there exists a strain density function explicitly dependent on the generalised strains, i.e. $\mathcal{W}(\mathsf{u}-\mathsf{u}_0, \mathsf{v}-\mathsf{v}_0, s)$, such that the components of the force $\mathsf{n} = (n_1, n_2, n_3)$ and moment $\mathsf{m} = (m_1, m_2, m_3)$ in the body are

$$m_i = \frac{\partial \mathcal{W}}{\partial u_i} \quad \text{and} \quad n_i = \frac{\partial \mathcal{W}}{\partial v_i}, \tag{3.8}$$

where u_0 and v_0 are the strains associated with the unstressed rod. If the rod is uniform then the constitutive relations are the same throughout the rod

$$\mathcal{W}(\mathsf{u}-\mathsf{u}_0, \mathsf{v}-\mathsf{v}_0) = \mathcal{W}(\mathsf{u}-\mathsf{u}_0, \mathsf{v}-\mathsf{v}_0, s)\,. \tag{3.9}$$

A hyperelastic rod will have a convex strain density function, that is the matrix of partial derivatives is positive definite

$$\begin{vmatrix} \partial \mathsf{m}/\partial \mathsf{u} & \partial \mathsf{m}/\partial \mathsf{v} \\ \partial \mathsf{n}/\partial \mathsf{u} & \partial \mathsf{n}/\partial \mathsf{v} \end{vmatrix} > 0. \tag{3.10}$$

Thus, an increase in the applied bending moment will accompany an increase in the bending strain. The hyperelastic strain function will also be coercive, that is

$$\frac{\mathcal{W}(\mathsf{u}-\mathsf{u}_0, \mathsf{v}-\mathsf{v}_0)}{\sqrt{|\mathsf{u}|^2 + |\mathsf{v}|^2}} \to \infty \quad \text{as} \quad |\mathsf{u}|^2 + |\mathsf{v}|^2 \to \infty. \tag{3.11}$$

This implies that extremal values of the stresses must accompany extremal values of the strains. Finally, the strain energy density will have a nondegenerate minimum at the

unstressed configuration

$$\mathbf{0} = \left.\frac{\partial \mathcal{W}}{\partial \mathsf{u}}\right|_{\mathsf{u}=\mathsf{u}_0,\,\mathsf{v}=\mathsf{v}_0} = \left.\frac{\partial \mathcal{W}}{\partial \mathsf{v}}\right|_{\mathsf{u}=\mathsf{u}_0,\,\mathsf{v}=\mathsf{v}_0}. \tag{3.12}$$

The convexity of the hyperelastic strain energy density function means that the strains can be inverted (locally) for the stresses. Hence a uniform hyperelastic function can be written as $\widetilde{\mathcal{W}}(\mathsf{m},\mathsf{n}) = \widetilde{\mathcal{W}}(\tilde{\mathsf{u}}(\mathsf{m},\mathsf{n}),\tilde{\mathsf{v}}(\mathsf{m},\mathsf{n}))$. This assumption is crucial in that it allows the hyperelastic function to be related to the Hamiltonion via the Legendre transform.

An important property of many rods is isotropy. If a rod is isotropic then there exists an orthogonal matrix Q of the form

$$Q = \begin{pmatrix} Q_{11} & Q_{12} & 0 \\ Q_{21} & Q_{22} & 0 \\ 0 & 0 & 1 \end{pmatrix}$$

such that

$$\tilde{\mathsf{u}}(Q\mathsf{m}, Q\mathsf{n}, s) = Q\tilde{\mathsf{u}}(\mathsf{m},\mathsf{n},s) \quad \text{and} \quad \tilde{\mathsf{v}}(Q\mathsf{m}, Q\mathsf{n}, s) = Q\tilde{\mathsf{v}}(\mathsf{m},\mathsf{n},s). \tag{3.13}$$

It has been shown [4] that for isotropic constitutive relationships the strain density function takes the form

$$\widetilde{\mathcal{W}} = \widetilde{\mathcal{W}}\left(m_1^2 + m_2^2, m_3, n_1^2 + n_2^2, n_3, m_1 n_1 + m_2 n_2, m_1 n_2 - m_2 n_1\right). \tag{3.14}$$

For an inextensible, unshearable rod the strain-density function for an initially straight and untwisted rod is a function of the strains u only with $\mathsf{u}_0 = (0,0,0)$ and $\mathsf{v} = \mathsf{v}_0 = (0,0,1)$. In fact, for a rod under tension and moment, nonlinear constitutive laws make little difference either in the underlying structure of the phase space, configurations or the effective localised buckling modes [3, 21]. However, in order to separate nonlinear geometric effects from those caused by material nonlinearity, linear constitutive laws will be taken throughout. For simplicity, quadratic form, linear constitutive relationships, satisfying Hooke's law are chosen. The strain density function is given by

$$\mathcal{W}(\mathsf{u},\mathsf{v}) = \frac{1}{2}B_1(u_1+u_0)^2 + \frac{1}{2}B_2u_2^2 + \frac{1}{2}Cu_3^2 + \frac{1}{2}Hv_1^2 + \frac{1}{2}Jv_2^2 + \frac{1}{2}Kv_3^2. \tag{3.15}$$

The constants $B_1 = EI_1$, $B_2 = EI_2$ and $C = GI_3$, where I_1 and I_2 are the principal moments of inertia about the $\boldsymbol{d}_1$ and $\boldsymbol{d}_2$ axes respectively, I_3 is the moment of inertia about the $\boldsymbol{d}_3$ axis, E is Young's modulus and

$$G = \frac{E}{2(1+\nu)}$$

is the shear modulus, where ν is Poisson's ratio. Thus B_1 and B_2 are the bending stiffnesses about the $\boldsymbol{d}_1$ and $\boldsymbol{d}_2$ axes respectively. The constants H and J are transverse shear stiffnesses and K is the axial stiffness. The constant u_0 is the initial curvature. It follows that m_1 and m_2 are associated with bending about the principal axes $\boldsymbol{d}_1$ and $\boldsymbol{d}_2$, m_3 with twist about $\boldsymbol{d}_3$, n_1 and n_2 with shearing forces and n_3 with tension if positive, compression if negative. In the case of isotropy then $B_1 = B_2$ and $H = J$.

3.3 Equilibrium Equations

In this section the static equilibrium balance equations of a family of rod are introduced. It is assumed that all forces and moments are suitable averages over the rod's cross section acting at the centreline of the rod. The balance equations are the final set of equations needed to close the system.

3.3.1 Force-Free Rod

The simplest rod model is that of a force-free rod. In the spatial frame the equilibrium equation is

$$\boldsymbol{m}' = \boldsymbol{0}. \tag{3.16}$$

In the director frame the equation can be written as a non-canonical Hamiltonian system

$$\mathsf{m}' = \mathcal{J}(\mathsf{m}) \nabla \mathcal{H}(\mathsf{m}), \tag{3.17}$$

where the skew-symmetric structure matrix $\mathcal{J} = \mathcal{J}(\mathsf{m})$ is given by

$$\mathcal{J} = -\mathcal{J}^T = \begin{pmatrix} 0 & -m_3 & m_2 \\ m_3 & 0 & -m_1 \\ -m_2 & m_1 & 0 \end{pmatrix} \tag{3.18}$$

and the Hamiltonian is

$$\mathcal{H} = \frac{1}{2}\mathsf{m} \cdot \mathsf{u}\left(\mathsf{m}\right), \tag{3.19}$$

for a set of strains given by a hyperelastic strain-density function $\mathcal{W}\left(\mathsf{u}\right)$. For any two functions, f and g of m, the Poisson bracket corresponding to the structure matrix (3.18), is given by

$$\{f, g\}_{(\mathsf{m})} = -\underbrace{\mathsf{m} \cdot \left(\nabla_{\mathsf{m}} f \times \nabla_{\mathsf{m}} g\right)}_{\text{twist}}. \tag{3.20}$$

Thus the governing equation (3.17) can be written as

$$\mathsf{m}' = \{\mathsf{m}, \mathcal{H}\}_{(\mathsf{m})} = \mathsf{m} \times \mathsf{u}. \tag{3.21}$$

The null-space of the structure matrix (3.18) is one-dimensional and is spanned by the gradient of the Casimir

$$\nabla C_1 = \frac{1}{2}\left(m_1, m_2, m_3\right)^T$$

and hence

$$C_1 = \mathsf{m} \cdot \mathsf{m} \tag{3.22}$$

is a Casimir. The Casimir describes the fact that the magnitude of the total moment is constant along the rod. Since $\mathcal{H}$ is an integral, it follows from the Arnol'd-Liouville theorem 2.1.5 that (3.21) is completely integrable. In fact, the force-free rod is globally superintegrable as the system has three degrees of freedom but configurations are described by two independent variables and hence confined to two-tori [39, 40, 46, 85].

3.3.2 Kirchhoff Rod

The equilibrium equations for a rod under end tension and moment are given by

$$\boldsymbol{m}' + \boldsymbol{r}' \times \boldsymbol{n} = \boldsymbol{0} \quad \text{and} \quad \boldsymbol{n}' = \boldsymbol{0}. \tag{3.23}$$

In the director frame the equations can be written in Hamiltonian form as

$$\begin{pmatrix} \mathsf{m} \\ \mathsf{n} \end{pmatrix}' = \mathcal{J}\left(\mathsf{m}, \mathsf{n}\right) \nabla \mathcal{H}\left(\mathsf{m}, \mathsf{n}\right), \tag{3.24}$$

where the structure matrix $\mathcal{J} = \mathcal{J}(\mathsf{m}, \mathsf{n})$ is given by

$$\mathcal{J} = -\mathcal{J}^T = \begin{pmatrix} \hat{\mathsf{m}} & \hat{\mathsf{n}} \\ \hat{\mathsf{n}} & 0 \end{pmatrix} \tag{3.25}$$

and the Hamiltonian is now

$$\mathcal{H} = \frac{1}{2}\mathsf{m} \cdot \mathsf{u} + \frac{1}{2}\mathsf{n} \cdot (\mathsf{v} - \mathrm{d}_3) + \mathsf{n} \cdot \mathsf{d}_3. \tag{3.26}$$

Equivalently, the governing equations are

$$\mathsf{m}' = \{\mathsf{m}, \mathcal{H}\}_{(\mathsf{m},\mathsf{n})} = \mathsf{m} \times \mathsf{u} + \mathsf{n} \times \mathsf{v}, \tag{3.27a}$$

$$\mathsf{n}' = \{\mathsf{n}, \mathcal{H}\}_{(\mathsf{m},\mathsf{n})} = \mathsf{n} \times \mathsf{u}. \tag{3.27b}$$

which are the Poisson equations on the Cartesian pairing (m, n) given by the bracket

$$\{f, g\}_{(\mathsf{m},\mathsf{n})} = -\mathsf{m} \cdot (\nabla_{\mathsf{m}} f \times \nabla_{\mathsf{m}} g) - \underbrace{\mathsf{n} \cdot (\nabla_{\mathsf{m}} f \times \nabla_{\mathsf{n}} g + \nabla_{\mathsf{n}} f \times \nabla_{\mathsf{m}} g)}_{\text{force}}. \tag{3.28}$$

An extra semidirect term [49], corresponding to the effect of the applied force has been added when compared to the previous Poisson bracket (3.20).

The additional term in the Hamiltonian breaks the full $SO(3)$ symmetry. The equations (3.27) are those for the motion of a heavy top when the rod is unshearable and inextensible.

The null-space of the structure matrix is two-dimensional and spanned by

$$\nabla C_1 = \begin{pmatrix} \mathsf{n} \\ \mathsf{m} \end{pmatrix} \quad \text{and} \quad \nabla C_2 = \frac{1}{2}\begin{pmatrix} 0 \\ \mathsf{n} \end{pmatrix}.$$

Hence the Casimirs are

$$C_1 = \mathsf{n} \cdot \mathsf{m}, \tag{3.29a}$$

$$C_2 = \mathsf{n} \cdot \mathsf{n}. \tag{3.29b}$$

The Casimir (3.29a) describes the conservation of the moment about the force vector, while (3.29b) describes the conservation of the magnitude of force in the rod.

In addition to the Hamiltonian and the two Casimirs, a single first integral is required if the system is to be completely integrable. There are two cases, both well-documented:

The Lagrange case has an integral given by

$$I_1 = \mathsf{m} \cdot \mathsf{d}_3 \quad \text{if} \quad B = B_1 = B_2. \tag{3.30}$$

Thus, if the two bending stiffnesses are equal then the (local) twist m_3 is a conserved quantity. For the Kirchhoff equation if the rod satisfies (3.13) then the Lagrange integral holds for arbitrary nonlinear constitutive relationships.

The Kovalevskaya case has an integral given by

$$I_1 = \left(B_1^2 m_1^2 - C^2 m_3^2 + n_3\right)^2 + \left(2B_1 C m_1 m_3 - n_1\right)^2 \quad \text{if} \quad B_1 = C = 2B_2. \tag{3.31}$$

Kovalevskaya found this integral by looking for the absence of certain types of singularities in complex time. Unlike the Lagrange integral the integral does not seem to have a clear physical interpretation.[1]

The condition on the bending stiffnesses renders the Kovalevskaya rod somewhat unphysical since it corresponds to a negative Poisson ratio. However, novel materials with negative effective Poisson ratio are now known. For instance, experimental measurements of bending and torsional stiffnesses of DNA molecules have led to the generally accepted range $0.7 < B_2/C < 1.5$ [80]. It is unknown how nonlinear constitutive relations or properties such as shear and extensibility effect the Kovalevskaya integral.

There is another case which is not completely integrable on the entire phase space but is completely integrable on a single symplectic leaf.

The Chaplygin-Goryachev case requires that the initial conditions must satisfy

$$\mathsf{m} \cdot \mathsf{n} = 0$$

then the integral

$$I_1 = B_2 m_2 \left(B_1^2 m_1^2 + B_2^2 m_2^2\right) - C m_3 n_2 \quad \text{if} \quad B_1 = 4B_2 = C \tag{3.32}$$

[1] Kovalevskaya won the Bordin Prize given by the Paris Academy of Sciences in 1886 and was considered such an achievement that the prize money was doubled.

renders the system integrable. Similarly to the Kovalevskaya integral, this case relies on linear stress-strain relationships and it is unknown whether a corresponding integral exist for nonlinear constitutive relations. The only natural interpretation of the condition on the Casimir is to not apply end moment and then the Chaplygin-Goryachev case can be considered an anisotropic case of the elastica.

It is simple to show that all the integrals (3.29), (3.26) and either (3.30), (3.31), or (3.32) are in involution with respect to the bracket (3.28) and that generically integrable configurations exist on three-tori.

3.3.3 An Elastic Conducting Rod in a Uniform Magnetic Field

Now consider a rod placed in a uniform magnetic field $\bar{\boldsymbol{B}}$. The rod carries a uniform current $\boldsymbol{I} = I\boldsymbol{r}'$ of strength I along the centreline, assuming the rod to be sufficiently slender for eddy currents within the cross section to be ignorable. The rod then experiences a Lorentz body force

$$\boldsymbol{n}' + \boldsymbol{F}_L = \boldsymbol{0} \quad \text{where} \quad \boldsymbol{F}_L = \boldsymbol{I} \times \bar{\boldsymbol{B}} = I\boldsymbol{r}' \times \bar{\boldsymbol{B}} = I\boldsymbol{v} \times \bar{\boldsymbol{B}}. \tag{3.33}$$

Let $\boldsymbol{B} = I\bar{\boldsymbol{B}}$ and let the magnetic field be aligned along the fixed axis $\boldsymbol{e}_3$ so that the equilibrium equations take the form

$$\boldsymbol{m}' + \boldsymbol{r}' \times \boldsymbol{n} = \boldsymbol{0}, \quad \boldsymbol{n}' + \boldsymbol{r}' \times \boldsymbol{B} = \boldsymbol{0} \quad \text{and} \quad \boldsymbol{B}' = \boldsymbol{0}. \tag{3.34}$$

It is necessary to assume that the current in the rod is moderate so that the effect of the magnetic field generated by the current is negligible compared to the external magnetic field.

In the director frame the governing equation is a non-canonical Hamiltonian system of the form

$$\begin{pmatrix} \mathsf{m} \\ \mathsf{n} \\ \mathsf{B} \end{pmatrix}' = \mathcal{J}\left(\mathsf{m}, \mathsf{n}, \mathsf{B}\right) \nabla \mathcal{H}\left(\mathsf{m}, \mathsf{n}\right), \tag{3.35}$$

where the structure matrix $\mathcal{J} = \mathcal{J}(\mathsf{m}, \mathsf{n}, \mathsf{B})$ is given by

$$\mathcal{J} = -\mathcal{J}^T = \begin{pmatrix} \hat{\mathsf{m}} & \hat{\mathsf{n}} & \hat{\mathsf{B}} \\ \hat{\mathsf{n}} & \hat{\mathsf{B}} & 0 \\ \hat{\mathsf{B}} & 0 & 0 \end{pmatrix} \tag{3.36}$$

and the Hamiltonian, once again, is

$$\mathcal{H} = \frac{1}{2}\mathsf{m} \cdot \mathsf{u} + \frac{1}{2}\mathsf{n} \cdot (\mathsf{v} - \mathsf{d}_3) + \mathsf{n} \cdot \mathsf{d}_3.. \tag{3.37}$$

Note that the Hamiltonian is a function of m and n only, but the gradient is taken with respect to the three field variables. The Hamiltonian is the same as for the Kirchhoff rod: the effect of the magnetic field is only present in the structure matrix. The governing equations can be written as

$$\mathsf{m}' = \{\mathsf{m}, \mathcal{H}\}_{(\mathsf{m},\mathsf{n},\mathsf{B})} = \mathsf{m} \times \mathsf{u} + \mathsf{n} \times \mathsf{v}, \tag{3.38a}$$

$$\mathsf{n}' = \{\mathsf{n}, \mathcal{H}\}_{(\mathsf{m},\mathsf{n},\mathsf{B})} = \mathsf{n} \times \mathsf{u} + \mathsf{B} \times \mathsf{v}, \tag{3.38b}$$

$$\mathsf{B}' = \{\mathsf{B}, \mathcal{H}\}_{(\mathsf{m},\mathsf{n},\mathsf{B})} = \mathsf{B} \times \mathsf{u}, \tag{3.38c}$$

where the Poisson bracket on $(\mathsf{m}, \mathsf{n}, \mathsf{B})$ given by

$$\begin{aligned} \{f, g\}_{(\mathsf{m},\mathsf{n},\mathsf{B})} = &-\mathsf{m} \cdot (\nabla_{\mathsf{m}} f \times \nabla_{\mathsf{m}} g) - \mathsf{n} \cdot (\nabla_{\mathsf{m}} f \times \nabla_{\mathsf{n}} g + \nabla_{\mathsf{n}} f \times \nabla_{\mathsf{m}} g) \\ &- \underbrace{\mathsf{B} \cdot (\nabla_{\mathsf{m}} f \times \nabla_{\mathsf{B}} g + \nabla_{\mathsf{B}} f \times \nabla_{\mathsf{m}} g)}_{\text{evolution of field}} - \underbrace{\mathsf{B} \cdot (\nabla_{\mathsf{n}} f \times \nabla_{\mathsf{n}} g)}_{\text{effect of field}}, \end{aligned} \tag{3.39}$$

has been extended from the previous bracket by the addition of two more terms. The first term, a semidirect extension, describes the evolution of the magnetic field in the director frame and does not affect the force and moment balance since the Hamiltonian is independent of B. The second term, a cocycle called a Leibniz extension [89], expresses the Lorentz force. This term makes the bracket extension non-semidirect.

There are three Casimirs, given by

$$C_1 = \frac{1}{2}\mathsf{n} \cdot \mathsf{n} + \mathsf{m} \cdot \mathsf{B}, \tag{3.40a}$$

$$C_2 = \mathsf{B} \cdot \mathsf{n}, \tag{3.40b}$$

$$C_3 = \mathsf{B} \cdot \mathsf{B}. \tag{3.40c}$$

The magnitude of the magnetic force is conserved, thus (3.40c). The magnitude of force is no longer conserved, but as a result of rotational symmetry the force component in the direction of the magnetic field is conserved resulting in (3.40b). Casimir (3.40a) however does not seem to have a physical interpretation; it states that half the magnitude of the force squared plus the moment about the direction of the magnetic field is a conserved quantity.

For linearly elastic, unshearable, inextensible and isotropic constitutive relations, (that is when $J = H = K = 0$ and $B = B_1 = B_2$), then two independent first integrals emerge

$$I_1 = \mathsf{m} \cdot \mathsf{d}_3, \tag{3.41a}$$

$$I_2 = \mathsf{n} \cdot \mathsf{m} + B\mathsf{B} \cdot \mathsf{d}_3. \tag{3.41b}$$

where $\mathsf{d}_3 = (0, 0, 1)$. As in the Lagrange case the first of these integrals expresses the conservation of twist in the rod. The second integral, like the Kovalevskaya integral, does not seem to have a physical interpretation. The Lagrange integrability condition $B_1 = B_2$ and $J = H$ is unaltered by the magnetic field, but now there are additional requirements on constitutive relations in the form of linear elasticity, inextensibilty and shearability $J = H = K = 0$. Numerical evidence presented in [90] in the form of chaotic orbits suggests that the linearly elastic, inextensible, unshearable the magnetic rod with $B_1 = C = 2B_2$ is not integrable. Of course, a perturbed condition on the stiffnesses may exist for which the system is integrable.

It is a straightforward task to check that all the integrals (3.37), (3.41a) and (3.41b) are independent and in involution with respect to the Poisson bracket (3.39). Hence in the isotropic case the system is completely integrable in the sense of Liouville and configurations lie on five-tori defined by two Casimirs, two integrals and the Hamiltonian.

3.3.4 An Elastic Conducting Rod in a Nonuniform Magnetic Field

By inspection of the structure matrices (3.18), (3.25) and (3.36) it is natural to consider the system

$$\boldsymbol{m}' + \boldsymbol{r}' \times \boldsymbol{n} = \boldsymbol{0}, \quad \boldsymbol{n}' + \boldsymbol{r}' \times \boldsymbol{B} = \boldsymbol{0}, \quad \boldsymbol{B}' + \boldsymbol{r}' \times \boldsymbol{D} = \boldsymbol{0} \quad \text{and} \quad \boldsymbol{D}' = \boldsymbol{0}. \tag{3.42}$$

The equation for $\boldsymbol{B}$ can be integrated to give $B_x = y$, $B_y = -x$, $B_z = 0$, where (x, y, z) and (B_x, B_y, B_z) are components of $\boldsymbol{r}$ and $\boldsymbol{B}$ relative to the fixed frame $\{\boldsymbol{e}_1, \boldsymbol{e}_2, \boldsymbol{e}_3\}$, and $\boldsymbol{e}_3$ is chosen to be in the direction of $\boldsymbol{D}$. Thus (3.42) can be thought of as describing a rod in a linearly-varying magnetic field generated by a uniform 'hypermagnetic' field $\boldsymbol{D}$.

In the director frame the equations take the Hamiltonian form

$$\begin{pmatrix} \mathsf{m} \\ \mathsf{n} \\ \mathsf{B} \\ \mathsf{D} \end{pmatrix}' = \mathcal{J}\left(\mathsf{m}, \mathsf{n}, \mathsf{B}, \mathsf{D}\right) \nabla \mathcal{H}\left(\mathsf{m}, \mathsf{n}\right), \quad \text{with} \quad \mathcal{H}\left(\mathsf{m}, \mathsf{n}\right) = \frac{1}{2}\mathsf{m} \cdot \mathsf{u} + \frac{1}{2}\mathsf{n} \cdot (\mathsf{v} - \mathrm{d}_3) + \mathsf{n} \cdot \mathrm{d}_3.$$

and structure matrix

$$\mathcal{J} = -\mathcal{J}^T = \begin{pmatrix} \hat{\mathsf{m}} & \hat{\mathsf{n}} & \hat{\mathsf{B}} & \hat{\mathsf{D}} \\ \hat{\mathsf{n}} & \hat{\mathsf{B}} & \hat{\mathsf{D}} & 0 \\ \hat{\mathsf{B}} & \hat{\mathsf{D}} & 0 & 0 \\ \hat{\mathsf{D}} & 0 & 0 & 0 \end{pmatrix}. \tag{3.43}$$

The governing equations can be expressed by a Poisson bracket

$$\mathsf{m}' = \{\mathsf{m}, \mathcal{H}\}_{(\mathsf{m},\mathsf{n},\mathsf{B},\mathsf{D})} = \mathsf{m} \times \mathsf{u} + \mathsf{n} \times \mathsf{v}, \tag{3.44a}$$

$$\mathsf{n}' = \{\mathsf{n}, \mathcal{H}\}_{(\mathsf{m},\mathsf{n},\mathsf{B},\mathsf{D})} = \mathsf{n} \times \mathsf{u} + \mathsf{B} \times \mathsf{v}, \tag{3.44b}$$

$$\mathsf{B}' = \{\mathsf{B}, \mathcal{H}\}_{(\mathsf{m},\mathsf{n},\mathsf{B},\mathsf{D})} = \mathsf{B} \times \mathsf{u} + \mathsf{D} \times \mathsf{v}, \tag{3.44c}$$

$$\mathsf{D}' = \{\mathsf{D}, \mathcal{H}\}_{(\mathsf{m},\mathsf{n},\mathsf{B},\mathsf{D})} = \mathsf{D} \times \mathsf{u}, \tag{3.44d}$$

where the Poisson bracket is constructed from (3.39) through the addition of two semidi-

rect and two Leibniz extensions:

$$\begin{aligned}\{f,g\}_{(\mathsf{m},\mathsf{n},\mathsf{B},\mathsf{D})} = &-\mathsf{m}\cdot(\nabla_{\mathsf{m}}f\times\nabla_{\mathsf{m}}g) - \mathsf{n}\cdot(\nabla_{\mathsf{m}}f\times\nabla_{\mathsf{n}}g+\nabla_{\mathsf{n}}f\times\nabla_{\mathsf{m}}g)\\ &- \mathsf{B}\cdot(\nabla_{\mathsf{m}}f\times\nabla_{\mathsf{B}}g+\nabla_{\mathsf{B}}f\times\nabla_{\mathsf{m}}g) - \mathsf{B}\cdot(\nabla_{\mathsf{n}}f\times\nabla_{\mathsf{n}}g)\\ &\underbrace{- \mathsf{D}\cdot(\nabla_{\mathsf{m}}f\times\nabla_{\mathsf{D}}g+\nabla_{\mathsf{D}}f\times\nabla_{\mathsf{m}}g)}_{\text{evolution of hyperfield}}\\ &\underbrace{- \mathsf{D}\cdot(\nabla_{\mathsf{B}}f\times\nabla_{\mathsf{n}}g) + \mathsf{B}\cdot(\nabla_{\mathsf{D}}f\times\nabla_{\mathsf{n}}g)}_{\text{effect of hyperfield}}.\end{aligned}$$

This twelve-dimensional system has four independent Casimirs:

$$C_1 = \mathsf{m}\cdot\mathsf{D} + \mathsf{n}\cdot\mathsf{B}, \tag{3.45a}$$

$$C_2 = \frac{1}{2}\mathsf{B}\cdot\mathsf{B} + \mathsf{n}\cdot\mathsf{D}, \tag{3.45b}$$

$$C_3 = \mathsf{B}\cdot\mathsf{D}, \tag{3.45c}$$

$$C_4 = \mathsf{D}\cdot\mathsf{D}. \tag{3.45d}$$

In the linearly elastic, unshearable, inextensible and isotropic case there are now three independent first integrals besides the Hamiltonian,

$$I_1 = B\mathsf{m}\cdot\mathsf{d}_3, \tag{3.46a}$$

$$I_2 = \mathsf{n}\cdot\mathsf{m} + B\mathsf{B}\cdot\mathsf{d}_3, \tag{3.46b}$$

$$I_3 = \frac{1}{2}\mathsf{n}\cdot\mathsf{n} + \mathsf{m}\cdot\mathsf{B} + B\mathsf{D}\cdot\mathsf{d}_3, \tag{3.46c}$$

making the system completely integrable. If $C_4 = 0$ then $\mathsf{D} = \mathsf{0}$ and the system reduces to that of the magnetic rod in the previous section. The system loses rank as the Casimir $C_4 = 0$ necessarily implies $C_3 = 0$ and the two Casimirs lose their independent meaning. Interestingly, the integral I_3 then becomes a Casimir (cf. (3.40a)), whose preservation does not rely on isotropy anymore.

By using the four Casimirs (3.45) the twelve-dimensional system can be reduced to an eight-dimensional canonical system. The reduced system would be parameterised by a coordinate chart which exists in a higher dimension than real space: generically configurations would have to be coupled to the evolution of the magnetic field.

3.4 A Lax Pair Formulation

In the previous sections a succession of rod models based on the form of the structure matrices was introduced and conditions on the constitutive relations determined whether a model was integrable or not. In this section a compact Lax pair formulation of the integrable family of linearly elastic, isotropic, inextensible, unshearable rod problems is given.

Consider the Lax pair with a spectral parameter μ

$$\frac{\mathrm{d}}{\mathrm{d}s}\Gamma(\mu) = \left[\Gamma(\mu), \hat{\mathsf{d}}_3\mu + \hat{\mathsf{u}}\right], \tag{3.47}$$

where

$$\Gamma(\mu) = B\hat{\mathsf{d}}_3\mu + \Gamma_0 + \Gamma_1\mu^{-1} + \ldots + \Gamma_n\mu^{-n} \in \mathfrak{so}(3), \quad n \in \mathbb{N},$$

with $B = B_1 = B_2$,

$$\hat{\mathsf{d}}_3 = \begin{pmatrix} 0 & -1 & 0 \\ 1 & 0 & 0 \\ 0 & 0 & 0 \end{pmatrix} \quad \text{and} \quad \hat{\mathsf{u}} = \begin{pmatrix} 0 & -u_3 & u_2 \\ u_3 & 0 & -u_1 \\ -u_2 & u_1 & 0 \end{pmatrix}$$

using the hat-map isomorphism (3.3). In (3.47) the bracket is the standard matrix commutator bracket given by

$$[a, b] = ab - ba, \quad \text{for} \quad a, b \in \mathbb{R}^{3\times 3}.$$

This Lax pair was proposed in [102] to study monodromy present in the generalised family of symmetric Lagrange tops.

The Lax pair describes our family of rod models if the terms in the expansion of Γ by μ (a spectral parameter) are associated with our field variables: $\Gamma_0 = \hat{\mathsf{m}}$, $\Gamma_1 = \hat{\mathsf{n}}$, $\Gamma_2 = \hat{\mathsf{B}}$, $\Gamma_3 = \hat{\mathsf{D}}$, etc. The non-canonical equations for the force-free rod ($n = 0$), Kirchhoff rod ($n = 1$), rod in uniform magnetic field ($n = 2$) and rod in nonuniform magnetic field ($n = 3$) are obtained by equating like powers of μ in (3.47). The first integrals are generated by

$$I_i = -\frac{1}{4}\mathrm{residue}_{\mu=0}\left(\mu^{i-1}\mathrm{trace}\left[\Gamma(\mu)^2\right]\right), \quad \text{for} \quad i = -1, 0, 1, \ldots, n-1, \tag{3.48}$$

the Casimirs are generated by

$$C_i = -\frac{1}{4}\text{residue}_{\mu=0}\left(\mu^{i-1}\text{trace}\left[\Gamma(\mu)^2\right]\right), \quad \text{for} \quad i = n, n+1, n+2, \ldots, 2n \tag{3.49}$$

and the Hamiltonian is given by

$$\mathcal{H} = \frac{I_0}{B} + \frac{B-C}{2BC}\left(\frac{I_{-1}}{B}\right)^2. \tag{3.50}$$

Chapter 4

Reduction of the Kirchhoff Rod

In this chapter the Casimirs of the Kirchhoff equations are used to reduce the non-canonical Hamiltonian system to a lower dimensional canonical system, allowing for a range of analytic tools to be applied. In the integrable Lagrange case planar phase diagrams are computed and fixed points and homoclinic solutions found. The reduction allows Mel'nikov's method to be applied for the nonintegrable perturbations of anisotropy and initial curvature and Poincaré sections to be computed. The consequences of non-integrability in these two cases are then outlined.

4.1 Reduction to a Canonical System

In this section the two Casimirs of the Kirchhoff equation (3.29) are used to reduce the six-dimensional non-canonical Hamiltonian system (3.28) in (m, n) to a four-dimensional canonical Hamiltonian system using Euler angles (A.1). The canonical coordinates are $q = (\theta, \phi, \psi)$ and their conjugate momenta $p = (p_\theta, p_\phi, p_\psi)$. The reduction is possible (at least locally) provided the structure matrix (3.25) is of constant rank everywhere [76, §6.2].

Firstly, in order to simplify the analysis the system is nondimensionalised. Let a torque, M, and tension, T, be applied in the direction of $\boldsymbol{d}_3$ at $s = \pm\infty$. By scaling the arclength by $\bar{s} = (M/B_1)\, s$ (as homoclinic solutions will be studied there is no natural

length scale) and scaling the forces and moments by

$$\bar{m}_1 = m_1/M, \quad \bar{m}_2 = m_2/M, \quad \bar{m}_3 = m_3/M,$$
$$\bar{n}_1 = n_1/T, \quad \bar{n}_2 = n_2/T \quad \text{and} \quad \bar{n}_3 = n_3/T$$

the system is nondimensional. For convenience in the notation the overbar is suppressed. From the general linear constitutive relations (3.15) the nondimensional parameters are

$$\begin{gathered} m = \frac{M}{\sqrt{B_2 T}}, \quad \rho = \frac{B_2}{B_1} - 1, \quad \nu = \frac{B_2}{C} - 1, \\ \epsilon = \frac{T}{J}, \quad \sigma = \frac{J}{H} - 1, \quad \gamma = \frac{K}{J} - 1 \quad \text{and} \quad \kappa_0 = \frac{B_1 u_0}{M}. \end{gathered} \tag{4.1}$$

Where m is the unified end loading parameter, $\rho + 1$ the anisotropy, $\nu + 1$ the ratio of torsional stiffness to bending stiffness, ϵ measures the ratio of shear to bending, γ and σ are the analogues of ρ and ν for shear and extensibility and κ_0 the initial curvature. If $\rho = 0$ then for circular rods ν is Poisson's ratio.

Let

$$R = \begin{pmatrix} \cos\theta\cos\phi\cos\psi - \sin\phi\sin\psi & \cos\theta\cos\phi\sin\psi + \cos\psi\sin\phi & -\sin\theta\cos\phi \\ -\cos\theta\sin\phi\cos\psi - \cos\phi\sin\psi & -\cos\theta\sin\phi\sin\psi + \cos\phi\cos\psi & \sin\theta\sin\phi \\ \sin\theta\cos\psi & \sin\theta\sin\psi & \cos\theta \end{pmatrix} \tag{4.2}$$

be a parameterisation of the rotation matrix (3.2) in terms of Euler angles. Following the convention used by Love [66], θ is the angle the tangent to the rod makes with the initially straight rod, ψ is the azimuthal angle about a fixed axis and ϕ is the twist angle about the centreline of the rod.

The force equation $\boldsymbol{n}' = \mathbf{0}$ is integrated subject to the condition that the force acts along the $\boldsymbol{e}_3$ axis at $s = \pm\infty$, thus $\boldsymbol{n} = \boldsymbol{e}_3$. Hence, in the body frame the force is then given by

$$\mathsf{n}(q) = (\sin\theta\cos\phi, -\sin\theta\sin\phi, \cos\theta)^T. \tag{4.3}$$

Using the Euler angles and expression of the strains (3.5), the strains $u_i(q, q')$ are

given by

$$u_1 = \theta' \sin\phi - \psi' \sin\theta \cos\phi, \tag{4.4a}$$

$$u_2 = \theta' \cos\phi + \psi' \sin\theta \sin\phi, \tag{4.4b}$$

$$u_3 = \phi' + \psi' \cos\theta. \tag{4.4c}$$

In the initially straight, inextensible, unshearable case, the stored energy-density functional (3.15) is given by

$$\mathcal{W}\left(q, q'\right) = \frac{1}{2}\left(\theta' \sin\phi - \psi' \sin\theta\cos\phi\right)^2 + \frac{1}{2}\left(1+\rho\right)\left(\theta' \cos\phi + \psi' \sin\theta \sin\phi\right)^2 + \frac{1}{2}\left(1+\nu\right)\left(\phi' + \psi'\cos\theta\right)^2. \tag{4.5}$$

The Lagrangian $\mathcal{L}\left(q, q'\right)$ is found by adding the (nondimensionalised) work done against end tension, which is given by $(n_3 - 1)$, to the energy stored in the rod. Thus, dropping the irrelevant constant term gives

$$\mathcal{L}\left(q, q'\right) = \frac{1}{2}\left(\theta' \sin\phi - \psi' \sin\theta\cos\phi\right)^2 + \frac{1}{2}\left(1+\rho\right)\left(\theta' \cos\phi + \psi' \sin\theta \sin\phi\right)^2 + \frac{1}{2}\left(1+\nu\right)\left(\phi' + \psi'\cos\theta\right)^2 - \frac{\cos\theta}{m^2}. \tag{4.6}$$

The conjugate momenta are defined as

$$p = \frac{\partial \mathcal{L}}{\partial q'}.$$

Hence

$$p_\theta = \left(\theta' \sin\phi - \psi' \sin\theta\cos\phi\right)\sin\phi + \left(1+\rho\right)\left(\theta' \cos\phi + \psi' \sin\theta \sin\phi\right)\cos\phi, \tag{4.7a}$$

$$p_\psi = -\left(\theta' \sin\phi - \psi' \sin\theta\cos\phi\right)\sin\theta\cos\phi + \left(1+\rho\right)\left(\theta' \cos\phi + \psi' \sin\theta \sin\phi\right)\sin\theta\sin\phi + \left(1+\nu\right)\left(\phi' + \psi'\cos\theta\right)\cos\theta, \tag{4.7b}$$

$$p_\phi = \left(1+\nu\right)\left(\phi' + \psi'\cos\theta\right). \tag{4.7c}$$

Due to the nondegeneracy conditions on the hyperelastic function (3.9)-(3.11) the equa-

tions (4.7) can be inverted

$$\theta' = p_\theta + \rho \sin\phi \left(p_\theta \sin\phi - \cos\phi \left(\frac{p_\psi - p_\phi \cos\theta}{\sin\theta} \right) \right), \tag{4.8a}$$

$$\phi' = (1+\nu)\, p_\phi - \cos\theta \left(\frac{p_\psi - p_\phi \cos\theta}{\sin^2\theta} \right) + \rho \frac{\cos\phi\cos\theta}{\sin\theta} \left(p_\theta \sin\phi - \cos\phi \left(\frac{p_\psi - p_\phi \cos\theta}{\sin\theta} \right) \right), \tag{4.8b}$$

$$\psi' = \left(\frac{p_\psi - p_\phi \cos\theta}{\sin^2\theta} \right) - \rho \frac{\cos\phi}{\sin\theta} \left(p_\theta \sin\phi - \cos\phi \left(\frac{p_\psi - p_\phi \cos\theta}{\sin\theta} \right) \right), \tag{4.8c}$$

From the strains (3.5), conjugate momenta (4.7) and using the constitutive relations (3.15), the conjugate momenta can be expressed in the form

$$p = L^{-1}(q)\, \mathsf{m} \quad \text{where} \quad L^{-1}(q) = \begin{pmatrix} \sin\phi & \cos\phi & 0 \\ -\sin\theta\cos\phi & \sin\theta\sin\phi & \cos\theta \\ 0 & 0 & 1 \end{pmatrix}. \tag{4.9}$$

That is,

$$p_\theta = m_1 \sin\phi + m_2 \cos\phi, \tag{4.10a}$$

$$p_\psi = -m_1 \cos\phi \sin\theta + m_2 \sin\phi \sin\theta + m_3 \cos\theta, \tag{4.10b}$$

$$p_\phi = m_3. \tag{4.10c}$$

The moments can be expressed as

$$\mathsf{m} = L(q)\, p \quad \text{where} \quad L(q) = \frac{1}{\sin\theta} \begin{pmatrix} \sin\theta\sin\phi & -\cos\phi & \cos\theta\cos\phi \\ \sin\theta\cos\phi & \sin\phi & -\cos\theta\sin\phi \\ 0 & 0 & \sin\theta \end{pmatrix} \tag{4.11}$$

or equivalently as

$$m_1 = p_\theta \sin\phi - \cos\phi \left(\frac{p_\psi - p_\phi \cos\theta}{\sin\theta} \right), \tag{4.12a}$$

$$m_2 = p_\theta \cos\phi + \sin\phi \left(\frac{p_\psi - p_\phi \cos\theta}{\sin\theta} \right), \tag{4.12b}$$

$$m_3 = p_\phi. \tag{4.12c}$$

Note that the polar singularity inherent in the Euler angle formulation manifests itself in the determinant of the matrix $L(q)$.

In order for the Poisson bracket (3.28) to be transformed into a canonical bracket it is necessary to verify that

$$G\mathcal{J}G^T = \bar{\mathcal{J}} \tag{4.13}$$

where $\mathcal{J}$ is the noncanonical structure matrix given by (3.25), $\bar{\mathcal{J}}$ is the four-by-four canonical structure matrix and G is the Jacobian of the transformation given by

$$G = \frac{\partial\,(q,p)}{\partial\,(\mathsf{m},\mathsf{n})}.$$

Using the relationships (4.12) and (4.3), the nontrivial variables (θ,ϕ) and conjugate momenta (p_θ, p_ϕ) can be expressed in terms of the force and moments

$$\theta = \cos^{-1} n_3, \quad \phi = \tan^{-1}\frac{-n_2}{n_1}, \quad p_\theta = \frac{m_1 n_2 - m_2 n_1}{\sqrt{1-n_3^2}} \quad \text{and} \quad p_\phi = m_3.$$

Thus

$$G = \frac{1}{\sin\theta}\begin{pmatrix} 0 & 0 & 0 & 0 & 0 & 1 \\ 0 & 0 & 0 & \sin\phi & \cos\phi & 0 \\ \sin\phi\sin\theta & \cos\phi\sin\theta & 0 & g_{34} & g_{35} & \cos\theta\left(p_\theta\sin^2\phi + p_\theta\cos\phi\right) \\ 0 & 0 & \sin\theta & 0 & 0 & 0 \end{pmatrix},$$

where

$$g_{34} = p_\theta\cos\phi + \sin\phi\left(\frac{p_\psi - p_\phi\cos\theta}{\sin\theta}\right) \quad \text{and} \quad g_{35} = p_\theta\sin\phi - \cos\phi\left(\frac{p_\psi - p_\phi\cos\theta}{\sin\theta}\right).$$

It is a straightforward task to check that (4.13) holds and hence the transformation reduces the noncanonical system to a canonical system. Thus the Hamiltonian is given by

$$\mathcal{H} = \frac{1}{2}p_\theta^2 + \frac{1}{2}\left(\frac{p_\psi - p_\phi\cos\theta}{\sin\theta}\right)^2 + \frac{1}{2}(1+\nu)\,p_\phi^2 + \frac{\cos\theta}{m^2} + \frac{1}{2}\rho\left(p_\theta\sin\phi - \cos\phi\left(\frac{p_\psi - p_\phi\cos\theta}{\sin\theta}\right)\right)^2. \tag{4.14}$$

The Casimirs do manifest themselves in the canonical formulation. The Hamiltonian is invariant under rotations about the $\boldsymbol{e}_3$ axis, so ψ is a cyclic variable and consequently

p_ψ is a constant of motion, which corresponds to the Casimir (3.29a). Thus, by (4.12) and (4.3)

$$\begin{aligned} p_\psi &= -m_1 \cos\phi \sin\theta + m_2 \sin\phi \sin\theta + m_3 \cos\theta \\ &= \mathsf{m} \cdot \mathsf{n} \\ &= \alpha. \end{aligned} \tag{4.15}$$

The parameterisation of the force (4.3) means that the Casimir (3.29b) ensures that the four-dimensional equations are nondegenerate, specifically $C_2 = \mathsf{n} \cdot \mathsf{n} \neq 0$ if $T \neq 0$, as was mentioned in §3.4.

While continuous symmetries correspond to conserved quantities, discrete symmetries correspond to multiplicities of solutions. The reduced system (4.14) admits two discrete symmetries for all constitutive relations. Firstly a rotation symmetry described by the translation in ϕ by π

$$Z_1 \,:\, \phi \mapsto \phi + \pi \tag{4.16}$$

which corresponds to a π-rotation about the $\boldsymbol{d}_3$ axis in the rod. Secondly, the reflection symmetry about the $\boldsymbol{e}_3$ axis in the spatial frame

$$Z_2 \,:\, (\theta, \phi, \psi, p_\theta, p_\phi, p_\psi) \mapsto (-\theta, -\phi, -\psi, -p_\theta, -p_\phi, -p_\psi)\,. \tag{4.17}$$

The action of this symmetry can be decomposed into two reversibilities, $Z_2 = R_1 \circ R_2$

$$R_1 \,:\, (\theta, \phi, \psi, p_\theta, p_\phi, p_\psi) \to (-\theta, -\phi, -\psi, p_\theta, p_\phi, p_\psi) \quad \text{as} \quad s \to -s \tag{4.18a}$$

and

$$R_2 \,:\, (\theta, \phi, \psi, p_\theta, p_\phi, p_\psi) \to (\theta, \phi, \psi, -p_\theta, -p_\phi, -p_\psi) \quad \text{as} \quad s \to -s. \tag{4.18b}$$

These symmetries imply that primary homoclinic solutions, that is homoclinic orbits with a single localised mode, have four distinct solutions - a pair of rotationally symmetric solutions which are reversible under R_1 and a pair of solutions reversible under R_2.

If the rod is isotropic ($\rho = 0$) the Lagrange integral (3.30) corresponds to the rotational invariance of the Hamiltonian about the $\boldsymbol{d}_3$ axis. Then ϕ is a cyclic variable and p_ϕ is a first integral corresponding to the conservation of twist in the rod

$$\begin{aligned} p_\phi &= m_3 \\ &= (1+\nu)\,\tau \\ &= \beta. \end{aligned} \tag{4.19}$$

As a set of rotations, the Euler angles are orientated in such a way as to describe the symmetries which generate the conserved quantaties (4.15) and (4.19). The two symmetries commute, as seen by the fact the integrals generated are independent with respect to the noncanonical Poisson bracket. Thus the integrable Hamiltonian is given by

$$\mathcal{H}_0\left(\theta, p_\theta\right) = \frac{1}{2}p_\theta^2 + \frac{1}{2}\left(\frac{\alpha - \beta\cos\theta}{\sin\theta}\right)^2 + \frac{1}{2}\left(1+\nu\right)\beta^2 + \frac{\cos\theta}{m^2}. \tag{4.20}$$

The constant term $(1+\nu)\,\beta^2/2$ is the stored energy-density due to twisting. This system is often described as a mechanical system or as an equivalent oscillator [99] as it can be expressed in the form

$$\mathcal{H}\left(\theta, p_\theta\right) = \frac{1}{2}p_\theta^2 + V\left(\theta\right) \quad \text{where} \quad V\left(\theta\right) = \frac{1}{2}\left(\frac{\alpha - \beta\cos\theta}{\sin\theta}\right)^2 + \frac{\cos\theta}{m^2} \tag{4.21}$$

on an (nondimensional) energy level $h = \mathcal{H}$. As a system of first order equations, the governing equations are given by

$$\theta' = p_\theta \quad \text{and} \quad p_\theta' = \frac{\sin\theta}{m^2} - \left(\frac{\beta - \alpha\cos\theta}{\sin\theta}\right)\left(\frac{\alpha - \beta\cos\theta}{\sin^2\theta}\right). \tag{4.22}$$

The evolution of the remaining angles are given by

$$\psi' = \frac{\alpha - \beta\cos\theta}{\sin^2\theta} \quad \text{and} \quad \phi' = \left(1+\nu\right)\beta - \left(\frac{\alpha - \beta\cos\theta}{\sin^2\theta}\right)\cos\theta. \tag{4.23}$$

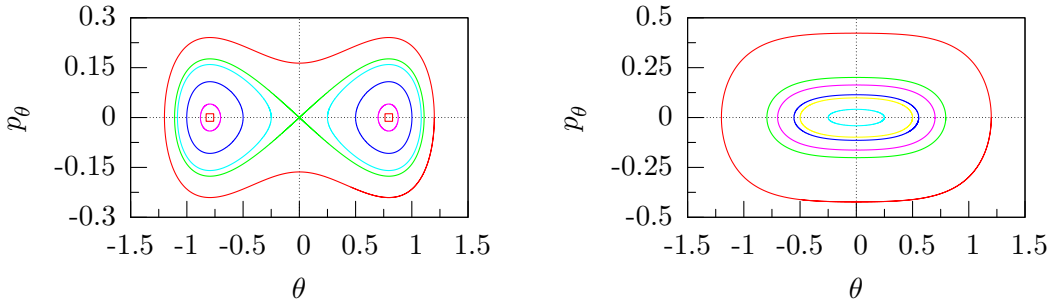

(a) Super-critical, $m = 1.7 < m_{\max}$ **(b)** Sub-critical, $m = 2.3 > m_{\max}$

Figure 4.1: Phase portraits of the equivalent oscillator for an isotropic, inextensible rods under uniform loading when $\alpha = \beta$ about the Hamiltonian-Hopf bifurcation at $m_{\max} = 2$. In subfigure 4.1(a) $m \leq m_{\max}$ and $h = 0.5934$ (red), $1/m^2 = 0.3402$ (green), 0.3689 (cyan), 0.3511 (blue), 0.3979 (magenta) and 0.4187 (red). In this case the phase portrait shows that a number of rod configurations are admissible: helices, localied and helix-on-helix configurations. In subfigure 4.1(b) $m \geq m_{\max}$ and $h = 0.5365$ (red), 0.2149 (green), 0.2778 (magneta), 0.2418 (blue), 0.2311 (yellow) and 0.1989 (cyan). In this case all orbits correspond to straight twisted rods.

Remark 4.1.1. *When expressed in terms of Euler angles the Kovalevskaya integral,* (3.31)*, conditional on* $\rho = -1/2$ *and* $\nu = -1/2$*, is given by*

$$\mathcal{I} = \left(\frac{1}{4}\left(p_\theta \sin\phi - \cos\phi\left(\frac{p_\psi - p_\phi\cos\theta}{\sin\theta}\right)\right)^2 - \frac{1}{4}p_\phi^2 + \frac{\cos\theta}{m^2}\right)^2 + \left(\frac{1}{4}p_\phi\left(p_\theta\sin\phi - \cos\phi\left(\frac{p_\psi - p_\phi\cos\theta}{\sin\theta}\right)\right) - \frac{\sin\theta\cos\phi}{m^2}\right)^2. \tag{4.24}$$

The Euler angle formulation gives a single pair of action-angle variables (ψ, p_ψ) *and a four-dimensional canonical Hamiltonian system in* $(\theta, \phi, p_\theta, p_\phi)$ *phase space with an integral. In [37] an algorithmic procedure was developed which associates the integrals with action integrals.*

4.2 Superintegrable Cases

Recently it has been shown that the relative equilibria of the noncanonical system (3.27) correspond to either straight rods or helices [26]. After performing the reduction in the isotropic case it is now shown that the equilibria (of the canonical system) are indeed either straight rods or helices. Furthermore it is shown that configurations

exist on tori of lower dimension.

As shown, the integrals α and β correspond to rotational invariances about the axes $\boldsymbol{e}_3$ in the spatial frame and $\boldsymbol{d}_3$ in the director frame. A straight twisted rod requires $\boldsymbol{d}_3$ to be aligned with $\boldsymbol{e}_3$. As a focus of this thesis will be on localised buckling from a straight twisted rod it is necessary to set $\alpha = \beta$ in order for such solutions to exist. For simplicity the values of the integrals (4.15) and (4.19) are set to unity

$$\alpha = \beta = 1. \tag{4.25}$$

For homoclinic solutions $\theta \to 0$ as $s \to \pm\infty$.

The governing equations (4.22) become

$$\theta' = p_\theta \quad \text{and} \quad p_\theta' = \frac{\sin\theta}{(1+\cos\theta)^2} - \frac{\sin\theta}{m^2}. \tag{4.26}$$

There are two fixed points of the governing equations (4.26), firstly, the trivial case given by

$$p_\theta = 0 \quad \text{and} \quad \sin\theta = 0. \tag{4.27}$$

The trivial fixed point corresponds to a straight twisted rod and is a hyperbolic saddle point $\boldsymbol{p} = (0, 0)$.

The additional conserved quantaties are m_1, m_2, n_1, n_2 and n_3 of which any two can be chosen which are independent with respect to the remaining integrals for the Poisson brackets (3.28). There are five independent integral: two Casimirs, a Hamiltonian, a first integral and two additional integrals. As a six-dimensional system with five independent integrals the straight twisted rod is maximally superintegrable and configurations exist on a one-torus given by

$$\mathcal{H}(p_\phi) = \frac{1}{2}(1+\nu)\, p_\phi^2 \quad \text{where} \quad \phi' = (1+\nu)\, p_\phi \quad \text{and} \quad p_\phi' = 0. \tag{4.28}$$

Secondly, the nontrivial case is given by

$$p_\theta = 0 \quad \text{and} \quad \theta = \cos^{-1}(m-1). \tag{4.29}$$

The nontrivial fixed point corresponds to a uniform helix. Closed form solutions of the helix are given by

$$m_1(s) = \mp\cos\left(\left(\nu+\frac{1}{m}\right)s\right)\left(\frac{2-m}{\sin\left(\cos^{-1}(m-1)\right)}\right), \tag{4.30a}$$

$$m_2(s) = \pm\sin\left(\left(\nu+\frac{1}{m}\right)s\right)\left(\frac{2-m}{\sin\left(\cos^{-1}(m-1)\right)}\right), \tag{4.30b}$$

$$m_3(s) = 1, \tag{4.30c}$$

$$n_1(s) = \mp\sin\left(\cos^{-1}(m-1)\right)\cos\left(\left(\nu+\frac{1}{m}\right)s\right), \tag{4.30d}$$

$$n_2(s) = \pm\sin\left(\cos^{-1}(m-1)\right)\sin\left(\left(\nu+\frac{1}{m}\right)s\right), \tag{4.30e}$$

$$n_3(s) = m-1. \tag{4.30f}$$

Expressing the nontrivial fixed point solution in the canonical formulation, the forces and moments can be described by the fixed points rotated by a constant angle

$$f = \pm\left(\nu+\frac{1}{m}\right).$$

As a consequence of the reversibilities (4.18), the sign of the angle f determines the chirality of the helix. The angle f is the angle between the principal directors and the normal and binormal in the Frenet frame [99].

An additional independent integral, in involution with all other integrals, can be chosen from either

$$n_3 \quad \text{or} \quad \mathsf{m}\cdot\mathsf{m}. \tag{4.31}$$

For the six-dimensional Kirchhoff system the additional integral means that there are four independent integrals and (3.26), (3.29), (3.30) and (4.31). Hence the helix is minimally superintegrable, existing on two-tori, rather than the generic three-tori. The Hamiltonian is now a function of the conjugate momenta only

$$\mathcal{H}(p_\phi, p_\psi) = \frac{\left(p_\psi - p_\phi(m-1)\right)^2}{m(2-m)} + \frac{1}{2}(1+\nu)p_\phi^2 + \frac{m-1}{m^2}$$

which are action variables. The angular coordinates move quasi-periodically on the two-tori with the frequencies given by

$$\psi' = \frac{1}{m} \quad \text{and} \quad \phi' = (1+\nu) + \frac{2-m}{m}. \tag{4.32}$$

The curvature, κ, and geometric torsion, τ_s, of the helices are constants given by

$$\kappa = \sqrt{u_1^2 + u_2^2} = \frac{2-m}{\sin\left(\cos^{-1}(m-1)\right)} \quad \text{and} \quad \tau_s = \tau - f' = 1 - \left(\frac{1}{m} + \nu\right).$$

Further information on the geometric classification of rod configurations can be found in [99].

4.3 Homoclinic Orbits

In this section the Hamiltonian vector field is integrated and homoclinic solutions calculated. Hamilton's equation $\theta' = p_\theta$ may be substituted into the Hamiltonian (4.20), which can then be rearranged as a first order ordinary differential equation in θ as

$$\frac{\mathrm{d}\theta}{\mathrm{d}s} = \frac{1}{\sqrt{2\left(h - \cos\theta/m^2\right)\left(1-\cos^2\theta\right) - \left(\alpha - \beta\cos\theta\right)^2}}. \tag{4.33}$$

From the substitution $u = \cos\theta$ the integral is

$$s = \int_{u(0)}^{u(s)} \frac{\mathrm{d}u}{\sqrt{2\left(h - u/m^2\right)\left(1-u^2\right) - \left(\alpha - \beta u\right)^2}} \quad -1 < u < 1, \quad m \neq 0. \tag{4.34}$$

Applying the torque condition $\alpha = \beta = 1$ yields

$$s = \int_{u(0)}^{u(s)} \frac{\mathrm{d}u}{\sqrt{(1-u)\left(2\left(h - u/m^2\right)(1+u) - (1-u)\right)}} \quad -1 < u < 1, \quad m \neq 0. \tag{4.35}$$

For homoclinic solutions emanating from the saddle at the origin from the Hamiltonian (4.21) the nondimensional energy-density is given by $h = 1/m^2$. Thus the integral becomes

$$s = \frac{m}{\sqrt{2}} \int_{u_0}^{u(s)} \frac{\mathrm{d}u}{(1-u)\sqrt{u-u_0}}, \quad -1 < u_0 < u < 1, \quad m \neq 0, \tag{4.36}$$

where $u_0 = m^2/2 - 1$. The substitution $u = u_0 + (1-u_0)\tanh^2 z$ simplifies the integral to

$$s = \frac{m\sqrt{2}}{\sqrt{1-u_0}} \int_{z_0}^{z(s)} \mathrm{d}z \quad \text{where} \quad z_0 = 0. \tag{4.37}$$

Hence, for homoclinic solutions the Euler angles and their conjugate variables are given by

$$\theta = \cos^{-1}\left(u_0 + (1-u_0)\tanh^2\left(\frac{\sqrt{1-u_0}}{m\sqrt{2}}s\right)\right), \tag{4.38a}$$

$$\psi = \frac{1}{2}s + \tan^{-1}\left(\sqrt{\frac{1-u_0}{1+u_0}}\frac{1-e^{-s/m\sqrt{m(1-u_0)}}}{1+e^{-s/m\sqrt{m(1-u_0)}}}\right), \tag{4.38b}$$

$$\phi = \left(\frac{1}{2}+\nu\right)s + \tan^{-1}\left(\sqrt{\frac{1-u_0}{1+u_0}}\frac{1-e^{-s/m\sqrt{m(1-u_0)}}}{1+e^{-s/m\sqrt{m(1-u_0)}}}\right), \tag{4.38c}$$

$$p_\theta = \theta', \tag{4.38d}$$

$$p_\psi = 1, \tag{4.38e}$$

$$p_\phi = 1. \tag{4.38f}$$

Note 4.3.1. *As the reversibilities dictate, $p_\theta(s)$ is an odd function while $\theta(s)$ is an even function of the arc-length s.*

The evolution of the angle θ and its conjugate momenta p_θ are illustrated in figure 4.2. The angular frequencies (4.23) are illustrated in figure 4.3. From the expressions of the homoclinic orbits in (4.38) at the critical value of the unified load parameter $m = m_{\max} = 2$ the homoclinic orbits undergo a subcritical Hamiltonian-Hopf bifurcation [98]. The super- and sub-critical phase portraits are illustrated in subfigures 4.1(a) and 4.1(b) respectively. Thus for decreasing m, a straight twisted rod, whose eigenvalues are a centre $\mu^c = \pm(i/2m)\sqrt{m^2-4}$ buckles into a localised or helical solution whose eigenvalues form a saddle $\mu^{s,u} = \pm(1/2m)\sqrt{4-m^2}$. For the analogous problem of a heavy spinning top the bifurcation corresponds to a fast, sleeping top supercritically bifurcating into a precessing top.

Remark 4.3.2. *Note that the homoclinic orbits emanate from the saddle but the fixed point $\boldsymbol{p} = (0,0)$ is not a part of the the orbit, since the saddle defines straight twisted rods which exist on one-tori. Thus, if the homoclinic orbit is denoted as $\boldsymbol{x}_0(s) = (\theta, p_\theta)$ then it is the union of the homoclinic and the fixed point $\Gamma = \{\boldsymbol{x}_0(s)\ \forall s \in \mathbb{R}\} \cup \{\boldsymbol{p}\}$ which, in subfigure 4.1(a), forms a closed curved in the two-dimensional phase space whose interior is filled with periodic orbits.*

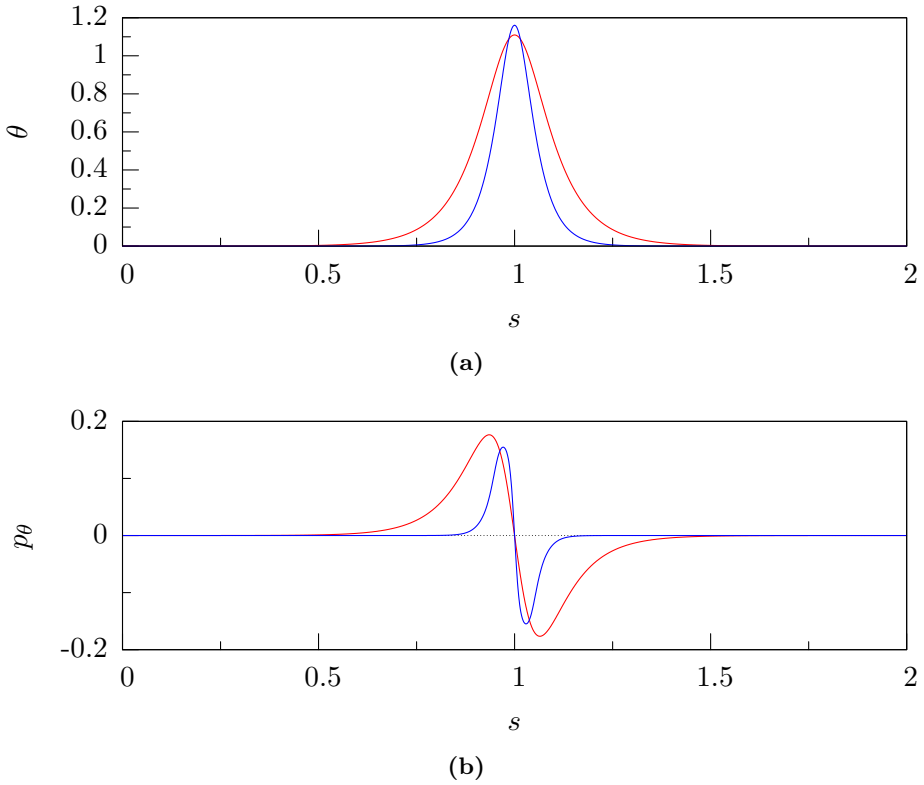

Figure 4.2: In subfigure 4.2(a) the evolution of the Euler angle θ (4.38a) is shown and in subfigure 4.2(b) the evolution of the conjugate variable conjugate p_θ (4.38d) is shown with respect to the normalised arclength s for the homoclinic orbit when $m = 1.7$ and $\nu = 1/3$.

4.3.1 Extensibility & Shearability

In [88] it was shown by finding explicit solutions, without exploiting the Hamiltonian structure, that an isotropic rod that is shearable and extensible is integrable. In this section, by exploiting the Hamiltonian structure, closed form expressions for homoclinic orbits are derived. These expressions are necessary when proving that extensibility is an integrability breaking parameter for a rod in a uniform magnetic field.

In the case of isotropic bending ($\rho = 0$) and shear ($\sigma = 0$) the governing equation can be reduced to a single degree of freedom Hamiltonian system by substituting the

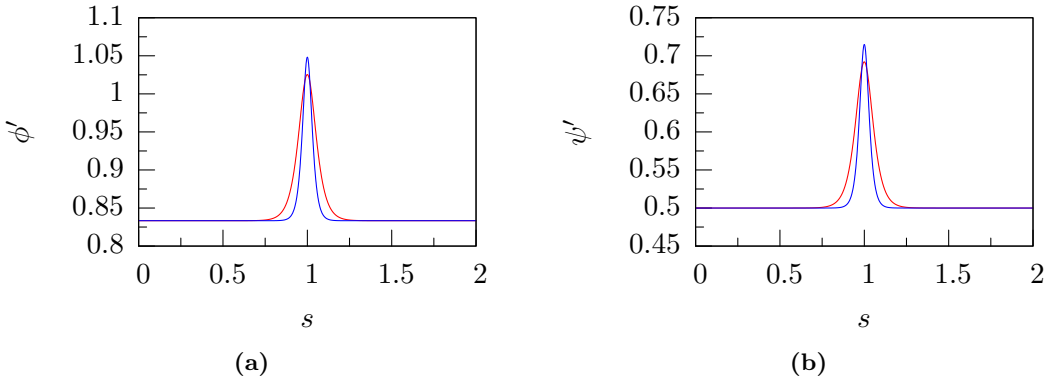

(a) **(b)**

Figure 4.3: The angular frequencies $\phi'(s)$ and $\psi'(s)$ are displayed in subfigures 4.3(a) and 4.3(b) respectively for the isotropic R_1-reversible homoclinic orbit with $m = 1.7$ and $\nu = 1/3$. The angular frequencies are given by substituting the homoclinic orbit (4.38a) into (4.32).

moments (4.12) and forces (4.3) into the Hamiltonian

$$\mathcal{H} = \frac{1}{2}m_1^2 + \frac{1}{2}m_2^2 + \frac{1}{2}(1+\nu)\,m_1^2 + \frac{1}{2m^2}\epsilon n_1^2 + \frac{1}{2m^2}\epsilon n_2^2 + \frac{1}{2m^2}\epsilon(1+\gamma)\,n_3^2 + \frac{n_3}{m^2} \quad (4.39)$$

which gives

$$\mathcal{H}_0(\theta, p_\theta) = \frac{1}{2}p_\theta^2 + \frac{1}{2}\left(\frac{p_\psi - p_\phi\cos\theta}{\sin\theta}\right)^2 + \frac{1}{2}(1+\nu)\,p_\phi^2 + \frac{\cos\theta\,(\epsilon\gamma\cos\theta + 2) + \epsilon}{2m^2}. \quad (4.40)$$

The additional constant term $\epsilon/2m^2$ is the (nondimensional) stored energy due to extensibility. Note that $\epsilon \geq 0$ and $\gamma \geq 0$ throughtout the analysis. When $\alpha = \beta = 1$, Hamilton's equations are given by

$$\theta' = p_\theta \quad \text{and} \quad p_\theta' = \frac{\sin\theta}{(1+\cos\theta)^2} - \frac{(\epsilon\gamma\cos\theta + 1)\sin\theta}{m^2}. \quad (4.41)$$

Solving for fixed point solutions yields the trivial solution, $p_\theta = 0$ and $\sin\theta = 0$, and the nontrivial solution given by $p_\theta = 0$ and θ is a solution of the cubic

$$0 = \epsilon\gamma\cos^3\theta + \cos^2\theta + \epsilon\gamma\cos\theta + 1 - m^2. \quad (4.42)$$

On linearisation the governing equation is identical to the linearisation of the inextensible case except that $1/m^2$ is now replaced by $1/(1+\epsilon\gamma)$. Thus, it is inferred that the nontrivial solutions correspond to helices which exist in the upper and lower limits

$$0 < m^2 < 4(1+\epsilon\gamma). \quad (4.43)$$

As $\cos\theta$ is an even function, if θ is a real solution then $-\theta$ is also a real solution, so helices still exist in chiral pairs. It should be noted that when $\epsilon\gamma$ is small the equation has two imaginary roots and a single real root. The condition for a cubic equation to have three real roots can be derived from Cardano's method [74]. For the cubic (4.42) the condition is

$$\left(1-\frac{1}{3}\frac{1}{\epsilon\gamma}\right)^3/27+\left(\frac{1}{\epsilon\gamma}\right)^2\left(\frac{2}{27}\left(\frac{1}{\epsilon\gamma}\right)^2+\frac{2}{3}-m^2\right)^2/4\geq 0. \tag{4.44}$$

At some values of $\epsilon\gamma$ large the cubic polynomial (4.42) will have three real roots and so three possible helices.

Following the procedure from the previous section, nontrivial solutions can be found from the integral

$$s=\int_{u(0)}^{u(s)}\frac{\mathrm{d}u}{\sqrt{2\left(h-u\left(u\epsilon\gamma/2+1\right)/m^2\right)\left(1-u^2\right)-\left(\alpha-\beta u\right)^2}}. \tag{4.45}$$

For homoclinic solutions emanating from the saddle at the origin, from the Hamiltonian (4.40) the nondimensional energy-density is given by

$$h=\frac{1}{m^2}\left(1+\frac{\epsilon\gamma}{2}\right)$$

which, along with the torque condition $\alpha=\beta=1$, yields the integral

$$s=\frac{m}{\sqrt{\epsilon\gamma}}\int_{u(0)}^{u(s)}\frac{\mathrm{d}u}{(1-u)\sqrt{f\left(u\right)}},\quad\text{where}\quad f\left(u\right)=u^2+2u\left(1+\frac{1}{\epsilon\gamma}\right)+1+\frac{2}{\epsilon\gamma}-\frac{m^2}{\epsilon\gamma}.$$

The quadratic $f\left(u\right)$ has roots

$$u_\pm=-\left(1+\frac{1}{\epsilon\gamma}\right)\pm\frac{1}{\epsilon\gamma}\sqrt{1+\epsilon\gamma m^2},$$

Substituting (4.43) into the roots of the quadratic gives the bounds

$$-\left(3+\frac{1}{2\epsilon\gamma}\right)<u_-<-\left(1+\frac{2}{\epsilon\gamma}\right)\quad\text{and}\quad-1<u_+<1. \tag{4.46}$$

Thus the roots are distinct. In the limit of small extensibility, that is $\epsilon\gamma m^2\ll 1$

$$\begin{aligned}u_+&=\frac{m^2}{2}-1-\frac{1}{8}\left(\epsilon\gamma m^2\right)^2+\frac{1}{16}\left(\epsilon\gamma m^2\right)^3+\mathcal{O}\left(\epsilon^4\right),\\ u_-&=-1-\frac{m^2}{2}-\frac{2}{\epsilon\gamma}+\frac{1}{8}\left(\epsilon\gamma m^2\right)^2-\frac{1}{16}\left(\epsilon\gamma m^2\right)^3+\mathcal{O}\left(\epsilon^4\right).\end{aligned}$$

The limits of integration become

$$s = \frac{m}{\sqrt{\epsilon\gamma}} \int_{u_+}^{u(s)} \frac{\mathrm{d}u}{(1-u)\sqrt{(u+u_-)(u-u_+)}}.$$

On the substitution $u(s) = -u_- + (u_- + u_+)\cosh^2 z(s)$ the integral becomes

$$s = \frac{2m}{(1+u_-)\sqrt{\epsilon\gamma}} \int_0^{z(s)} \frac{\mathrm{d}z}{1 - k\cosh^2 z}, \quad \text{with} \quad k = \frac{u_- + u_+}{1+u_-}. \tag{4.48}$$

From the bounds on the roots of the quadratic $f(u)$ given in equation (4.46) it is evident that $k > 1$ for all parameter values. Thus, the integral is given by

$$\int \frac{\mathrm{d}z}{1 - k\cosh^2 z} = \frac{-2}{\sqrt{k^2-1}} \tan^{-1}\left(\sqrt{\frac{k+1}{k-1}} \tanh\frac{z}{2}\right). \tag{4.49}$$

Hence, homoclinic solutions are given by

$$\cos\theta = u_- + (u_+ + u_-)\cosh^2\left(2\tanh^{-1}\left(\sqrt{\frac{k-1}{k+1}}\tan\left(\frac{-s(1+u_-)\sqrt{\epsilon\gamma(k^2-1)}}{4m}\right)\right)\right), \tag{4.50}$$

$$p_\theta = \theta'. \tag{4.51}$$

In the limit of $\epsilon \to 0$ the Kirchhoff homoclinic solution (4.38) is recovered. The evolutions of the Euler angles and their conjugates are displayed in figures 4.2 and 4.3 in blue.

4.4 Nonintegrable Perturbations

In this section the perturbations of anisotropy and initial curvature [23, 95] are shown to destroy integrability through the loss of the Lagrange integral p_ϕ. In both cases the constitutive relations change but the force and moment balance remain the same. Thus, the Casimirs (3.29) remain and hence the reduction to a canonical system holds. Both cases have been studied before but in a different formulation using Deprit variables [64, 70].

The Hamiltonian system now takes the general form

$$\mathcal{H}_\epsilon(\theta, \phi, p_\theta, p_\phi, p_\psi) = \mathcal{H}_0(\theta, p_\theta, p_\phi, p_\psi) + \varepsilon\mathcal{H}_1(\theta, \phi, p_\theta, p_\phi, p_\psi),$$

where the unperturbed Hamiltonian is given by (4.20), the equilibrium point (4.27) from which the unperturbed homoclinic orbit (4.38) emanates from is a hyperbolic saddle and the frequency of the angle ϕ in the unperturbed case is given by

$$\omega_0 = \frac{\partial \mathcal{H}_0}{\partial p_\phi} = \nu + \frac{2}{m^2 + (4+m^2)\tanh^2\left(\dfrac{\sqrt{4+m^2}}{2m}s\right)}.$$

Thus if $\nu \geq 0$ then $\omega_0 \geq \delta > 0$ for a small, fixed δ. Thus, Mel'nikov's method, as described in §2.2, may be applied.

The partial derivatives of the unperturbed Hamiltonian and angular frequency evaluated at the (nondimensional) homoclinic energy level when $p_\psi = p_\phi = 1$ are given by

$$\frac{\partial \mathcal{H}_0}{\partial \theta} = \frac{\sin\theta}{(1+\cos\theta)^2} - \frac{\sin\theta}{m^2}, \quad \frac{\partial \mathcal{H}_0}{\partial p_\theta} = p_\theta, \quad \frac{\partial \omega_0}{\partial \theta} = \frac{\sin\theta}{(1+\cos\theta)^2} \quad \text{and} \quad \frac{\partial \omega_0}{\partial p_\theta} = 0.$$

4.4.1 Anisotropy

When the rod is linearly elastic, unshearable, inextensible, initially straight and anisotropic the hyperelastic function is given by

$$\mathcal{W}(\mathsf{u}) = \frac{1}{2}B_1 u_1^2 + \frac{1}{2}B_2 u_1^2 + \frac{1}{2}C u_3^2. \tag{4.52}$$

The nondimensional Hamiltonian is given by

$$\mathcal{H}_\rho = \frac{1}{2}p_\theta^2 + \frac{1}{2}\left(\frac{p_\psi - p_\phi\cos\theta}{\sin\theta}\right)^2 + \frac{1}{2}(1+\nu)\,p_\phi^2 + \frac{\cos\theta}{m^2} + \frac{1}{2}\rho\left(p_\theta\sin\phi - \cos\phi\left(\frac{p_\psi - p_\phi\cos\theta}{\sin\theta}\right)\right)^2. \tag{4.53}$$

Hamilton's equations are

$$\theta' = p_\theta + \rho \sin\phi \left(p_\theta \sin\phi - \cos\phi \left(\frac{p_\psi - p_\phi \cos\theta}{\sin\theta} \right) \right), \tag{4.54a}$$

$$\begin{aligned}\phi' = (1+\nu)\, p_\phi - \cos\theta \left(\frac{p_\psi - p_\phi \cos\theta}{\sin^2\theta} \right) \\ + \rho \frac{\cos\phi \cos\theta}{\sin\theta} \left(p_\theta \sin\phi - \cos\phi \left(\frac{p_\psi - p_\phi \cos\theta}{\sin\theta} \right) \right),\end{aligned} \tag{4.54b}$$

$$\psi' = \left(\frac{p_\psi - p_\phi \cos\theta}{\sin^2\theta} \right) - \rho \frac{\cos\phi}{\sin\theta} \left(p_\theta \sin\phi - \cos\phi \left(\frac{p_\psi - p_\phi \cos\theta}{\sin\theta} \right) \right), \tag{4.54c}$$

$$\begin{aligned}p_\theta' = \frac{\sin\theta}{m^2} - \left(\frac{p_\phi - p_\psi \cos\theta}{\sin\theta} \right) \left(\frac{p_\psi - p_\phi \cos\theta}{\sin^2\theta} \right) \\ - \rho \cos\phi \left(\frac{p_\psi - p_\phi \cos\theta}{\sin^2\theta} \right) \left(p_\theta \sin\phi - \cos\phi \left(\frac{p_\phi - p_\psi \cos\theta}{\sin\theta} \right) \right),\end{aligned} \tag{4.54d}$$

$$p_\phi' = \rho \left(p_\theta \cos\phi + \sin\phi \left(\frac{p_\phi - p_\psi \cos\theta}{\sin\theta} \right) \right) \left(p_\theta \sin\phi - \cos\phi \left(\frac{p_\phi - p_\psi \cos\theta}{\sin\theta} \right) \right), \tag{4.54e}$$

$$p_\psi' = 0. \tag{4.54f}$$

Expressing $\phi(s) = \bar{\phi}(s) + \phi_0$, the perturbation to the Hamiltonian is

$$\begin{aligned}\mathcal{H}_1 = \frac{1}{2}\cos 2\phi_0 \left(\cos 2\bar{\phi} \left(p_\theta^2 + \frac{1-\cos\theta}{1+\cos\theta} \right) - p_\theta \sin 2\bar{\phi} \left(\frac{1-\cos\theta}{\sin\theta} \right) \right) \\ - \frac{1}{2}\sin 2\phi_0 \left(\sin 2\bar{\phi} \left(p_\theta^2 + \frac{1-\cos\theta}{1+\cos\theta} \right) + p_\theta \cos 2\bar{\phi} \left(\frac{1-\cos\theta}{\sin\theta} \right) \right) \\ - \frac{1}{2}p_\theta^2 + \frac{1}{2}\left(\frac{1-\cos\theta}{1+\cos\theta} \right)\end{aligned} \tag{4.55}$$

where $p_\psi = p_\phi = 1$. The partial derivatives of the perturbation are given by

$$\begin{aligned}\frac{\partial \mathcal{H}_1}{\partial \theta} = \frac{1}{2} p_\theta \left(\cos 2\phi_0 \cos 2\bar{\phi} - \sin 2\phi_0 \sin 2\bar{\phi} - 1 \right) \\ + \left(1 - \frac{1}{2}\left(\cos 2\phi_0 \cos 2\bar{\phi} - \sin 2\phi_0 \sin 2\bar{\phi} \right) \right) \left(\frac{1-\cos\theta}{(1+\cos\theta)\sin\theta} \right),\end{aligned} \tag{4.56a}$$

$$\begin{aligned}\frac{\partial \mathcal{H}_1}{\partial p_\theta} = \frac{1}{2} p_\theta \left(\cos 2\phi_0 \cos 2\bar{\phi} - \sin 2\phi_0 \sin 2\bar{\phi} - 1 \right) \\ - \frac{1}{2}\left(\sin 2\phi_0 \cos 2\bar{\phi} - \cos 2\phi_0 \sin 2\bar{\phi} \right) \left(\frac{1-\cos\theta}{\sin\theta} \right).\end{aligned} \tag{4.56b}$$

Hence the first order Mel'nikov integral is given by

$$\mathcal{M}_h^{(1)}(\phi_0) = \sin\phi_0 \int_{-\infty}^{+\infty} A(s)\, \mathrm{d}s + \cos\phi_0 \int_{-\infty}^{+\infty} B(s)\, \mathrm{d}s + \int_{-\infty}^{+\infty} C(s)\, \mathrm{d}s$$

where

$$A(s) = \frac{1}{2}\left(\frac{1+\cos\theta}{m^2} + \frac{1}{1+\cos\theta} + p_\theta^2\right)\left(p_\theta \sin\theta \sin 2\bar{\phi} - (1-\cos\theta)\cos 2\bar{\phi}\right) + \frac{1}{2}p_\theta^2 \cos\theta\left(\cos 2\bar{\phi} + \sin 2\bar{\phi}\left(\frac{1-\cos\theta}{\sin\theta}\right)\right), \tag{4.57a}$$

$$B(s) = \frac{1}{2}\left(\frac{1+\cos\theta}{m^2} + \frac{1}{1+\cos\theta} + p_\theta^2\right)\left(p_\theta \sin\theta \cos 2\bar{\phi} - (1-\cos\theta)\sin 2\bar{\phi}\right) + \frac{1}{2}p_\theta^2 \cos\theta\left(\sin 2\bar{\phi} - \cos 2\bar{\phi}\left(\frac{1-\cos\theta}{\sin\theta}\right)\right), \tag{4.57b}$$

$$C(s) = \frac{1}{2}p_\theta\left(\frac{1-\cos\theta}{\sin\theta} + \frac{1+\cos\theta}{m^2} + \frac{1}{1+\cos\theta} + p_\theta^2\right). \tag{4.57c}$$

Then the condition for simple zeroes is given by

$$\left|\frac{c}{\sqrt{a^2+b^2}}\right| < 1$$

where

$$a = \int_{-\infty}^{\infty} A(s)\,\mathrm{d}s, \quad b = \int_{-\infty}^{\infty} B(s)\,\mathrm{d}s \quad \text{and} \quad c = \int_{-\infty}^{\infty} C(s)\,\mathrm{d}s.$$

In figure 4.4.1 the first order Mel'nikov integral $\mathcal{M}_h^{(1)}(\phi_0)$ is evaluated for a variety of values for m.

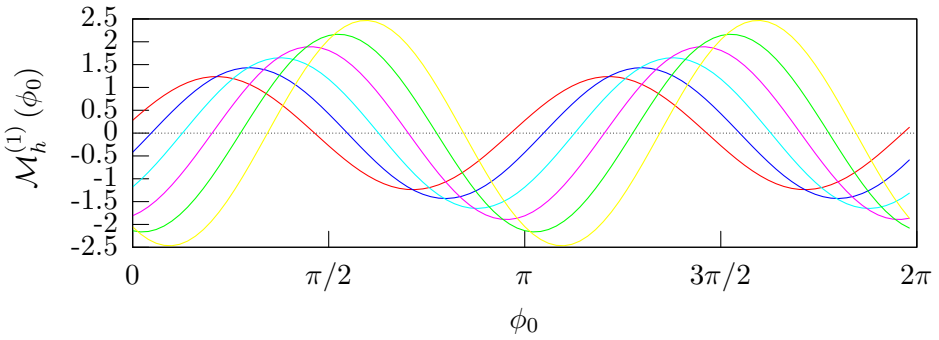

Figure 4.4: Mel'nikov integral (4.57) for anisotropic rod with $\nu = 1/3$ and $m = 1.70$ (red), 1.72 (blue), 1.74 (cyan), 1.76 (magenta), 1.78 (yellow), 1.80 (green) at the nondimensional homoclinic energy level. From the figure it is clear that the Mel'nikov integral has simple zeroes and that via the construction of a Bernoulli shift map, the system will become sensitive to initial conditions. In the context of rod theory this means that multimodal rod configurations are possible.

4.4.2 Initial Curvature

For an initially curved isotropic rod the hyperelastic function takes the form

$$\mathcal{W}(\mathsf{u}) = \frac{1}{2}B_1 u_1^2 - u_0 u_1 + \frac{1}{2}B_1 u_2^2 + \frac{1}{2}C u_3^2.$$

In the initially curved case the nondimensionalised Hamiltonian is given by

$$\mathcal{H}_{\kappa_0} = \frac{1}{2}p_\theta^2 + \frac{1}{2}\left(\frac{p_\psi - p_\phi\cos\theta}{\sin\theta}\right)^2 + \frac{1}{2}(1+\nu)\,p_\phi^2 + \frac{\cos\theta}{m^2} + \frac{1}{2}\kappa_0\left(p_\theta\sin\phi - \cos\phi\left(\frac{p_\psi - p_\phi\cos\theta}{\sin\theta}\right)\right). \tag{4.58}$$

Remark 4.4.1. *It is interesting to observe that the perturbation for initial curvature is the square root of the perturbation for anisotropy.*

The governing equations are

$$\theta' = p_\theta + \kappa_0\sin\phi, \tag{4.59a}$$

$$\phi' = (1+\nu)\,p_\phi - \cos\theta\left(\frac{p_\psi - p_\phi\cos\theta}{\sin^2\theta}\right) + \kappa_0\frac{\cos\theta\cos\phi}{\sin\theta}, \tag{4.59b}$$

$$\psi' = \left(\frac{p_\psi - p_\phi\cos\theta}{\sin^2\theta}\right) - \kappa_0\frac{\cos\phi}{\sin\theta}, \tag{4.59c}$$

$$p_\theta' = \frac{\sin\theta}{m^2} - \left(\frac{p_\phi - p_\psi\cos\theta}{\sin\theta}\right)\left(\frac{p_\psi - p_\phi\cos\theta}{\sin^2\theta}\right) - \kappa_0\cos\phi\left(\frac{p_\phi - p_\psi\cos\theta}{\sin^2\theta}\right), \tag{4.59d}$$

$$p_\phi' = -\kappa_0\left(p_\theta\cos\phi + \sin\phi\left(\frac{p_\psi - p_\phi\cos\theta}{\sin\theta}\right)\right), \tag{4.59e}$$

$$p_\psi' = 0. \tag{4.59f}$$

The perturbation to the Hamiltonian is given by

$$\mathcal{H}_1 = \sin\phi_0\left(p_\theta\cos\bar{\phi} + \sin\bar{\phi}\left(\frac{1-\cos\theta}{\sin\theta}\right)\right) + \cos\phi_0\left(p_\theta\sin\bar{\phi} - \cos\bar{\phi}\left(\frac{1-\cos\theta}{\sin\theta}\right)\right)$$

when $p_\psi = p_\phi = 1$. The partial derivatives of the perturbation to the Hamiltonian are given by

$$\frac{\partial\mathcal{H}_1}{\partial\theta} = \frac{\sin\phi_0\sin\bar{\phi} - \cos\phi_0\cos\bar{\phi}}{1+\cos\theta} \quad \text{and} \quad \frac{\partial\mathcal{H}_1}{\partial p_\theta} = \sin\phi_0\cos\bar{\phi} + \sin\bar{\phi}\cos\phi_0. \tag{4.60}$$

It follows from the reversibilities of the homoclinic solutions that the first order Mel'nikov function can be simplified over the half range

$$\mathcal{M}_h^{(1)}(\phi_0) = 2\cos\phi_0 \int_0^{+\infty} \sin\bar{\phi}\sin\theta\left(\frac{1+\cos\theta}{m^2} + \frac{1}{1+\cos\theta} + p_\theta^2\right) \mathrm{d}s + 2\sin\phi_0 \int_0^{+\infty} p_\theta \cos\theta \sin\bar{\phi}\,\mathrm{d}s.$$

In contrast to the anisotropic case, there is no constant term in the Mel'nikov function, there are no bounds on the existence of transverse intersections of the stable and unstable manifolds.

In figure 4.4.2 Poincaré sections which show the loss of integrability are presented. The Poincaré sections were computed by fixing the integrals $p_\psi = 1$, $\mathcal{H} = h = 1/m^2$ and placing the initial conditions near the (unperturbed) saddle: $p_\theta(0) = \theta(0) = 10^{-3}$ with $p_\phi(0) = 1$ and solving $\mathcal{H}_0(\theta, p_\theta, \phi, p_\phi) = h$ for $\phi(0)$ on the nondimensional homoclinic energy level when $m = 1.7$. The section itself was defined by

$$\Sigma^0 = \{\cos\phi = 0 \,:\, \theta,\, p_\phi,\, p_\theta \in \mathbb{R}\}.$$

4.5 Consequences of Spatial Chaos

The construction of a Poincaré section is a little more involved of that for the Duffing oscillator and follows the sections constructed by Devaney in [32]. Firstly let $\Sigma^{u,s}$ be general sections transverse to the flow of the unstable and stable manifolds respectively, then consider sections on the homoclinic energy level $\Sigma_h^{u,s} = \Sigma_{u,s} \cap \mathcal{H}^{-1}(h)$. Now let $\sigma^{u,s}$ denote the intersection of the local stable manifold with $\Sigma_h^{u,s}$. So $\sigma^{u,s}$ are the central circles of the solid tori $\Sigma_0^{u,s}$. For a homoclinic orbit $\boldsymbol{\gamma}$ let $q^{u,s} = \boldsymbol{\gamma} \cap \sigma^{u,s}$.

Now define the Poincaré map Φ as the composition of two maps Φ_0 and Φ_1. Let $D^{u,s}$ be discs in $\Sigma_0^{u,s}$ centred at the points $q^{u,s}$. As the discs are on the homoclinic energy surface and are tranverse to the flow the energy level there exists a Poincaré section $\Phi_1 : D^u \mapsto D^s$. If D^s is sufficiently small, then a Poincaré map $\Phi_0 : D^s - \sigma^s \mapsto \Sigma_0^u$ also

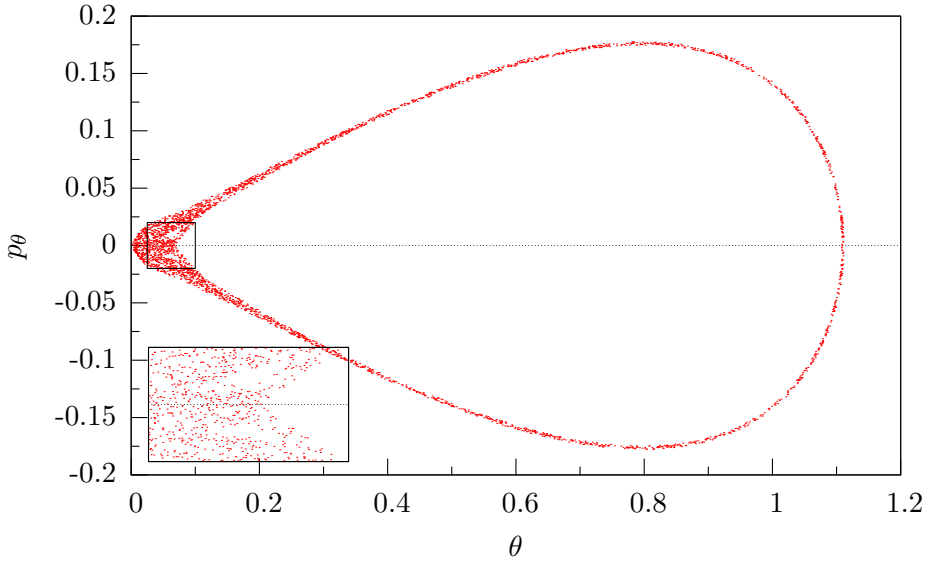

(a) $\kappa_0 = 0.001$

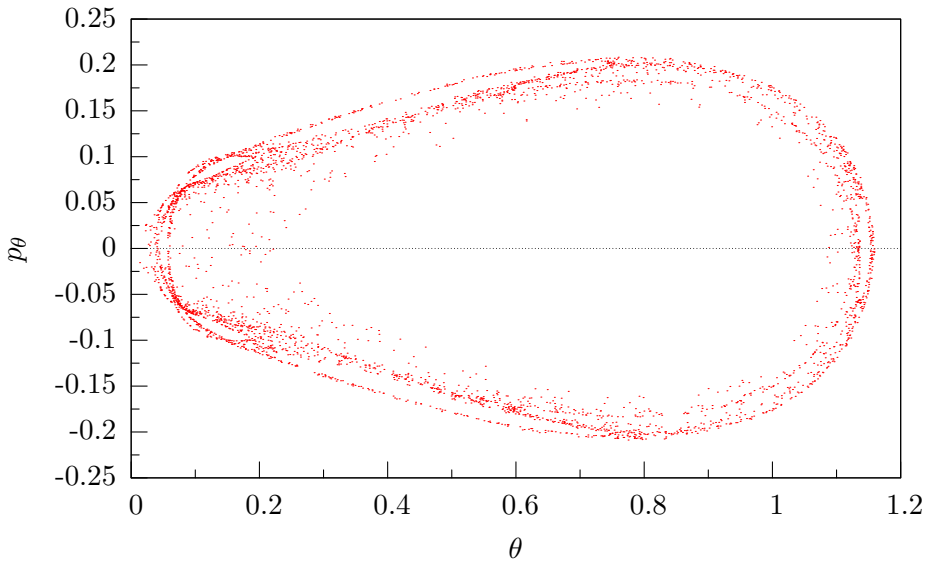

(b) $\kappa_0 = 0.01$

Figure 4.5: Poincaré sections for initially curved rods on the unperturbed nondimensional homoclinic energy level $h = 1/m^2$ when $m = 1.7$ for varying levels of κ_0 on the hypersection determined by $\cos\phi = 0$. The figures illustrates a consequence of simple zeroes of the Mel'nikov function as the lose of integrability which occurs for $\kappa_0 \neq 0$ through the typical plots, referred to as "stochastic layers" in [45, pg. 222], associated with the Poincaré-Birkhoff theorem.

exists. Let the Poincaré map for orbits $\boldsymbol{\gamma}$ on the local transverse sections D^s be defined by $\Phi : \Phi_1 \circ \Phi_0$.

In a manner described in §2.3 and using the Poincaré section Φ then, by the Smale-Birkhoff theorem there then exists a compact, invariant, hyperbolic set $\Lambda \subset \Sigma$ on which the Poincaré map is topologically conjugate to a Bernoulli shift.The physical implications of the existence of horseshoes on the Poincaré section of the perturbed homoclinic are that multi-modal configurations, with extreme sensitivity to initial conditions, now exist when either $\rho \neq 0$ or $\kappa_0 \neq 0$.

For each reversibility there are two disjoint closed sets in the unperturbed phase space with a pair of homoclinic orbits acting as a separatrix between right- and left-handed solutions, see figure 4.1(a) for an illustration of the unperturbed phase space. The dynamics in the vicinity of the homoclinic tangency however are spatially chaotic. Now the perturbed solutions may pass through the regions in any prescribed sequence. The sets can be chosen to lie in the vicinity of the saddle point; in the event of a multi-modal homoclinic orbit, this implies that the perturbed solution passes through different members of the set in any order. Thus the Poincaré map on the level set of the perturbed homoclinic orbit is conjugate to a Bernoulli shift on two symbols. Consequently a multiplicity of solutions with an arbitrary large number of localised modes now exist. To first order non-periodic orbits in the neighbourhood of the transverse homoclinic orbit are quasi-random superpositions of single unperturbed homoclinic orbit.

The computation and continuation of multimodal solutions between two hyperbolic fixed points is well known, so detail is presented in appendix §B.2 and §B.3 and can be seen in figures 4.6, 4.7(a) and 4.7(b). Homoclinic orbits of the nonintegrable Kirchhoff rod have a well defined bifurcation structure determined by accumulation and coalescence rules [23, 95] which are described in detail in §B.5.

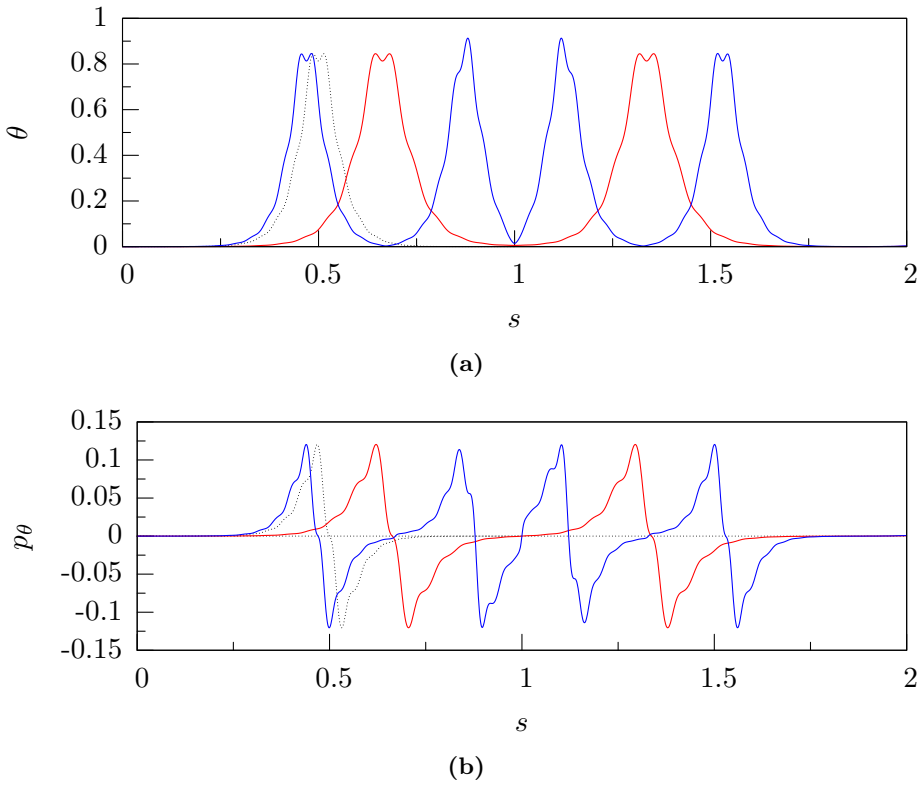

Figure 4.6: The evolution of the Euler angle θ and its conjugate p_θ, with respect to the normalised arclength for the bimodal (red) and quadmodal (blue) homoclinic orbits when $m = 1.7$, $\nu = 1/3$ and $\rho = 1/4$. For comparison the primary (dotted) homoclinic orbit is displayed over the half range. Note that the evolutions of the both θ and p_θ in this case are different from the integrable primary homoclinic orbit displayed in figure 4.2.

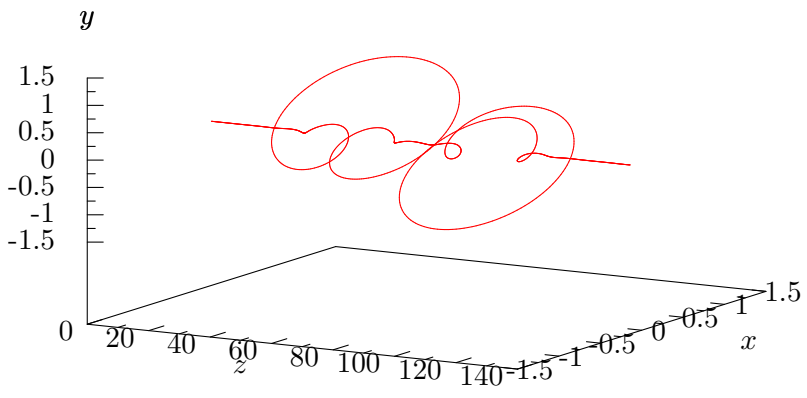

(a)

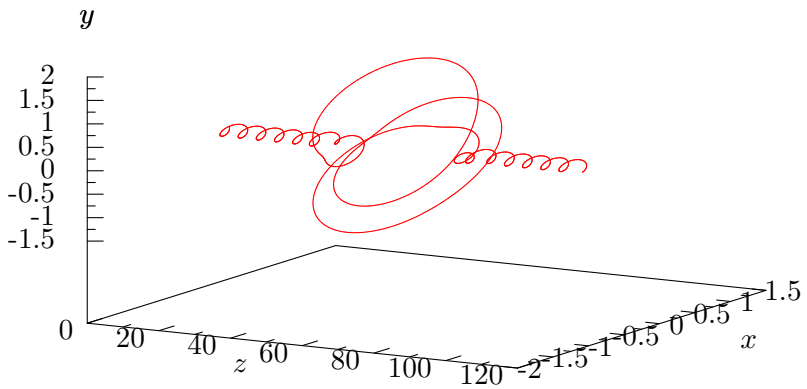

(b)

Figure 4.7: As a consequence of the transverse intersection of the perturbed stable and unstable manifolds, anisotropic or initially curved rod will admit a multiplicity of multimodal localised solutions. Subfigure 4.7(a) displays a R_1-reversible bimodal homoclinic orbit, that is a localised configuration essentially comprised of two primary localisations, labelled $(P_1, 0, P_2)$, for an anisotropic rod when $\rho = 1/4$, $\nu = 1/3$, $m = 1.70$ and $\kappa_0 = 0$. The shooting parameters are given by $\delta = 3.339928$ and $\mathcal{T} = 70.86311$. Subfigure 4.7(b) displays a R_2-reversible bimodal (P_1, P_1) homoclinic orbit for an initially curved rod when $\rho = 0$, $\nu = 1/3$, $m = 1.70$ and $\kappa_0 = 0.1$. The shooting parameters are given by $\delta = 1.27835$ and $\mathcal{T} = 50.3568$. For detail on the computation of such solutions, please see appendix §B.

Chapter 5

Spatial Chaos in Extensible Rods in a Uniform Magnetic Field

In this chapter the nine-dimensional noncanonical equilibrium equations for a rod in a magnetic field are reduced by the three Casimirs to a six-dimensional canonical system using Euler Angles. In the integrable case the reduction gives a four-dimensional canonical system with a first integral and a Hamiltonian. By specifying an energy level to constrain the orbits to a surface in three-dimensions, Poincaré sections yield closed curves. By Mel'nikov's method it is shown that for an extensible rod the presence of the magnetic field destroys complete integrability through the loss of a first integral, illustrated by Poincaré sections, in contrast to the regular dynamics of the integrable case.

5.1 Reformulation

For clarity when describing the family of rod models, in §3 the governing equations for a rod in a uniform magnetic field were presented in terms of the three field variables $(\mathsf{m}, \mathsf{n}, \mathsf{B})$. However, in order to apply a suitable perturbation to a canonical Hamiltonian system it is necessary to express the magnetic field in terms of the unit vector e_3 and a bifurcation parameter relating to the magnitude of the magnetic effects $\lambda = |\boldsymbol{B}|$. Thus

the governing equations (3.36) can be expressed as

$$\begin{pmatrix} \mathsf{m} \\ \mathsf{n} \\ \mathsf{e}_3 \end{pmatrix}' = \begin{pmatrix} \hat{\mathsf{m}} & \hat{\mathsf{n}} & \hat{\mathsf{e}}_3 \\ \hat{\mathsf{n}} & \lambda\hat{\mathsf{e}}_3 & 0 \\ \hat{\mathsf{e}}_3 & 0 & 0 \end{pmatrix} \begin{pmatrix} \mathsf{u} \\ \mathsf{v} \\ 0 \end{pmatrix}. \tag{5.1}$$

The Casimirs of the system (3.40) are now given by

$$C_1 = \frac{1}{2}\mathsf{n}\cdot\mathsf{n} + \lambda\mathsf{m}\cdot\mathsf{e}_3, \tag{5.2a}$$

$$C_2 = \mathsf{n}\cdot\mathsf{e}_3, \tag{5.2b}$$

$$C_3 = \mathsf{e}_3\cdot\mathsf{e}_3. \tag{5.2c}$$

The integrals (3.41), conditionally dependent on $B := B_1 = B_2$ and $J = K = H = 0$ are now given by

$$I_1 = m_3, \tag{5.3a}$$

$$I_2 = \mathsf{m}\cdot\mathsf{n} + B\lambda e_{33}. \tag{5.3b}$$

5.2 Reduction to a Canonical System

In this section the three Casimirs (5.2) are used to reduce the nine-dimensional non-canonical Hamiltonian system (5.1) to a six-dimensional canonical Hamiltonian system using Euler angles. This is possible (at least locally) provided the structure matrix (3.36) is of constant rank everywhere [76, §6.2]. The reduction is performed by constructing a coordinate transformation from the nine coordinates $(\mathsf{m}, \mathsf{n}, \mathsf{e}_3)$ to three Euler angles $q = (\theta, \psi, \phi)$ and their canonical momenta $p = (p_\theta, p_\psi, p_\phi)$. The reduction follows [90] but here the system is shown to be canonical. As it happens, the transformation is only canonical subject to a non-alignment condition. The aligned case is also of interest and is treated in §5.2.2.

If the magnetic field is directed along the $\boldsymbol{e}_3$ vector of the fixed coordinate system, in the director frame it can be parameterised as

$$\mathsf{e}_3(q) = R(q)\,k = \begin{pmatrix} -\sin\theta\cos\phi \\ \sin\theta\sin\phi \\ \cos\theta \end{pmatrix}, \tag{5.4}$$

where $k = (0,0,1)^T$ and $R(q)$ is the rotation matrix (4.2).

On inserting the Euler angles into the strains (3.5) and using the constitutive relations (3.8) and the orthonormality of the directors, the moments are parametrised by (4.12)

$$\begin{aligned} m_1 &= p_\theta \sin\phi - \cos\phi \left(\frac{p_\psi - p_\phi \cos\theta}{\sin\theta} \right), \\ m_2 &= p_\theta \cos\phi + \sin\phi \left(\frac{p_\psi - p_\phi \cos\theta}{\sin\theta} \right), \\ m_3 &= p_\phi. \end{aligned}$$

The moments can be expressed in the compact matrix form as $\mathsf{m} = Lp$ (see (4.11)). The force may be written as

$$\mathsf{n}(q,p) = R(q)\, v(q,p),$$

for some non-constant triple v. Decomposing v into components parallel and perpendicular to the magnetic field yields

$$v(q,p) = v_\perp(q,p)\, i_\perp + v_\parallel(q,p)\, i_\parallel,$$

where $i_\parallel$ and $i_\perp$ are the unit triples parallel and perpendicular to k respectively. Thus (5.2b) yields

$$\begin{aligned} C_2 = \mathsf{n} \cdot \mathsf{e}_3 &= Rv \cdot Rk \\ &= v \cdot \left(R^T R\right) k \\ &= v_\parallel. \end{aligned} \tag{5.6}$$

Hence the component of the force in the rod parallel to the magnetic field is constant. Furthermore, from (5.2c)

$$\begin{aligned} C_1 = \frac{1}{2}\mathsf{n} \cdot \mathsf{n} + \lambda \mathsf{m} \cdot \mathsf{e}_3 &= \frac{1}{2} Rv \cdot Rv + \lambda Lp \cdot Rk \\ &= \frac{1}{2} C_2^2 + \frac{1}{2} v_\perp^2 + \lambda p \cdot \left(LR^T\right) k, \end{aligned} \tag{5.7}$$

which allows expressions for $v_\perp$ as

$$\begin{aligned} v_\perp(q,p) &= \sqrt{2C_1 - C_2^2 - 2\lambda p \cdot (LR^T)\, k} \\ &= \sqrt{2C_1 - C_2^2 - 2\lambda p_\psi}, \end{aligned} \tag{5.8}$$

where, without loss of generality, the positive solution is taken. If the vector perpendicular to k is taken to be $i_\perp = (1,0,0)^T$ then

$$\begin{aligned} \mathsf{n} = C_2 &\begin{pmatrix} -\sin\theta\cos\phi \\ \sin\theta\sin\phi \\ \cos\theta \end{pmatrix} \\ &+ \sqrt{2C_1 - C_2^2 - 2\lambda p_\psi} \begin{pmatrix} \cos\theta\cos\phi\cos\psi - \sin\phi\sin\psi \\ -\cos\theta\sin\phi\cos\psi - \cos\phi\sin\psi \\ \sin\theta\cos\psi \end{pmatrix}. \end{aligned} \tag{5.9}$$

Note that this transformation is well-defined as

$$v_\perp^2 = 2C_1 - C_2^2 - 2\lambda p_\psi \geq 0. \tag{5.10}$$

In contrast to the reduction of the Kirchhoff equations, the equations (5.4), (4.12) and (5.9) give a representation of the three field variables in terms of all of the Euler angles. In order for the noncanonical bracket (3.39) to be transformed into canonical form it is necessary to verify that

$$G\mathcal{J}G^T = \bar{\mathcal{J}},$$

where $\mathcal{J}$ is the structure matrix defined in (3.36) and $\bar{\mathcal{J}}$ is the standard canonical structure matrix in $\mathbb{R}^6$ and the G is the Jacobian matrix

$$G = \frac{\partial(q,p)}{\partial(\mathsf{m},\mathsf{n},\mathsf{e}_3)}. \tag{5.11}$$

Inverting the non-canonical variables (5.4), (4.12) and (5.9) yields

$$\begin{aligned}
\theta &= \cos^{-1} e_{33},\\
p_\theta &= \frac{m_1 e_{32} - m_2 e_{31}}{\sqrt{1-e_{33}^2}},\\
\phi &= \tan^{-1}\frac{-e_{32}}{e_{31}},\\
p_\phi &= m_3,\\
\psi &= \cos^{-1}\left(\frac{n_3 - C_2 e_{33}}{\sqrt{\left(1-e_{33}^2\right)\left(2C_1 - C_2^2 - 2\lambda\left(m_1 e_{31} + m_2 e_{32} + m_3 e_{33}\right)\right)}}\right),\\
p_\psi &= \left(m_1 e_{31} + m_2 e_{32} + m_3 e_{33}\right).
\end{aligned}$$

Explicitly, the transformation matrix G is given by

$$G = \begin{pmatrix}
0 & 0 & 0 & 0 & 0 & 0 & 0 & 0 & -\sqrt{\frac{1}{1-e_{33}^2}}\\
0 & 0 & 0 & 0 & 0 & 0 & \frac{e_{32}}{e_{31}^2+e_{32}^2} & \frac{-e_{31}}{e_{31}^2+e_{32}^2} & 0\\
g_{31} & g_{32} & g_{33} & g_{34} & g_{35} & g_{36} & g_{37} & g_{38} & g_{39}\\
\frac{e_{32}}{\sqrt{1-e_{33}^2}} & \frac{-e_{31}}{\sqrt{1-e_{33}^2}} & 0 & 0 & 0 & 0 & \frac{-m_2}{\sqrt{1-e_{33}^2}} & \frac{m_1}{\sqrt{1-e_{33}^2}} & \frac{\left(m_1 e_{32} - m_2 e_{31}\right)e_{33}}{\left(1-e_{33}^2\right)^{3/2}}\\
0 & 0 & 1 & 0 & 0 & 0 & 0 & 0 & 0\\
e_{31} & e_{32} & e_{33} & 0 & 0 & 0 & m_1 & m_2 & m_3
\end{pmatrix},$$

where

$$\begin{aligned}
&g_{31} = -\frac{e_{31}\left(n_3 - C_2 e_{33}\right)}{\Delta}, \quad g_{32} = -\frac{e_{32}\left(n_3 - C_2 e_{33}\right)}{\Delta}, \quad g_{33} = -\frac{e_{33}\left(n_3 - C_2 e_{33}\right)}{\Delta},\\
&g_{34} = 0, \quad g_{35} = 0, \quad g_{36} = -\frac{1}{\Delta}, \quad g_{37} = -\frac{m_1\left(n_3 - C_2 e_{33}\right)}{\Delta}, \quad g_{38} = -\frac{m_2\left(n_3 - C_2 e_{33}\right)}{\Delta}
\end{aligned}$$

and

$$\begin{aligned}
g_{39} = &\frac{C_2\left(2C_1 - C_2^2 - 2\lambda \mathsf{m}\cdot\mathsf{e}_3\right)}{\Delta}\\
&- \frac{\left(n_3 - C_2 e_{33}\right)\left(e_{33}\left(2C_1 - C_2^2 - 2\lambda \mathsf{m}\cdot\mathsf{e}_3\right) - m_3\left(1 - e_{33}/C_2\right)\right)}{\Delta}
\end{aligned}$$

with the denominator given by

$$\Delta = \left(2C_1 - C_2^2 - 2\lambda \mathsf{m}\cdot\mathsf{e}_3\right)\sqrt{\left(1-e_{33}^2\right)\left(2C_1 - C_2^2 - 2\lambda \mathsf{m}\cdot\mathsf{e}_3\right) - \left(n_3 - C_2 e_{33}\right)^2}.$$

The non-canonical structure matrix is given by

$$\mathcal{J} = \begin{pmatrix} 0 & -m_3 & m_2 & 0 & -n_3 & n_2 & 0 & -e_{33} & e_{32} \\ m_3 & 0 & -m_1 & n_3 & 0 & -n_1 & e_{33} & 0 & -e_{31} \\ -m_2 & m_1 & 0 & -n_2 & n_1 & 0 & -e_{32} & e_{31} & 0 \\ 0 & -n_3 & n_2 & 0 & -e_{33} & e_{32} & 0 & 0 & 0 \\ n_3 & 0 & -n_1 & e_{33} & 0 & -e_{31} & 0 & 0 & 0 \\ -n_2 & n_1 & 0 & -e_{32} & e_{31} & 0 & 0 & 0 & 0 \\ 0 & -e_{33} & e_{32} & 0 & 0 & 0 & 0 & 0 & 0 \\ e_{33} & 0 & -e_{31} & 0 & 0 & 0 & 0 & 0 & 0 \\ -e_{32} & e_{31} & 0 & 0 & 0 & 0 & 0 & 0 & 0 \end{pmatrix},$$

while the canonical structure matrix is given by

$$\bar{\mathcal{J}} = \begin{pmatrix} 0 & 0 & 0 & 1 & 0 & 0 \\ 0 & 0 & 0 & 0 & 1 & 0 \\ 0 & 0 & 0 & 0 & 0 & 1 \\ -1 & 0 & 0 & 0 & 0 & 0 \\ 0 & -1 & 0 & 0 & 0 & 0 \\ 0 & 0 & -1 & 0 & 0 & 0 \end{pmatrix}.$$

The calculation can be verified using a symbolic manipulation program. The transformation is proper *provided* that $v_\perp > 0$, i.e., provided that n and e_3 are not aligned. Without this condition the necessary inverse transformation does not exist as $\Delta = 0$. Note that n and e_3 are aligned if and only if

$$2C_1 - C_2^2 = 2\lambda \mathsf{m} \cdot \mathsf{e}_3. \tag{5.12}$$

By differentiating the Casimir (5.2a) and using the governing equation (5.1) the following holds

$$2\lambda \frac{\mathrm{d}}{\mathrm{d}s}(\mathsf{m} \cdot \mathsf{e}_3) = -\frac{\mathrm{d}}{\mathrm{d}s}(\mathsf{n} \cdot \mathsf{n}) = 2\mathsf{d}_3 \cdot (\mathsf{e}_3 \times \mathsf{n}), \tag{5.13}$$

which is zero if n and e_3 are aligned. Thus the alignment condition is well defined: *if the force and the magnetic field are aligned anywhere on the rod they are aligned everywhere along the rod.* As remark 4.3.2 states, the alignment condition does not prohibit the existence of homoclinic orbits.

5.2.1 The Isotropic Case

In the isotropic case ($B := B_1 = B_2$) the Hamiltonian (3.37) reduces to

$$\mathcal{H} = \frac{1}{2B}p_\theta^2 + \frac{\left(p_\psi - p_\phi \cos\theta\right)^2}{2B\sin^2\theta} + \frac{1}{2C}p_\phi^2 + C_2\cos\theta + \sin\theta\cos\psi\sqrt{2C_1 - C_2^2 - 2\lambda p_\psi}. \tag{5.14}$$

Since this Hamiltonian does not depend on the angle ϕ the momentum $p_\phi = m_3$ is a constant. The isotropic Hamiltonian still has rotational symmetry about the $\boldsymbol{d}_3$ axis. Note that the rod is no longer rotationally symmetric about the axis $\boldsymbol{e}_3$. Also note that the effect of the magnetic field, which previously was encoded in the Casimirs is now in the Hamiltonian.

The additional integral (3.41b) in canonical variables reads

$$\mathcal{I} = \lambda B\cos\theta + C_2 p_\psi - \sqrt{2C_1 - C_2^2 - 2\lambda p_\psi}\left(p_\theta\sin\psi - \cos\psi\left(\frac{p_\phi - p_\psi\cos\theta}{\sin\theta}\right)\right), \tag{5.15}$$

rendering the system completely integrable.

Hamilton's equations are

$$\theta' = \frac{p_\theta}{B}, \tag{5.16a}$$

$$\psi' = \frac{(p_\psi - p_\phi\cos\theta)}{B\sin^2\theta} - \frac{\lambda\cos\psi\sin\theta}{\sqrt{2C_1 - C_2^2 - 2\lambda p_\psi}}, \tag{5.16b}$$

$$p_\theta' = \frac{\left(p_\psi\cos\theta - p_\phi\right)\left(p_\psi - p_\phi\cos\theta\right)}{B\sin^3\theta} + C_2\sin\theta - \cos\theta\cos\psi\sqrt{2C_1 - C_2^2 - 2\lambda p_\psi}, \tag{5.16c}$$

$$p_\psi' = \sin\theta\sin\psi\sqrt{2C_1 - C_2^2 - 2\lambda p_\psi}. \tag{5.16d}$$

Helical solutions about $\boldsymbol{e}_3$ have fixed point solutions $\theta = \theta^* \neq 0$ and $\psi' = \psi^* \neq 0$. On substituting the conditions in to the governing equations then (5.16d) is separable

$$p_\psi' = -\sin\theta^*\sin\left(\psi^* s + \psi_0\right)\sqrt{2C_1 - C_2^2 - 2\lambda p_\psi} \tag{5.17}$$

and can be integrated so that an expression for p_ψ can be found

$$p_\psi(s) = \frac{2C_1 - C_2^2}{2\lambda} - \frac{1}{2\lambda}\left(\sqrt{2C_1 - C_2^2 - 2\lambda p_\psi(0)} + \frac{\lambda}{\psi^*}(1-\sin\theta^*)\cos(\psi^* s + \psi_0)\right)^2 \tag{5.18}$$

Inserting the result into (5.16b) yields

$$\psi^* = \frac{2C_1 - C_2^2 - 2\lambda p_\phi \cos\theta}{2\lambda \sin^2\theta^*} - \frac{\psi^*\sqrt{2C_1 - C_2^2 - 2\lambda p_\psi(0)} + \lambda(1-\sin\theta^*)\cos(\psi^* s + \psi_0)}{2\lambda\psi^* \sin^2\theta^*} + \frac{\lambda \sin\theta^* \cos\psi^* s}{2\sqrt{\sqrt{2C_1 - C_2^2 - 2\lambda p_\psi(0)} + \frac{\lambda}{\psi^*}(1-\sin\theta^*)\cos(\psi^* s + \psi_0)}}$$

which does not permit solutions for $\psi' = \psi^*$ and $\theta^* \neq 0$. Thus helices can not be expressed in this parameterisation.

By fixing the level sets of the integrals $\mathcal{I}$ and $\mathcal{H}$, solution of the four-dimensional Hamiltonian system (5.16) exist in a three-dimensional space. Through Poincaré sections closed curves can be computed in the plane. Figure 5.1 shows Poincaré sections for

$$\Sigma^\alpha = \{\cos\psi = \alpha \,:\, \theta,\, p_\psi,\, p_\theta \in \mathbb{R}\} \tag{5.19}$$

with $\alpha = 0.3$, 0.5, 0.7 and 0.9 for a variety of values of $\mathcal{H}$ when the integral is fixed as $\mathcal{I} = 1.00995$. The self intersection is an artifact of the projection onto the (θ, p_θ) plane.

Remark 5.2.1. *The situation is comparable to the Kovalevskaya case for the Kirchhoff rod* (4.24) *in that the Euler angles reduce the system to a four-dimensional canonical Hamiltonian system with a first integral. Figure 5.1 gives insight into the topology of the energy surfaces. If a 'comprehensive Poincaré section' as in [37, Figure 2] could be created which distinguishes between configurations, then in the four-dimensional phase space the integrals* (5.14) *and* (5.15) *could be associated with action integrals. Thus energy surfaces could be constructed in the space of action variables.*

5.2.2 Alignment of Force and Field – the Superintegrable Case

It has already been shown that if force and field are aligned anywhere then they are aligned everywhere. From (3.34) it follows that $\boldsymbol{d}_3 \times \boldsymbol{e}_3 = \boldsymbol{0} = \boldsymbol{d}_3 \times \boldsymbol{n}$, i.e., $\boldsymbol{n}$ is aligned

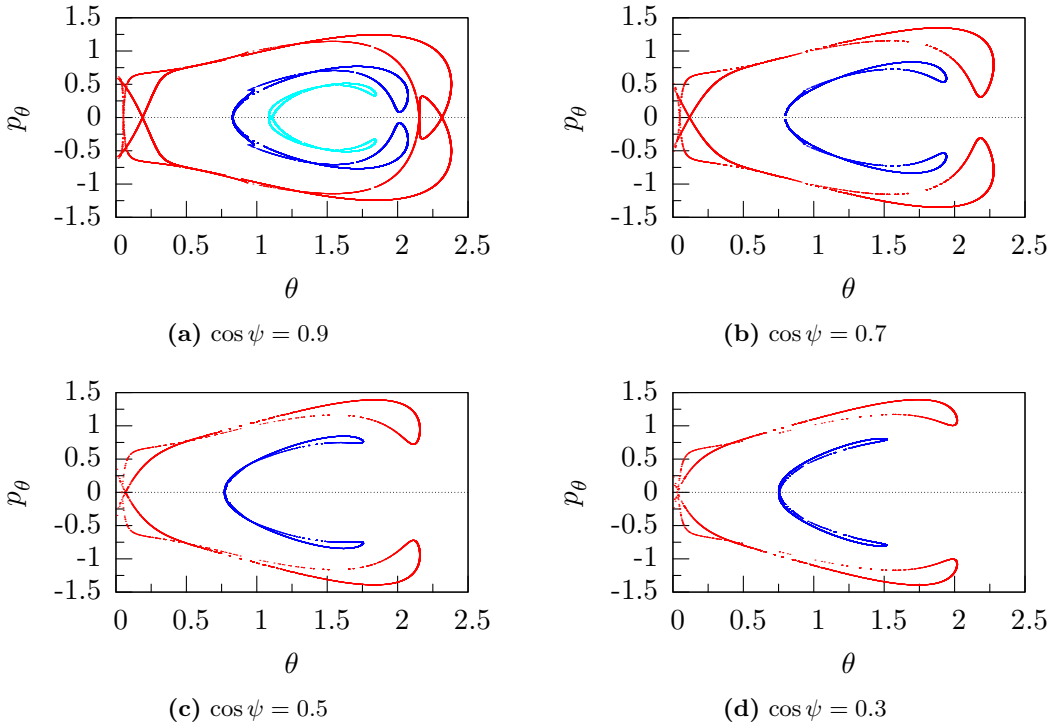

(a) $\cos\psi = 0.9$ **(b)** $\cos\psi = 0.7$

(c) $\cos\psi = 0.5$ **(d)** $\cos\psi = 0.3$

Figure 5.1: Poincaré plots for (5.16) with various sections. In each diagram orbits are displayed for energy levels $\mathcal{H} = 1.90$ (red), 1.50 (blue) and 1.37 (cyan), while $\mathcal{I} = 1.00995$, $\lambda = 0.1$, $C_1 = 1.02$, $C_2 = C_3 = p_\phi = 1$ and $C/B = 3/4$.

with $\boldsymbol{d}_3$. If this is the case it then follows from the governing equation (5.1) that $\boldsymbol{m}$ is constant also. This means that solutions are twisted straight rods. Hence the aligned case is maximally superintegrable with solutions lying on one-tori. The corresponding result holds for the rod in a non-uniform magnetic field (3.44). In this case if the magnetic field and the curvature of the field are aligned anywhere on the rod they are aligned everywhere along the rod and hence aligned along d_3. Note that this conclusion holds irrespective of whether the rod is isotropic or not.

5.3 The Application of Mel'nikov's Theory

It has been shown in §4.3.1 and §3.3.3 that both an isotropic, extensible Kirchhoff rod and an isotropic, inextensible rod in a magnetic field are completely integrable. A

condition on both the Lax pair (3.47) and the integral (3.41b) is that the rod must be inextensible. In this section, by decomposing the possible perturbations applied to the Hamiltonian of an extensible rod in a magnetic field, it will be shown that it is the *interaction* between extensibility and the magnetic field which destroys integrability as alone neither effect alters the integrability of the unperturbed system.

When the field variables $(\mathsf{m}, \mathsf{n}, \mathsf{e}_3)$ are parametrised by (4.12), (5.4) and (5.9) the Hamiltonian function for an extensible rod in a magnetic field is given by

$$\begin{aligned}\mathcal{H}(\theta, \psi, p_\theta, p_\psi, p_\phi) = \frac{1}{2B}p_\theta^2 + \frac{1}{2B}\left(\frac{p_\psi - p_\phi\cos\theta}{\sin\theta}\right)^2 + C_2\cos\theta\left(C_2\cos\theta\left(\frac{1}{K}-\frac{1}{J}\right)+1\right)\\ + \left(C_2\cos\theta\left(\frac{1}{K}-\frac{1}{J}\right)+1\right)\sin\theta\cos\psi\sqrt{2C_1 - C_2^2 - 2\lambda p_\psi}\\ + \left(\frac{1}{K}-\frac{1}{J}\right)\sin^2\theta\cos^2\psi\left(2C_1 - C_2^2 - 2\lambda p_\psi\right). \qquad (5.20)\end{aligned}$$

The Hamiltonian is constant on the energy-density level with $E = \mathcal{H}(\theta, \psi, p_\theta, p_\psi, p_\phi)$. It can be shown, as was performed in the previous section, that the transformation is canonical.

From the Hamiltonian (5.20) there are three possible cases to be considered:

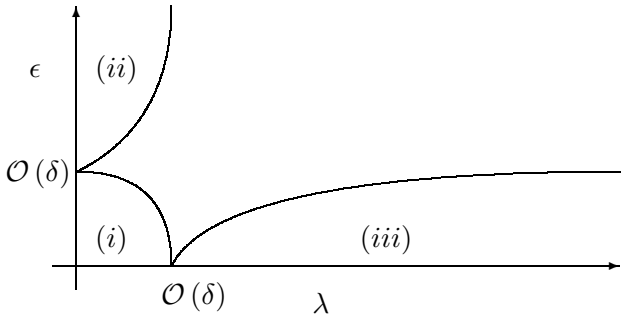

- (i) Firstly to consider the unperturbed system to be the Kirchhoff system and let both extensibility and the magnetic field be rescaled as perturbation of equal order.

- (ii) Secondly to consider the unperturbed system to be the extensible Kirchhoff rod and let the effect of the magnetic field be the perturbation parameter.

(*iii*) Finally to consider the unperturbed system to be an inextensible rod in a uniform magnetic field and let the effect of extensibility be the perturbation parameter.

As proved in lemma 2.2.3, the first order approximation of the Mel'nikov integral can be computed from a canonical Poisson bracket. From the bilinearity of the Poisson bracket when both extensibility and the magnetic field are of equal order and sufficiently small, as in case (*i*), the first order terms are the *sum* of the two integrable perturbations. To first order the Mel'nikov integral is zero. However, the second order terms in the Melnikov integral are from the *product* of the two integrable perturbations. It will be shown that the interaction between the two integrable perturbations results in simple zeroes of the Mel'nikov function and the loss of integrability.

If extensibility is an order of magnitude greater than the magnetic field, as in case (*ii*), then the interaction between the two integrable perturbations will appear at first order in the Mel'nikov integral since there will be coupling through the unperturbed homoclinic orbit (which is dependent on extensibility) and the first order perturbation (which is dependent on the magnetic field). Thus, for cases (*ii*) and (*iii*) it is sufficient to perform Mel'nikov analysis to first order to find simple zeroes. However, for case (*iii*) the unperturbed system has yet to be expressed as a single degree of freedom system. Instead case (*iii*) and the parameter regime where both extensibility and the magnetic field are $\mathcal{O}(1)$ will be investigated numerically in §6.2.1.

5.3.1 Case (*i*): Perturbing the Kirchhoff Rod

For the reduced canonical system (5.20), on setting

$$2C_1 - C_2^2 = 0, \quad \lambda = 0 \quad \text{and} \quad C_2^2\left(\frac{1}{J} - \frac{1}{K}\right) = 0 \tag{5.21}$$

the unperturbed inextensible system (4.20) is recovered. In order to apply a suitable perturbation to the Hamiltonian it is necessary to scale the system as

$$2C_1 - C_2^2 = a\delta^2, \quad \lambda = b\delta^2 \quad \text{and} \quad C_2^2\left(\frac{1}{J} - \frac{1}{K}\right) = c\delta \tag{5.22}$$

for a, b, $c \in \mathbb{R}$ where a, b, $c \sim \mathcal{O}(1)$ such that $a > 2bp_\psi$ and δ is a small perturbation. Thus, the δ-perturbed Hamiltonian takes the form

$$\mathcal{H}_\delta(\theta, p_\theta, \psi, p_\psi) = \mathcal{H}_0(\theta, p_\theta, p_\psi) + \delta\left(\mathcal{H}_1^\lambda(\theta, \psi, p_\psi) + \mathcal{H}_1^\epsilon(\theta)\right) + \delta^2\mathcal{H}_2^{\epsilon\lambda}(\theta, \psi, p_\psi) + \delta^3\mathcal{H}_3^{\epsilon\lambda^2}(\theta, \psi, p_\psi) + \mathcal{O}\left(\delta^4\right) \quad (5.23)$$

where

$$\mathcal{H}_0 = \frac{1}{2B}p_\theta^2 + \frac{1}{2B}\left(\frac{p_\psi - p_\phi\cos\theta}{\sin\theta}\right)^2 + C_2\cos\theta, \quad (5.24a)$$

$$\mathcal{H}_1^\lambda = \sqrt{a - 2bp_\psi}\sin\theta\cos\psi, \quad (5.24b)$$

$$\mathcal{H}_1^\epsilon = c\cos^2\theta, \quad (5.24c)$$

$$\mathcal{H}_2^{\epsilon\lambda} = c\sqrt{a - 2bp_\psi}\cos\theta\sin\theta\cos\psi, \quad (5.24d)$$

$$\mathcal{H}_3^{\epsilon\lambda^2} = c\left(a - 2bp_\psi\right)\sin^2\theta\cos^2\psi \quad (5.24e)$$

In (5.23) the subscripts of the perturbations are the orders of magnitude of the perturbation and the superscripts describe the composition of the perturbation.

When $\delta = 0$ the trivial equilibrium (4.26) is a hyperbolic saddle and from (4.38) so $\omega_0(s) > 0\,\forall s$. Thus the two conditions (H1) and (H2) specified in §2.2 are satisfied. Hence Mel'nikov's method can be performed. From lemma 2.2.3 the first order Mel'nikov integral can be expressed through a canonical Poisson bracket formulation. The bilinearity of the bracket allows the perturbartions to be decomposed into their constituent parts.

$$\mathcal{M}_h^{(1)}(\psi_0) = \int_{-\infty}^{+\infty}\left\{\mathcal{H}_0, \frac{\mathcal{H}_1^\epsilon + \mathcal{H}_1^\lambda}{\omega_0}\right\}_{(\theta,p_\theta)}\mathrm{d}s = \int_{-\infty}^{+\infty}\left\{\mathcal{H}_0, \frac{\mathcal{H}_1^\epsilon}{\omega_0}\right\}_{(\theta,p_\theta)} + \left\{\mathcal{H}_0, \frac{\mathcal{H}_1^\lambda}{\omega_0}\right\}_{(\theta,p_\theta)}\mathrm{d}s.$$

where the frequency $\omega_0(s)$ is given by

$$\omega_0(s) = \frac{\partial\mathcal{H}_0}{\partial p_\psi} = \frac{p_\psi - p_\phi\cos\theta}{\sin^2\theta} = \frac{1}{1 + \cos\theta} \quad (5.25)$$

with $p_\psi = p_\phi = 1$ for homoclinic solutions (4.38).

The partial derivatives are given by

$$\frac{\partial \mathcal{H}_0}{\partial \theta} = \sin\theta \left(\frac{1}{B\left(1+\cos\theta\right)^2} - C_2 \right), \tag{5.26a}$$

$$\frac{\partial \mathcal{H}_0}{\partial p_\theta} = \frac{p_\theta}{B}, \tag{5.26b}$$

$$\frac{\partial \omega_0}{\partial \theta} = \frac{\sin\theta}{B\left(1+\cos\theta\right)^2}, \tag{5.26c}$$

$$\frac{\partial \omega_0}{\partial p_\theta} = 0, \tag{5.26d}$$

$$\frac{\partial \mathcal{H}_1^\lambda}{\partial \theta} = -2c\sin\theta\cos\theta, \tag{5.26e}$$

$$\frac{\partial \mathcal{H}_1^\lambda}{\partial p_\theta} = 0, \tag{5.26f}$$

$$\frac{\partial \mathcal{H}_1^\lambda}{\partial \theta} = \sqrt{a-2bp_\psi}\sin\theta\cos\psi, \tag{5.26g}$$

$$\frac{\partial \mathcal{H}_1^\lambda}{\partial p_\theta} = 0. \tag{5.26h}$$

As the perturbation (2.9) is independent of ψ so following [45, Eq. (4.5.15)] and using Green's theorem, the natural result appears

$$\begin{aligned}
\int_{-\infty}^{+\infty} \left\{ \mathcal{H}_0, \frac{\mathcal{H}_1^\epsilon}{\omega_0} \right\}_{(\theta,p_\theta)} \mathrm{d}s &= \int_{-\infty}^{+\infty} f_0 \wedge f_1 \, \mathrm{d}\psi \\
&= \int_{-\infty}^{+\infty} \left(\frac{\partial I^{(0)}}{\partial \theta}\frac{\partial I^{(1)}}{\partial p_\theta} - \frac{\partial I^{(0)}}{\partial p_\theta}\frac{\partial I^{(1)}}{\partial \theta} \right) \mathrm{d}\psi \\
&= \int_{-\infty}^{+\infty} \left(\frac{\partial I^{(1)}}{\partial p_\theta} p_\theta' - \frac{\partial I^{(1)}}{\partial \theta}\theta' \right) \mathrm{d}\psi \\
&= \oint_{\partial\Gamma} \left(\frac{\partial I^{(1)}}{\partial p_\theta}\,\mathrm{d}p_\theta - \frac{\partial I^{(1)}}{\partial \theta}\,\mathrm{d}\theta \right) \\
&= \iint_\Gamma \left(\frac{\partial^2 I^{(1)}}{\partial p_\theta \partial \theta} - \frac{\partial^2 I^{(1)}}{\partial \theta \partial p_\theta} \right) \mathrm{d}\theta\,\mathrm{d}p_\theta = 0.
\end{aligned} \tag{5.27a}$$

By recalling that $\theta(s)$ is an even function of arc-length and $p_\theta(s)$ an odd function, it follows that

$$\int_{-\infty}^{+\infty} \left\{ \mathcal{H}_0, \frac{\mathcal{H}_1^\lambda}{\omega_0} \right\}_{(\theta,p_\theta)} \mathrm{d}s = -\sqrt{a-2bp_\psi} \int_{-\infty}^{+\infty} p_\theta \cos\theta \left(1+\cos\theta\right) \mathrm{d}s = 0. \tag{5.27b}$$

Hence, the first order Mel'nikov integral, comprised of the combined first order effects is trivially zero, i.e. $\mathcal{M}_h^{(1)}(\psi_0) = 0$. Thus, as described in §2.2 higher order terms must

be computed. The analysis must now be performed in a nonautonomous system (2.17) where the action integral p_ψ plays the role of the Hamiltonian and ψ acts as the new time variable. For this case the first order approximations to the homoclinic orbit $\theta_1^{s,u}(\psi, \psi_0)$, $p_{\theta_1}^{s,u}(\psi, \psi_0)$ must be computed.

On inverting the Hamiltonian, the unperturbed action integral is given by

$$I^{(0)}(\theta, p_\theta) = p_\phi \cos\theta \pm \sin\theta \sqrt{2EB - 2C_2 B\cos\theta - p_\theta^2}. \tag{5.28}$$

For consistency the positive square root is taken at all times. The frequency $\omega_0(\psi)$ is given by

$$\omega_0(\psi) = \frac{\sqrt{2EB - 2C_2 B\cos\theta - p_\theta^2}}{\sin\theta}. \tag{5.29}$$

The unperturbed nonautonomous integrable system is

$$\frac{\mathrm{d}}{\mathrm{d}\psi}\theta = \frac{p_\theta \sin\theta}{\sqrt{2EB - 2C_2 B\cos\theta - p_\theta^2}}, \tag{5.30a}$$

$$\frac{\mathrm{d}}{\mathrm{d}\psi}p_\theta = -p_\phi \sin\theta + \cos\theta\sqrt{2EB - 2C_2 B\cos\theta - p_\theta^2} + \frac{C_2 B\sin^2\theta}{\sqrt{2EB - 2C_2 B\cos\theta - p_\theta^2}}. \tag{5.30b}$$

The unperturbed vector field is denoted by $f_0 = \left(\partial I^{(0)}/\partial p_\theta, -\partial I^{(0)}/\partial\theta\right)^T$. This nonlinear coupled system is integrable and admits a homoclinic orbit. However, closed form expressions for the homoclinic orbit are difficult to find. For example, it is not possible to solve the system as was done in §4.3. Nor is it possible to use (4.38) to invert $\psi = \psi(s)$ for s so that an expression for $s = s(\psi)$ can be substituted into the homoclinic orbit $\theta = \theta(s)$ to give $\theta = \theta(\psi)$. Instead the orbit is evaluated numerically by noting that the system is still reversible, so that $p_\theta(0) = 0$ and thus from the homoclinic energy level $\theta(0) = 2\pi/3$. From this point the homoclinic orbit can be found by integrating forwards and backwards in ψ from $\psi = 0$.

The derivative of ω_0 with respect to p_ψ is required in order to find the second order

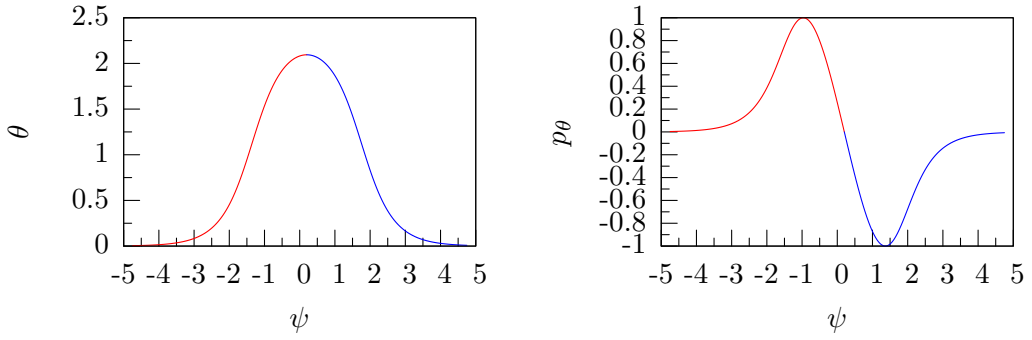

Figure 5.2: Homoclinics of the transformed unperturbed system integrated forwards and backwards from $\psi_0 = 0$.

terms from the expansion of the Hamiltonian (2.16). Hence

$$\frac{\partial^2 \mathcal{H}_0}{\partial I^{(0)}} = \frac{\partial \omega_0}{\partial p_\psi} = \frac{1}{\sin^2\theta}. \tag{5.31}$$

Thus, from (2.16) the first order nonautonomous perturbation is then given by

$$I^{(1)}(\theta, p_\theta, \psi) = \frac{\sin\theta\left(\cos^2\theta + \sin\theta\cos\psi\sqrt{a - 2b\sqrt{p_\phi\cos\theta + \sin\theta\sqrt{2EB - 2C_2B\cos\theta - p_\theta^2}}}\right)}{\sqrt{2EB - 2C_2B\cos\theta - p_\theta^2}}. \tag{5.32}$$

Thus f_1 can be found and hence its Jacobian Df_1. Their closed form expressions are long and complex and thus are omitted.

The second order perturbation is given by

$$I^{(2)} = Bb\sin^4\cos^2\psi + \frac{Bbc\cos^2\theta\sin^3\theta\cos\psi}{\sqrt{a - b\sqrt{p_\phi\cos\theta \pm \sin\theta\sqrt{2EB - 2C_2B\cos\theta - p_\theta^2}}}} + Bc\sin^3\theta\cos\theta\cos\psi\sqrt{a - b\sqrt{p_\phi\cos\theta \pm \sin\theta\sqrt{2EB - 2C_2B\cos\theta - p_\theta^2}}}. \tag{5.33}$$

Hence f_2 can be found. Again, the closed form expressions are extremely long and are omitted.

From f_1 and Df_0 the first order approximations to the tangential flow can be found

from the first order variational equation (2.34) linearised about the homoclinic solutions (5.30)

$$\begin{pmatrix} \theta_1^{s,u} \\ p_{\theta_1}^{s,u} \end{pmatrix}' = \begin{pmatrix} -\partial^2 I^{(0)}/\partial\theta\partial p_\theta & -\partial^2 I^{(0)}/\partial\theta^2 \\ \partial^2 I^{(0)}/\partial p_\theta^2 & \partial^2 I^{(0)}/\partial p_\theta \partial\theta \end{pmatrix} \begin{pmatrix} \theta_1^{s,u} \\ p_{\theta_1}^{s,u} \end{pmatrix} + \begin{pmatrix} -\partial I^{(1)}/\partial p_\theta \\ \partial I^{(1)}/\partial\theta \end{pmatrix}.$$

As the equation is linearised about a homoclinic solution which cannot be found analytically, the equation must be solved numerically. The solutions to the equation (2.34) must be bounded and transverse to the flow of the unperturbed homoclinic orbit (2.35). This condition essentially requires the initial conditions $\theta_1^{s,u}(\psi_0, \psi_0)$, $p_{\theta_1}^{s,u}(\psi_0, \psi_0)$ to be those such that the solutions have exponential dichotomies (see §B.3.1 for further details). In [77, Corollary 4.3] it is shown that as the linearised vector field $Df_0(\boldsymbol{x}_0)$ has an exponential dichotomy, then if $\left(-\partial I^{(1)}/\partial p_\theta,\, \partial I^{(1)}/\partial\theta\right)^T$ is bounded and its partial derivatives continuous then the variational equation linearised about the homoclinic solution has a *unique* solution with an exponential dichotomy. Figure 5.3 shows that the necessary conditions are satisfied.

An algorithm to compute the second order Mel'nikov integral (2.33) is outlined as follows:

(*i*) Fix a value of ψ_0.

(*ii*) Compute the homoclinic orbit (θ, p_θ), the first and second order perturbations f_1 and f_2 and their partial derivatives over the ranges $[-\mathcal{T}, \psi_0]$ and $[\psi_0, +\mathcal{T}]$ by integrating forwards and backwards from ψ_0. The length $\mathcal{T}$ should be chosen so that the homoclinic orbit is less than a prescribed tolerance close to the saddle point.

(*iii*) The integral $\int_{-\mathcal{T}}^{+\mathcal{T}} f_0(x_0(\psi - \psi_0)) \wedge f_2(x_0(\psi - \psi_0), \psi)\, \mathrm{d}\psi$ can be computed directly from the homoclinic orbit.

In order to compute $\theta_1^{s,u}(\psi, \psi_0)$ and $p_{\theta_1}^{s,u}(\psi, \psi_0)$ as solutions to the first order variational equation (2.34), from (2.35) the solutions must be bounded and transverse to the unperturbed homoclinic orbits. Thus, the two pairs of initial conditions for the stable and unstable first order approximations $\theta_1^{s,u}(\psi_0, \psi_0)$ and $p_{\theta_1}^{s,u}(\psi_0, \psi_0)$ must be chosen so that they satisfy these two conditions. This is done as follows

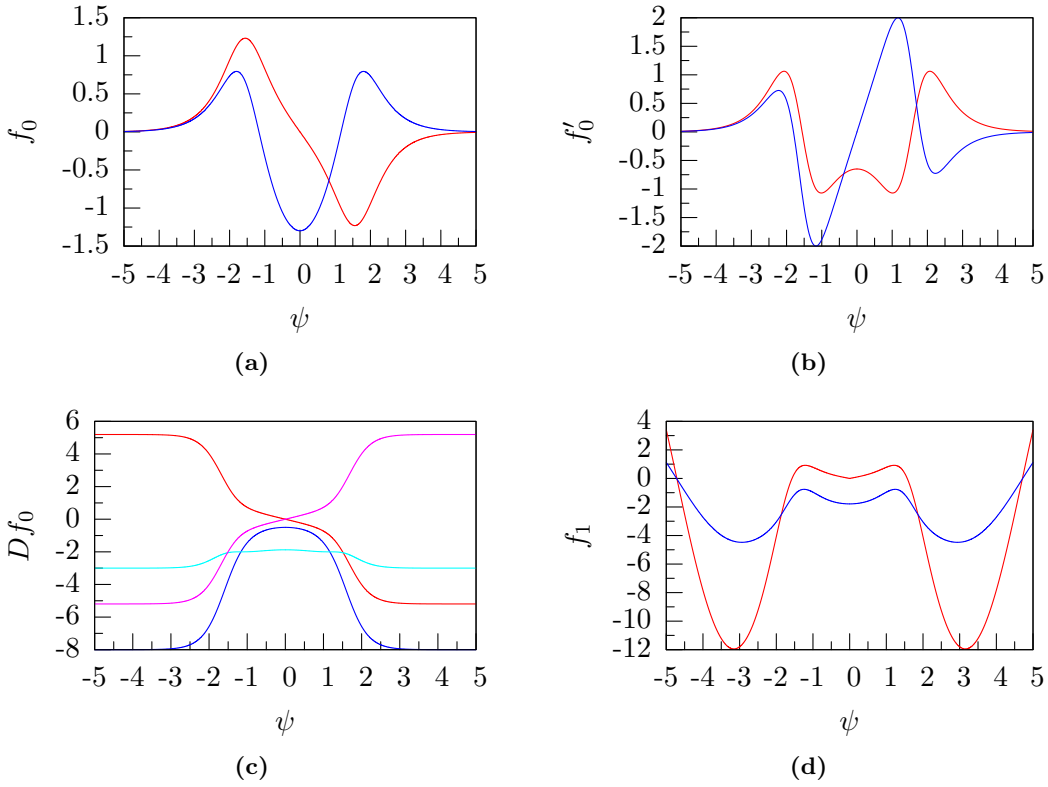

Figure 5.3: In subfigure 5.3(a) the first components of the forces are in red, the second components in blue. In subfigure 5.3(b) the total derivatives are displayed while in subfigure 5.3(c) the partial derivatives $\partial f_{01}/\partial\theta$ (red), $\partial f_{01}/\partial p_\theta$ (blue), $\partial f_{02}/\partial\theta$ (cyan) and $\partial f_{02}/\partial p_\theta$ (magenta) are displayed. Note that $\partial f_{01}/\partial\theta = -\partial f_{02}/\partial p_\theta$ as the system is Hamiltonian, hence trace $(Df_0) = 0$. In the subfigures $a = 5$, $b = 1$ and $c = 1$. $B = 1$, $C_1 = 1.665$, $C_2 = 1$ and $E = C_2$.

(*iv*) Specify the transversality condition using the initial conditions

$$\theta_1^{s,u}(\psi_0, \psi_0) = -\frac{p_{\theta_1}^{s,u}(\psi_0, \psi_0)\,\dfrac{\partial I_0}{\partial\theta}}{\dfrac{\partial I_0}{\partial p_\theta}}$$

(*v*) Determine an interval by upper and lower bounds which diverge to $-\infty$ and $+\infty$ respectively and use a bisection method to trap the initial condition $p_{\theta_1}^{s,u}(\psi_0, \psi_0)$ which determines bounded and transverse solutions of $\theta_1^{s,u}(\psi, \psi_0)$ and $p_{\theta_1}^{s,u}(\psi, \psi_0)$.

(*vi*) For the correct initial conditions compute the first order approximation to the stable and unstable manifolds and then compute the appropriate integrals via a quadrature subroutine `cubint.f`.

(*vii*) Incrementally change ψ_0 by a sufficiently small amount and repeat the algorithm from step (*ii*) until simple zeroes are detected.

The tolerances for the convergence of the bisection method were set as 10^{-10} and the tolerances for the truncated homoclinic set as 10^{-12}. The error returned by the subroutine `cubint.f` was of order 10^{-6}. For step (*i*) the initial phase condition was $\psi_0 = 0$ and a suitable truncation length was $\mathcal{T} = 5$.

The bisection method was chosen as it was found to behave in a more robust manner than other solvers such as the Newton-Raphson method. However, the algorithm requires the correct solution to be within a specified interval. In order for the root to be trapped for successive iterations the interval was large, this along with the linear convergence of the method meant the algorithm converges very slowly. As both stable and unstable approximations need to be computed the search for the correct initial conditions was a rather time consuming process.

The algorithm is not shown to be well posed, but was successfully tested on the rotator pendulum system [78] and the modified Duffing oscillator. Indeed, after finding that many examples of second order Mel'nikov integrals were from the rotator-pendulum system, the modified Duffing oscillator was formulated to provide an alternative model which allowed the algorithm to be tested against a known solution.

Figure 5.4 illustrates that the second order Mel'nikov integral has a simple zero. Performing Mel'nikov analysis numerically does not prove that generically the stable and unstable manifolds intersect transversely as there is no closed form analytical expression of the splitting of the manifolds. The numerical results only shows that at a certain set of values the stable and unstable manifolds intersect transversely.

The contributions to the second order Mel'nikov integral from the first order approximations $\theta_1^{s,u}(\psi, \psi_0)$ and $p_{\theta_1}^{s,u}(\psi, \psi_0)$ dominated in contrast to the far smaller sinusoidal term provided by $\int_{-\mathcal{T}}^{+\mathcal{T}} f_0 \wedge f_2 \, \mathrm{d}\psi$. This behaviour was also observed for the modified Duffing oscillator as illustrated in figure 2.4.

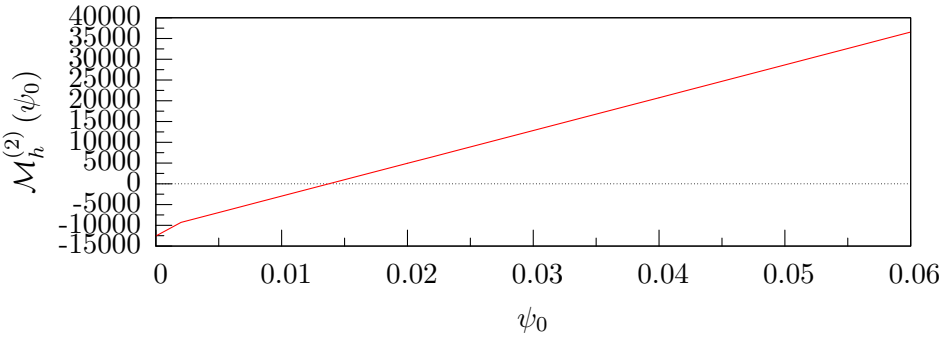

Figure 5.4: Second order Mel'nikov integral showing the existence of a simple zero.

5.3.2 Case (ii): Perturbing the Extensible Rod

For the reduced canonical system (5.20), on setting

$$2C_1 - C_2^2 = 0 \quad \text{and} \quad \lambda = 0 \tag{5.34}$$

the unperturbed extensible system (4.40) is recovered. The trivial equilibrium is a hyperbolic saddle and $\omega_0(s) > 0 \ \forall s$. Thus, having satisfied the two conditions specified in §2.2 Mel'nikov's method can be performed on the unperturbed inextensible Hamiltonian. However, in order to express the Hamiltonian in the appropriate form (2.5) it is necessary to introduce a parameter δ such that

$$2C_1 - C_2^2 = a\delta \quad \text{and} \quad \lambda = b\delta^2. \tag{5.35}$$

for a, $b \in \mathbb{R}$, where a, $b \sim \mathcal{O}(1)$ such that $a > 2bp_\psi$ and δ is a small parameter. Hence when an extensible conducting rod is perturbed by the effect of a uniform magnetic field the perturbation of the Hamiltonian takes the form

$$\mathcal{H}_\delta(\theta, \psi, p_\theta, p_\psi, p_\phi) = \mathcal{H}_0(\theta, p_\theta, p_\psi, p_\phi) + \delta\mathcal{H}_1(\theta, \psi, p_\theta, p_\psi, p_\phi) + \mathcal{O}\left(\delta^2\right),$$

where the unperturbed system is given by

$$\mathcal{H}_0 = \frac{1}{2B}p_\theta^2 + \frac{1}{2B}\frac{\left(p_\psi - p_\phi\cos\theta\right)^2}{\sin^2\theta} + \frac{1}{2C}p_\phi^2 + C_2\cos\theta + C_2^2\left(\frac{1}{K} - \frac{1}{J}\right)\cos^2\theta \tag{5.36}$$

and the first order term is given by

$$\mathcal{H}_1(\theta,\psi,p_\psi)=\sqrt{a-2bp_\psi}\left(C_2\left(\frac{1}{K}-\frac{1}{J}\right)\cos\theta+1\right)\sin\theta\cos\psi.$$

Thus Mel'nikov's method can be applied to give an approximation to the splitting of the stable and unstable manifolds.

The frequency of the angle ψ in the unperturbed case when $p_\psi=p_\phi=B$ is given by

$$\omega_0=\frac{\partial\mathcal{H}_0}{\partial p_\psi}=\frac{1}{1+\cos\theta} \tag{5.37}$$

where the closed form expressions for the angle $\theta(s)$ and its conjugate $p_\theta(s)$ are known and given from (4.50). Hence $\psi(s)$ can be found directly. Let $\psi(s)=\bar{\psi}(s)+\psi_0$ so that the first order perturbation to the Hamiltonian is

$$\mathcal{H}_1=\sqrt{a-2bp_\psi}\left(C_2\left(\frac{1}{K}-\frac{1}{J}\right)\cos\theta+1\right)\sin\theta\left(\cos\bar{\psi}\cos\psi_0-\sin\bar{\psi}\sin\psi_0\right).$$

From the first order Mel'nikov integral (2.36), the canonical Poisson bracket can be expanded as

$$\begin{aligned}\mathcal{M}_h^{(1)}(\psi_0)&=\int_{-\infty}^{+\infty}\left\{\mathcal{H},\frac{\mathcal{H}_1}{\omega_0}\right\}_{(\theta,p_\theta)}\mathrm{d}s\\&=\int_{-\infty}^{+\infty}\frac{1}{\omega_0}\left\{\mathcal{H}_0,\mathcal{H}_1\right\}_{(\theta,p_\theta)}+\frac{\mathcal{H}_1}{\omega_0^2}\left\{\mathcal{H}_0,\omega_0\right\}_{(\theta,p_\theta)}\mathrm{d}s.\end{aligned} \tag{5.38}$$

The partial derivatives are given by

$$\begin{aligned}\frac{\partial\mathcal{H}_0}{\partial\theta}&=\sin\theta\left(\frac{1}{(1+\cos\theta)^2}-C_2\left(1+\left(\frac{1}{K}-\frac{1}{J}\right)\cos\theta\right)\right),\\\frac{\partial\mathcal{H}_0}{\partial p_\theta}&=\frac{p_\theta}{B},\\\frac{\partial\omega_0}{\partial\theta}&=\frac{\sin\theta}{(1+\cos\theta)^2},\\\frac{\partial\omega_0}{\partial p_\theta}&=0,\\\frac{\partial\mathcal{H}_1}{\partial\theta}&=\sqrt{a-2bp_\psi}\left(\cos\theta+C_2\left(\frac{1}{K}-\frac{1}{J}\right)\cos 2\theta\right)\left(\cos\psi_0\cos\bar{\psi}-\sin\psi_0\sin\bar{\psi}\right),\\\frac{\partial\mathcal{H}_1}{\partial p_\theta}&=0.\end{aligned}$$

Hence, the brackets may be evaluated as

$$\frac{1}{\omega_0}\left\{\mathcal{H}_0,\mathcal{H}_1\right\}_{(\theta,p_\theta)} = \frac{1}{B}\sqrt{a-2bp_\psi}\,(1+\cos\theta)\,p_\theta\left(\cos\theta + C_2\left(\frac{1}{K}-\frac{1}{J}\right)\cos 2\theta\right)\cos\bar{\psi}\cos\psi_0 - \frac{1}{B}\sqrt{a-2bp_\psi}\,(1+\cos\theta)\,p_\theta\left(\cos\theta + C_2\left(\frac{1}{K}-\frac{1}{J}\right)\cos 2\theta\right)\sin\bar{\psi}\sin\psi_0$$

and

$$\frac{\mathcal{H}_1}{\omega_0^2}\left\{\mathcal{H}_0,\omega_0\right\}_{(\theta,p_\theta)} = \frac{1}{B}\sqrt{a-2bp_\psi}p_\theta\left(C_2\left(\frac{1}{K}-\frac{1}{J}\right)\cos\theta+1\right)\sin\theta\left(\cos\bar{\psi}\cos\psi_0-\sin\bar{\psi}\sin\psi_0\right).$$

Thus, in contrast to the previous analysis, a closed form expression for the Mel'nikov integral can be found as

$$\begin{aligned}\mathcal{M}_h^{(1)}(\psi_0) = {}& \frac{1}{B}\sqrt{a-2bp_\psi}\cos\psi_0\int_{-\infty}^{+\infty} p_\theta\cos\bar{\psi}\left((1+\cos\theta)\left(\cos\theta+C_2\left(\frac{1}{K}-\frac{1}{J}\right)\cos 2\theta\right)\right.\\ &\left.+\sin\theta\left(1+C_2\left(\frac{1}{K}-\frac{1}{J}\right)\right)\right)\mathrm{d}s\\ &-\frac{1}{B}\sqrt{a-2bp_\psi}\sin\psi_0\int_{-\infty}^{+\infty} p_\theta\sin\bar{\psi}\left((1+\cos\theta)\left(\cos\theta+C_2\left(\frac{1}{K}-\frac{1}{J}\right)\cos 2\theta\right)\right.\\ &\left.+\sin\theta\left(1+C_2\left(\frac{1}{K}-\frac{1}{J}\right)\right)\right)\mathrm{d}s. \qquad (5.40)\end{aligned}$$

As $p_\theta(s)$ is an odd function and $\theta(s)$ an even function of the arclength s, the first and fourth parts of the Mel'nikov integral (5.40) are odd functions and are zero when integrated over a symmetric range. Thus

$$\begin{aligned}\mathcal{M}_h^{(1)}(\psi_0) = {}& \frac{2}{B}\sqrt{a-2bp_\psi}\cos\psi_0\int_0^{+\infty} p_\theta\cos\bar{\psi}\sin\theta\left(1+C_2\left(\frac{1}{K}-\frac{1}{J}\right)\cos\theta\right)\mathrm{d}s\\ &-\frac{2}{B}\sqrt{a-2bp_\psi}\sin\psi_0\int_0^{+\infty} p_\theta\sin\bar{\psi}\,(1+\cos\theta)\left(\cos\theta+C_2\left(\frac{1}{K}-\frac{1}{J}\right)\cos 2\theta\right)\mathrm{d}s.\end{aligned}$$

Generically the Mel'nikov integral will have simple zeroes when $a-2bp_\psi>0$. Indeed, the restriction is a natural facet of the scaling since

$$a-2bp_\psi=0 \Longleftrightarrow 2C_1-C_2-2\lambda p_\psi=0$$

which is in fact the alignment condition (5.10). There may be isolated points, dependent on the constitutive relations and the values of the Casimirs, where the Mel'nikov integral is zero but these will form a codimension-one set since the Mel'nikov integral is

analytic [52]. In figure 5.5 the Mel'nikov integral is displayed showing that the integral possesses simple zeroes.

Hence by Mel'nikov's theorem 2.2.1 the transversal intersection of the unstable and unstable manifolds lead to Smale horseshoes on the Poincaré section of the homoclinic energy level which are conjugate to a Bernoulli shift in exacly the same manner as illustrated in the previous chapter §4.5 as both systems have qualatatively the same unperturbed phase space. In the next chapter the bifurcation structure of the multimodal solutions are investigated.

By the corollary 2.2.2 the system is no longer completely integrable. This phenomena is illustrated in figure 5.6 which clearly show the breakup of integrability into the typical plots, referred to as "stochastic layers" in [45, pg. 222], associated with the Poincaré-Birkhoff theorem. The Poincaré sections were computed by fixing the integrals $p_\phi = 1$, $\mathcal{H} = E = C_2\left(1 + C_2\left(1/K - 1/J\right)\right)$ and placing the initial conditions near the (unperturbed) saddle: $p_\theta\left(0\right) = \theta\left(0\right) = 10^{-3}$ with $p_\phi\left(0\right) = 1$ and solving $\mathcal{H}_0\left(\theta, p_\theta, \phi, p_\phi\right) = E$ for $\psi\left(0\right)$ on the nondimensional homoclinic energy level. The two-dimensional section was defined by

$$\Sigma^{-0.95} = \left\{\cos\phi = -0.95 \,:\, \theta,\, p_\psi,\, p_\theta \in \mathbb{R}\right\}.$$

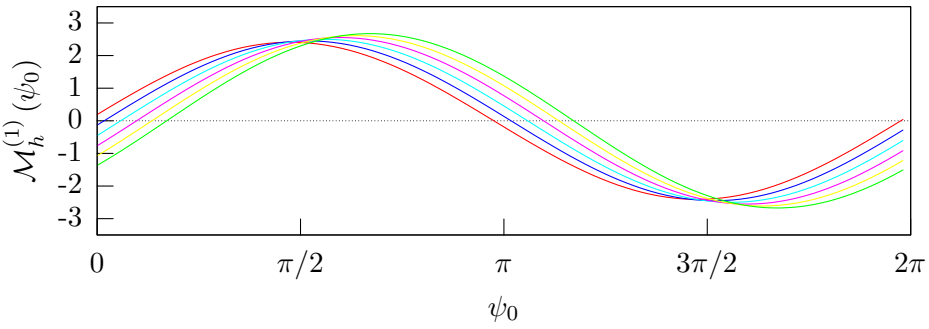

(a)

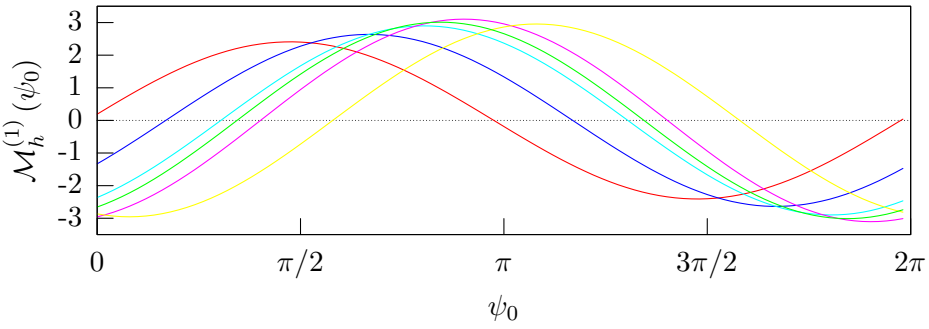

(b)

Figure 5.5: Mel'nikov integrals evaluate at homoclinic energy density level $E = C_2\,(1 + C_2\,(1/K - 1/J))$ where $B = 1$, $M = 1.70$, $T = 1$. Subfigure 5.5(a) displays a functions at differing degrees of extensibility $(1/K - 1/J) = 0.1$ (red), 0.12 (blue), 0.14 (cyan), 0.16 (magenta), 0.18 (yellow) and 0.2 (green) when $C_2 = 1$. In subfigure 5.5(a) extensibility is fixed $(1/K - 1/J) = 1$ and $C_2 = 1$ (red), 1.2 (blue), 1.4 (cyan), 1.6 (magenta), 1.8 (yellow) and 2 (green).

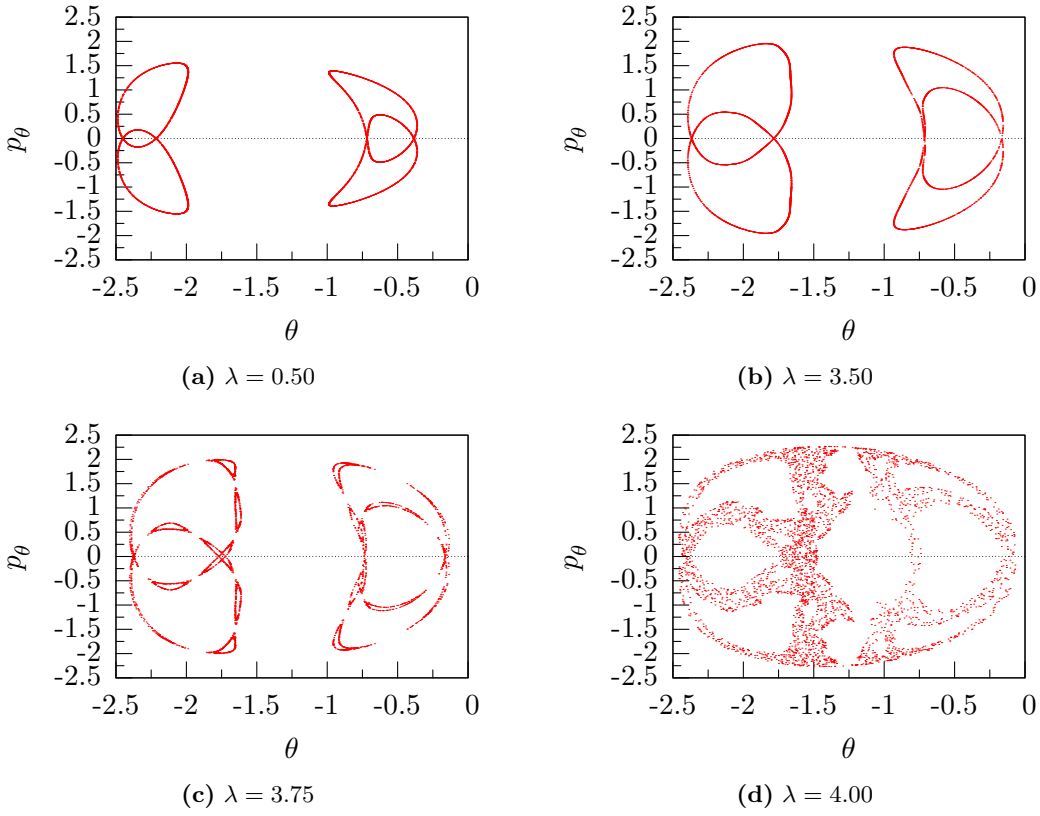

(a) $\lambda = 0.50$ **(b)** $\lambda = 3.50$

(c) $\lambda = 3.75$ **(d)** $\lambda = 4.00$

Figure 5.6: Poincaré sections on the homoclinic energy level $h = 1.109756$ for varying levels of λ at the section determined by $\cos\psi = -0.95$. The Casimirs are $C_1 = C_2 = C_3 = 1$, the bending stiffness $B = 1$, the torsional stiffness $C = 4/3$, the applied moment is $M = 1.70$ and the compressive stiffnesses are $J = 1$, $K = 50/41$.

Chapter 6

Homoclinic Bifurcation of a Rod in a Magnetic Field

Having proved the existence of spatially chaotic solutions for an extensible rods in a magnetic field in §5.3, in this chapter homoclinic solutions are computed and their bifurcation structure investigated for both primary and multimodal solutions.

The computation and continuation of homoclinic solutions requires that the arc-length be truncated from the infinite domain to a finite interval. The computation of homoclinic orbits then becomes a boundary value problem where the lefthand boundary conditions are placed in the unstable mainfold of the trivial equilibrium and, for reversible systems the righthand boundary conditions in the symmetric section of a reversibility (6.21). The boundary value problem is then solved by a shooting method using the Newton-Raphson method to solve a variational equation with respect to a set of shooting parameters. Configurations are then followed using continuation software by exploiting the exponential trichotomies of the system. Due to the magnetic effects the trivial solution is a periodic orbit, so specific details of the computation and continuation of homoclinic orbits are explained in this chapter. However, for details on the computation and continuation of homoclinic solutions, see appendix §B.

6.1 Problem Setting

In order to increase computational efficiency the Euler parameters $q = (q_1, q_2, q_3, q_4)$ are used to reduce the dimension of the full system by parameterising the directors. The rotation matrix (3.2) is then given by

$$R = \begin{pmatrix} q_1^2 - q_2^2 - q_3^2 + q_4^2 & 2\,(q_1 q_2 - q_3 q_4) & 2\,(q_1 q_3 + q_2 q_4) \\ 2\,(q_1 q_2 + q_3 q_4) & q_2^2 + q_4^2 - q_1^2 - q_3^2 & 2\,(q_2 q_3 - q_1 q_4) \\ 2\,(q_1 q_3 - q_2 q_4) & 2\,(q_1 q_4 + q_2 q_3) & q_3^2 + q_4^2 - q_1^2 - q_2^2 \end{pmatrix}. \tag{6.1}$$

The four Euler parameters give a double covering of the set of rotations subject to the constraint

$$Q = q \cdot q = q_1^2 + q_2^2 + q_3^2 + q_4^2 = 1. \tag{6.2}$$

The Euler parameters are robust in that unlike the Euler angles there is no polar singularity. For more details on the Euler parameters and their relation to the Euler angles see appendix §A.

From (3.5) the strains can be written as

$$u_i = \frac{2\,A_i\,q \cdot q'}{q \cdot q} \quad \text{for} \quad i = 1, 2, 3 \tag{6.3}$$

where the A_i are four-by-four skew-symmetric matrices satisfying the relationships

$$\begin{aligned} A_1 q &= (q_4, q_3, -q_2, -q_1)\,, \\ A_2 q &= (-q_3, q_4, q_1, -q_2)\,, \\ A_3 q &= (q_2, -q_1, q_4, -q_3)\,. \end{aligned}$$

The four vectors $\{q, A_1 q, A_2 q, A_3 q\}$ form an orthonormal basis in $\mathbb{R}^4$. Thus (6.3) subject to (6.2) can be inverted and solved for the derivatives of the Euler parameters as

$$q_1' = (u_1 q_4 - u_2 q_3 + u_3 q_2)\,/2, \tag{6.4a}$$

$$q_2' = (u_1 q_3 + u_2 q_4 - u_3 q_1)\,/2, \tag{6.4b}$$

$$q_3' = (-u_1 q_2 + u_2 q_1 + u_3 q_4)\,/2, \tag{6.4c}$$

$$q_4' = (-u_1 q_1 - u_2 q_2 - u_3 q_3)\,/2. \tag{6.4d}$$

From (6.1) the triple e_3 can be expressed as a function of the Euler parameters.

$$\mathsf{e}_3(q) = \begin{pmatrix} 2(q_1q_3 + q_2q_4) \\ 2(q_2q_3 - q_1q_4) \\ q_3^2 + q_4^2 - q_1^2 - q_2^2 \end{pmatrix}. \tag{6.5}$$

The constitutive relations take the form

$$u_1 = m_1/B_1, \quad u_2 = m_2/B_2, \quad u_3 = m_3/C \quad \text{and} \quad v_3 = 1 + n_3/J \tag{6.6}$$

where $B = B_1 = B_2$ so that the rod is isotropic. It is assumed that a moment, M, and tension, T, are applied axially at $s = \pm\infty$. The system is then nondimensionalised by

$$\begin{gathered} \bar{s} = (M/B)\, s, \quad x_1 = n_1/T, \quad x_2 = n_2/T, \quad x_3 = (n_3 - T)/T, \\ x_4 = m_1/M, \quad x_5 = m_2/M, \quad x_6 = (m_3 - M)/M, \\ x_7 = q_1, \quad x_8 = q_2, \quad x_9 = q_3 \quad \text{and} \quad x_{10} = q_4. \end{gathered} \tag{6.7}$$

The nondimensional parameters for an extensible rod are then given by

$$m = \frac{M}{\sqrt{BT}}, \quad \bar{\lambda} = \frac{\lambda B}{M}, \quad \nu = \frac{B}{C} - 1 \quad \text{and} \quad \epsilon = \frac{T}{J}. \tag{6.8}$$

The nondimensional parameters are the same as those in (4.1) with the additional parameter $\bar{\lambda}$ as the (magnetic) body force parameter. The bar notation is suppressed from this point onwards. Thus, explicitly the governing equations are

$$x_1' = (1+\nu)\, x_2x_6 - x_3x_5 + 2\lambda(1+\epsilon x_3)(x_7x_{10} + x_8x_9), \tag{6.9a}$$

$$x_2' = x_3x_4 - (1+\nu)\, x_1x_6 - 2\lambda(1+\epsilon x_3)(x_7x_9 - x_8x_{10}), \tag{6.9b}$$

$$x_3' = x_1x_5 - x_2x_4, \tag{6.9c}$$

$$x_4' = \nu x_5x_6 + x_2(1+\epsilon x_3)/m^2, \tag{6.9d}$$

$$x_5' = -\nu x_4x_6 - x_1(1+\epsilon x_3)/m^2, \tag{6.9e}$$

$$x_6' = 0, \tag{6.9f}$$

$$x_7' = (x_4x_{10} - x_5x_9 + (1+\nu)\, x_6x_8)/2, \tag{6.9g}$$

$$x_8' = (x_4x_9 + x_5x_{10} - (1+\nu)\, x_6x_7)/2, \tag{6.9h}$$

$$x_9' = (-x_4x_8 + x_5x_7 + (1+\nu)\, x_6x_{10})/2, \tag{6.9i}$$

$$x_{10}' = (-x_4x_7 - x_5x_8 - (1+\nu)\, x_6x_9)/2. \tag{6.9j}$$

It is a straightforward exercise to check that the Casimirs (3.40),

$$C_1 = \frac{1}{2}x_1^2 + \frac{1}{2}x_2^2 + \frac{1}{2}x_3^2 + 2\lambda x_4\left(x_7x_9 + x_8x_{10}\right) + 2\lambda x_5\left(x_8x_9 - x_7x_{10}\right) + \lambda x_6\left(x_{10}^2 + x_9^2 - x_8^2 - x_7^2\right), \tag{6.10a}$$

$$C_2 = x_1\left(x_7x_9 + x_8x_{10}\right) + x_2\left(x_8x_9 - x_7x_{10}\right) + x_3\left(x_{10}^2 + x_9^2 - x_8^2 - x_7^2\right), \tag{6.10b}$$

$$C_3 = \left(x_7x_9 + x_8x_{10}\right)^2 + \left(x_8x_9 - x_7x_{10}\right)^2 + \left(x_{10}^2 + x_9^2 - x_8^2 - x_7^2\right)^2, \tag{6.10c}$$

first integrals (3.41)

$$I_1 = x_6, \tag{6.11a}$$

$$I_2 = x_1x_4 + x_2x_5 + x_3x_6 + \lambda\left(x_{10}^2 + x_9^2 - x_8^2 - x_7^2\right) \tag{6.11b}$$

and constraint (6.2)

$$Q = x_7^2 + x_8^2 + x_9^2 + x_{10}^2 \tag{6.12}$$

are all conserved quantities.

Incorporating the evolution of a fixed vector in the spatial frame into the governing equations (in the director frame) results in the trivial configuration, a straight twisted rod, being a periodic orbit. The periodic orbit $\boldsymbol{\gamma}(s)$ with period $\tau = 4\pi/(1+\nu)$ which satisfies the constraint and the correct orientation of the director frame is given by

$$\boldsymbol{\gamma}(s) = \left(0,0,0,0,0,0,0,0,\sin\left(s\left(1+\nu\right)/2\right),\cos\left(s\left(1+\nu\right)/2\right)\right). \tag{6.13}$$

Under the τ-mapping $\boldsymbol{\gamma}(n\tau) = \boldsymbol{p}$ the periodic orbit is the fixed point

$$\boldsymbol{p} = \boldsymbol{\gamma}_0(\tau) = (0,0,0,0,0,0,0,0,0,1). \tag{6.14}$$

The straight twisted rod does not intersect the lines of flux of the magnetic field, so the trivial solution does not feature any dependence on the magnetic field.

Evaluating the conserved quantities about the trivial solution (6.13) yields

$$C_1 = 0, \quad C_2 = 0, \quad C_3 = 1, \quad I_1 = 0, \quad I_2 = \lambda \quad \text{and} \quad Q = 1. \tag{6.15}$$

Note that the body force is incorporated into the boundary conditions through the values of the conserved quantities and not through the scaling of the field variables $(\mathsf{m}, \mathsf{n}, \mathsf{e}_3)$.

The formulation of the governing equations based on the force and moment balance equations (3.38a), (3.38b) with the evolution of the Euler parameters (6.4) and body force (6.5), subject to the constraint (6.2) is a dynamical system of the form

$$\boldsymbol{x}' = f(\boldsymbol{x}, \boldsymbol{\mu}), \quad \boldsymbol{x} \in \mathbb{R}^{10} \quad \text{and} \quad \boldsymbol{\mu} \in \mathbb{R}^p \quad \text{with} \quad s \in (-\infty, +\infty) \tag{6.16}$$

where p is the number of independent nondimensional parameters under consideration.

Computation of homoclinic orbits requires local knowledge of the solutions near equilibria, specifically the trajectories by which homoclinic orbits leave the unstable manifold and approach the stable manifold. The monodromy matrix gives insight into the local dynamics of the system as a linear approximation of the flow at the fixed point of the map [82]. Consider the linearised equation about the periodic solution (6.13)

$$\Psi' = \frac{\partial f(\boldsymbol{\gamma}, \boldsymbol{\mu})}{\partial \boldsymbol{x}} \Psi = A(\boldsymbol{\gamma}, \boldsymbol{\mu}) \Psi \quad \text{with} \quad \Psi(0) = \mathbb{I}_{10} \tag{6.17}$$

Then the monodromy matrix is defined as $M := \Psi(\tau)$ and determined by the solution to the system of ordinary differential equations (6.17) evaluated at $s = \tau$.

In this thesis the monodromy matrix is computed column-wise, that is for the i^{th}-column of M a system of linear differential equations $\boldsymbol{z}' = A\boldsymbol{z}$ is integrated up to $s = \tau$ with the i^{th}-column of the identity matrix $\mathbb{I}_{10}$ as initial conditions [82, §7.5.1].

On linearising the system (6.9) about the periodic solution (6.13) then the linearised differential equation takes the form

$$\boldsymbol{z}' = A(s)\, \boldsymbol{z} \quad \text{for} \quad \boldsymbol{z} = (x_1, x_2, x_4, x_5, x_7, x_8, x_3, x_6, x_9, x_{10})^T$$

On reordering the variables the periodic matrix A decouples into two periodic matrices

$$A = \begin{pmatrix} A_1 & \mathbf{0} \\ \mathbf{0}^T & A_2 \end{pmatrix} \quad \text{with} \quad \mathbf{0} \in \mathbb{R}^{4\times 6}, \quad A_1 \in \mathbb{R}^{6\times 6} \quad \text{and} \quad A_2 \in \mathbb{R}^{4\times 4}.$$

A_1 is a six-by-six matrix containing the nontrivial dynamics $A_1 =$

$$\begin{pmatrix} 0 & (1+\nu) & 0 & -1 & 2\lambda(1+\epsilon)\cos(\tau s/2\pi) & 2\lambda(1+\epsilon)\sin(\tau s/2\pi) \\ -(1+\nu) & 0 & 1 & 0 & 2\lambda(1+\epsilon)\sin(\tau s/2\pi) & 2\lambda(1+\epsilon)\cos(\tau s/2\pi) \\ 0 & \dfrac{(1+\epsilon)}{m^2} & 0 & \nu & 0 & 0 \\ -\dfrac{(1+\epsilon)}{m^2} & 0 & -\nu & 0 & 0 & 0 \\ 0 & 0 & \dfrac{\cos(\tau s/2\pi)}{2} & -\dfrac{\sin(\tau s/2\pi)}{2} & 0 & \dfrac{(1+\nu)}{2} \\ 0 & 0 & \dfrac{\sin(\tau s/2\pi)}{2} & -\dfrac{\cos(\tau s/2\pi)}{2} & -\dfrac{(1+\nu)}{2} & 0 \end{pmatrix}$$

and A_2 is a four-by-four matrix containing the trivial dynamics.

$$A_2 = \begin{pmatrix} 0 & 0 & 0 & 0 \\ 0 & 0 & 0 & 0 \\ 0 & \dfrac{(1+\nu)}{2}\cos(\tau s/2\pi) & 0 & 0 \\ 0 & \dfrac{(1+\nu)}{2}\sin(\tau s/2\pi) & 0 & 0 \end{pmatrix}.$$

Thus monodromy matrix decouples into two submatrices, M_1 comprising of solutions to the linear system for A_1 and M_2 comprising of solutions to the linear system for A_2. The submatrix M_1 contains the dynamics of the system and the submatrix M_2 contains the trivial dynamics.

The submatrix M_2 yields a trivial Floquet multiplier $\mu^t = 1$ with algebraic and geometric multiplicity equal to four. The matrix of the trivial dynamics is spanned by the gradients of the three Casimirs (6.10) and constraint (6.12) when evaluated at the fixed point of the stroboscopic map $\boldsymbol{p}$. When the spectrum of Floquet multipliers are not all on the unit circle, the nontrivial monodromy matrix M_1 has a pair of complex conjugate unstable Floquet multipliers, $|\mu^u| > 1$, a pair of complex conjugate stable Floquet multipliers, $|\mu^s| <1$, and a pair of complex conjugates on the unit circle, $|\mu^c| = 1$. The local stable, centre and unstable manifolds are all two dimensional.

For general linear systems with periodic coefficients the monodromy matrix will have a unit Floquet multiplier $\mu^t = +1$ but in reversible or Hamiltonian formulations the roots of the associated characteristic polynomial occur in conjugate pairs (cf. lemma B.1.2). Hence the monodromy matrix will have a double Floquet multiplier at $\mu^t = +1$. For more detail on monodromy matrices, see [82, §7].

Generically homoclinic orbits are at least a codimension-one phenomena but if the system is Hamiltonian homoclinic orbits may be a codimension-zero phenomena [33]. The explanation is as follows: for non-Hamiltonian systems the sum of the dimensions of the stable and unstable manifolds is equal to the dimension of the ambient manifold, so the two manifolds can never intersect transversely so homoclinic orbits will be at least a codimension-one phenomenom. For Hamiltonian systems the intersection of the stable and unstable manifolds occurs along a constant 'energy' level defined by the Hamiltonian function and is thus of codimension-zero.

In the system (6.9) the centre-stable and centre-unstable manifolds are three-dimensional and their intersection occurs along an energy level, hence homoclinic solutions are codimension-zero.

The Floquet multipliers can only be computed numerically, so were computed using the highly accurate integrator `dop853.f` and the eigenvalue/eigenvector subroutine `f02agf.f`. The spectrum of Floquet multipliers was computed for a variety of (loading) parameters (λ, m) and is displayed in figure 6.1. In figure 6.1 the coloured regions correspond to elliptic regimes where all Floquet multipliers are on the unit circle and homoclinic solutions cannot exist. The colours correspond to various degrees of extensibility where $\epsilon = 0$ (blue), $\epsilon = 0.05$ (cyan) and $\epsilon = 0.1$ (magenta). The corresponding dotted lines are where all of the pairs of Floquet multipliers are stationary with respect to the principal continuation parameter, that is

$$\frac{\partial \mu^c}{\partial \lambda} = \frac{\partial \mu^s}{\partial \lambda} = \frac{\partial \mu^u}{\partial \lambda} = 0. \tag{6.18}$$

On these curves the Floquet multipliers reverse direction. At the cusp points, (where the dashed lines meets the coloured regions) there are codimension-two points (λ_c, m_c) at which the pairs of Floquet multipliers satisfy

$$\frac{\partial \mu^c}{\partial \lambda} = \frac{\partial \mu^s}{\partial \lambda} = \frac{\partial \mu^u}{\partial \lambda} = 0 \quad \text{and} \quad \mu^c = \mu^s = \mu^u. \tag{6.19}$$

Thus, at the codimension-two point all Floquet multipliers lie on the same point on the unit circle and have zero derivative, hence the stable and unstable Floquet multipliers

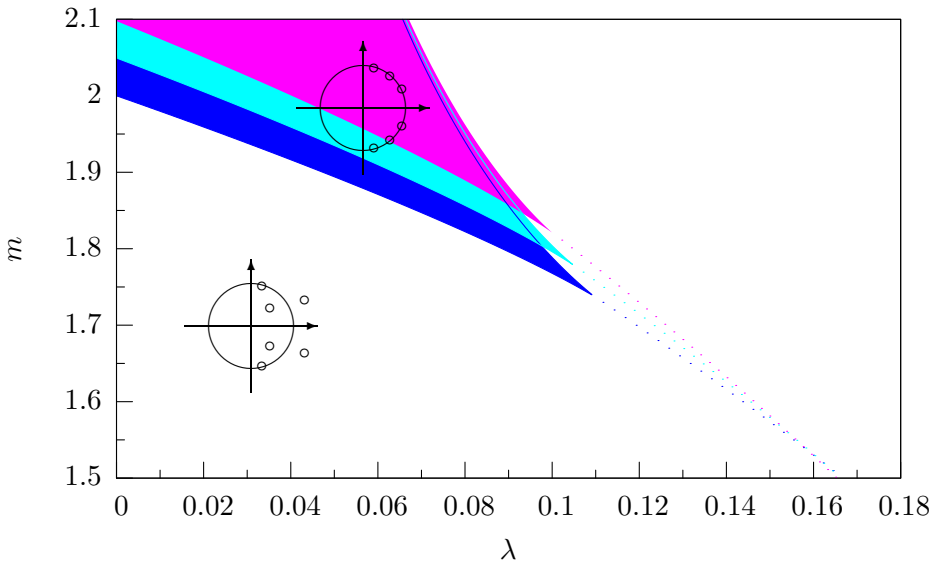

Figure 6.1: Spectrum of the monodromy matrix of the governing equation (6.9) about the trivial periodic solution (6.13) when $\nu = 1/3$. The coloured regions correspond elliptic periodic orbits, the dashed lines is the codimension-one curve at which the Floquet multipliers are stationary and reverse direction and the cusp points are co-dimension two points. Here $\epsilon = 0$ (blue), $\epsilon = 0.05$ (cyan) and $\epsilon = 0.1$ (magenta). In the unshaded region the spectrum of Floquet multipliers show the stable Floquet multipliers μ^s within the unit circle, centre Floquet multipliers μ^c on the unit circle and unstable Floquet multipliers μ^u outside the unit circle. In this region localised solutions are computed.

Table 6.1: Codimension-two points when $\nu = 1/3$ for a variety of rods with different degrees of extensibility. The codimension-two points were computed from the monodromy matrix of the governing equations about the periodic solution. The codimension-two points were identified as the cusp points of the spectrum of Floquet multipliers. The codimension-two points are of significance as the Hamiltonian-Hopf-Hopf bifurcation occurs at this point for primary homoclinic solutions and the codimension two points act as organising centres for the multimodal solutions.

ϵ	m_c	λ_c
0.00	1.7398	0.10897200
0.01	1.7451	0.10897395
0.02	1.7537	0.10790956
0.03	1.7622	0.10687853
0.04	1.7708	0.10583647
0.05	1.7793	0.10482703
0.06	1.7877	0.10384922
0.07	1.7961	0.10288132
0.08	1.8045	0.10192327
0.09	1.8129	0.10089494
0.10	1.8211	0.10007644

graze the unit circle (cf. figure 6.11(b)). Codimension-two points have been computed for a variety of degrees of extensibility and are displayed in table 6.1. It will be shown that the codimension-two points plays a significant role in the bifurcation structure of the rod in a magnetic field and the dashed line plays a role in the rod configurations near the codimension-two point.

6.2 Computation of Homoclinic orbits

The computation of solutions over an infinite domain is impossible. Thus it is necessary to truncate the domain to a finite interval. In this section the reversibilities of the system are exploited to formulate a well-posed boundary value problem over the half range. The boundary value problem is then solved with a shooting method by forming a variation problem with respect to the shooting parameters so that the righthand boundary conditions ensure that solutions are reversible.

The range of the dynamical system (6.16) is truncated and scaled over the unit

interval

$$\boldsymbol{x}' = \mathcal{T} f(\boldsymbol{x}, \boldsymbol{\mu}), \quad \boldsymbol{x} \in \mathbb{R}^{2n} \quad \text{and} \quad \boldsymbol{\mu} \in \mathbb{R}^{p} \quad \text{with} \quad s \in [0,1] \tag{6.20}$$

where $\mathcal{T}$ is the (as yet unknown) truncated length of half a homoclinic orbit.

The reflection symmetry Z is given by

$$Z : (x_1, x_2, x_3, x_4, x_5, x_6, x_7, x_8, x_9, x_{10}) \mapsto (-x_1, -x_2, x_3, -x_4, -x_5, x_6, -x_7, -x_8, -x_9, -x_{10}).$$

The discrete symmetry can be decomposed into two reversing involutions $Z = R_1 \circ R_2$ where $R_i^2 = \mathbb{I}_{10}$. The reversibilities are given by

$$R_1 : (x_1, x_2, x_3, x_4, x_5, x_6, x_7, x_8, x_9, x_{10}) \mapsto (-x_1, x_2, x_3, -x_4, x_5, x_6, x_7, -x_8, -x_9, x_{10}),$$
$$R_2 : (x_1, x_2, x_3, x_4, x_5, x_6, x_7, x_8, x_9, x_{10}) \mapsto (x_1, -x_2, x_3, x_4, -x_5, x_6, x_7, -x_8, -x_9, x_{10})$$

as $s \mapsto -s$ so that the trivial solution is also reversible and the fixed point $\boldsymbol{p}$ is invariant under both reversing involutions. The symmetric section $\mathcal{S}_1$, the fixed point set of a τ-periodic solution $\boldsymbol{\gamma}(s)$ for the reversing involution R_1, is given by

$$\mathcal{S}_1 = \mathrm{Fix}(R_1) \quad \text{for} \quad \boldsymbol{\gamma}(n\tau) = \boldsymbol{p} \quad \text{where} \quad f(\boldsymbol{p}) = \boldsymbol{0} \quad \text{with} \quad \boldsymbol{p} \in \mathcal{S}_1 \tag{6.21a}$$

so that

$$\mathcal{S}_1 = \left\{ \boldsymbol{x} \in \mathbb{R}^{10} : x_1(1) = x_4(1) = x_{10}(1) - 1 = 0 \right\}. \tag{6.21b}$$

The righthand boundary conditions are determined by the symmetric section $\mathcal{S}_i$, hence the three righthand boundary conditions for a R_1-reversible solution are

$$x_1(1) = x_4(1) = x_{10}(1) - 1 = 0. \tag{6.22a}$$

Similarly for a R_2-reversible solution the righthand boundary conditions are

$$x_2(1) = x_5(1) = x_{10}(1) - 1 = 0. \tag{6.22b}$$

Recalling that the system, reduced by the Casimirs and constraint yields a canonical six-dimension system and that the monodromy matrix decouples into a trivial four-dimensional matrix and non-trivial six-dimensional matrix, as the symmetric section is three-dimensional the reversibilities are reversibilities in the classical sense.

As the reversibilities define a three-dimensional symmetric section (6.22), so three shooting parameters are required in order to satisfy the righthand boundary conditions (6.22). Letting the three shooting parameters be $(\delta_1, \delta_2, \mathcal{T})$, where $\delta_1 \sim \mathcal{O}(1)$, $\delta_2 \in (0, 2\pi)$ and $\mathcal{T} \gg \delta_1$ then the lefthand boundary conditions are

$$\boldsymbol{x}(0) = \boldsymbol{p} + \varepsilon\,\delta_1\,(\boldsymbol{v}_1 \sin\delta_2 + \boldsymbol{v}_2 \cos\delta_2)\,. \tag{6.23}$$

The fixed point of the return map (6.14) is denoted by $\boldsymbol{p}$, $\varepsilon = 10^{-5}$ is a small perturbation, the shooting parameter δ_1 is a measure of the perturbation away from the equilibrium solution, δ_2 ensures that the perturbation remains transverse to the flow, and $\boldsymbol{v}_1$ and $\boldsymbol{v}_2$ are the real and imaginary parts of the eigenvectors that span the unstable (generalised) eigenspace of the monodromy matrix M_1. For $\nu = 1/3$, $m = 1.90$, $\lambda = 0.1$ and $\epsilon = 0.1$ the eigenvectors $\boldsymbol{v}_1 \pm \boldsymbol{v}_2 i$ corresponding to the unstable Floquet multipliers $\mu^u = -1.2861 \pm 2.5236i$ are

$$\begin{aligned}
\boldsymbol{v}_1 &= (0.5307, 0, 0, 0.2024, -0.02854, 0, 0.1367, -0.3974, 0, 0)\,,\\
\boldsymbol{v}_2 &= (0, 0.5307, 0, 0.02854, 0.2024, 0, 0.3974, 0.1367, 0, 0)\,.
\end{aligned}$$

Note that the eigenspace is a subspace of $\mathbb{R}^{10}$ but, due to the zeroes in the Floquet multipliers from the decomposition of the monodromy matrix, is homomorphic to $\mathbb{R}^6$, the dimension of the reduced phase space. This is because on linearisation the trivial dynamics decouple from the nontrivial dynamics so the four zeroes in the vectors correspond to the eigenspace spanned by eigenvectors of the trivial multiplier μ^t.

Effectively the shooting parameters δ_1 and δ_2 parametrise a solution along the (local) unstable manifold about a fixed point $\boldsymbol{p}$ of the stroboscopic map and $\mathcal{T}$ parametrises 'time' along one such trajectory. Since the initial conditions place a solution $\mathcal{O}(\varepsilon)$ away from the fixed point when $\delta_1 \sim \mathcal{O}(1)$, decreasing the distance from the fixed point leads to an increase in the truncation length $\mathcal{T}$ and vice versa.

If $\mathcal{T}$ is sufficiently large and ε sufficiently small, then equation (6.16) subject to the boundary conditions (6.23) and (6.22a) forms a well-posed boundary value problem for the computation of a reversible homoclinic about to the trivial solution (6.13).

Table 6.2: Data showing quadratic convergence of the shooting method from an suitable initial guess for the trimodal orbit in table 6.5. Due to restrictions of space shooting parameters for iterations $n = 3, 4$ and 5 all appear the same to six significant figures. The residue of the truncation length is defined as $\left|\mathcal{T}^{(i-1)} - \mathcal{T}^{(i)}\right|$ and similarly for δ_1 and δ_2. After 5 iterations the Newton-Raphson method has found the shooting parameters to within the specified tolerance of 10^{-12}.

n	δ_1	δ_2	$\mathcal{T}$	residue δ_1	residual δ_2	residual $\mathcal{T}$
0	4.00000	1.00000	111.000	–	–	–
1	3.03854	0.873004	112.611	0.961458E+00	0.126996E+00	0.161133E+01
2	3.14319	0.882138	112.390	0.104651E+00	0.913415E-02	0.220915E+00
3	3.14253	0.882213	112.392	0.665358E-03	0.758128E-04	0.146157E-02
4	3.14253	0.882213	112.392	0.510191E-09	0.385818E-08	0.190802E-08
5	3.14253	0.882213	112.392	0.799361E-14	0.461853E-13	0.426326E-13

Having formulated the boundary value problem as a three-parameter shooting problem, a forty-dimensional equation is constructed from the ten-dimensional system (6.9) coupled to a thirty dimensional variation equation of the partial derivatives of the phase variables with respect to the three shooting parameters $(\delta_1, \delta_2, \mathcal{T})$. The variational equation is then solved using the Newton-Raphson method. Each iteration is not computationally expensive but choosing three good initial guesses is often quite delicate. When a suitable initial guess is found the shooting method converges quadratically in accordance with the Newton-Raphson scheme, so shown in table 6.2. Homoclinic solutions are found for all parameter values which are not purely elliptic for isolated continua of the shooting parameters. Consistent with the Hamiltonian formulation, homoclinic orbits are a codimension-zero phenomena. For more details on how the variational equation was formulated and the shooting method was solved, see appendix §B.2.

There is a relationship between the shooting parameters δ_2 and $\mathcal{T}$ which is illustrated in figure 6.2. The truncation length $\mathcal{T}$ can be shifted by the phase $\tau/2 = 2\pi/(1+\nu)$ and δ_2 then scaled by a factor $\sqrt{\ln|\mu^u|}$. This gives a greater value for the truncation length and places the initial condition nearer the fixed point of the map, giving a better approximation to the homoclinic orbit. There does not appear to be any pattern to the behaviour of the shooting parameter δ_1 under this phase shift.

Reversible pairs of solutions can be found in one of two ways; either by adding π to δ_1 or by taking $-\delta_2$ rather than δ_2.

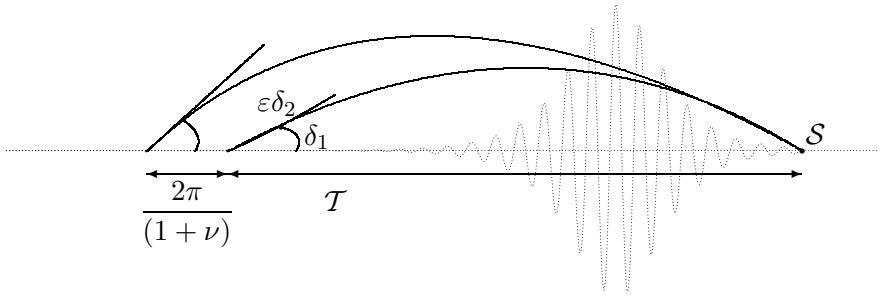

Figure 6.2: Schematic diagram of the shooting method into the symmetric section S_i for a bimodal homoclinic illustrating the failure to locate families of bimodal solutions as had been done for the Kirchhoff rod [95]. The diagram shows the interpretation of the shooting parameters and shows the choice of starting position is arbitrary up to a phase $2\pi/(1+\nu)$.

Given the two involutions R_1 and R_2, four distinct primary homoclinic orbits are expected to exist; two for each of the reversibilities. Primary homoclinic orbits are homoclinic orbits with a single localisation and are labelled as P_i for $i = 1, 2, 3, 4$ where $P_{1,2}$ are reversible under R_1 and $P_{3,4}$ are reversible under R_2. Multimodal homoclinic solutions are characterised by a number of distinct primary localisations separated by a number of smaller oscillations.

Table 6.3 gives shooting parameters for a set of primary homoclinic orbits within the non-elliptic region. Shooting parameters for a selection of bimodal and trimodal homoclinic orbits are given in tables 6.4 and 6.5 respectively. Sample configurations of a primary homoclinic orbit are displayed in figure 6.3. Components of the body force due to the magnetic effects, that is $\boldsymbol{F}_L$ in (3.33), are displayed in figure 6.4. Components of multimodal homoclinic orbits from the tables 6.4 and 6.5 are displayed in figure 6.5.

For the Kirchhoff rod the shooting method can be used to detect a multiplicity of multimodal configurations according to a well-defined set of accumulation rules (for more detail see §B.5). As shall be demonstrated in §6.5 using continuation, while families of multimodal solutions *do* exist in this system, the shooting method is unable to find

Table 6.3: Shooting data for the reversible primary homoclinic orbits when $\nu = 1/3$, $m = 1.90$, $\epsilon = 0.1$ and $\lambda = 0.1$. Note that as the homoclinics are reversible that $\mathcal{T}$ is the distance to the symmetric section and is half the length of the full homoclinic.

		δ_1	δ_2	$\mathcal{T}$
R_1	P_1	1.058975	1.374092	60.61385
	P_2	4.200569	1.374092	60.61385
R_2	P_3	0.2069183	1.082621	58.26191
	P_4	3.348511	1.082621	58.26191

Table 6.4: Shooting data for some reversible bimodal homoclinic orbits when $\nu = 1/3$, $m = 1.90$, $\epsilon = 0.1$ and $\lambda = 0.1$. Once again, note that as the homoclinics are reversible that $\mathcal{T}$ is the distance to the symmetric section and is half the length of the full homoclinic.

		δ_1	δ_2	$\mathcal{T}$
R_1	(P_1, P_1)	3.900605	2.809424	82.48046
	(P_2, P_1)	0.7590124	2.809424	82.48046
R_2	(P_3, P_3)	0.8877950	1.797026	81.18148
	(P_4, P_3)	4.029388	1.797026	81.18148

members in a systematic way, in constrast to the Kirchhoff rod. Instead of finding a bimodal solution with an extra quarter turn often the shooting method would find a bimodal solution with the truncation length shifted by one period τ.

Multimodal solutions are found in the anisotropic system when $B_1 \neq B_2$, as shown in figure 6.6, providing numerical evidence that, as in the Kirchhoff rod, anisotropy is an integrability breaking parameter for the linearly elastic, inextensible, unshearable rod in

Table 6.5: Shooting data for some reversible trimodal homoclinic orbits when $\nu = 1/3$, $m = 1.90$, $\epsilon = 0.1$ and $\lambda = 0.1$. Once again, note that as the homoclinics are reversible that $\mathcal{T}$ is the distance to the symmetric section and is half the length of the full homoclinic.

		δ_1	δ_2	$\mathcal{T}$
R_1	(P_2, P_2, P_2)	3.142530	0.8822137	112.3920
	(P_3, P_1, P_4)	6.284123	0.8822137	112.3920
R_2	(P_1, P_4, P_1)	0.5914260	6.264897	99.38831
	(P_2, P_3, P_2)	3.7330187	6.264897	99.38831

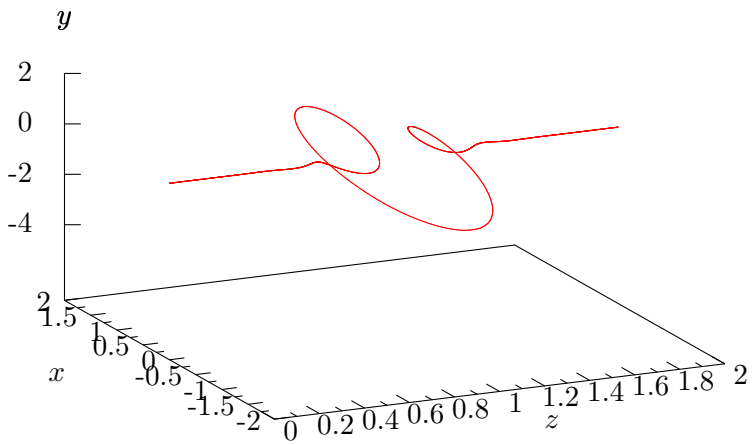

Figure 6.3: Configuration of primary homoclinic P_1 orbits in table 6.3. The reversible configuration was computed using the shooting method over the half length and then reflected.

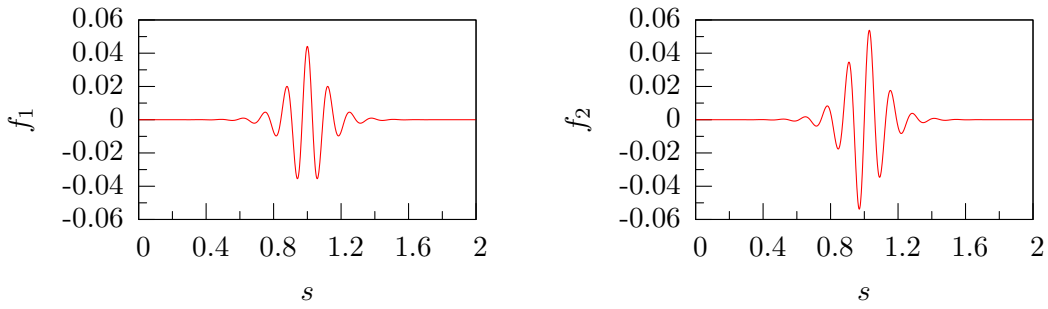

Figure 6.4: External forces due to magnetic effects for the P_1 orbits in table 6.3. The component in $\boldsymbol{d}_1$ is given by $f_1 = 2\,(1+\epsilon x_3)\,(x_7x_{10} + x_8x_9)$ and the component in $\boldsymbol{d}_2$ is given by $f_2 = 2\,(1+\epsilon x_3)\,(x_7x_9 - x_8x_{10})$. Note that the external forces are reversible: the configuration was computed using the shooting method over the half length and then reflected.

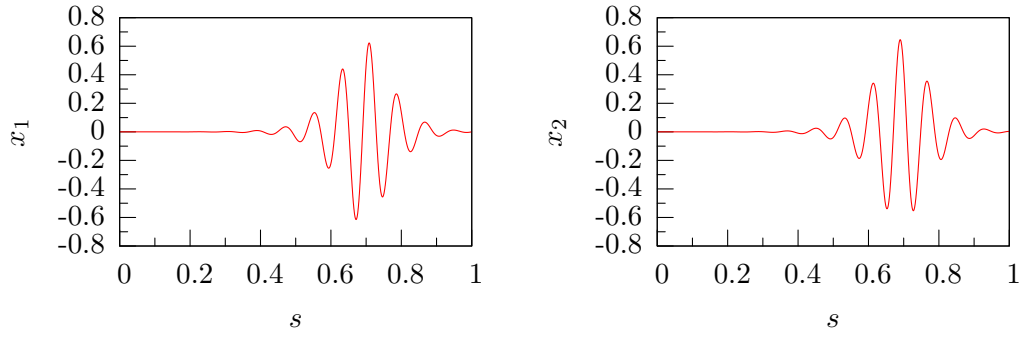

(a) (P_1, P_1)

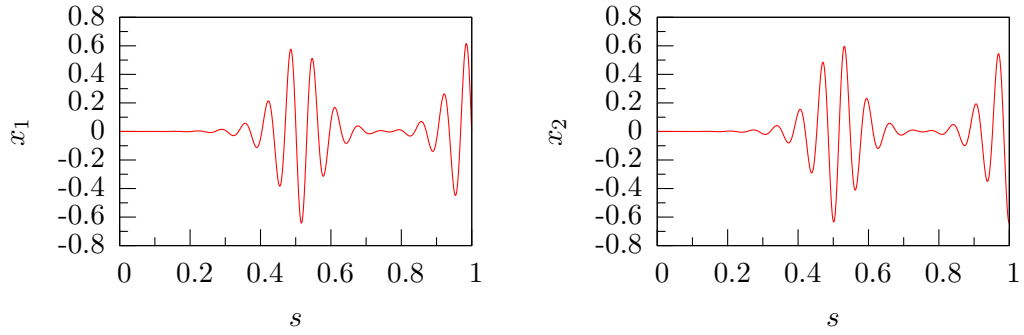

(b) (P_2, P_2, P_2)

Figure 6.5: Force components x_1 and x_2 over the half range of the bimodal orbit (P_1, P_2) from table 6.4 and for the trimodal orbit (P_2, P_2, P_2) in table 6.5.

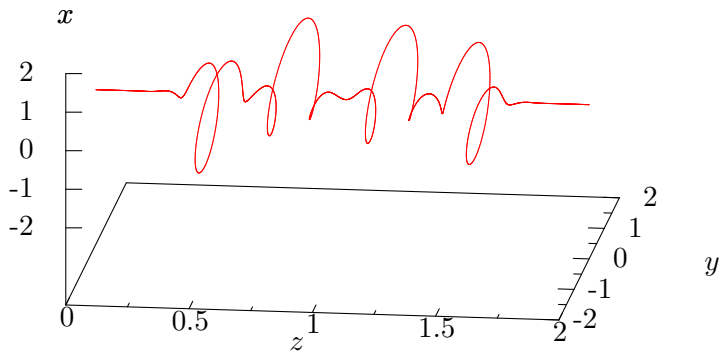

Figure 6.6: An anisotropic quadmodal homoclinic with parameters are $\nu = 1/3$, $\lambda = 0.01$, $m = 1.70$ and $\rho = 0.1$. The shooting parameters are given by $\delta_1 = 5.2433$, $\delta_2 = 2.1968$ and $\mathcal{T} = 85.509$. The multimodal configuration provides strong numerical evidence that anisotropy is an integrability breaking parameter which leads to transverse intersections of the stable and unstable manifolds and spatially chaotic solutions, as has been seen in the Kirchhoff case.

a uniform magnetic field.

6.2.1 Case (iii): Multimodal Configurations of a weakly extensible rod in a strong magnetic field

A mulitplicity of multimodal homoclinic solutions for rods with small ϵ, large λ were found by the shooting method. Figure 6.7 gives data for a selection of R_2-reversible multimodal orbits with $m = 1.70$, $\nu = 1/3$ $\lambda = 1/5$ and $\epsilon = 0.0001$ in region (iii) from §5.3 which are then displayed in figure 6.7. Numerical evidence strongly suggests that extensibility destroys the non-transverse intersection of the stable and unstable manifolds for a rod in a magnetic field [16]. It is difficult to label the multimodal solutions with many modes, such as the five- and six-modal in terms of the primary orbits of which they are composed.

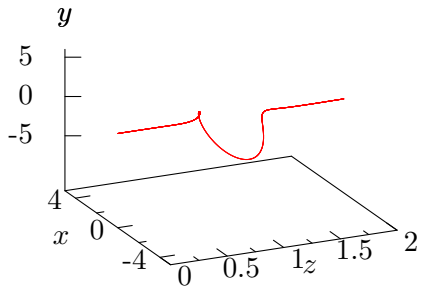

(a) primary

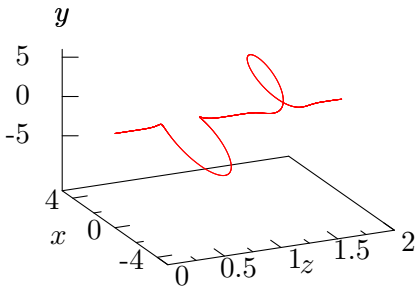

(b) bimodal

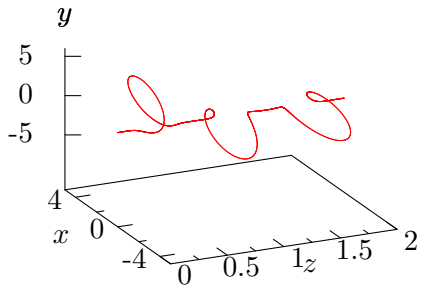

(c) trimodal

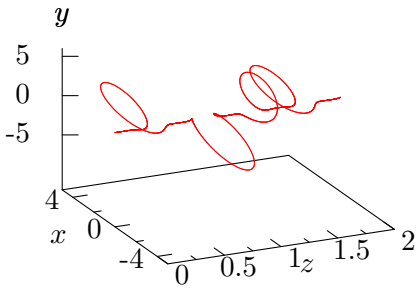

(d) quadmodal

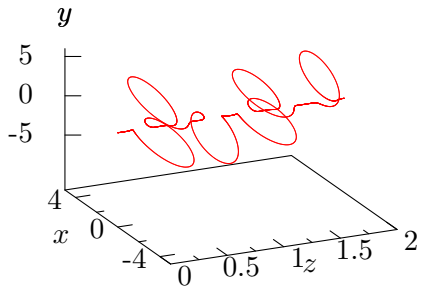

(e) five-modal

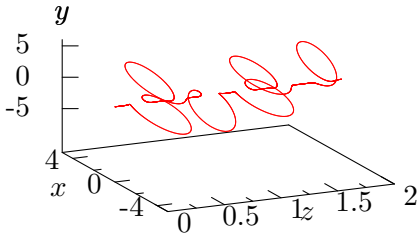

(f) six-modal

Figure 6.7: A selection of multimodal solutions in the regime of parameter space where $\lambda >> \epsilon$. The parameters are with $m = 1.70$, $\nu = 1/3$ $\lambda = 1/5$ and $\epsilon = 0.0001$. Shooting data for each configuration is displayed in table 6.6. Note that the solutions were computed by the shooting method and reflected about the symmetric section.

Table 6.6: Shooting data for R_2-reversible homoclinic orbits when $\nu = 1/3$, $m = 1.70$, $\epsilon = 0.0001$ and $\lambda = 1/5$.

	δ_1	δ_2	$\mathcal{T}$
primary	3.947947	1.653330	45.66977
bimodal	2.653258	2.527768	73.78479
trimodal	4.847755	0.01053711	102.0591
quadmodal	2.734204	1.122803	141.5829
five-modal	2.297042	1.611518	171.7983
six-modal	1.902365	2.581330	201.9815

6.3 Continuation

In this section the continuation of homoclinic orbits is performed using projection boundary conditions [12, 13] exploiting the exponential trichotomies the system possesses [58]. The method places solutions in the linear subspace which approximates the flow near the fixed point of the map. The approximation error caused by the truncation has been shown to decay exponentially [12]. For more information on projection boundary conditions see §B.3.1.

In this system the continuation of periodic-to-periodic homoclinic orbits is simplified [8, 19, 34] by knowing the underlying periodic orbit (6.13). The stable, centre and unstable projection matrices L_s, L_c and L_u respectively, are formed by the normalised stable, centre and unstable eigenvectors of the transpose of the monodromy matrix. Projecting back onto the two-dimensional centre and unstable (generalised) eigenspaces about the phase condition (6.14) yields the four lefthand boundary conditions

$$L_s(\boldsymbol{\mu})(\boldsymbol{x}(0) - \boldsymbol{p}) = \mathbf{0}, \quad L_s(\boldsymbol{\mu}) \in \mathbb{R}^{2\times 10}, \tag{6.25a}$$

$$L_c(\boldsymbol{\mu})(\boldsymbol{x}(0) - \boldsymbol{p}) = \mathbf{0} \quad \text{and} \quad L_c(\boldsymbol{\mu}) \in \mathbb{R}^{2\times 10}. \tag{6.25b}$$

Applying the symmetric section boundary conditions, for R_1 as in (6.22a), yields three righthand boundary conditions

$$x_1(1) = x_4(1) = x_{10}(1) = 0. \tag{6.26}$$

Finally, specifying the three Casimir (6.10) and the constraint fixing conditions (6.12) at $s = 0$ gives four lefthand boundary conditions

$$x_3(0) = x_6(0) = x_9(0) = x_{10}(0) - 1 = 0. \tag{6.27}$$

The system (6.9) with boundary conditions (6.25), (6.26) and (6.27) is over-determined as there are eleven boundary conditions for a ten-dimensional system (6.9). Specifically, the projection boundary conditions (6.25) provide an extra condition, as there are four boundary conditions determining a flow which can be uniquely characterised by three (shooting) parameters. Thus, in order to make the problem well-posed the truncation length, $\mathcal{T}$, is allowed to vary along with the principal continuation parameter λ.

Continuation is performed using AUTO97 [35]. The continuation software uses Gaussian collocation, which is equivalent to a symplectic Runge-Kutta scheme. Symplectic Runge-Kutta methods exactly conserve the value of any integrals of the system that are quadratic functions of the phase variables [24]. Thus, as all of the conserved quantities are quadratic functions of the phase variables, they will be preserved by the numerical scheme. Indeed, the Lax pair formulation presented in §3.4, shows all the conserved quantities of the integrable subfamily are quadratic and hence will be preserved by the numerical scheme.

It should be noted that while there is no restriction on the sign of λ, that when performing continuation an increase in λ acts in the direction of the end load parameter m and decreasing λ acts against the end load parameter. Although λ is both increased and decreased, in all continuation runs λ will be positive. When continuation was performed with λ negative no bifurcation was found.

In order to visualise the rod configurations the centreline $\boldsymbol{r}(s) = (x, y, z)$, which evolves according to (3.6), is computed from the initial condition

$$\boldsymbol{r}(0) = \mathbf{0}. \tag{6.28}$$

Hence the end-rotation and (dimensionless) end-displacement can be calculated while continuing along solution branches of homoclinic orbits for the two parameters λ and $\mathcal{T}$.

End-rotation and end-displacement are solution measures, called load-deflections, which represent the contributions due to the effect of loading on configurations by removing the trivial contributions from a unbuckled straight rod. The end-displacement, $\tilde{\mathcal{D}}$, is simply the length of the localised configuration subtracted from the length of the straight twisted rod. The relative end-rotation is the additional twisting due to loading and is calculated by subtracting the end rotation of the straight twisted rod from the end rotation of a localised rod configuration. The end-displacement, $\tilde{\mathcal{D}}$ and relative end-rotation $\tilde{\mathcal{R}}$ are given by

$$\tilde{\mathcal{D}} = (1+\epsilon)\,\mathcal{T} - z\,(1)\,, \tag{6.29a}$$

$$\tilde{\mathcal{R}} = \frac{\mathcal{R} - (1+\nu)\,\mathcal{T}}{2\pi}. \tag{6.29b}$$

For the end rotation $\mathcal{R}$ of a straight twisted rod the directors evolve according to $\boldsymbol{d}_{1,2}'' = -(1+\nu)\,\boldsymbol{d}_{1,2}$, so that for a rod of length $\mathcal{T}$ the angle turned by the end point is $(1+\nu)\,\mathcal{T}$. Thus

$$\cos\mathcal{R} = \langle \boldsymbol{d}_1\,(1)\,, \boldsymbol{d}_1\,(0)\rangle = \langle \boldsymbol{d}_1\,(1)\,, (1,0,0)\rangle \quad \text{and} \quad \sin\mathcal{R} = \langle \boldsymbol{d}_1\,(1)\,, (0,1,0)\rangle\,.$$

As all configurations computed are reversible, found shooting over the half range into a symmetric section, load-deflection curves are computed by simply doubling the values the from half-length solutions. Varying $\mathcal{T}$ has no effect on the values of the load deflections since the contributions from varying the truncation length produce trivial contributions, i.e. almost straight twisted rod segments, which do not effect the load deflections. The method is validated through continuation in m and $\mathcal{T}$ in the isotropic, inextensible case, which recovers the classical buckling value $m = m_{\max} = 2$ and post-buckling path.

6.4 Bifurcation

In this section the bifurcation behaviour of primary homoclinic orbits is investigated numerically. It is found that the rod buckles in a twice generalised Hopf bifurcation: firstly by being Hamiltonian and secondly by being a bifurcation of a periodic orbit.

From the analysis of the Floquet multipliers in figure 6.1, the codimension-two point distinguishes between primary homoclinic configurations which can buckle at two values $\lambda = \lambda_+$, $\lambda = \lambda_-$, one value, $\lambda = \lambda_c$ or which do not buckle. Load-deflection diagrams presented in figure 6.8 illustrates all three possible situations. From subfigure 6.8(a) it can be seen that localised configurations can either buckle from the right at $\lambda_+ = 0.076370$ or from the left at $\lambda_- = 0.087626$. (The buckling values predicted through the Floquet multipliers are $\lambda_+ = 0.076482$ and $\lambda_- = 0.087562$). As can be seen from subfigure 6.8(b) if $m = m_c = 1.8211$ the load deflection curves are discontinuous at $\lambda = \lambda_c = 0.10007644$ as the curves merge from the left and right. Thus at the codimension-two point a double Hamiltonian-Hopf bifurcation occurs. Subfigure 6.8(c) shows that the load-deflection diagrams are smooth for all λ if $m < m_c$. Note that the mimina of the load-deflection curves are accurately predicted by the stationary point of the Floquet multipliers which is illustrated by the dotted line in figure 6.1. Thus, just below the critical value m_c there is a linear approximation to the point at which the configurations cease to delocalise and begin to localise.

As illustrated in subfigure 6.9(a), configurations which exist when $\lambda > \lambda_+$ and $m > m_c$ are highly localised and buckle in a more pronounced way than those configurations which exist for $\lambda < \lambda_-$ and $m > m_c$. However, the rod configurations are qualitatively similar whether the bifurcation values are approached from either the left or the right. It is interesting to note that straight twisted rods will actually buckle with λ either decreasing or increasing. Also note that the post-buckling paths of a rod due to a magnetic field, in figures 6.9 and 6.8, are not dissimilar to the post-buckling paths due to end force and moment, in figure 6.12.

Figures 6.8 and 6.9 illustrate that the effect of the magnetic field on the configurations produces two distinct scenarios depending on the value of end loading m in relation to the critical value m_c. If $m < m_c$ then localising-buckling occurs, as illustrated in subfigure 6.9(a) but if $m > m_c$ then due to the residual effect of the codimension-two point localising-delocalising-localising behaviour occurs, as illustrated by subfigure 6.9(b).

For values of m far below the critical value m_c the load-deflection diagrams are

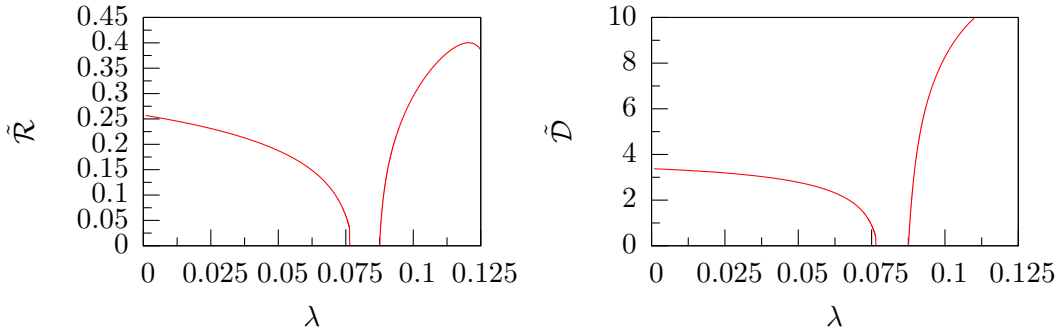

(a) $m = 1.9 > m_c$

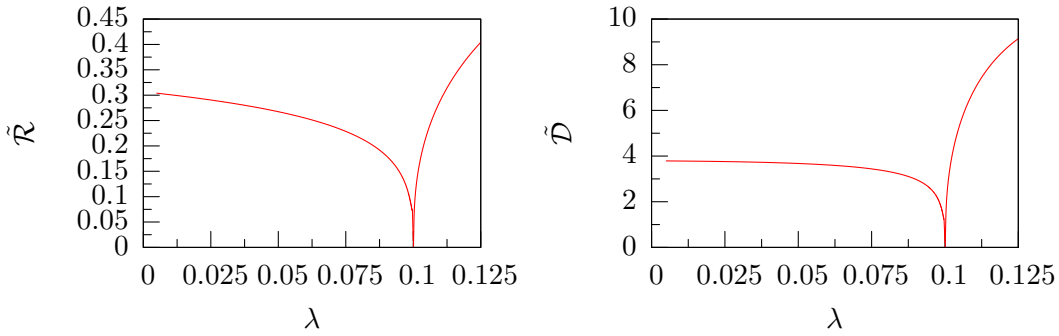

(b) $m = 1.8211 = m_c$

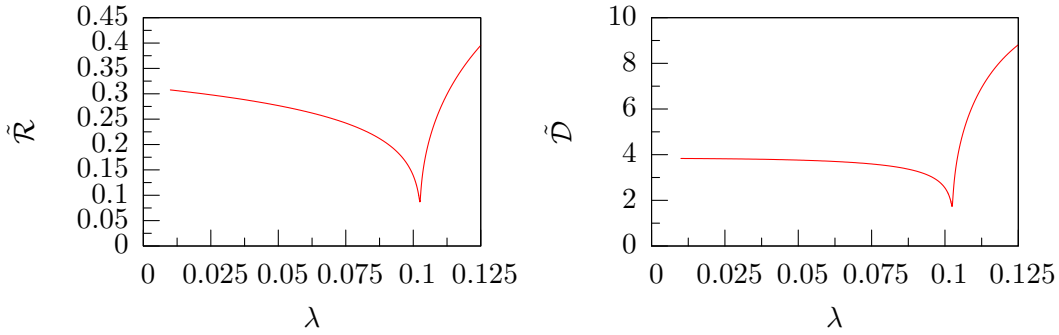

(c) $m = 1.81 < m_c$

Figure 6.8: Load-deflection diagrams of a primary reversible homoclinic solution for λ, when m is above, equal and below the codimension-two point m_c. When $m > m_c$ two Hamiltonian-hopf bifurcations occur at $\lambda_\pm$. When $m = m_c$ the two bifurcations occur similtaneously and there is a Hamiltonian-Hopf-Hopf bifurcation at λ_c When $m < m_c$ then no bifurcation occurs.

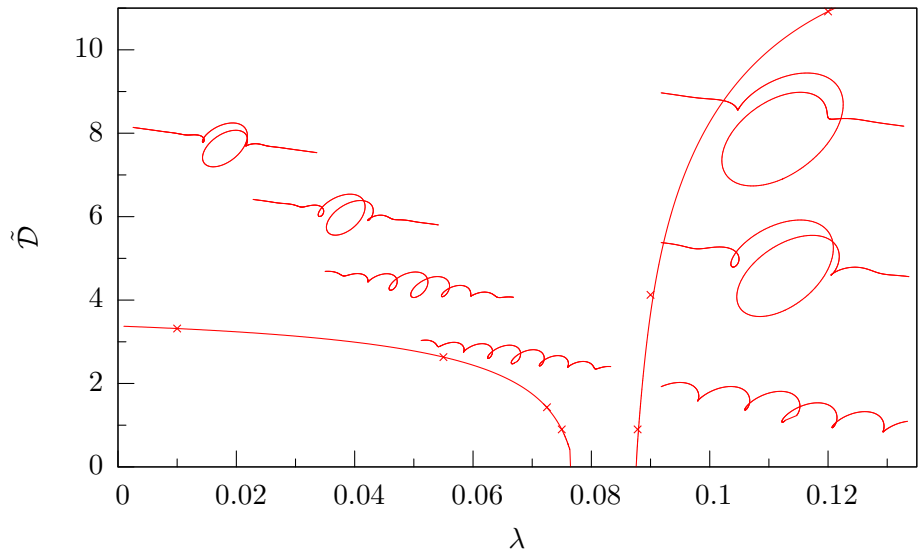

(a) $m = 1.90 > m_c$

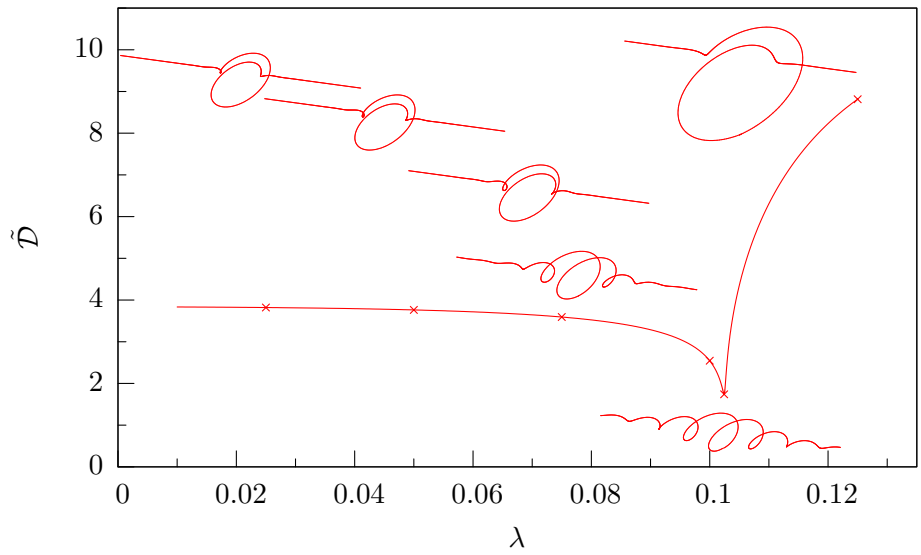

(b) $m = 1.81 < m_c$

Figure 6.9: Subfigure 6.9(a) shows buckling for both $\lambda_+ = 0.07637$ and $\lambda_- = 0.087626$ above the codimension-two point when $m = 1.90$. Subfigure 6.9(b) shows the localisation-delocalisation-localisation behaviour below the codimension-two point at $m = 1.81$. Again, in both subfigures $\nu = 1/3$ and $\epsilon = 0.1$. The marks $\times$ on the bifurcation curves correspond to the configurations they appear besides.

qualitatively different from those load deflection diagrams where the values of m are near or greater than m_c. As can be seen from figure 6.10 for $m = 1.7398$ initially as λ increases so $\tilde{\mathcal{R}}$ decreases while $\tilde{\mathcal{D}}$ increases, in contrast to the behaviour in subfigure 6.8(c). For values of m just below the critical value m_c the minima of the load-deflection curves are accurately predicted by the stationary values of the Floquet multipliers, but far below the critical value m_c the minimum and point of inflection are not accurately predicted by the behaviour of the Floquet multipliers. Quantitatively in this regime localisation dominates over the diminishing effect of the codimension-two point.

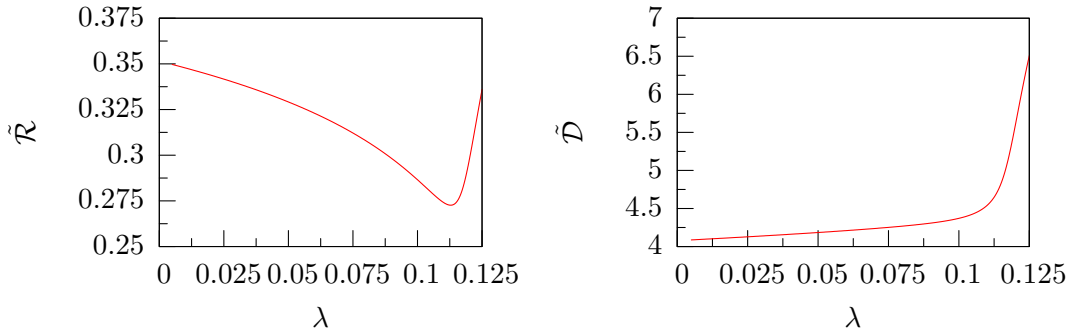

Figure 6.10: Load-deflection diagrams for λ far below the codimension two point at $m = 1.7398 \ll m_c$. The critical value of λ is given by $\lambda = 0.1128947$ although there seems to be little quantitative difference between solutions near this value. Note that the scale on the y-axes are different from figure 6.8. This diagrams illustrates that far below the codimension-two point the localisation-delocalation-localisation effect is neglible.

Schematic diagrams in figure 6.11 illustrate the observed bifurcation in terms of the spectrum of the six nontrivial Floquet multipliers. Subfigure 6.11(a) illustrates the case when $m > m_c$. Starting from $\lambda = 0$, while the centre Floquet multipliers move from $(1, 0)$ around the unit circle, the stable and unstable Floquet multipliers collide on the unit circle when $\lambda = \lambda_-$. At the bifurcation the pair of Floquet multipliers split and move around the unit circle in opposite directions before one pair collides with the centre multipliers when $\lambda = \lambda_+$. The multipliers then split again to become pairs of stable and unstable multipliers. As can be inferred from figure 6.9 the process can be described in reverse as λ decreases from a large value.

As subfigure 6.11(b) illustrates, when $m = m_c$ the centre Floquet multipliers now move around the unit centre with sufficient speed so that at $\lambda = \lambda_c$ all the Floquet multipliers collide on the unit circle. At this point there is a triple resonance between the Floquet multipliers. After the collision one pair remain on, one pair within and one pair outside of the unit circle.

When $m < m_c$ the stable and unstable Floquet multipliers approach the unit circle but slow down, stop then reverse direction heading away from the unit circle.

It is clear that six is the minimal dimension at which two distinct Hamiltonian-Hopf bifurcations can occur similtaneously. It is unfortunate that due to the underlying periodicity of the trivial solution no analytical expressions for the codimension-two point can be found. One can understand that the two loading parameters λ and m 'unfold' the dynamics in the sense that there exists a parameter $\eta^1 = \eta^1(\lambda, m)$ which determines the two Hamiltonian-Hopf bifurcations and a parameter $\eta^2 = \eta^2(\lambda, m)$ which determines the distance between the bifurcations such that at the critical values $\eta_c^1 = \eta_c^1(\lambda_c, m_c)$ and $\eta_c^2 = \eta_c^2(\lambda_c, m_c)$ the two bifurcations occur simultaneously. As will be seen later, the codimension-two point is an organising centre for the bifurcation set of primary and multimodal homoclinics.

For comparison the effect of a constant magnetic field when $\lambda < \lambda_c$ on the buckling of a rod due to end loading m is illustrated in figure 6.12 . It is observed that the presence of the magnetic field decreases the critical buckling loads. This bifurcation is also a Hamiltonian-Hopf bifurcation of a periodic orbit.

Similarly, the effect of the magnetic field on the buckling of the rod due to anisotropy is illustrated in figure 6.13. Once again the presence of the magnetic field leads to a decrease in the buckling value and the overall post-buckling paths.

6.5 Coalescence of Multimodal Homoclinic Orbits

From the analysis presented in §5.3 it is shown that multimodal solutions cannot exist in the integrable limit as either λ or ϵ approaches zero. Instead pairs of reversible multimodal solutions coalesce at limit points. As has been seen in figure 6.8, for primary

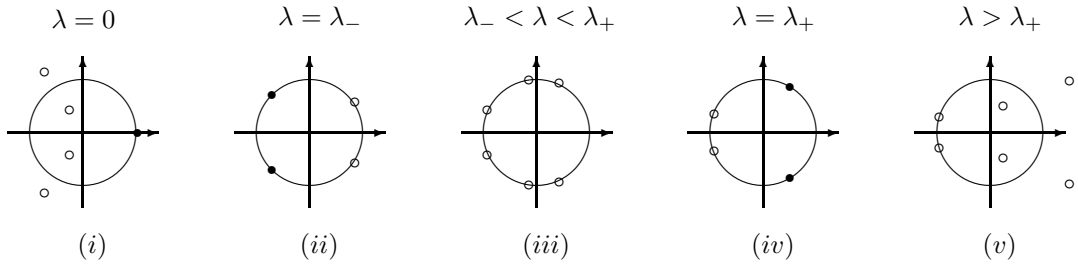

(a) $m > m_c$

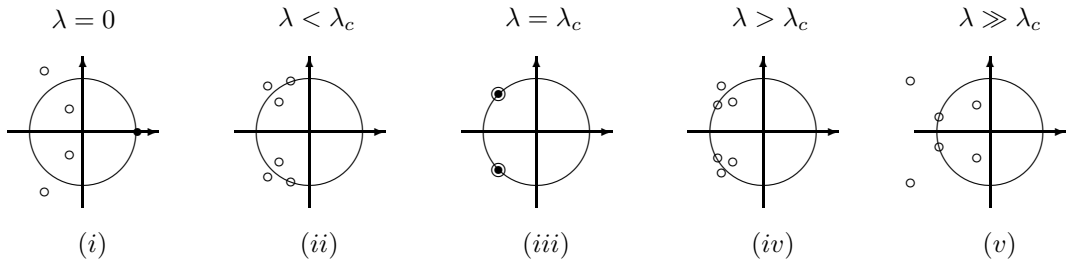

(b) $m = m_c$

Figure 6.11: Schematic diagrams of the motion of the Floquet multipliers for the twice generalised Hopf bifurcation at $m > m_c$ at which two Hamiltonian-Hopf bifurcations occur at $\lambda_\pm$ and at $m = m_c$ at which the two bifurcations occur similtaneously at λ_c. There is no diagram for the region $m < m_c$ as the is no bifurcation. In this regime the stable and untable Floquet multipliers approach the unit circle and reverse direction. The centre multipliers reverse direction also.

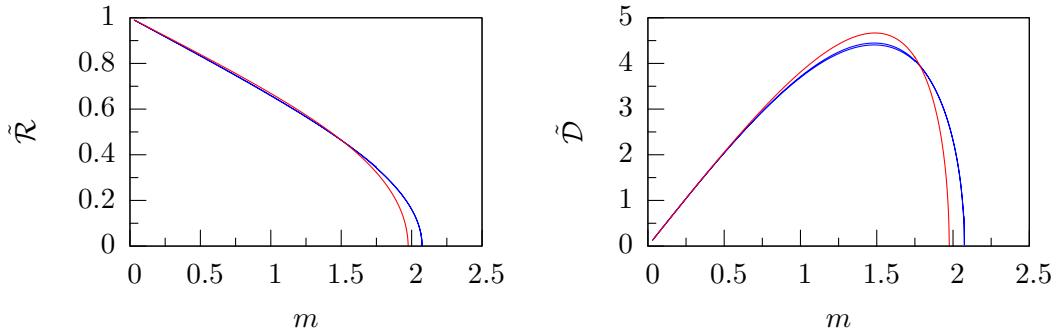

Figure 6.12: Load-deflection diagrams for primary homoclinics when $\nu = 1/3$, $\epsilon = 0.1$. When $\lambda = 0.01$ (blue) then the rod buckles at $m = 2.074667$ and if $\lambda = 0.05$ (red) the rod buckles at $m = 1.975754$. Qualitatively the bifurcation diagram is the same as the Kirchhoff case but the effect of the magnetic field lowers the buckling value.

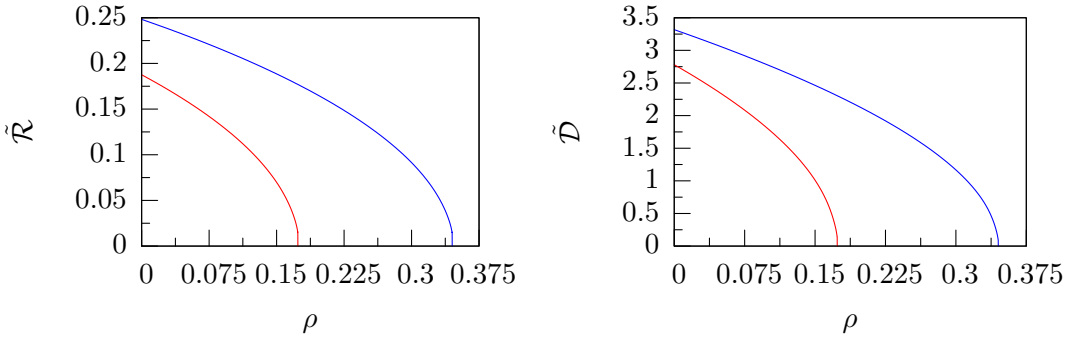

Figure 6.13: Load-deflection diagrams for homoclinics when $\nu = 1/3$, $\epsilon = 0.1$ and $m = 1.90$. The blue line corresponds to $\lambda = 0.01$ and buckles at $\rho = 0.3451724$ and the red line corresponds to $\lambda = 0.05$ and this buckles at $\rho = 0.1736441$. Qualitatively the bifurcation diagram is the same as the Kirchhoff case but the effect of the magnetic field lowers the buckling value.

homoclinic orbits the codimension-two point separates regimes which have two, one or zero bifurcation values; in this section the effect of the codimension-two point on the persistence of multimodal solutions and bifurcation structure of multimodal solutions is investigated numerically. The bifurcation structure of the Kirchhoff rod is presented in §B.5.

Figure 6.14 shows the continuation of a bimodal solution in m when $\lambda = 0.20$. There are three branches, labelled b_1 (blue), b_2 (cyan) and b_3 (red) connected by two limit points at $lp_1 = (0.2, 1.791139)$ and $lp_2 = (0.2, 2.033325)$. As can be seen in the inset diagrams the limit point lp_1 connects branches b_1 and b_2 and the limit point lp_2 connects branches b_2 and b_3. Branch b_1 can be continued further with m increasing and branch b_3 be continued further with m decreasing.

Figure 6.15 shows the configurations on the three branches b_1 (blue), b_2 (cyan) and b_3 (red) at fixed values of $m = 1.80 > lp_1$ and $m = 2.00 < lp_2$. Note that the configurations displayed in subfigures 6.15(a) and 6.15(c) and those in subfigures 6.15(d) and 6.15(f) are qualitatively similar as the selected values of m are near the limit points at which they coalesce. Subfigures 6.15(a), 6.15(b) and 6.15(c) show that for branch b_2 when $m = 1.80$ configurations have the same number of quarter turns as configurations on branch b_1. Subfigures 6.15(d), 6.15(e) and 6.15(f) show that when $m = 2.00$ configurations have

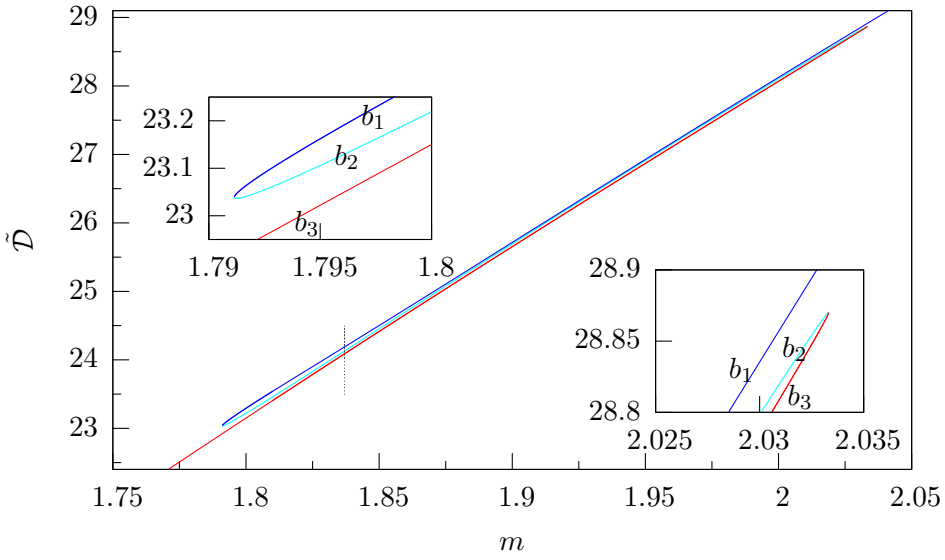

Figure 6.14: Three connected branches of bimodal orbits b_1 (blue), b_2 (cyan) and b_3 (red) at $\lambda = 0.20$ with $\nu = 1/3$ and $\epsilon = 0.1$. From continuation in m the branches b_1 and b_2 coalesce at $m = 1.791139$, while the b_2 and b_3 curves coalesce at $m = 2.033325$. The dashed line marks the point at which b_2 switches from connecting b_1 to connecting b_3.

the same number of quarter turns as configurations on branch b_1. Thus at the limit points lp_1 configurations on the branch b_2 gain a quarter turn and at the limit point lp_2 configurations on the branch b_2 loss a quarter turn.

Figure 6.16 shows that when continuation is performed in λ decreasing near the limit point lp_1 a succession of branches passing through b_1 and b_2 coalesce. A corresponding result holds near the limit point lp_2 where a succession of branches which pass through b_3 and b_2 coalesce.

When continuation is performed in λ for $lp_1 < m < 1.837$ the branch b_2 coalesces with b_1 whereas for $1.837 < m < lp_2$ the branch b_2 switches to coalesce with branch b_3. Figure 6.17 shows two branches of solutions which pass through b_2 (cyan), one of which, with $m = 1.8369$, connects with a branch which passes through b_1 (blue) the other, with $m = 1.8373$, is connected to a branch of solutions which passes though b_3 (red).

When continued in λ decreasing with m sufficiently smaller than m_c the branch b_3 passes beyond λ_c and merges with another branch. Thus, in order to merge with other

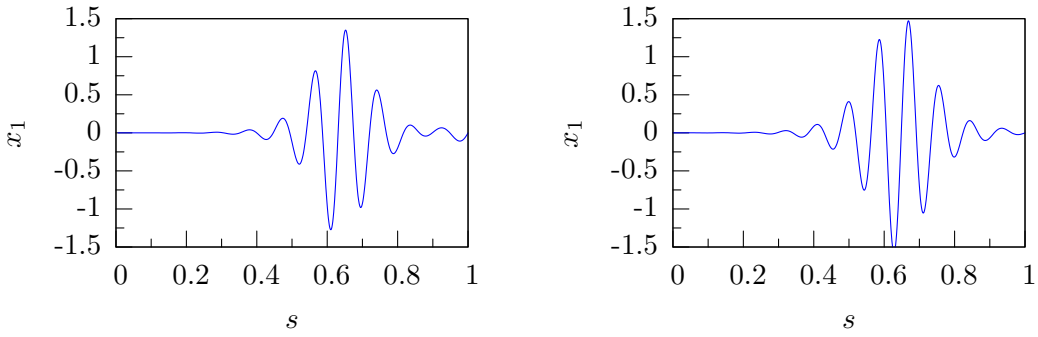

(a) b_1, $m = 1.80$

(b) b_1, $m = 2.00$

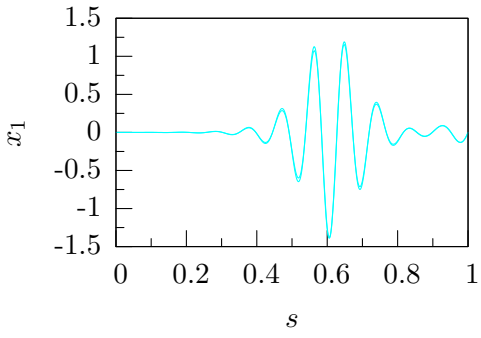

(c) b_2, $m = 1.80$

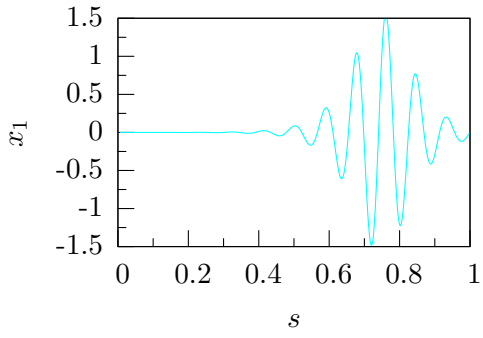

(d) b_2, $m = 2.00$

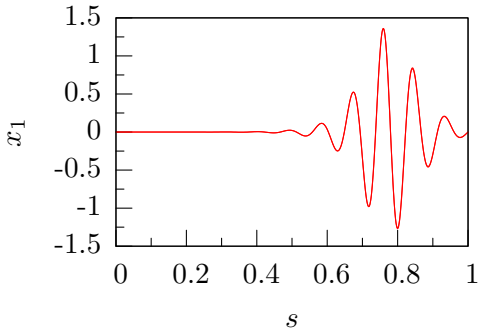

(e) b_3, $m = 1.80$

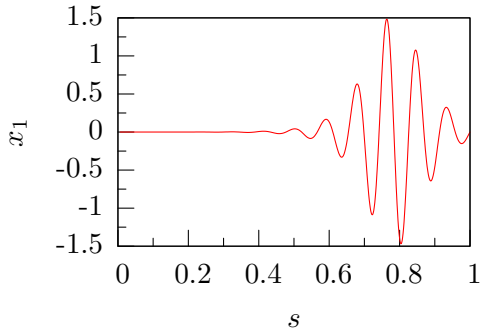

(f) b_3, $m = 2.00$

Figure 6.15: Nondimensionalised force components x_1 of bimodal configurations found by continuation along the branches b_1 (blue), b_2 (cyan) and b_3 (red) in figure 6.14. The parameters are $\nu = 1/3$, $\epsilon = 1/10$, $\lambda = 2/10$.

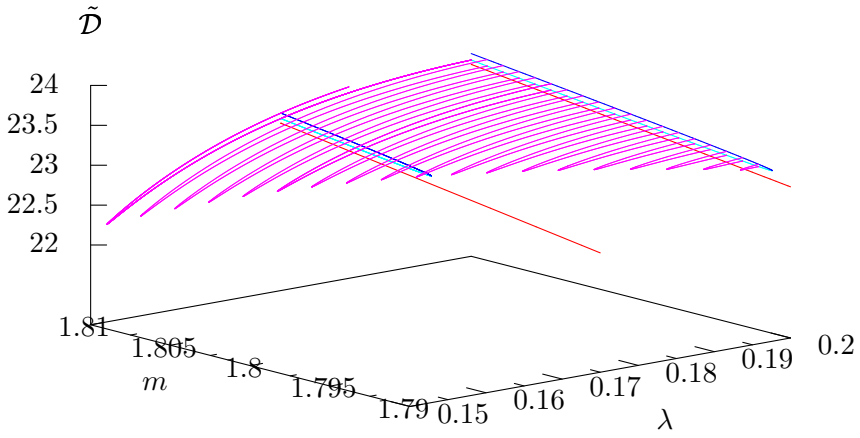

Figure 6.16: Continuation in m and λ showing a succession of coalescence curves (magenta) connecting the branches b_1 (blue) and b_2 (cyan) when $\epsilon = 0.1$ and $\nu = 1/3$. Branches on the curve b_3 (red) are able to be continued further and merge with branches as in figure 6.18.

branches beyond the codimension-two point branches b_1 and b_2 must be continued in either m or λ onto branch b_3.

Figure 6.18 shows that under continuation in λ the primary (red), bimodal (blue) and trimodal (cyan) solutions exist in isolated regions which only merge if m is less than a critical value. Note that the primary solutions are single branches but the multimodal solutions are pairs of solution branches connected by limit points, which unfortunately due to solution measures chosen give the impression of being a single branch. As subfigure 6.18(a) illustrates, at $m = 1.9$ the primary, bimodal and trimodal homoclinic orbits all exist on distinct branches, separated by intervals which contain λ_c. Subfigure 6.18(b) shows that soon after the critical value of m_c is passed at $m = 1.81$, the branches of primary homoclinic orbits have merged while the branches of bimodal and trimodal orbits remain as distinct branches. As subfigure 6.18(c) then illustrates, by $m = 1.7750$ the pairs of bimodal branches have merged while the pairs of trimodal branches remain separated. Finally, as subfigure 6.18(d) illustrates by $m = 1.7398$ the trimodal branches

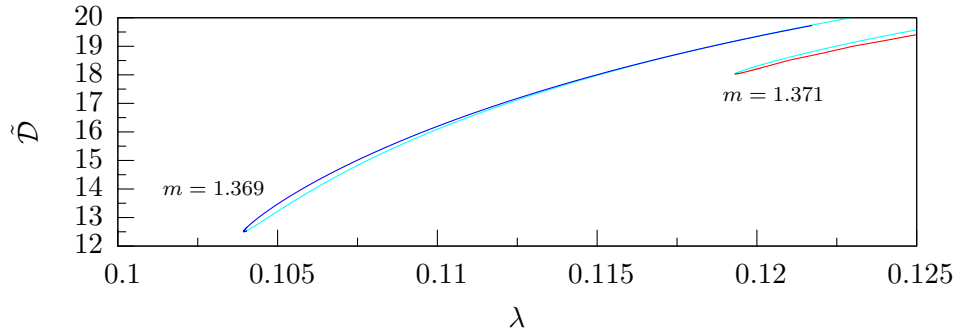

Figure 6.17: The figure shows two branches of solutions which pass through b_2 (cyan), one of which, with $m = 1.8369$, connects with a branch which passes through b_1 (blue) the other, with $m = 1.8373$, is connected to a branch of solutions which passes though b_3 (red).

have merged.

The numerical investigations were performed in figure 6.18 on multimodal solutions with a minimal number of small oscillations between localised modes so that a fair comparison of merging behaviour could be observed.

For each n-modal solution found there exists a critical value of the end loading parameter $m_c^{(n)}$ for which the branch of n-modal orbits can merge when continued in λ from the left and the right. Let the critical value of λ at which branches of n-modal solutions merge be denoted by $\lambda_c^{(n)}$. Numerical evidence presented in figure 6.18 strongly suggests that there appears to be a sequential merging of limit points for each pair of branches of n-modal solutions

$$m_c = m_c^{(1)} < m_c^{(2)} < \ldots < m_c^{(n-1)} < m_c^{(n)} < m_c^{(n+1)} < \ldots .$$

Branches of homoclinic orbits merge in the neighbourhood of the codimension-two point defining a double Hamiltonian-Hopf bifurcation. It should be emphasised that while the first member of the sequence of coalescence points can be predicted through Floquet theory, as the double Hamiltonian-Hopf bifurcation point $\left(\lambda_c^{(1)}, m_c^{(1)}\right)$, all subsequent values are double limit points and as such must be computed numerically using continuation software.

Near the codimension-two point the effect of λ on the multimodal homoclinic orbits

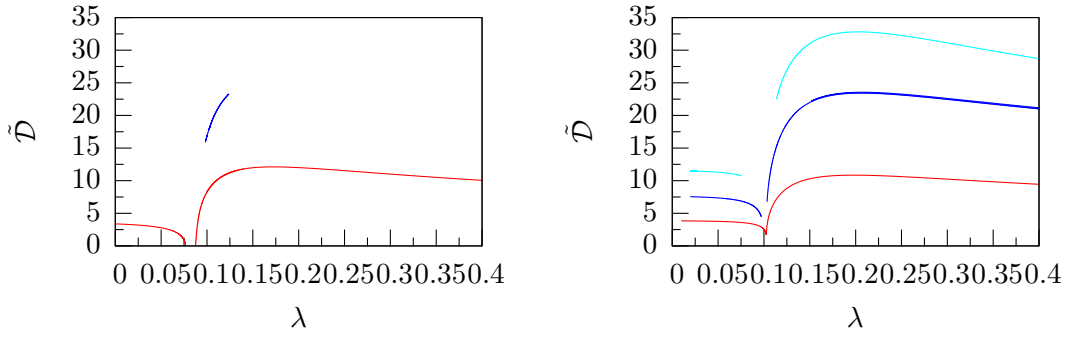

(a) $m = 1.9$ **(b)** $m = 1.81$

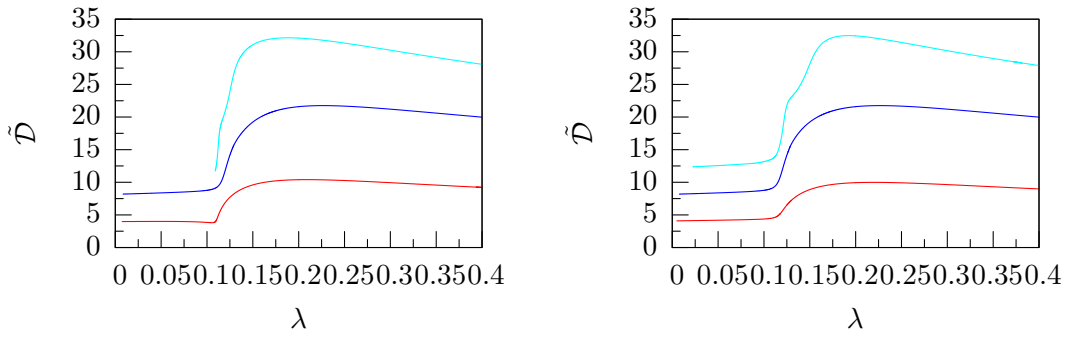

(c) $m = 1.7750$ **(d)** $m = 1.7398$

Figure 6.18: Load-deflection diagrams for a number of primary (red), bimodal (blue) and trimodal (cyan) homoclinic orbits for $\nu = 1/3$, $\epsilon = 0.1$ under a variety of end loads illustrating the sequential merging of distinct solution branches of multimodal solutions near the codimension-two point. In subfigures 6.18(a) and 6.18(c) some multimodal orbits were unable to be adequately continued and so were not displayed.

delocalises configurations so that the individual localisations become indistinct. The numerical evidence suggests that, in a sense, the primary orbits can sustain a greater degree of delocalisation than bimodal orbits, which can sustain a greater degree of delocalisation than trimodal orbits. Away from the codimension-two point the delocalisation-localisation phenomenon is less pronounced, cf. figure 6.10, and the multimodal orbits exist throughout continuation, as seen in figure 6.18(d).

A rich bifurcation structure clearly exists, for example, through continuation in λ decreasing just beyond lp_2 the branch b_1 coalesces with another branch at $(\lambda, m) = (0.2, 1.975411)$ which is not connected with the branches b_1, b_2 or b_3 through continuation in m. Figure 6.19 shows that a number of coalescence scenarios occur for bimodal orbits for continuation with λ increasing, i.e. away from the buckling line.

The (λ, m) parameter space was explored and collection of limit points computed for a number of bimodal orbits. The results are presented in figure 6.20. Again, note that the figure does not give an global picture of the bifurcation structure of the bimodal orbits as continuation was performed from a single solution on the branch b_2, which connects many others.

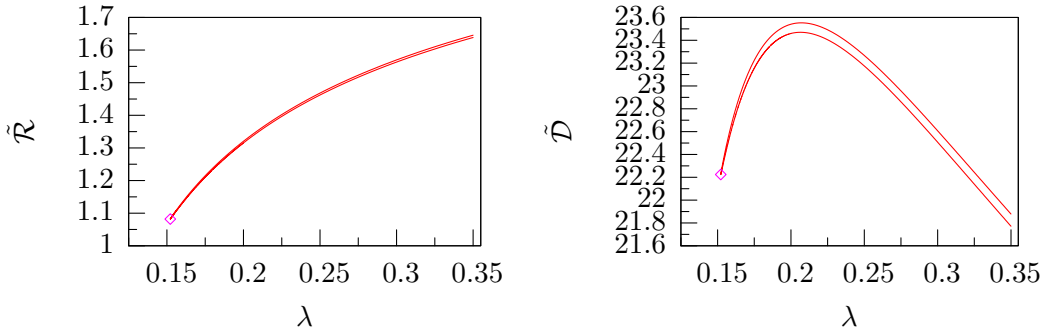

(a) $m = 1.81$

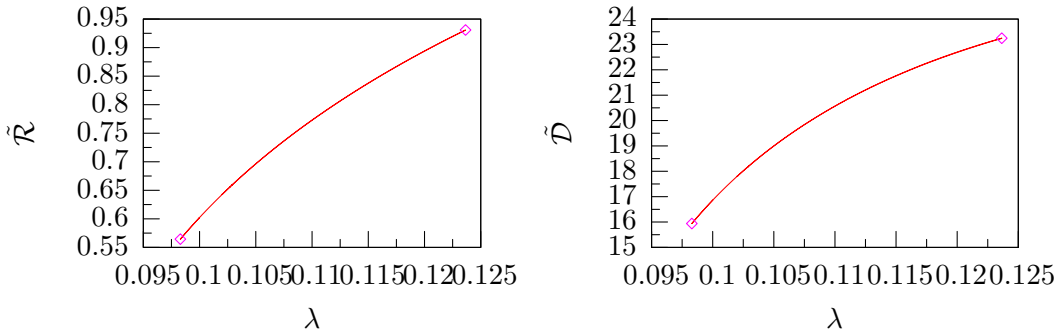

(b) $m = 1.91$

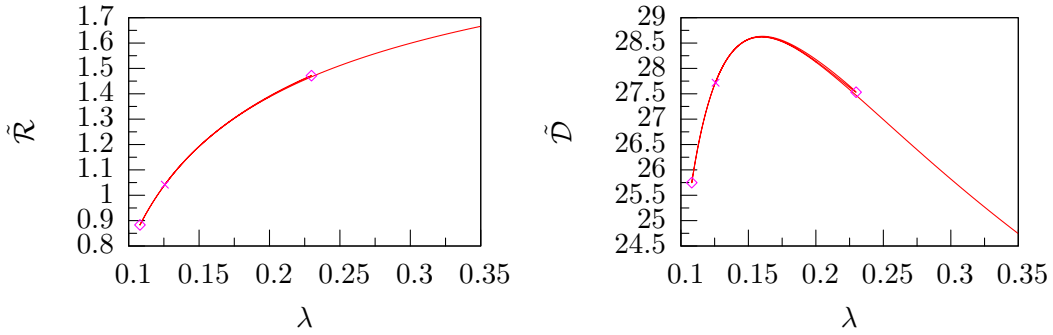

(c) $m = 2.00$

Figure 6.19: A variety of load-deflection diagrams for bimodal solutions in λ showing different classes of bifurcation diagram for a variety of values of m. The limit points are denoted by the diamond ($\diamond$). In subfigure 6.19(c) the cross ($\times$) denotes the point at which the continuation software fails to converge.

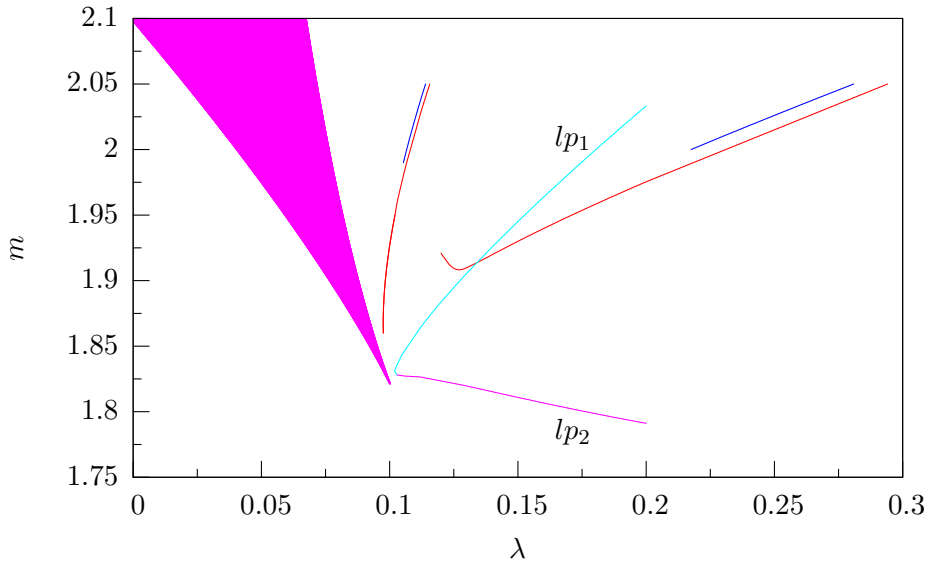

Figure 6.20: A succession of limit points for a set of bimodals against the spectrum of Floquet multipliers when $\epsilon = 0.1$ and $\nu = 1/3$ in the (λ, m) parameter plane. As in figure 6.1 the shaded area is the elliptic regime and the dotted line the codimension-one curve (6.18). The various colours relate to different branches of bimodals, for example the limit point lp_1 is cyan, the limit point lp_2 in magenta. Note that the two curves meet close to the codimension-two point at $(0.1006, 1.837)$.

Chapter 7

Conclusion

The objective of this thesis was to investigate the behaviour of an elastic conducting rod in a uniform magnetic field. Three main results are presented, firstly, the identification of the static equilibrium equations with a noncanonical Hamiltonian system, in contrast to previous work [81, 104–109], which for a class of constitutive relations is *completely integrable* in the sense of Liouville. The governing equations gave a physical realisation to the abstract 'twisted top' [90]. Secondly, through detailed perturbation analysis it was shown that if an extensible conducting rod is placed in a magnetic field the governing equations will no longer be integrable. Furthermore it was shown that it is the interaction between the magnetic effects and extensibility which leads to spatial chaos and *multiplicity of localised multimodal solutions*. Thirdly, for critical values of the nondimensional end and body loading parameters (λ, m) the rod undergoes a codimension-two *double Hamiltonian-Hopf bifurcation*. The codimension-two point has been shown to act as an organising centre for the nearby dynamics. The three main contributions of integrability, localisation and bifurcation are stated in the title of this thesis

Perhaps the most important step in the investigation was recognising that the static equilibrium equations were a noncanonical system as the Hamiltonian structure is exploited throughout the thesis. For example, the Hamiltonian structure is necessary in order to prove complete integrability in the unperturbed system, in the Mel'nikov analysis and, by exploiting the codimension of homoclinic solutions in Hamiltonian systems,

to produce load-deflection diagrams.

The equilibrium equations were shown to be, like the Kirchhoff equations, Lie-Poisson equations. The new Lie-Poisson bracket was produced via Leibniz and semidirect extensions to the Kirchhoff bracket. Interestingly, the Hamiltonian remains unchanged as the effect of the magnetic field results from the bracket extensions. The Poisson bracket was generalised and the equilibrium equations found to sit, as the third member, in a family of rod equations in generalised hyper-magnetic fields. As the Hamiltonian remains unchanged the contributions of each new generalised force on the rod are provided by the bracket extensions.

An integrable subfamily of equations was found which are described by a Lax pair. The Lax pair assumed a number of conditions on the constitutive relations in order for all the members of the family of rod equations to be completely integrable which for some members are not necessary conditions. For example, the first member of the integrable subfamily, the force-free rod is (super)integrable regardless of anisotropy or extensibility, in contrast to the the second member, (the Kirchhoff rod) which requires isotropy in order to be integrable. A rod in a magnetic field requires the additional condition of inextensibility to be integrable, in contrast to the two previous members.

It is interesting to note that in the Lax pair formulation some Casimirs are 'promoted' to first integrals (and thus become conditional on the constitutive relations) as a new field is added in going to the next 'generation' of the family. For instance, at the second level of the family n is added as a uniform field and hence $\frac{1}{2}\mathsf{n}\cdot\mathsf{n}$ is a Casimir. In the next perturbation, by the field B, the Casimir is perturbed to $\frac{1}{2}\mathsf{n}\cdot\mathsf{n}+\mathsf{m}\cdot\mathsf{B}$. After one more perturbation, by the field D, this Casimir is turned into the first integral $\frac{1}{2}\mathsf{n}\cdot\mathsf{n}+\mathsf{m}\cdot\mathsf{B}+B\mathsf{D}\cdot\mathsf{d}_3$. By contrast, the Casimir $\mathsf{n}\cdot\mathsf{m}$ at the second level is perturbed directly into the integral $\mathsf{n}\cdot\mathsf{m}+B\mathsf{B}\cdot\mathsf{d}_3$ at the next level and remains the same one level up.

For the integrable subfamily, configurations can be classified by their motion on Liouville tori. Generically, a rod in a uniform magnetic field exists on a five-torus. Through analysis of previous members of the integrable subfamily superintegrable configurations

can be classified. For example, configurations on one-tori are either straight twisted rods or untwisted rings, on two-tori configurations are helices and on three-tori configurations are (generically) quasi-periodic helices. However, the form of minimally superintegrable configurations (on a four-torus) remains unknown.

It remains an open question as to whether two Kovalevskaya-type integrals exist for the rod in a magnetic field so that the system would be integrable. If this were the case an integral would exist that as $\lambda \to 0$ recovered the Kovalevskaya integral. There is numerical evidence, in the form of non-zero Lyapunov exponents, which suggests that at the original condition on the bending stiffnesses no such integral exists [90] but the condition itself may be different. The form of a prospective second integral remains unknown. A Lax pair does exist for a generalised Kovalevskaya top [14] but unfortunately in the context of rod theory the model generalises a class of body moments rather than body forces. One possible approach to finding a new integrable case would be to replicate Kovalevskaya's original analysis. This approach would give a condition on the nondimensional parameters such that the system was integrable, but would not reveal the form of the two integrals.

The noncanonical equilibrium equations of a rod in a uniform magnetic field were reduced using the three Casimirs to a six-dimensional canonical Hamiltonian system with an integral. It was shown as a rank degeneracy condition that if the force in the rod is aligned anywhere with the magnetic field it is aligned everywhere with the field. In this case the rod is simply a straight twisted rod.

Mel'nikov's method was then used to show that for an extensible rod the presence of the magnetic field leads to the transverse intersections of the stable and unstable manifolds of the homoclinic orbit, Smale horsehoes and the existence of spatially chaotic solutions. As a corollary complete integrability is destroyed through the loss of the integral. Through detailed scaling arguments and using a basic algorithm to compute a first order approximation to the homoclinic orbit, it was shown that it is the *interaction* between extensibility (a 'material' nonlinearity) and magnetic effects (a 'geometric' nonlinearity) which destroys integrability as neither perturbation alone alters either the

integrability or the transversality of the system. Specifically, to first order (the *sum* of the two perturbations) the Mel'nikov function is zero but to second order (the *product* of the two perturbations) the Mel'nikov function has simple zeroes. This implies the existence of a multiplicity of localised configurations exist.

It is conjectured that a rod with nonlinear constitutive relations or a shearable rod in a magnetic field will have spatially chaotic solutions as both linear elasticity and shearability, like inextensibility, are necessary conditions on the integral (3.41b).

Having proved the existence of multimodal solutions for an extensible rod in a magnetic field, localised solutions were then computed. Due to the coupling between the spatial and director frames by the magnetic field, standard numerical procedures for the computation and continuation of homoclinic solutions needed to be adapted to deal with the periodicity of the trivial solution. The spectrum of Floquet multipliers in the nondimensional load parameter plane (λ, m) was investigated. Localised solutions were computed using a three parameter shooting method by exploiting the reversibilities of the system. Solutions were then continued with pseudo-arclength continuation software using projection boundary conditions which utilised the exponential trichotomies of the system. The post-buckling path of a rod in a magnetic field λ was found to be qualitatively similar to the post-buckling path of a rod under end force and moment m. It was shown that the presence of the magnetic field decreased the value at which the rod buckled due to end loading, although care must be taken to avoid general statements when dealing with buckling due to dimensionless parameters.

A codimension-two point (λ_c, m_c) was identified at which a double Hamiltonian-Hopf bifurcation occurred. The codimension-two point determined whether a primary homoclinic solution could bifurcate at one of either two critical values of the field strength $\lambda = \lambda_+$ or $\lambda = \lambda_-$, one critical value $\lambda = \lambda_c$ or did not bifurcate. It is believed that this is the first example of a double Hamiltonian-Hopf bifurcation found. The bifurcation structure of multimodal configurations was then investigated. The codimension-two point was found to be an organising centre for the bifurcation set of both primary and multimodal homoclinic solutions. Double coalescence points were observed as two pairs

of branches of bimodal and trimodal homoclinic solutions merged at critical values of the load parameters.

If the rod was not subject to an end moment, i.e. $M = 0$, the trivial configuration would be a straight and untwisted rod and the trivial solution would be a fixed point. Preliminary numerical evidence on the spectrum of the eigenvalues suggests that a codimension two point (λ_c, m_c) exists, so an analytical condition could be formulated. Nonlinear normal form analysis about the fixed point solution could be performed through a reduction of the nine-dimensional governing equations by the three Casimirs, then by a Lyapunov-Schmidt reduction [101].

The Mel'nikov analysis, which implied the existence of multimodal solutions, only applied for a small δ-perturbation, while multimodal solutions could be computed for all non-zero values of λ when the Floquet multipliers where not on the unit circle. This is because the Mel'nikov analysis provides an approximation to the splitting of the stable and unstable manifolds for the perturbation based on inverting the Hamiltonian and solving for an expansion of an action integral by the implicit function theorem. However, Devaney's theorem, which states that a Hamiltonian system with a transverse point will have a multiplicity of multimodal homoclinic orbits, only requires that the intersection of the stable and unstable manifolds be transverse, which is a global phenomenon for hyperbolic homoclinic orbits in Hamiltonian systems since the intersections will occur along an 'energy' level [21].

An important question which has not been discussed in this thesis is the question of the stability of localised configurations. Stability is likely to be the exception rather than the rule as it has been shown, for the related problem of a beam on an elastic foundation [79], that all multimodal configurations are unstable regardless of how the loading is applied. It is reasonable to conjecture that similar instability occurs.

It has been shown [5] that neglecting the effect of the magnetic field and seeking travelling wave solutions for $\eta = s - ct$ of the dynamic system derived in [83] yields an Hamiltonian system which can be shown to be integrable. This is a suprising result as numerical evidence showing solition interaction [27] strongly suggests that the full dy-

namic system is not integrable. Note that by seeking travelling wave solutions of the full equations, there are far more admissible solutions such as hetroclinic and discontinuous solutions. If the Lorentz force on the rod is included and it is assumed, as in [105], that the velocity of the rod is small then the stationary solutions of the governing equation will have an equivalent form to (3.38). However any restriction on the motion of the rod is at odds with the geometrically exact formulation as it is assumed the rod can undergo arbitarily large deformations then it is natural to assume the rod can move in an arbitary fashion. The motion of the rod will induced an electro-motive force which opposes the motion rod. The magnitude of this force is proportional to the rate of change of the enclosed magnetic flux [110]. Thus, without restriction on the seeking stationary solutions of an exact partial differential will not yield an equivalent system to the static equilibrium formulation investigated in this thesis.

Preliminary numerical investigations of the spectrum of Floquet multipliers in the (λ, ρ) parameter plane indicates that a rich bifurcation structure is present. Once again the monodromy matrix decouples into a four-dimensional trivial matrix, containing the Casimirs and the constraint, and a six-dimensional non-trivial matrix containing the dynamics of the system. A codimension-two point determined by critical values $(\lambda_c, \rho_c) = (0.01, 1.10533)$ given $m = 1.4247$, $\epsilon = 0$ and $\nu = 1/3$ was found which distinguishes between strongly and weakly anisotropic buckling due to the magnetic field. Weakly anisotropic rods have a pair of unstable, centre and stable Floquet multipliers and the strongly anisotropic system have two pairs of centre multipliers and a stable and an unstable Floquet multiplier on the real line. Following from [98], the buckling mechanism for a weakly anisotropic rod is a Hamiltonian-Hopf bifurcation of a periodic solution, while in the strongly anisotropic case the rods buckle in a Hamiltonian-Pitchfork bifurcation of a periodic solution.

Whether a Poisson bracket formulation can model another family of generalised body forces on a rod or if the model presented here is unique, is another open question.

Appendix A

Parameterisation

In order to convert any quantities in the spatial frame into the director frame a form of parameterisation is needed that perserves length and orientation. There are two forms of parameterisation used in this thesis: the Euler angles and the Euler parameters. In this appendix both forms of parameterisation are outlined.

The Euler angles are easily expressed in closed form and have a distinct physical interpretation, making them amenable to analytical methods, yet have an inherent polar singularity which, along with the appearance of trigonometric functions, makes them less suitable for computation. The Euler parameters are a set of unit quarternions and have little physical meaning. Indeed, with the exception of [57] there is little analytical work in this formulation relating to rods. The Euler parameters have the property of 'double covering' which removes the polar singularity and are numerically straightforward to implement[1].

There are other forms of parameterisation, most notably the Deprit-Andoyer variables [70]. However, they are well chosen choices for the co-terminal rotations and say no more than the Euler Angles.

[1]Goldstein, writing without knowledge of today's computation power in an earlier edition of his text on classical mechanics alludes to the supposed redundancy of quaternions by dismissively referring to them as "musty mathematics" but this quote has been removed from the latter editions [43].

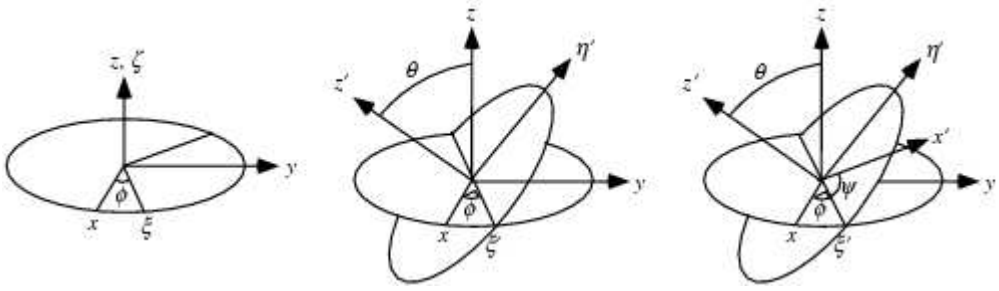

Figure A.1: Representation of the three consecutive rotations R_1, R_2 and R_3 by the corresponding angles ϕ, θ and ψ which produces the Euler angles.

A.1 Euler Angles

The Euler angles are defined by three consecutive rotations which convert quantities in the spatial frame into the director frame preserving the length and orientation. Let $\left(x^{(0)}, y^{(0)}, z^{(0)}\right)$ denote components of a vector in the spatial frame $\{\boldsymbol{e}_1, \boldsymbol{e}_2, \boldsymbol{e}_3\}$ and let $\left(x^{(3)}, y^{(3)}, z^{(3)}\right)$ denote components of a 3-tuple written in the director frame $\{\boldsymbol{d}_1, \boldsymbol{d}_2, \boldsymbol{d}_3\}$. Components of 3-tuples in intermediate bases will be denoted with intermediate superscripts accordingly. There is no standard notation for Euler angle formulations[2] but following [99] and adopting the conventions of the so-called British school of Love, Whittaker and Pars *et al.*, the transformation can be defined by the following three consecutive rotations:

(i) A rotation $R_1(\phi)$ about z_0 by ϕ mapping $x^{(0)}$ and $y^{(0)}$ onto $x^{(1)}$ and $y^{(1)}$.

(ii) A rotation $R_2(\theta)$ about x_1 by θ mapping $y^{(1)}$ and $z^{(1)}$ onto and $y^{(2)}$ and $z^{(2)}$.

(iii) A rotation $R_3(\psi)$ about $z^{(2)}$ by ψ mapping $x^{(2)}$ and $y^{(2)}$ onto $x^{(3)}$ and $y^{(3)}$.

Explicitly, the rotation R_1 acts by

$$\begin{pmatrix} x^{(1)} \\ y^{(1)} \\ z^{(1)} \end{pmatrix} = \begin{pmatrix} \sin\phi & \cos\phi & 0 \\ \cos\phi & -\sin\phi & 0 \\ 0 & 0 & 1 \end{pmatrix} \begin{pmatrix} x^{(0)} \\ y^{(0)} \\ z^{(0)} \end{pmatrix},$$

[2]There are twelve distinct sequences of rotations.

the second rotation R_2 is given by

$$\begin{pmatrix} x^{(2)} \\ y^{(2)} \\ z^{(2)} \end{pmatrix} = \begin{pmatrix} 1 & 0 & 0 \\ 0 & \cos\theta & -\sin\theta \\ 0 & \sin\theta & \cos\theta \end{pmatrix} \begin{pmatrix} x^{(1)} \\ y^{(1)} \\ z^{(1)} \end{pmatrix}$$

and the final rotation R_3 is given by

$$\begin{pmatrix} x^{(3)} \\ y^{(3)} \\ z^{(3)} \end{pmatrix} = \begin{pmatrix} -\sin\psi & \cos\psi & 0 \\ \cos\psi & \sin\psi & 0 \\ 0 & 0 & 1 \end{pmatrix} \begin{pmatrix} x^{(2)} \\ y^{(2)} \\ z^{(2)} \end{pmatrix}.$$

Thus, evaluating the rotations consecutively gives the matrix

$$R(\theta, \psi, \phi) = R_1(\phi) R_2(\theta) R_3(\psi),$$

which, by direct calculation is

$$R = \begin{pmatrix} \cos\theta\cos\phi\cos\psi - \sin\phi\sin\psi & \cos\theta\cos\phi\sin\psi + \cos\psi\sin\phi & -\sin\theta\cos\phi \\ -\cos\theta\sin\phi\cos\psi - \cos\phi\sin\psi & -\cos\theta\sin\phi\sin\psi + \cos\phi\cos\psi & \sin\theta\sin\phi \\ \sin\theta\cos\psi & \sin\theta\sin\psi & \cos\theta \end{pmatrix}.$$

The set of rotations are displayed in figure A.1.

The parameterisation of the directors is given explicitly by

$$\boldsymbol{d}_1(\theta, \phi, \psi) = \begin{pmatrix} \cos\psi\cos\theta\cos\phi - \sin\psi\sin\phi \\ \cos\psi\cos\theta\sin\phi + \sin\psi\cos\phi \\ -\cos\psi\sin\theta \end{pmatrix}, \tag{A.1a}$$

$$\boldsymbol{d}_2(\theta, \phi, \psi) = \begin{pmatrix} -\sin\psi\cos\theta\cos\phi + \sin\psi\cos\phi \\ -\sin\psi\cos\theta\sin\phi + \cos\psi\cos\phi \\ \sin\psi\sin\theta \end{pmatrix}, \tag{A.1b}$$

$$\boldsymbol{d}_3(\theta, \phi) = \begin{pmatrix} \sin\theta\cos\phi \\ \sin\theta\sin\phi \\ \cos\theta \end{pmatrix}. \tag{A.1c}$$

Here θ measures the displacement from an initially straight rod, ψ is the azimuthal angle about a fixed axis and ϕ is the twist angle about the centreline of the rod. In the terminology of rigid body mechanics θ is the nutation angle, ψ is the precession angle and ϕ is the spin angle. It is evident from the construction of R that when there is no nutation that spin and precession are no longer independent.

A.2 Euler Parameters

If a unit vector in the spatial frame, $\boldsymbol{k} = k_1\boldsymbol{e}_1 + k_2\boldsymbol{e}_2 + k_3\boldsymbol{e}_3$, is rotated by an angle Φ, then the Euler parameters may be defined as

$$\begin{array}{ll} q_j & = \boldsymbol{k}\cdot\boldsymbol{e}_j \sin\left(\Phi/2\right), \quad j = 1,2,3. \\ q_4 & = \cos\left(\Phi/2\right), \end{array} \tag{A.2}$$

subject to the normalisation condition

$$q_1^2 + q_2^2 + q_3^2 + q_4^2 = 1. \tag{A.3}$$

This is equivalent to making the substitutions

$$q_1 = \cos\frac{\psi+\phi}{2}\cos\frac{\theta}{2}, \quad q_2 = \cos\frac{\psi-\phi}{2}\sin\frac{\theta}{2}, \quad q_3 = \sin\frac{\psi-\phi}{2}\sin\frac{\theta}{2}$$

and

$$q_4 = \sin\frac{\psi+\phi}{2}\cos\frac{\theta}{2}$$

into the matrix (A.1). Thus the rotation matrix R is given by

$$R = \begin{pmatrix} q_1^2 - q_2^2 - q_3^2 + q_4^2 & 2\left(q_1q_2 - q_3q_4\right) & 2\left(q_1q_3 + q_2q_4\right) \\ 2\left(q_1q_2 + q_3q_4\right) & q_2^2 + q_4^2 - q_1^2 - q_3^2 & 2\left(q_2q_3 - q_1q_4\right) \\ 2\left(q_1q_3 - q_2q_4\right) & 2\left(q_1q_4 + q_2q_3\right) & q_3^2 + q_4^2 - q_1^2 - q_2^2 \end{pmatrix}. \tag{A.4}$$

The determinant of this matrix, due to the normalisation condition (A.3), is unity.

In terms of Euler parameters the directors are given by

$$\boldsymbol{d}_1 = \begin{pmatrix} q_1^2 - q_2^2 - q_3^2 + q_4^2 \\ 2\left(q_1q_2 + q_3q_4\right) \\ 2\left(q_1q_3 - q_2q_4\right) \end{pmatrix}, \tag{A.5a}$$

$$\boldsymbol{d}_2 = \begin{pmatrix} 2\left(q_1q_2 - q_3q_4\right) \\ q_2^2 + q_4^2 - q_1^2 - q_3^2 \\ 2\left(q_1q_4 + q_2q_3\right) \end{pmatrix}, \tag{A.5b}$$

$$\boldsymbol{d}_3 = \begin{pmatrix} 2\left(q_1q_3 + q_2q_4\right) \\ 2\left(q_2q_3 - q_1q_4\right) \\ q_3^2 + q_4^2 - q_1^2 - q_2^2 \end{pmatrix}. \tag{A.5c}$$

If the set of quaternions q corresponds to the rotation of $\boldsymbol{k}$ by Φ then $-q$ corresponds to the co-terminal rotation of $\boldsymbol{k}$ by $\Phi + 2\,\pi$. Hence q and $-q$ describe the same rotation and thus there is a homomorphic two-to-one relationship between representations by

the Euler parameters and rotations, referred to as the double covering of the Euler parameters. This is because the Euler parameters provide a representation of the group $SU(2)$ as well as $SO(3)$.

The evolution of the Euler parameters can be derived by substituting the equations (A.5) into (3.4) to give

$$\begin{pmatrix} q_1 \\ q_2 \\ q_3 \\ q_4 \end{pmatrix}' = \frac{1}{2} \begin{pmatrix} q_4 & -q_3 & q_2 \\ q_3 & q_4 & -q_1 \\ -q_2 & q_1 & q_4 \\ -q_1 & -q_2 & -q_3 \end{pmatrix} \begin{pmatrix} u_1 \\ u_2 \\ u_3 \end{pmatrix}. \tag{A.6}$$

In one respect the normalisation condition (A.3) can be interpreted as a Casimir as it is independent of any parameters. However, the normalisation condition can not be recovered from the equation (A.6) as the matrix is not square [48]. Instead the normalisation condition can be (correctly) interpreted as a geometric constraint. The Euler parameters are constrained to lie on the surface of a four-dimensional unit hyper-sphere [36]. The constraint is holonomic, i.e., it does not depend on the derivatives of the Euler parameters so does not affect the integrability of the parameterised system [1, pg. 624].

Appendix B

Numerical Analysis

This appendix gives an overview of the numerical procedures outlined in §4.5 and §6 as well as many of the programs, routines and procedures used. The numerical analysis is consists of two parts: the construction and the continuation of homoclinic solutions. Throughout this thesis, homoclinic solutions are constructed by using an approximation to the flow about the equilibrium and by exploiting the reversibilities of the system [20]. From a given solution there are two principal methods of computing solutions using continuation software: projection boundary conditions [11–13, 61] and explicit boundary conditions [41]. The explicit and projection boundary conditions are mathematically equivalent in that both procedures require a knowledge of the invariant subspace structure near the equilibrium by stipulating that the solutions be in the linear subspaces which approximate the stable and unstable manifolds.

In order to construct homoclinic orbits some preliminary results are necessary. Further detail can be found in any relevant textbook, for example [45].

B.1 Preliminary Results

Let an even-dimension dynamical system take the form

$$\boldsymbol{x}' = f_0\left(\boldsymbol{x}, \boldsymbol{\mu}\right), \quad \boldsymbol{x} \in \mathbb{R}^{2n}, \quad \boldsymbol{\mu} \in \mathbb{R}^p \quad \text{with} \quad s \in (-\infty, +\infty) \tag{B.1}$$

Definition B.1.1. *A dynamical system is doubly reversible if there exists a pair of linear*

involutions R_1 and R_2 such that ,

$$R_i \circ f_0(\boldsymbol{x}) = -f_0(R_i \circ \boldsymbol{x}), \quad R_i^2 = \mathbb{I}^{2n} \quad \textit{and} \quad \mathcal{S}_i = \operatorname{fix}(R_i) \cong \mathbb{R}^n \quad \textit{for} \quad i = 1, 2$$

where the linear subspace $\mathcal{S}_i$ is defined as the symmetric section of the reversibility R_i.

Lemma B.1.2. *Let $\boldsymbol{p}$ be a fixed point so that $f_0(\boldsymbol{p}) = \mathbf{0}$ and without loss of generality assume $\boldsymbol{p} = \mathbf{0}$. Then if $f_0(\boldsymbol{x})$ is reversible then the spectrum of the eigenvalues of the linearised vector field $Df_0(\mathbf{0})$ will also be reversible, i.e., have reflection symmetry about the imaginary axis.*

Proof. By the reversibility

$$Df_0(\mathbf{0}) \circ R_i = -R_i \circ Df_0(\mathbf{0}),$$

thus, forming a characteristic polynomial in μ

$$|Df_0(\mathbf{0}) - \mu\mathbb{I}| = |-R_i \circ (Df_0(\mathbf{0}) \circ R_i) - \mu\mathbb{I}| = |Df_0(\mathbf{0}) + \mu\mathbb{I}|.$$

Hence all roots of the characteristic polynomial, the eigenvalues, will occur in reversible (conjugate) pairs. □

The stable manifold theorem gives an insight into the structure of the invariant subspaces. For a dynamical system with a fixed point at the origin the following subspaces may be constructed

Definition B.1.3. *The stable, centre and unstable subspaces of a linearised dynamical system are given by*

(i) $\mathcal{E}^{(s)}(\mathbf{0}) = \operatorname{span}\{\boldsymbol{v}_1, \boldsymbol{v}_2, \ldots, \boldsymbol{v}_k\}$ *where* $\Re\mu_1, \ldots, \Re\mu_k \leq 0$.

(ii) $\mathcal{E}^{(c)}(\mathbf{0}) = \operatorname{span}\{\boldsymbol{v}_{k+1}, \boldsymbol{v}_{k+2}, \ldots, \boldsymbol{v}_{k+l}\}$ *where* $\Re\mu_{k+1}, \ldots, \Re\mu_{k+l} = 0$.

(iii) $\mathcal{E}^{(u)}(\mathbf{0}) = \operatorname{span}\{\boldsymbol{v}_{k+l+1}, \boldsymbol{v}_{k+l+2}, \ldots, \boldsymbol{v}_{k+l+m}\}$ *where* $\Re\mu_{k+l+1}, \ldots, \Re\mu_{k+l+m} \geq 0$.

Where $\dim \mathcal{E}^{(s)} = k$, $\dim \mathcal{E}^{(c)} = l$ *and* $\dim \mathcal{E}^{(u)} = m$. *Hence* $2n = k + l + m$ *and* $\mathbb{R}^{2n} = \mathcal{E}^{(s)}(\mathbf{0}) \oplus \mathcal{E}^{(c)}(\mathbf{0}) \oplus \mathcal{E}^{(u)}(\mathbf{0})$.

If the system is reversible then $k = m$ and l is even. If the system is also strictly hyperbolic then $l = 0$ and $k = m = n$. The linear subspaces can be related to the flow of the corresponding nonlinear system near an equilibrium solution by the centre manifold theorem

Theorem B.1.4 (The Centre Manifold). *For a nonlinear dynamical system with a fixed point at the origin,*

(i) There exists local stable, centre and unstable manifolds W^s_{loc}, W^c_{loc} and W^u_{loc} of dimension k, l and m respectively.

(ii) The local stable, centre and unstable manifolds are tangent to the stable, centre and unstable subspaces of the linearised system at the fixed point.

(iii) The stable and unstable manifolds are uniquely defined but the centre manifold need not be.

Proof of B.1.4. See [45, §3.2] and the references therein. □

Now, consider a perturbation to the vector field (B.1) of the form

$$\boldsymbol{x}' = f_0(\boldsymbol{x}) + \varepsilon f_1(\boldsymbol{x}, s) + \mathcal{O}\left(\varepsilon^2\right) \tag{B.2}$$

with a solution to the unperturbed system $\boldsymbol{x}_0$. By the centre manifold theorem, the flow of the perturbed vector field can be approximated near the stable and unstable manifolds. Thus for the unstable part, about the equilibrium the solution $\boldsymbol{x}_0$ can be approximated by

$$\boldsymbol{x}^u_\varepsilon(s_0, s_0) = \boldsymbol{x}_0(0) + \varepsilon \boldsymbol{v}_1 + \mathcal{O}\left(\varepsilon^2\right) \tag{B.3}$$

which in general is [45, Lemma 4.5.2]

$$\boldsymbol{x}^u_\varepsilon(s, s_0) = \boldsymbol{x}_0(s - s_0) + \varepsilon \boldsymbol{x}^u_1(s, s_0) + \mathcal{O}\left(\varepsilon^2\right), \quad \text{for} \quad s \in (-\infty, s_0] \tag{B.4}$$

where

$$\boldsymbol{x}^u_1(s_0, s_0) = \boldsymbol{v}_1. \tag{B.5}$$

The vector $\boldsymbol{v}_1$ is in the set of normalised orthogonal real eigenvectors spanning the unstable eigenspace of the linearised vector field and s_0 determines the phase of a solution. The terms of the expansion (B.4) can be determined through a succession of variational equations. The variational equations can be constructed by differentiating (B.2) and (B.4) and then equating coefficients of ε of the Taylor expansion

$$\begin{aligned}\frac{\mathrm{d}}{\mathrm{d}s}\boldsymbol{x}_\varepsilon^u &= f_0\left(\boldsymbol{x}_\varepsilon^u\right) + \varepsilon f_1\left(\boldsymbol{x}_\varepsilon^u, s\right) + \mathcal{O}\left(\varepsilon^2\right) \\ &= f_0\left(\boldsymbol{x}_0\left(s-s_0\right) + \varepsilon\boldsymbol{x}_1^u\left(s,s_0\right) + \mathcal{O}\left(\varepsilon^2\right)\right) + \varepsilon f_1\left(\boldsymbol{x}_0\left(s-s_0\right) + \varepsilon\boldsymbol{x}_1^u\left(s,s_0\right) + \mathcal{O}\left(\varepsilon^2\right)\right) \\ &\qquad + \mathcal{O}\left(\varepsilon^2\right) \\ &= f_0\left(\boldsymbol{x}\left(s-s_0\right)\right) + \varepsilon Df_0\left(\boldsymbol{x}_0\left(s-s_0\right)\right)\boldsymbol{x}_1^u\left(s,s_0\right) + \varepsilon f_1\left(\boldsymbol{x}_0\left(s-s_0\right), s\right) + \mathcal{O}\left(\varepsilon^2\right).\end{aligned}$$

Therefore, the first order approximation $\boldsymbol{x}_1^u\left(s,s_0\right)$ can be found through

$$\frac{\mathrm{d}}{\mathrm{d}s}\boldsymbol{x}_1^u\left(s,s_0\right) = Df_0\left(\boldsymbol{x}_0\left(s-s_0\right)\right)\boldsymbol{x}_1^u\left(s,s_0\right) + f_1\left(\boldsymbol{x}_0\left(s-s_0\right), s\right). \tag{B.6}$$

A similar expression for the unstable part over $s \in [s_0, \infty)$ can be found in exactly the same way. Thus, through the centre manifold theorem there are ways of approximating the flow of nonlinear systems near fixed points. Knowledge of the area about an equilibrium can be exploited to give a *global* description of the dynamics when the system admits homoclinic orbits.

B.2 Shooting for Homoclinic Orbits

The computation of a homoclinic orbit over an infinite domain is impossible. Hence, it is necessary to truncate the arc-length parameter to $s \in [0, \mathcal{T}]$ for a finite but arbitrarily large $\mathcal{T}$ in order to form a good approximation of a homoclinic orbit. Consequently, the truncation requires the system to be treated as a boundary-value problem. For reversible dynamical systems, the discrete reversing symmetry can be exploited to simplify the calculations. The left-hand side conditions are placed in the unstable mainfold of the trivial equilibrium and the right-hand side conditions are placed in the symmetric section. The resulting boundary-value problem is then solved using a shooting method where the Newton-Raphson method solves a variational equation with respect to a set of shooting

parameters which satisfy a reversibility. The method can easily be adapted to non-reversible systems and periodic systems [7].

For simplicity a reversible, hyperbolic system is considered. Let $\{\boldsymbol{v}_1, \boldsymbol{v}_2, \ldots \boldsymbol{v}_n\}$ be normalised orthogonal real eigenvectors spanning the unstable (generalised) eigenspace of the linearised vector field (B.1). A solution to the governing equation can be approximated by the linearised flow by the centre manifold theorem as

$$\boldsymbol{x}(s) = \varepsilon \boldsymbol{v} + \mathcal{O}\left(\varepsilon^2\right) \quad \text{with} \quad s \in (0, s^*)$$

for s^* and ε sufficiently small and where $\boldsymbol{v} \in \operatorname{span}\{\boldsymbol{v}_1, \boldsymbol{v}_2, \ldots \boldsymbol{v}_n\}$. Now consider the truncated system as a boundary-value problem over the unit interval

$$\boldsymbol{x}' = \mathcal{T} f_0(\boldsymbol{x}, \boldsymbol{\mu}), \quad \boldsymbol{x} \in \mathbb{R}^{2n}, \quad \boldsymbol{\mu} \in \mathbb{R}^p \quad \text{with} \quad s \in [0, 1], \tag{B.7}$$

subject to the boundary conditions

$$\boldsymbol{x}(0) = \varepsilon\left(a_1 \boldsymbol{v}_1 + a_2 \boldsymbol{v}_2 + \ldots + a_n \boldsymbol{v}_n\right), \quad \boldsymbol{v} \in \mathbb{R}^{2n}, \tag{B.8a}$$

$$\boldsymbol{x}(1) \in \mathcal{S}, \tag{B.8b}$$

where $\mathcal{T}$ is the truncated arclength and $\mathcal{S} \in \mathbb{R}^n$ is given in definition (B.1.1). The a_i are weighted functions of the shooting parameters δ_i. They are subject to the normalisation constraint

$$\sum_{i=1}^{n} a_i^2 = 1. \tag{B.9}$$

In order to construct a well-posed shooting problem there must be n independent shooting parameters δ_i, as the righthand boundary condition is a subspace of $\mathbb{R}^n$. However, the system (B.7) with boundary conditions (B.8) subject to the normalisation condition (B.9) is ill-posed: there are more boundary conditions than independent shooting parameters. This is because the shooting parameters need to satisfy n righthand boundary conditions and are formulated in terms of the initial conditions via n functions a_i but due to the normalisation condition (B.9) only $n-1$ of the functions are independent.

Thus, the truncationed length is treated as an additional variable which satisfies the equation

$$\mathcal{T}' = 0. \tag{B.10}$$

Hence the boundary value problem for the governing equation (B.7) satisfying boundary conditions (B.8), subject to the normalisation condition (B.9) and with a constant but undetermined truncation length (B.10) is now well-posed. Since the vectors $\boldsymbol{v}_i$ form a basis for the unstable subspace, the perturbation (B.8a) is tangential to the flow about the fixed point and hence is a good approximation for the initial trajectory of a homoclinic orbit if $\mathcal{T}$ is sufficiently large and ε is sufficiently small.

Having constructed a well-posed boundary-value problem it is now necessary to find the shooting parameters which satisfy the boundary conditions. Let the n independent shooting parameters be denoted by $\boldsymbol{y}$, where

$$\boldsymbol{y} = (\boldsymbol{\delta}, \mathcal{T}) \quad \text{with} \quad \boldsymbol{\delta} = (\delta_1, \delta_2, \ldots, \delta_{n-1}). \tag{B.11}$$

Hence the left-hand boundary condition (B.8a) can be expressed as a function of the shooting parameters

$$\boldsymbol{x}(0) = \varepsilon \left(a_1(\boldsymbol{\delta})\, \boldsymbol{v}_1 + a_2(\boldsymbol{\delta})\, \boldsymbol{v}_2 + \ldots + a_n(\boldsymbol{\delta})\, \boldsymbol{v}_n \right).$$

The weighted functions a_i are explicitly dependent on the shooting parameters $\boldsymbol{\delta}$ whereas $\mathcal{T}$ is implicitly dependent on the constant ε. A solution $\boldsymbol{x}(s)$ of the boundary-value problem will satisfy the righthand boundary condition (B.8b), which may be reformulated as the function b where

$$b : \mathbb{R}^{2n} \mapsto \mathbb{R}^n \quad \text{so that} \quad b(\boldsymbol{x}(1)) = \mathbf{0}. \tag{B.12}$$

Suppose that $\boldsymbol{w}(s; \boldsymbol{y})$ is a solution to the *initial-value* problem

$$\boldsymbol{w}'(s; \boldsymbol{y}) = \mathcal{T} f_0(\boldsymbol{w}, \boldsymbol{\mu}) \quad \text{for} \quad \boldsymbol{w} \in \mathbb{R}^{2n}, \quad \boldsymbol{\mu} \in \mathbb{R}^p, \quad \boldsymbol{y} \in \mathbb{R}^n, \tag{B.13a}$$

$$\boldsymbol{w}(0) = \varepsilon \left(a_1 \boldsymbol{v}_1 + a_2 \boldsymbol{v}_2 + \ldots + a_n \boldsymbol{v}_n \right). \tag{B.13b}$$

Now define the function

$$G(\boldsymbol{y}) = b(\boldsymbol{w}(s;\boldsymbol{y}))|_{s=1}.$$

Given a good initial guess $\boldsymbol{y}^{(0)}$, in order to solve the boundary-value problem it is necessary to generate a sequence of improved guesses $\{\boldsymbol{y}^{(0)}, \boldsymbol{y}^{(1)}, \boldsymbol{y}^{(2)}, \ldots\}$ such that

$$\lim_{n\to\infty} G\left(\boldsymbol{y}^{(n)}\right) = \mathbf{0}$$

so that the righthand boundary condition (B.8b) will be satisfied by solutions of the initial-value problem. To generate the sequence of successive guesses the Newton-Raphson method is used

$$\boldsymbol{y}^{(n+1)} = \boldsymbol{y}^{(n)} - \frac{G\left(\boldsymbol{y}^{(n)}\right)}{DG\left(\boldsymbol{y}^{(n)}\right)}, \tag{B.14}$$

where DG is the Jacobian of the function G with respect to the shooting parameters. The Jacobian is given by

$$\begin{aligned} DG\left(\boldsymbol{y}^{(n)}\right)_{i,j} &= \left.\frac{\partial b_i(\boldsymbol{w}(s;\boldsymbol{y}))}{\partial y_j}\right|_{s=1,\,\boldsymbol{y}=\boldsymbol{y}^{(n)}} \\ &= \sum_{k=1}^{2n} \left.\frac{\partial b_i(\boldsymbol{w}_i(s;\boldsymbol{y}))}{\partial w_k(s;\boldsymbol{y})} \cdot \frac{\partial w_k(s;\boldsymbol{y})}{\partial y_j}\right|_{s=1,\,\boldsymbol{y}=\boldsymbol{y}^{(n)}}. \end{aligned} \tag{B.15}$$

In order to solve the Newton-Raphson equation for an initial guess $\boldsymbol{y}^{(0)}$ a variational equation of $\boldsymbol{w}(s,\boldsymbol{y})$ with respect to the shooting parameters is formed. Let the partial derivatives of $\boldsymbol{w}$ with respect to the shooting parameters $\boldsymbol{y}$ be denoted by

$$z_{k,j}(s;\boldsymbol{y}) = \frac{\partial w_k(s;\boldsymbol{y})}{\partial y_j}. \tag{B.16}$$

The Jacobian may now be written as

$$DG\left(\boldsymbol{y}^{(n)}\right)_{i,j} = \sum_{k=1}^{2n} \left.\frac{\partial b_i(w_i(s;\boldsymbol{y}))}{\partial w_k(s;\boldsymbol{y})} z_{k,j}(s;\boldsymbol{y})\right|_{s=1,\,\boldsymbol{y}=\boldsymbol{y}^{(n)}}, \tag{B.17}$$

where $z_{k,j}(s,\boldsymbol{y})$ satisfies the auxiliary variational equations

$$z'_{k,j}(s;\boldsymbol{y}) = \mathcal{T}\sum_{l=1}^{2n} \frac{\partial f_{0k}(\boldsymbol{w}(s;\boldsymbol{y}))}{\partial w_l(s;\boldsymbol{y})} z_{l,j}(s;\boldsymbol{y}) \quad j = 1,2,\ldots n-1 \quad \text{and} \quad k = 1,2,\ldots 2n, \tag{B.18a}$$

$$z'_{k,n}(s;\boldsymbol{y}) = \mathcal{T}\sum_{l=1}^{2n} \frac{\partial f_{0k}(\boldsymbol{w}(s;\boldsymbol{y}))}{\partial w_l(s;\boldsymbol{y})} z_{l,n}(s;\boldsymbol{y}) + f_{0k}(\boldsymbol{w}(s;\boldsymbol{y})) \quad k = 1,2,\ldots 2n. \tag{B.18b}$$

The auxiliary equations (B.18) are found by differentiating (B.16) with respect to arc-length implicitly and using equation (B.13a). Similarly the auxiliary boundary conditions can be found by differentiating the boundary conditions (B.8a) with respect to the shooting parameters

$$z_{k,j}(0;\boldsymbol{y}) = \varepsilon \sum_{l=1}^{2n} \frac{\partial a_l(\boldsymbol{\delta})}{\partial \delta_j} v_{l_k} \quad j = 1, 2, \ldots, n-1 \quad \text{and} \quad k = 1, 2, \ldots, 2n, \tag{B.19a}$$

$$z_{k,n}(0;\boldsymbol{y}) = 0 \quad k = 1, 2, \ldots, 2n. \tag{B.19b}$$

The coupled equations (B.13a) and (B.18) with initial conditions (B.13b) and (B.19) constitute a well-posed initial-value problem. From the p^{th}-iterate the initial-value problem $\boldsymbol{w}\left(s;\boldsymbol{y}^p\right)$ can be integrated up to $s = 1$ to find values of $z_{k,j}(1;\boldsymbol{y}^{(p)})$ which can then be substituted into the Newton-Raphson equation (B.14) in order to compute the next iterate for the shooting parameters $\boldsymbol{y}^{(p+1)}$, in turn creating a new initial-value problem for $\boldsymbol{w}\left(s;\boldsymbol{y}^{(p+1)}\right)$. From a good initial guess the successive solutions will then produce the correct shooting parameters for the associated boundary-value problem (B.7), (B.8).

B.3 Continuation of Homoclinic Orbits

Having computed a homoclinic solution on specifying the correct boundary conditions, numerical continuation software can follow solutions under small changes in the parameters. Continuation software discretises the solution and then under a slight change of a parameter uses the mesh points of the decretised solution as suitable initial guesses for a Newton-Raphson type method to find a new set of mesh points. The new solution is then reconstructed using a collocation algorithm [82].

As previously mentioned at the start of the chapter there are two types of boundary condition commonly employed to follow homoclinic solutions using continuation software, the explicit [41] and the projection boundary conditions [11–13, 61]. The explicit boundary conditions require a smooth basis of the stable and unstable manifolds, while the projection boundary conditions require a smooth projection onto the stable and unstable manifolds. The explicit boundary conditions require additional free parameters

which increase the dimension of the problem but can accommodate a wider variety of connecting orbits.

B.3.1 Projection Boundary Conditions

The stable, centre and unstable projection matrices onto the respective eigenspaces of the equilibrium $\boldsymbol{p}$ are composed of the stable, centre and unstable eigenvectors of the transpose of the matrix of the vector field linearised about the equilibrium. For a vector field such as that described in definition B.1.3, the projections onto the k-dimensional stable, l-dimensional centre and m-dimensional unstable manifolds are given by the three matrices $L_s(\boldsymbol{\mu})$, $L_c(\boldsymbol{\mu})$ and $L_u(\boldsymbol{\mu})$, where

$$\begin{aligned}
&L_s(\boldsymbol{\mu})(\boldsymbol{x}(0)-\boldsymbol{p}) = \mathbf{0}, \quad L_s(\boldsymbol{\mu}) \in \mathbb{R}^{k\times 2n},\\
&L_c(\boldsymbol{\mu})(\boldsymbol{x}(0)-\boldsymbol{p}) = L_c(\boldsymbol{\mu})(\boldsymbol{x}(1)-\boldsymbol{p}) = \mathbf{0}, \quad L_c(\boldsymbol{\mu}) \in \mathbb{R}^{l\times 2n},\\
&L_u(\boldsymbol{\mu})(\boldsymbol{x}(1)-\boldsymbol{p}) = \mathbf{0} \quad \text{and} \quad L_u(\boldsymbol{\mu}) \in \mathbb{R}^{m\times 2n}.
\end{aligned}$$

Projection matrices have the property of *exponential trichotomies* [58]. Hence there exist trichotomy constants $\alpha_s < -\alpha_c < 0 < \alpha_c < \alpha_u$ and $K > 0$ such that all the projection matrices satisfy

$$|\,\Phi(s,s_0)\,L_s(\boldsymbol{\mu})\,| \le Ke^{+\alpha_s(s-s_0)}, \qquad |\,\Phi(s,s_0)\,L_c(\boldsymbol{\mu})\,| \le Ke^{+\alpha_c(s-s_0)} \qquad \text{for} \quad s \ge s_0$$

and

$$|\,\Phi(s,s_0)\,L_c(\boldsymbol{\mu})\,| \le Ke^{-\alpha_c(s-s_0)}, \qquad |\,\Phi(s,s_0)\,L_u(\boldsymbol{\mu})\,| \le Ke^{+\alpha_u(s-s_0)} \qquad \text{for} \quad s_0 \ge s$$

where $\Phi(s,s_0)$ is a solution to the linearised system $\boldsymbol{x}' = Df_0\,\boldsymbol{x}$ with a phase s_0.

The existence of the exponential trichotomy means that solutions that start in the image of the stable projection matrix decay exponentially with a rate of at least $e^{-\alpha_s}$ as $s \to +\infty$. Solutions in the projection of the centre-space will not decay faster than $e^{-\alpha_c s}$ and will not increase faster than $e^{\alpha_c s}$ as $s \to +\infty$. Solutions in the image of the unstable projection decay exponentially with a rate of at least $e^{+\alpha_u}$ as $s \to -\infty$.

An important property of exponential trichotomies is that under small perturbations the resulting system also has exponential trichotomies. Thus,

Lemma B.3.1. *If the variational equation of a vector field* (B.1) *about an orbit* $\boldsymbol{x}_0$ *has an exponential trichotomy on* $\mathbb{R}^+$*, then*

$$\text{image}\left[L_s\left(\boldsymbol{\mu}\right)\right] = T_{\boldsymbol{x}_0(s)}W^s \quad \textit{and} \quad \text{image}\left[L_s\left(\boldsymbol{\mu}\right) + L_c\left(\boldsymbol{\mu}\right)\right] = T_{\boldsymbol{x}_0(s)}W^{cs},$$

where $T_{\boldsymbol{x}_0(s)}W^s$ *is the tangent space of the stable manifold associated with the orbit* $\boldsymbol{x}_0\left(s\right)$ *and* W^{cs} *is the centre-stable manifold and 'can be seen as the union of stable manifolds of the orbits lying in the centre manifold' [58].*

Proof. See [58, Lemma 2.1]. □

The lemma states that the projection conditions are stable under small perturbations and are suitable for continuation of homoclinic solutions. An analogous statement holds for projections on $\mathbb{R}^-$ with the same centre projection rates α_c. If the centre, stable and unstable projections on $\mathbb{R}^-$ are the same as those on $\mathbb{R}^+$ the exponential trichotomy is said to be a *total* exponential trichotomy.

The Kirchhoff equations in §4 were continued using the exponential dichotomies of the system. Exponential dichotomies are properties of systems which posses stable and unstable projection matrices $L_{s,u}\left(\boldsymbol{\mu}\right)$ on $\mathbb{R}^+$ for which $\left|\,\Phi\left(s,s_0\right)L_s\left(\boldsymbol{\mu}\right)\right| \leq Ke^{+\alpha_s(s-s_0)}$ for $s \geq s_0$ and $\left|\,\Phi\left(s,s_0\right)L_u\left(\boldsymbol{\mu}\right)\right| \leq Ke^{+\alpha_u(s-s_0)}$ for $s_0 \geq s$. An analogous statement holds for projections on $\mathbb{R}^-$.

B.3.2 Computation & Continuation of Periodic-to-Homoclinic Solutions

There is a great deal of literature on the computation and continuation of connecting orbits between hyperbolic equilibria, whereas periodic-to-homoclinic solutions (often called periodic-to-periodic connections) have yet to be investigated as extensively. However, much of the theoretical framework from the fixed point case can be extended to include a periodic orbit.

In this section only homoclinic periodic-to-periodic connections shall be considered. Only systems with a hyperbolic periodic orbit [34] (also refered to as a periodic orbit of saddle-type [19]) are considered. These are systems with a single conjugate pair of

Floquet multipliers on the unit circle. In this thesis both connecting orbits between hyperbolic equilibria and periodic-to-periodic connections are computed. However, the periodic-to-periodic connection is highly degenerate: firstly the system is Hamiltonian, secondly the system is reversible and thirdly the periodic orbit is known. In this section a general method shall be described before showing how each degeneracy of the system reduces the overall complexity of the system.

In [19] the authors investigated the computation shallow water waves in the presence of gravity and surface tension, a problem which has a similar two parameter bifurcation plane (in Bond and Froude numbers) to anisotropic Kirchhoff rods [98] (in m and ρ, see figure B.4). Curiously, solitary waves which are assympotic to non-decaying ripples at infinity were found to exist generically, whereas solitary waves which are assymptotic to a fixed point, i.e. ripples which decay to zero were found to be a codimension-one phenomena. The authors constructed a general boundary-value method for the continuation of homoclinic orbits to periodic orbits in Hamiltonian and reversible systems. The method was then extended in [34] for more general systems.

General Case

In the most general case, a periodic-to-periodic homoclinic connection is a codimension-zero phenomena, that is such connections persist under perturbation. A general method for their computation essentailly involves solving a pair of coupled systems: one system for the periodic orbit and one system for the homoclinic connection.

The τ-periodic solution $\boldsymbol{\gamma}(s)$ is the solution to the boundary value problem

$$\boldsymbol{v}' = \tau f(\boldsymbol{v}(s), \boldsymbol{\mu}) \quad s \in [0,1], \quad \boldsymbol{\mu} \in \mathbb{R}^p, \tag{B.21a}$$

subject to the periodic boundary condition

$$\boldsymbol{v}(0) = \boldsymbol{v}(1) \tag{B.21b}$$

and a scalar equation which determines the phase

$$\Psi(\boldsymbol{v}(s), \tau, \boldsymbol{\mu}) = \bar{p}. \tag{B.21c}$$

The homoclinic connection is given by the solution to the boundary value problem

$$\boldsymbol{w}' = \mathcal{T} f\left(\boldsymbol{w}\left(s\right), \boldsymbol{\mu}\right) \quad s \in [0,1], \quad \boldsymbol{\mu} \in \mathbb{R}^p, \tag{B.22a}$$

subject to the projection boundary conditions

$$L_s\left(\boldsymbol{\mu}\right)\left(\boldsymbol{w}\left(0\right) - \boldsymbol{v}\left(0\right)\right) = \mathbf{0}, \quad L_s\left(\boldsymbol{\mu}\right) \in \mathbb{R}^{2n\times(n-1)}, \tag{B.22b}$$

$$L_c\left(\boldsymbol{\mu}\right)\left(\boldsymbol{w}\left(0\right) - \boldsymbol{v}\left(0\right)\right) = \mathbf{0} \quad \text{or} \quad L_c\left(\boldsymbol{\mu}\right)\left(\boldsymbol{w}\left(1\right) - \boldsymbol{v}\left(1\right)\right) = \mathbf{0}, \quad L_c\left(\boldsymbol{\mu}\right) \in \mathbb{R}^{2n\times 2}, \tag{B.22c}$$

$$L_u\left(\boldsymbol{\mu}\right)\left(\boldsymbol{w}\left(1\right) - \boldsymbol{v}\left(1\right)\right) = \mathbf{0} \quad L_u\left(\boldsymbol{\mu}\right) \in \mathbb{R}^{2n\times(n-1)}. \tag{B.22d}$$

The coupling between the two systems is through the projection boundary conditions. In order for the system to be well-posed two artifical parameters are introduced into the system: the period τ and the truncated length of the homoclinic connection $\mathcal{T}$. Homoclinic solutions can be continued under changes in the parameter $\mu \in \boldsymbol{\mu}$.

Hamiltonian Case

If the system is Hamiltonian the periodic orbit satisfies

$$\boldsymbol{v}' = \tau\left(J\nabla\mathcal{H}\left(\boldsymbol{v}\left(s\right), \boldsymbol{\mu}\right) + \lambda_1 \nabla\mathcal{H}\left(\boldsymbol{v}\left(s\right), \boldsymbol{\mu}\right)\right) \quad s \in [0,1] \tag{B.23a}$$

subject to the periodic boundary condition

$$\boldsymbol{v}\left(0\right) = \boldsymbol{v}\left(1\right) \tag{B.23b}$$

and along with a condition which fixes the 'energy' of the Hamiltoninan

$$\mathcal{H}\left(\boldsymbol{v}\left(s\right), \boldsymbol{\mu}\right) = h \tag{B.23c}$$

and a phase condition

$$\Psi\left(\gamma, \boldsymbol{\mu}\right) = p. \tag{B.24}$$

The homoclinic connection is satisfies the boundary value problem

$$\boldsymbol{w}' = \mathcal{T}\left(J\nabla\mathcal{H}\left(\boldsymbol{w}, \lambda\right) + \lambda_2 \nabla\mathcal{H}\left(\boldsymbol{w}, \lambda\right)\right) \quad s \in [0,1] \tag{B.25a}$$

subject to the projection boundary conditions

$$L_s(\boldsymbol{\mu})(\boldsymbol{w}(0)-\boldsymbol{v}(0))=\mathbf{0}, \quad L_s\in\mathbb{R}^{2n\times(n-1)}, \tag{B.25b}$$

$$L_c(\boldsymbol{\mu})(\boldsymbol{w}(0)-\boldsymbol{v}(0))=\mathbf{0} \quad \text{or} \quad L_c(\boldsymbol{\mu})(\boldsymbol{w}(1)-\boldsymbol{v}(1))=\mathbf{0}, \quad L_c\in\mathbb{R}^{2n\times 2)} \tag{B.25c}$$

$$L_u(\boldsymbol{\mu})(\boldsymbol{w}(1)-\boldsymbol{v}(1))=\mathbf{0} \quad L_u\in\mathbb{R}^{2n\times(n-1)} \tag{B.25d}$$

where λ_2 is a Hamiltonian breaking parameter.

There are now four artifical parameters introduced in order for the system to be well-posed: the period τ, the trunacation length $\mathcal{T}$ and the two Hamiltonain breaking parameters λ_1 and λ_2. There are now two free parameters which can be continued either $\mu\in\boldsymbol{\mu}$ or h. If h is the free parameter then the periodic orbit will be change. If μ is the free parameter then continuation will follow connections between a single periodic orbit.

Hamiltonian & Symmetric Case

Considering the special case where the system is reversible, the construction of the periodic orbit is given by

$$\boldsymbol{v}'=\tau\left(J\nabla\mathcal{H}(\boldsymbol{v}(s),\lambda)+\lambda_1\nabla\mathcal{H}(\boldsymbol{v}(s),\lambda)\right) \quad s\in[0,1] \tag{B.26a}$$

subject to the periodic boundary condition

$$\boldsymbol{v}(0)=\boldsymbol{v}(1) \tag{B.26b}$$

and along with a condition which fixes the 'energy' of the Hamiltoninan

$$\mathcal{H}(\boldsymbol{v}(s),\boldsymbol{\mu})=h. \tag{B.26c}$$

Solutions which are reversible must satisfy the n-dimensional constraint

$$\boldsymbol{w}(1)\in\mathcal{S}$$

thus for symmetric orbits the Hamiltonian breaking parameter λ_2 can be removed, so that the second set of coupled equations is given by

$$\boldsymbol{w}'=\mathcal{T}\nabla\mathcal{H}(\boldsymbol{w}(s),\boldsymbol{\mu}) \quad s\in[0,1] \tag{B.27a}$$

subject to the boundary conditions

$$L_s(\boldsymbol{\mu})(\boldsymbol{w}(0)-\boldsymbol{v}(0))=\mathbf{0}, \quad L_s\in\mathbb{R}^{2n\times(n-1)} \tag{B.27b}$$

$$L_c(\boldsymbol{\mu})(\boldsymbol{w}(0)-\boldsymbol{v}(0))=\mathbf{0} \quad \text{or} \quad L_c(\boldsymbol{\mu})(\boldsymbol{w}(1)-\boldsymbol{v}(1))=\mathbf{0}, \quad L_c\in\mathbb{R}^{2n\times 2}. \tag{B.27c}$$

There are three artifical free parameters introduced in order for the system to be well-posed: τ, $\mathcal{T}$ and λ_1.

Hamiltonian, Symmetric with a Given Periodic Orbit

If the periodic orbit can be constructed then the parameter τ is known and as $\boldsymbol{\gamma}$ is an exact solution so $\lambda_1=0$. Thus, the governing equation can be simplified further as the system can be discarded. Now there is only one free parameter $\mathcal{T}$.

$$\boldsymbol{w}'=\mathcal{T}f(\boldsymbol{w}(s),\boldsymbol{\mu}) \quad s\in[0,1] \tag{B.28a}$$

subject to the boundary conditions

$$L_s(\boldsymbol{\mu})(\boldsymbol{w}(0)-\boldsymbol{v}(0))=\mathbf{0}, \quad L_s\in\mathbb{R}^{2n\times(n-1)} \tag{B.28b}$$

$$L_c(\boldsymbol{\mu})(\boldsymbol{w}(0)-\boldsymbol{v}(0))=\mathbf{0} \quad \text{or} \quad L_c(\boldsymbol{\mu})(\boldsymbol{w}(1)-\boldsymbol{v}(1))=\mathbf{0}, \quad L_c\in\mathbb{R}^{2n\times 2} \tag{B.28c}$$

This is the method implimented in chapter §6.

B.3.3 Explicit Boundary Conditions

The explicit boundary conditions [41] allow for an 'adaptive' shooting procedure to be performed with continuation software by placing the lefthand and righthand boundary conditions of a truncated homoclinic orbit in the unstable and stable tangent spaces of an equilibrium. The tangent spaces are spanned by the set of vectors of the linearised vector field about an equilibrium. The key assumption is that the problem is generic in the sense that the boundary conditions perturb the homoclinic orbit transversally.

As the only systems which are investigated in this thesis are reversible, the boundary conditions only need to place lefthand boundary conditions in the tangent space of

the unstable manifold as the righthand boundary conditions can be placed in the n-dimensional symmetric section. Once again the tangent space of the unstable manifold is approximated as

$$\begin{aligned}\boldsymbol{x}(0) &= \varepsilon\left(a_1\boldsymbol{v}_1 + a_2\boldsymbol{v}_2 + \ldots + a_n\boldsymbol{v}_n\right),\\ \boldsymbol{x}(1) &\in \mathcal{S}.\end{aligned}$$

As in §B.2 the n normalised functions a_i are parameterised by $n-1$ free parameters $\boldsymbol{\delta}$ and $\boldsymbol{v}_i \in \mathbb{R}^{2n}$ are vectors in the linearised subspace $\mathcal{E}^u(0)$. As there are $3n$ boundary conditions (n conditions for $\boldsymbol{x}(0)$, n conditions on the functions a_i and n conditions on the symmetric section) for a $2n$-dimensional problem with $n-1$ free parameters $\boldsymbol{\delta}$, once again it is necessary to allow $\mathcal{T}$ to be a free parameter in order for the boundary value problem to be well-posed.

Introducing the functions a_i and increasing the number of continuation parameters $(\boldsymbol{\delta}, \mathcal{T})$ of the problem is computationally expensive in comparison with the projection boundary conditions. Another drawback is that when approaching critical values $\lambda = \lambda_\pm$ the shooting parameters δ_1 and δ_2 vary dramatically, decreasing computational speed. Numerically as critical buckling values are approached the problem becomes similar to the existence of a boundary layer in singular perturbation problems [95]. However, the explicit boundary conditions seem to provide a better approximation of the linear subspaces than projection boundary conditions as they can be continued closer to the critical values.

B.4 Numerical Subroutines Implimented

A variety of numerical subroutines were implimented in this thesis. In this section they are described, along with their advantages and disadvantes.

Quadrature

The quadrature subroutine `cubint.f` was used in the computation of the second-order Mel'nikov integral. This package was used primarily because takes the unequally

spaced output from the adaptive integrator and approximates an integral using cubic polynomial interpolation of data. The choice of cubic polynomial is the natural one since linear interpolation is inaccurate and higher order polynomials are seldom reliable for unevenly spaced data. The returned absolute and relative errors were always low, i.e. 10^{-12}.

Eigenvalue & Eigenvector computation

Initially the Eispack routine `rg.f` was used to calculate eigenvalues of the monodromy matrix and the unstable vectors $\boldsymbol{v}_1$ and $\boldsymbol{v}_2$ which were used in the computation and continuation of the homoclinic orbits. However, for continuity with the continuation software used the nag subroutine `f02agf.f` was used instead.

The subroutine takes a matrix M which is first balanced and then reduced to upper Hessenberg form using real stabilised elementary similarity transformations. The eigenvalues and eigenvectors of the Hessenberg matrix are calculated using the QR-algorithm. The eigenvectors of the Hessenberg matrix are back-transformed to give the eigenvectors of the original matrix M.

It should be noted that this subroutine has been discontinued and has been replaced with `f02ebf.f`.

Numerical solution of systems of first order equations

Throughout the majority of this thesis systems of first order differential equations were solved with the subroutine `dop853.f`. This is an explicit, highly accurate, adaptive Runge-Kutta method of order 8 for first order non-stiff systems due to Dormand and Prince. The local error estimation and step-size control are based on embedded formulas of orders 5 and 3 respectively. The method provides dense output of order 7.

At first a basic explicit, non-adaptive, fourth-order Runge-Kutta routine was implimented but in comparison with the higher-order method was slow. For example when shooting to find homoclinic orbits each step of the Newton-Raphson iteration requires the integration of an initial value problem and this method became slow when the large

solutions were computed.

It should be noted that the solver is not a symplectic or geometric integrator, that is it does not exploit the Hamiltonian structure of the system to conserve the phase space. However the solver does conserve the integrals to a great degree of accuracy. For example when computing solutions from the shooting algorithm with the relative and absolute tolerances set to 10^{-14}, all of the integrals are conserved to at least 10^{-10}. When computing Poincaré sections, such as figures 4.4.2 and 5.6 over exceptionally long time periods the Hamiltonian remained bounded and had an error of order 10^{-7}. To overcome this a symplectic integrator was used.

Due to the symmetry in the system the Hamiltonian is not separable in terms of kinetic plus potential energy, so explicit rather than implicit runge-kutta type algorithms must be applied. Thus, in practice, one has to solve the implicit algebraic equations for the intermediate stage values using some iterative approximation method. In general, with an approximation based on a finite number of iterations, the resulting integration scheme is no longer symplectic. Error analysis on the structural conservation, like the analysis on the numerical accuracy, provides insight into a numerical method and helps in making judicious choices of integration schemes - but still these methods are "almost symplectic".

Solutions from the eighth order explicit integrator were contrasted against the symplectic implicit S-stage Gauss-Legendre method of order $2S$ when $S = 1, 2, 3$. Note that when $S = 1$ the S-stage Gauss-Legendre method corresponds to the midpoint rule. The Poincaré sections were similar in appearance illustrating stochastic layers. The implicit S-stage Gauss-Legendre methods took far greater time and memory than the implicit Runge-Kutta method but conserved the Hamiltonian to with 10^{-12} and so was used to compute the Poincaré sections in figures 4.4.2 and 5.6.

Continuation Software

The program `auto97` is the standard continuation software and was used throughout the thesis. The program discretizes ordinary differential equation boundary value prob-

lems by the method of orthogonal collocation using piecewise polynomials and continues the solutions using psuedo arc-length continuation. The mesh automatically adapts to the solution to equi-distribute the local discretization error. It is a psuedo-arclength continuation package which uses a combined Newton and Chord iteration to compute paths of solutions.

The maximum number of Newton-Raphson iterations was $\texttt{NWTN} = 3$ and the maximum number of combined Newton-Raphson/Chord iterations was $\texttt{ITNW} = 5$. The criteria for convergence of solution components and equation parameters was set to $\texttt{EPSL} = 10^{-8}$, $\texttt{EPSU} = 10^{-8}$. The criteria for the detection of special solutions, such as limit points, was $\texttt{EPSS} = 10^{-6}$. If the combined Newton-Raphson and Chord methods failed to converge then the stepsize, initially given as $\texttt{DS} = 10^{-5}$, was halved until a minimum stepsize is reached, $\texttt{DSMIN} = 10^{-12}$. The maximum stepsize was given as $\texttt{DS} = 10^{-2}$. In all computations the number of mesh intervals was $\texttt{NTST} = 100$ and the number of collocation points per interval was $\texttt{NCOL} = 4$.

B.5 Application to the Kirchhoff rod

From the Mel'nikov analysis presented in §4.4, if a rod is anisotropic or initially curved then a multiplicity of multimodal configurations exists with a well-defined bifurcation structure determined by a set of *accumulation* and *coalescence* rules [23, 95]. Following from the rather general description of the computation and continuation of homoclinic orbits to hyperbolic fixed points in the previous section, as an illustrative example the computation and continuation of homoclinic orbits of the Kirchhoff rod is presented in this section.

In the spatial frame the static equilibrium equations are given by (3.23) and in the director frame by (3.27). The governing equations in the director frame a six-dimensional noncanonical Hamiltonian system with two Casimirs given by (3.29). Let the constitutive relations be given by (4.52) and let a torque, M, and tension, T, be applied in the direction of $\boldsymbol{d}_3$ at $s = \pm\infty$. As homoclinic solutions shall be studied there is no natural length scale, thus the arclength is nondimensionalised by $\bar{s} = (M/B_1)\, s$. Scaling the

forces and moments by

$$x_1 = m_1/M, \quad x_2 = m_2/M, \quad x_3 = (m_3 - M)/M,$$
$$x_4 = n_1/T, \quad x_5 = n_2/T \quad \text{and} \quad x_6 = (n_3 - T)/T$$

the equilibrium equations $\boldsymbol{x}' = f(\boldsymbol{x})$ become

$$\begin{array}{ll} x_1' & = (1+\nu)x_2(1+x_6) - (x_3+1)x_5, \\ x_2' & = (1+\rho)(x_3+1)x_4 - (1+\nu)x_1(1+x_6), \\ x_3' & = x_1x_5 - (1+\rho)x_2x_4, \\ x_4' & = \nu x_5(1+x_6) + x_2/m^2, \\ x_5' & = (\rho-\nu)x_4(1+x_6) - x_1/m^2, \\ x_6' & = -\rho x_4x_5, \end{array} \tag{B.30}$$

subject to $\boldsymbol{x} \to \boldsymbol{0}$ as $\bar{s} \to \pm\infty$. The nondimensional parameters are described in (4.1). The bar notation shall be suppressed from thsi point onwards.

The linearised governing equation is given by

$$\boldsymbol{x}' = A\boldsymbol{x} \quad \text{where} \quad A = \begin{pmatrix} 0 & (1+\nu) & 0 & 0 & -1 & 0 \\ -(1+\nu) & 0 & 0 & (1+\rho) & 0 & 0 \\ 0 & 0 & 0 & 0 & 0 & 0 \\ 0 & 1/m^2 & 0 & 0 & \nu & 0 \\ -1/m^2 & 0 & 0 & (\rho-\nu) & 0 & 0 \\ 0 & 0 & 0 & 0 & 0 & 0 \end{pmatrix}. \tag{B.31}$$

The matrix has a two-dimensional kernel so the nontrivial linearised dynamics take place in a four-dimensional phase space. In accordance with the centre manifold theorem, the dimensions of the linearised subspaces correspond to the dimensions of the stable, centre and unstable manifolds of the reduced system (4.54).

In order to compute the homoclinic solutions over a truncated range the governing equations are scaled as $\boldsymbol{x}' = \mathcal{T} f(\boldsymbol{x})$ over the unit interval $[0,1]$. The computation of homoclinic orbits will exploit the reversibilities of the system and compute solutions over half the range. As shown in (4.18) the canonical system is invariant under the action of Z_2. For the noncanonical system the action of Z is given by

$$Z_2 \,:\, (x_1, x_2, x_3, x_4, x_5, x_6) \mapsto (-x_1, -x_2, x_3, -x_4, -x_5, x_6)\,.$$

The reversibilities are given by

$$R_1 \,:\, (x_1, x_2, x_3, x_4, x_5, x_6) \mapsto (-x_1, x_2, x_3, -x_4, x_5, x_6) \quad \text{as} \quad s \mapsto -s$$

and

$$R_2 : (x_1, x_2, x_3, x_4, x_5, x_6) \mapsto (x_1, -x_2, x_3, x_4, -x_5, x_6) \quad \text{as} \quad s \mapsto -s.$$

For the R_1-reversibility the fixed point set of the reversibilities, referred to as the symmetric section, is given by

$$\mathcal{S}_1 = \left\{ \boldsymbol{x} \in \mathbb{R}^6 \, : \, x_1(1) = x_4(1) = 0 \right\}. \tag{B.33a}$$

Similarly for the R_2-reversibility the symmetric section is given by

$$\mathcal{S}_2 = \left\{ \boldsymbol{x} \in \mathbb{R}^6 \, : \, x_2(1) = x_5(1) = 0 \right\}. \tag{B.33b}$$

When the fixed point is a saddle-node with stable and unstable eigenvalues $\mu^{s,u} = \pm\eta \pm i\omega$ (with $\eta, \omega > 0$) of the linearised system A, a suitable lefthand boundary condition is given by

$$\boldsymbol{x}(0) = \varepsilon \left(\boldsymbol{v}_1 \sin\delta_1 + \boldsymbol{v}_2 \cos\delta_1 \right) \tag{B.34}$$

where the $\boldsymbol{v}_1 \pm i\boldsymbol{v}_2$ is the eigenvector corresponding to the unstable eigenvalue μ^u, $\varepsilon = 10^{-5}$ is a small perturbation away from the saddle and δ_1 is a shooting parameter which ensures the perturbation is transversal to the flow about the equilibrium. When $m = 1.7$, $\nu = 1/3$ and $\rho = 1/4$ then

$$\begin{aligned} \boldsymbol{v}_1 &= (0.646691, 0.0414290, 0, 0.339329, -0.117096, 0), \\ \boldsymbol{v}_2 &= (0, 0.587457, 0, 0.150579, 0.288856, 0). \end{aligned}$$

The shooting parameter $\mathcal{T}$, corresponding to the 'time' spent outside the local unstable manifold, is in the rescaled equations, whereas δ features in the lefthand boundary condition.

The righthand boundary conditions are determined by the symmetric section of a reversibility (B.33).

Thus for the six-dimensional system (B.30) an eighteen-dimensional equation is constructed, as in equation (B.16), to solve for the shooting parameters δ and $\mathcal{T}$ which

determine solutions which satisfy the symmetric section boundary conditions (B.33). The eighteen-dimensional was comprised of the six-dimensional initial value problem $\boldsymbol{w}$ coupled to a twelve-dimensional variational equation $z_i = \partial w_i/\partial\delta$, $i = 1, \ldots, 6$ and $z_i = \partial w_i/\partial\mathcal{T}$, $i = 7, \ldots, 12$. The equation is

$$
\begin{aligned}
w_1' &= \mathcal{T}\left((1+\nu)\, w_2\,(1+w_6) - (w_3+1)\, w_5\right),\\
w_2' &= \mathcal{T}\left((1+\rho)\,(w_3+1)\, w_4 - (1+\nu)\, w_1\,(1+w_6)\right),\\
w_3' &= \mathcal{T}\left(w_1 w_5 - (1+\rho)\, w_2 w_4\right),\\
w_4' &= \mathcal{T}\left(\nu w_5\,(1+w_6) + w_2/m^2\right),\\
w_5' &= \mathcal{T}\left((\rho-\nu)\, w_4\,(1+w_6) - w_1/m^2\right),\\
w_6' &= -\mathcal{T}\rho w_4 w_5,
\end{aligned}
$$

and

$$
\begin{aligned}
z_1' &= \mathcal{T}\left((1+\nu)\,(z_2\,(1+w_6) + w_2 z_6) - (z_5\,(w_3+1) + w_5 z_3)\right),\\
z_2' &= \mathcal{T}\left((1+\rho)\,(z_4\,(w_3+1) + w_4 z_3) - (1+\nu)\,(z_1\,(1+w_6) + w_1 z_6)\right),\\
z_3' &= \mathcal{T}\left(z_1 w_5 + w_1 z_5 - (1+\rho)\,(z_2 w_4 + w_2 z_4)\right),\\
z_4' &= \mathcal{T}\left(\nu\,(z_5\,(1+w_6) + w_5 z_6) + z_2/m^2\right),\\
z_5' &= \mathcal{T}\left((\rho-\nu)\,(z_4\,(1+w_6) + w_4 z_6) - z_1/m^2\right),\\
z_6' &= -\mathcal{T}\rho\,(z_4 w_5 + w_4 z_5),\\
z_7' &= \mathcal{T}\left((1+\nu)\,(z_8\,(1+w_6) + w_2 z_{12}) - (z_{11}\,(w_3+1) + w_5 z_9)\right.\\
&\qquad \left. + (1+\nu)\, w_2\,(1+w_6) - (w_3+1)\, w_5,\right.\\
z_8' &= \mathcal{T}\left((1+\rho)\,(z_{10}\,(w_3+1) + w_4 z_9) - (1+\nu)\,(z_7\,(1+w_6) + w_1 z_{12})\right)\\
&\qquad + (1+\rho)\,(w_3+1)\, w_4 - (1+\nu)\, w_1\,(1+w_6),\\
z_9' &= \mathcal{T}\left(z_7 w_5 + w_1 z_{11} - (1+\rho)\,(z_8 w_4 + w_2 z_{10})\right) + w_1 w_5 - (1+\rho) w_2 w_4,\\
z_{10}' &= \mathcal{T}\left((\nu(z_{11}\,(1+w_6) + w_5 z_{12}) + z_8/m^2\right) + \nu w_5\,(1+w_6) + w_2/m^2,\\
z_{11}' &= \mathcal{T}\left((\rho-\nu)\,(z_{10}\,(1+w_6) + w_4 z_{12}) - z_7/m^2\right) + (\rho-\nu)\, w_4\,(1+w_6) - w_1/m^2,\\
z_{12}' &= -\mathcal{T}\rho\,(z_{10} w_5 + w_4 z_{11}) - \rho w_4 w_5,
\end{aligned}
$$

subject to the initial conditions

$$\boldsymbol{w}(0) = \varepsilon(\boldsymbol{v}_1 \cos\delta + \boldsymbol{v}_2 \sin\delta)$$

and

$$z_i(0) = \varepsilon(v_{2i}\cos\delta - v_{1i}\sin\delta) \quad i = 1,\ldots,6 \quad \text{and} \quad z_k(0) = 0 \quad k = 7,\ldots,12.$$

The shooting parameters $\delta, \mathcal{T}$ need to be found so that they minimize a function which corresponds to the symmetric section boundary condition. For the R_1-reversibility for the function (B.12) was given as

$$b(\boldsymbol{x}(1)) = (x_1(1), x_4(1))^T \tag{B.35}$$

so that when solving the variational equation for the initial value problem the function G was given by

$$G(\delta, \mathcal{T}) = (w_1(1;\delta,\mathcal{T}), w_4(1;\delta,\mathcal{T}))^T \tag{B.36}$$

so that a solution to the variational equation will lie in the symmetric section of a reversibility. For the R_2-reversibility the corresponding function to be minimized was given by

$$G(\delta, \mathcal{T}) = (w_2(1;\delta,\mathcal{T}), w_5(1;\delta,\mathcal{T})). \tag{B.37}$$

When ε is sufficiently small and $\mathcal{T}$ is sufficiently large, for a good initial guess $\left(\delta^{(0)}, \mathcal{T}^{(0)}\right)$ the successive values of the shooting parameter converged quadratically to minimize G and hence solve the boundary value problem for truncated homoclinic orbits.

The computed homoclinic solutions were then continued with AUTO97 using projection boundary conditions. From the transpose of the linearised system A^T, the normalised eigenvectors $\bar{\boldsymbol{v}}_1 \pm i\bar{\boldsymbol{v}}_2$ of the stable eigenvalue $\mu^s = +\eta \pm i\omega$ define the stable projection matrix as

$$L_s(m,\rho,\nu) = (\bar{\boldsymbol{v}}_1, \bar{\boldsymbol{v}}_2)^T \in \mathbb{R}^{2\times 6}. \tag{B.38}$$

The lefthand boundary conditions were given by projecting back onto the stable eigenspace of the equilibrium

$$L_s(m,\rho,\nu)\,\boldsymbol{x}(0) = \mathbf{0} \tag{B.39}$$

along with

$$x_3(0) = 0 \quad \text{and} \quad x_6(0) = 0 \tag{B.40}$$

which fixed the values of the Casimirs (3.29). From the reversibilities of the solution, the appropriate righthand boundary conditions placed the solution in the symmetric section of a reversibility (B.33). Thus for the R_1-reversibility

$$x_1(1) = 0 \quad \text{and} \quad x_4(1) = 0 \tag{B.41a}$$

and for the R_2-reversibility

$$x_1(2) = 0 \quad \text{and} \quad x_5(1) = 0. \tag{B.41b}$$

From the discrete symmetries of the Kirchhoff rod, there are four distinct primary homoclinic orbits, labelled P_i where $i = 1,\ldots,4$. Shooting parameters for the primary orbits are given in table B.1, a configuration is displayed in figure B.1 and components of the force x_1 and x_2 displayed in figure B.2.

Table B.1: Shooting values for primary homoclinic orbits computed by the method outlined in §B.2 when $m = 1.7$, $\nu = 1/3$ and $\rho = 1/4$. All values shall be given to seven significant figures. Note that as the homoclinics are reversible that $\mathcal{T}$ is the distance to the symmetric section and is half the length of the full homoclinic.

		δ	$\mathcal{T}$
R_1	P_1	3.338506	46.99226
	P_2	0.1969133	46.99226
R_2	P_3	1.707908	46.92438
	P_4	4.8495001	46.92438

Multimodal solutions are then characterised by a number of distinct primary localisations separated by a number of smaller oscillations. Each oscillation is a quarter turn

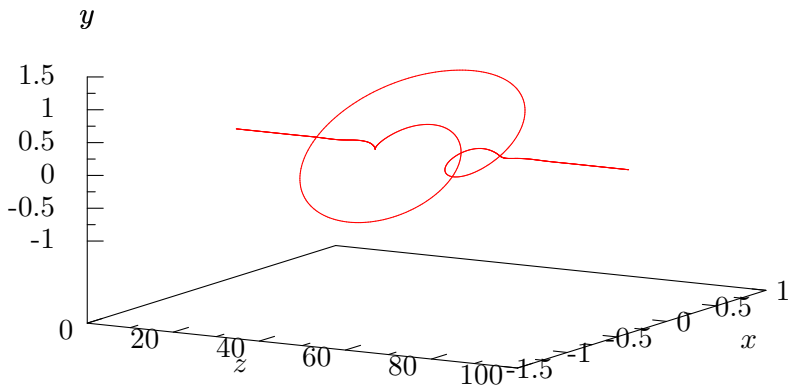

Figure B.1: Configuration of the P_4 primary homoclinic orbit when $m = 1.7$, $\nu = 1/3$ and $\rho = 1/4$. The shooting parameters, over the half range are given in table B.1 as $\delta = 4.8495001$ and $\mathcal{T} = 46.92438$. In order to visualise the entire configuration the half range solution is reflected by the R_2 involution (4.18b).

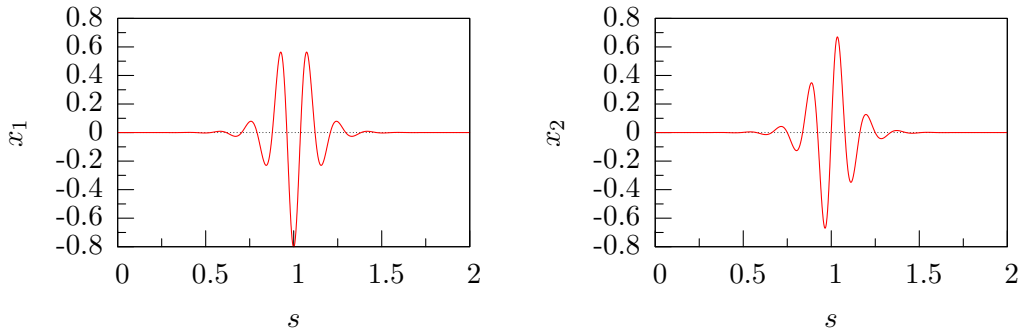

Figure B.2: Components of force x_1 and x_2 for a anisotropic primary homoclinic orbit for primary homoclinic orbit P_4 when $m = 1.7$, $\nu = 1/3$ and $\rho = 1/4$.

the rod makes between localised modes. Bimodals orbits are denoted by (P_i, n, P_j) where n denotes the number of small oscillations separating the primary localisations. When n is small then the correspondence between a primary homoclinic orbit and a mode of a bimodal orbit is not immediately evident but when n is large the correspondence becomes clear as the two modes *accumulate* onto the respective primary homoclinic orbits.

Table B.2 presents shooting parameters for a succession of bimodal homoclinic orbits of the form (P_1, n, P_1). From the table B.2 it can be seen that as n increases so the shooting parameter δ_n approaches the value of the shooting parameter δ for the primary orbit which is the first mode of a bimodal orbit. It can be seen that as n increases so the difference between successive truncation lengths $|\mathcal{T}_n - \mathcal{T}_{n-1}|$ tends to $\pi/2\omega$ where ω is the positive imaginary part of the eigenvalue μ^u. The additional 'time' taken is due to the fact that the dynamics occurs near the equilibria where, by the centre manifold theorem, the governing equations are "governed, very nearly, by the linear equations" [22].

Table B.2: Shooting values for R_1-reversible bimodal homoclinic orbits (P_1, n, P_1) when $m = 1.7$, $\nu = 1/3$ and $\rho = 1/4$ and corresponding limit points under continuation in m.

n	δ_n	$\mathcal{T}_n$	$\mathcal{T}_n - \mathcal{T}_{n-1}$	limit point $m^{(n)}$
0	2.766753	59.85963	–	1.700431
1	3.446896	62.78099	2.921359	1.739740
2	3.299746	64.64873	1.867743	1.741342
3	3.351155	66.76810	2.119364	1.765862
4	3.334243	68.80146	2.033367	1.766433
5	3.339928	70.86311	2.061650	1.783191
10	3.338500	81.13418	2.054381	1.804975
15	3.338506	91.40702	2.054572	1.822971

	δ	$\mathcal{T}$	$\pi/2\omega$	bifurcation point m
P_1	3.338506	46.99226	2.054567	1.861290

Since the minimum number of turns found is rather arbitrary, the only reliable way to label a multimodal homoclinic orbit correctly is by increasing the number of turns from the accumulation rules and to assign the label according to which configuration emerges. Thus, families of solutions rather than individual orbits are labelled.

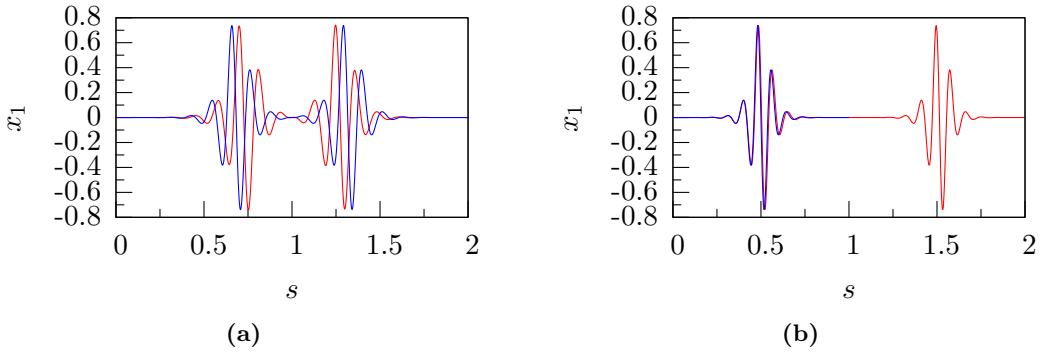

Figure B.3: Nondimensionalised force component x_1 of a bimodal homoclinic orbit with $\rho = 1/4$, $\nu = 1/3$ and $m = 1.70$ as given in table B.2 over a normalised arclength. Subfigure B.3(a) shows force components of bimodal orbits with $n = 2$ (red) and $n = 4$ (blue), illustrating how the bimodal orbits change as the number of quarter turns between localisations increases. Subfigure B.3(b) then shows the bimodal orbit $n = 15$ (red) against a primary bimodal (blue), illustrating that as n increases so each localisation of a bimodal becomes more like the corresponding primary localisation.

Multimodal solutions cannot exist in the integrable limit as either ρ or κ_0 approaches zero. In this limit pairs of reversible solutions *coalesce* at limit points and pairs of non-reversible solutions bifurcate in a Hamiltonian-Hopf bifurcation, (cf. figure 6.18). Pairs of multimodal solutions also coalesce as they approach a critical value of end loading for the buckling of primary solutions $m_{\max}$. For reversible multimodal solutions the limit points are not a change of stability but an exchange of stability through the switching of an unstable branch to a branch which is less unstable [17, 79] as all branches are unstable. The following coalescence rules were found for R_1-reversible bimodal orbits under continuation of ρ, m, and κ_0

$$
\begin{aligned}
(P_1, 2n+1, P_1) &\longleftrightarrow (P_3, 2n+1, P_4)\,, \\
(P_1, 2n+2, P_1) &\longleftrightarrow (P_4, 2n+2, P_3)\,, \\
(P_2, 2n+1, P_2) &\longleftrightarrow (P_4, 2n+1, P_3)\,, \\
(P_2, 2n+2, P_2) &\longleftrightarrow (P_3, 2n+2, P_4)
\end{aligned}
$$

and for R_2-reversible bimodal orbits the coalesce rules are

$$(P_1, 2n+1, P_2) \longleftrightarrow (P_3, 2n+1, P_3)\,,$$
$$(P_1, 2n+2, P_2) \longleftrightarrow (P_4, 2n+2, P_4)\,,$$
$$(P_2, 2n+1, P_1) \longleftrightarrow (P_4, 2n+1, P_4)\,,$$
$$(P_2, 2n+2, P_1) \longleftrightarrow (P_3, 2n+2, P_3)\,.$$

The exchange of stability which occurs at the limit points is due to a nontransverse intersection of the stable and unstable manifolds rather than a local bifurcation. Coalescence only affects multimodal solutions since for reversible Hamiltonian systems the stable and unstable manifolds of a primary homoclinic orbit continue to intersect the symmetric section transversely [18]. As yet no accumulation or coalescence rules for trimodals or higher modes have been formulated.

In table B.2 it is clear that as n increases the modes of the bimodal orbits becomes more like the primary orbits, so the limit points $m^{(n)}$ approach the bifurcation value for the primary orbits.

From the accumulation and coalescence rules a coherent picture of the bifurcation structure emerges. Using limit point continuation in the pseudo arclength continuation software AUTO97, a codimension-one curve of coalescence values for reversible bimodal, trimodal and sixmodal orbits in the nondimensional (ρ, m) parameter plane is presented in figure B.4(a). Note that all the curves approach the codimension-two point (with four-fold zero eigenvalues) at $(\rho_c, m_c) = (1.1064, 1.4295)$. The codimension-two point separates weakly anisotropic rods, which buckle in Hamiltonian-Hopf bifurcations, and strongly anisotropic rods, which buckle in Hamiltonian-pitchfork bifurcations [98].

The limit points for the bimodal orbits calculated in table B.2 when $\rho = 1/4$ can be seen in figure B.4(b), showing the differences in the bifurcation characteristics within a family of bimodal solutions. Although the limit point curves for bimodal orbits with small n are further from the buckling line than those orbits with large n, the curves can be continued closer to the codimension-two point.

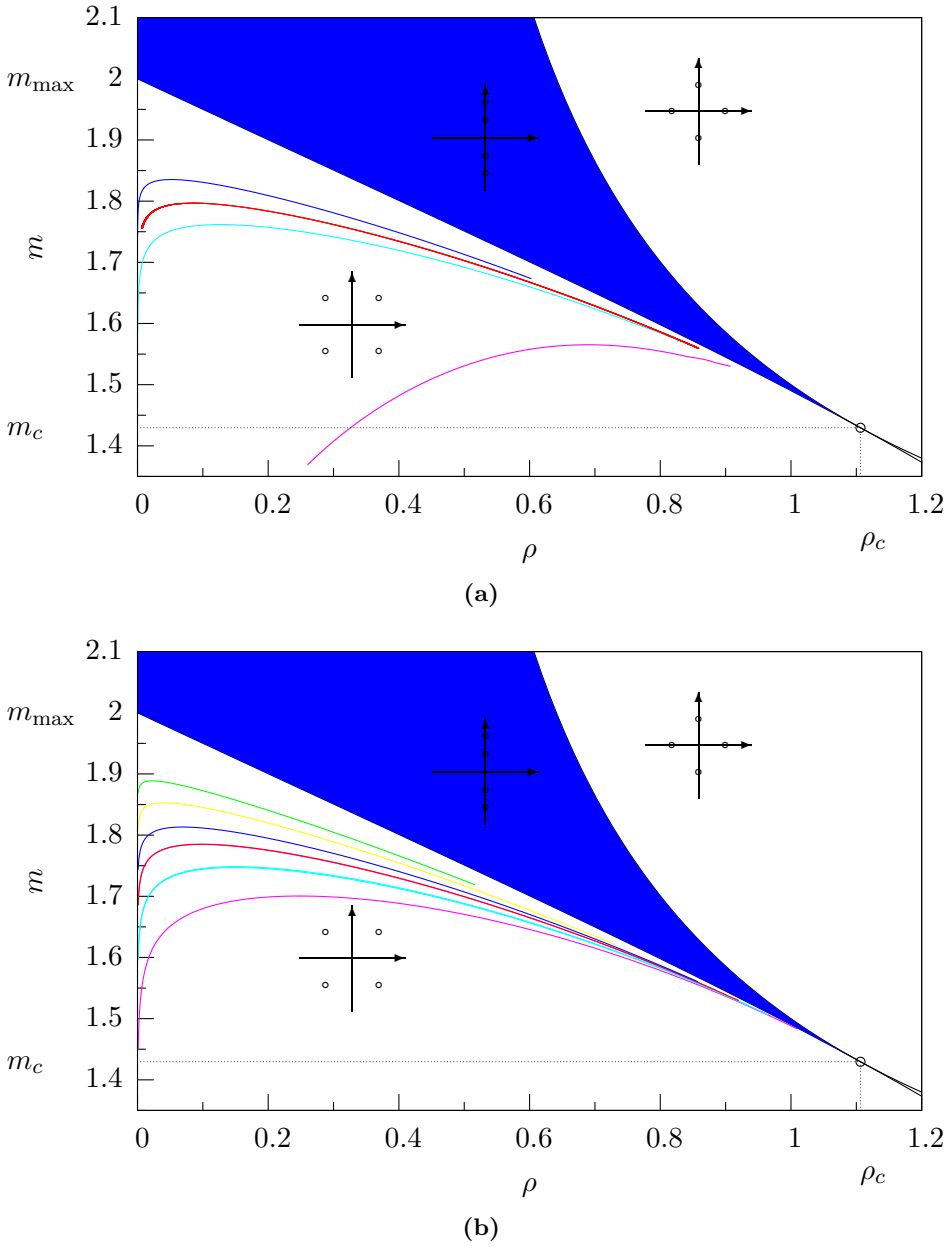

Figure B.4: Subfigure B.4(a) shows the limit point curves for anisotropic multimodal solutions in the (ρ, m) parameter plane the multimodal solutions are computed are bimodal (blue), trimodal (red), quadmodal (cyan) and six modal (magenta) orbits. . The coloured region is the elliptic region in which localised solutions cannot exist. The subfigure illustrates that higher order multimodal solutions tend to bifurcation before lower order multimodal solutions. Subfigure B.4(b) shows the limit point curves of the bimodal family in table B.2. As the limit point curves essentially occur in pairs, so $n = 0$ (magenta), $n = 1$, 2 (cyan), $n = 3$, 4 (red), $n = 5$ (blue), $n = 10$ (yellow), $n = 15$ (green) . The subfigure illustrates that as those bimodals which have a large number of quarter-turns are better approximations to the corresponding primary orbits, they bifurcate closer to the bifurcation values of the primary orbits.

Bibliography

[1] R. Abraham, J. E. Marsden, and T. S. Ratiu, *Manifolds, Tensor Analysis and Applications*, 2nd ed., Applied Mathematical Sciences, no. 75, Springer-Verlag, New York, NY, 1988.

[2] S. S. Antman, *Nonlinear Problems of Elasticity*, 2nd ed., Applied Mathematical Sciences, no. 107, Springer-Verlag, New York, NY, 1995.

[3] S. S. Antman and K. B. Jordan, *Qualitative aspects of the spatial deformation of nonlinearly elastic rods*, Proc. R. Soc. Edinburgh Sect. A **73** (1975), 85–105.

[4] S. S. Antman and C. S. Kenney, *Large buckled states of nonlinearly elastic rods under torsion, thrust, and gravity*, Arch. Ration. Mech. Anal. **76** (1981), 289–338.

[5] S. S. Antman and T. P. Liu, *Travelling waves in hyperelastic rods*, Quart. Appl. Math. **36** (1979), 377–399.

[6] V. I. Arnol'd, *Mathematical Methods of Classical Mechanics*, 2nd ed., Graduate Texts in Mathematics, no. 60, Springer-Verlag, New York, NY, 1989.

[7] F-S. Bai and A. R. Champneys, *Numerical detection and continuation of saddle-node homoclinic bifurcations of codimension one and two*, J. Dyn. Stab. Sys. **11** (1996), 327–348.

[8] F-S. Bai, G. J. Lord, and A. Spence, *Numerical computations of connecting orbits in discrete and continuous dynamical systems*, Internat. J. Bif. Chaos Appl. Sci. Engrg. **6** (1996), 1281–1293.

[9] L. A. Belyakov and L. P. Šil'nikov, *Homoclinic curves and complex solitary waves*, Selecta Math. Soviet. **9** (1990), 219–228.

[10] F. Bertails, B. Audoly, L. Querleux, J-L. Lévêque, and M-P. Cani, *Predicting natural hair shapes by solving the statics of flexible rods*, Eurographics 2005, 2005.

[11] W. J. Beyn, *Global bifurcations and their numerical computation*, Continuation and Bifurcations: Numerical Techniques and Applications (Dordrecht) (D. Roose, B. de Dier, and A. Spence, eds.), NATO ASI C: Mathematical and Physical Sciences, no. 313, Kluwer, 1990, pp. 169–181.

[12] ———, *The numerical computation of connecting orbits in dynamical systems*, IMA J. Numer. Anal. **9** (1990), 379–405.

[13] ———, *On well-posed problems for connecting orbits in dynamical systems*, Chaotic Numerics (Providence, RI) (P. E. Kloeden and K. J. Palmer, eds.), Contemporary Mathematics, no. 172, American Mathematical Society, 1994, pp. 131–168.

[14] A. I. Bobenko, A. G. Reyman, and M. A. Semenov-Tian-Shansky, *The Kowalewski top 99 years later: a Lax pair generalizations and explicit solutions*, Comm. Math. Phys. **122** (1989), 321–354.

[15] V. Brunsden and P. J. Holmes, *Power spectra of strange attractors near homoclinic orbits*, Phy. Rev. Lett. **58** (1987), no. 17, 1699–1702.

[16] B. Buffoni, *Shooting methods and topological transversality*, Proc. Roy. Soc. Edinburgh Sect. A **125** (1999), 1137–1155.

[17] B. Buffoni, A. R. Champneys, and J. F. Toland, *Bifurcation and coalescence of a plethora of homoclinic orbits for a Hamiltonian system*, J. Dynam. Differential Equations **8** (1996), 221–279.

[18] A. R. Champneys, *Homoclinic orbits in reversible systems and their applications in mechanics, fluids and optics*, Phys. D **112** (1998), 158–186.

[19] A. R. Champneys and G. J. Lord, *Computation of homoclinic solutions to periodic orbits in a reduced water-wave problem*, Phys. D **102** (1997), 101–124.

[20] A. R. Champneys and A. Spence, *Hunting for homoclinic orbits in reversible systems: a shooting technique*, Adv. Comput. Math. **1** (1993), 81–108.

[21] A. R. Champneys and J. M. T. Thompson, *A multiplicity of localized buckling modes for twisted rod equations*, Proc. R. Soc. London A **452** (1996), 2467–2491.

[22] A. R. Champneys and J. F. Toland, *Bifurcation and a plethora of multi-modal homoclinic orbits for automonous Hamiltonian systems*, Nonlinearity **6** (1993), 665–721.

[23] A. R. Champneys, G. H. M. van der Heijden, and J. M. T. Thompson, *Spatially complex localization after one-twist-per-wave equilibria in twisted circular rods with initial curvature*, Phil. Trans. R. Soc. London A **355** (1997), 2151–2174.

[24] P. J. Channell and C. Scovel, *Symplectic integration of Hamiltonian systems*, Nonlinearity **3** (1990), 231–259.

[25] P. Chossat, J-P. Ortega, and T. S. Ratiu, *Hamiltonian-Hopf bifurcation with symmetry*, Arch. Ration. Mech. Anal. **163** (2002), 1–33.

[26] N. Chouaïeb and J. H. Maddocks, *Kirchhoff's problem of helical equilibria of uniform rods*, J. Elasticity **77** (2004), 221–247.

[27] B. D. Coleman and J-M. Xu, *On the interaction of solitary waves of flexure in elastic rods*, Acta Mech. **110** (1995), 173–182.

[28] J. Coyne, *Analysis of the formation and elimination of loops in twisted cables*, IEEE J. Oceanic Engrg. **15** (1990), 72–83.

[29] R. Cushman and H. Knörrer, *The energy momentum map of the Lagrange top*, Differential Gemeotric Methods in Mathematical Physics (Berlin) (H. D. Doebner and J. D. Hennig, eds.), Lecture Notes in Mathematics, no. 1139, Springer-Verlag, 1985, pp. 12–24.

[30] R. Cushman and J-C. van der Meer, *The Hamiltonian-Hopf bifurcation in the Lagrange top*, Geométrié Symplectique et Méchanique (Berlin) (C. Albert, ed.), Lecture Notes in Mathematics, no. 1416, Springer-Verlag, 1990, pp. 26–38.

[31] R. Dandoloff and G. Grahovski, *The Kirchhoff rod as a XY spin chain model*, Unpublished, available as an eprint from `http://www.arXiv:nlin/0512069`, 2005.

[32] R. L. Devaney, *Homoclinic orbits in Hamiltonian systems*, J. Differential Equations **21** (1976), 431–438.

[33] ———, *Transversal homoclinic orbits in an integrable system*, Amer. J. Math. **100** (1978), 631–642.

[34] L. Dieci and J. Rebaza, *Point-to-Periodic and Periodic-to-Periodic Connections*, BIT Numerical Mathematics **44** (2004), 41–62.

[35] E. Doedel, A. R. Champneys, T. F. Fairgrieve, Y. A. Kuznetsov, B. Sandstede, and X. Wang, *AUTO97: Software for continuation and bifurcation problems in ordinary differential equations (with HomCont)*, California Institute of Technology, Pasadena, CA, 1998.

[36] H. R. Dullin, *Inflation of Hamiltonian system: the spinning top in projective space*, Unpublished, available as an eprint from `http://www.arXiv:chao-dyn/9604015`, 1996.

[37] H. R. Dullin, M. Juhnke, and P. H. Ritcher, *Action integrals and energy surfaces of the Kovalevskaya top*, Internat. J. Bifur. Chaos Appl. Sci. Engrg. **4** (1994), 1535–1562.

[38] M. S. El Naschie and T. Kapitaniak, *Soliton chaos models for mechanical and biological elastic chains*, Phys. Lett. A **147** (1990), 275–281.

[39] F. Fassò, *The Euler-Poinsot top: A non-commutatively integrable system without global action-angle coordinates*, Zeitschrift für Angewandte Mathematik und Physik (ZAMP) **47** (1996), 953–976.

[40] ———, *Superintegrable Hamiltonian systems: geometry and perturbations*, Acta Appl. Math. **87** (2005), 93–121.

[41] M. J. Friedman and E. J. Doedel, *Numerical computation and continuation of invariant manifolds connecting fixed points*, SIAM J. Numer. Anal. **28** (1991), 789–808.

[42] G. Gallavotti, *Twistless KAM tori, quasi flat homoclinic intersections, and other cancellations in the perturbation series of certain completely integrable Hamiltonian systems. A review*, Rev. Math. Phys. **6** (1994), 343–411.

[43] H. Goldstein, C. Poole, and J. Safko, *Classical Mechanics*, 3rd ed., Addison-Wesley, New York, NY, 2002.

[44] A. Goriely and M. Tabor, *Spontaneous helix hand reversal and tendril perversion in climbing plants*, Phys. Rev. Lett. **80** (1998), 1564–1567.

[45] J. Guckenheimer and P. J. Holmes, *Nonlinear Oscillations, Dynamical systems, and Bifurcations of Vector Fields*, Applied Mathematical Sciences, no. 42, Springer-Verlag, New York, NY, 1983.

[46] H. Hanßmann, *Perturbations of integrable and superintegrable Hamiltonian systems*, Proc. of the 5th EUROMECH Nonlinear Dynamics Conference (ENOC 2005), Eindhoven, Netherlands, 7-12 August 2005 (D. H. van Campen, M. D. Lazurko, and W. P. J. M. van den Oever, eds.), (CD), 2005, pp. 1527–1536.

[47] H. Hasimoto, *Motion of a vortex filament and its relation to elastica*, J. Phys. Soc. Jap. **31** (1971), 293–294.

[48] B. Hernández-Bermejo and V. Fairén, *Simple evaluation of Casimir invariants in finite-dimensional Poisson systems*, Phys. Lett. A **241** (1998), 148–154.

[49] D. D. Holm, J. E. Marsden, and T. S. Ratiu, *The Euler-Poincaré equations and semidirect products with applications to continuum theories*, Adv. Math. **137** (1998), 1–81.

[50] P. J. Holmes, J. Jenkins, and N. E. Leonard, *Dynamics of the Kirchhoff equations I: coincident centers of gravity and bouyancy*, Phys. D **118** (1998), 311–342.

[51] P. J. Holmes and J. E. Marsden, *Mel'nikov's method and Arnol'd diffusion for perturbations of integrable Hamiltonian systems*, J. Math. Phys. **23** (1982), 669–675.

[52] ———, *Horseshoes and Arnol'd diffusion for Hamiltonian systems on Lie groups*, Indiana Univ. Math. J. **32** (1983), 273–309.

[53] J. Horák, G. J. Lord, and M. A. Peletier, *Cylinder Buckling: the mountain pass as an organizing center*, SIAM J. Appl. Math. (2005), 1793–1824.

[54] L. Johnson and M. Herrman, *International Space Station Electrodynamic Tether Reboost Study*, Tech. Report NASA/TP–1998–208538, Marshall Space Flight Center, 1998.

[55] S. Kar, *A simple mechanical analog of the field theory of tachyon matter*, Unpublished, available as an eprint from `http://arxiv.org/hep-th/0210108`, 2002.

[56] S. Kehrbaum, *Hamiltonian Formulations of the Equilibrium Conditions Governing Elastic Rods: Qualitative Analysis and Effective Properties*, Ph.D. thesis, University of Maryland, 1997.

[57] S. Kehrbaum and J. H. Maddocks, *Elastic rods, rigid bodies, quaternions and the last quadrature*, Phil. Trans. R. Soc. London A **355** (1997), 2117–2136.

[58] J. Klaus and J. Knobloch, *Bifurcation of a homoclinic orbit to a saddle-center in reversible systems*, Internat. J. Bif. Chaos Appl. Sci. Engrg. **13** (2003), 2603–2622.

[59] L. Langer and D. A. Singer, *Lagrangian aspects of the Kirchhoff elastic rod*, SIAM Rev. **38** (1996), 605–618.

[60] S. Lenci and G. Rega, *Higher-order Melnikov functions for single-DOF mechanical oscillators: theoretical treatment and applications*, Math. Probl. Eng. **2004** (2004), 145–168.

[61] M. Lentini and H. B. Keller, *Boundary-value problems on semi-infinite intervals and their numerical solution*, SIAM J. Numer. Anal. **17** (1980), 577–604.

[62] N. E. Leonard, *Stability of bottom heavy underwater vehicle*, Automatica **33** (1997), 331–346.

[63] N. E. Leonard and J. E. Marsden, *Stability and drift of underwater vehicles: mechanical systems with rigid motion symmetry*, Phys. D **105** (1997), 130–162.

[64] A. Y. T. Leung and J. L. Kuang, *Spatial chaos of 3-D elastica with the Kirchhoff gyrostat analogy using Mel'nikov integrals*, Int. J. Numer. Meth. Engng. **61** (2004), 1674–1709.

[65] Z. Liu and G. Gu, *Second order Melnikov function and its application*, Phys. Letts. A **143** (1990), 213–216.

[66] A. E. H. Love, *A Treatise on the Mathematical Theory of Elasticity*, 4$^{\text{th}}$ ed., Dover, New York, NY, 1994.

[67] J. E. Marsden and T. S. Ratiu, *Introduction to Mechanics and Symmetry*, 2$^{\text{nd}}$ ed., Texts in Applied Mathematics, no. 17, Springer-Verlag, New York, 1999.

[68] T. McMillen and A. Goriely, *Tendril perversion in intrinsically curved rods*, Nonlinear Sci. **12** (2002), 241–281.

[69] V. K. Mel'nikov, *On the stability of the center for time periodic perturbations*, Trans. Moscow Math. Soc **12** (1963), 1–57.

[70] A. Mielke and P. J. Holmes, *Spatially complex equilibria of buckled rods*, Arch. Ration. Mech. Anal. **101** (1988), 319–348.

[71] F. C. Moon, *Experiments on choatic motions of a forced nonlinear oscillator: strange attractors*, J. Appl. Mech. **47** (1980), 638–644.

[72] ———, *Magneto-solid Mechanics*, Wiley, New York, NY, 1984.

[73] F. C. Moon and P. J. Holmes, *A magnetoelastic strange attractor*, J. Sound Vib. **65** (1979), 275–296.

[74] R. W. D. Nickalls, *A new approach to solving the cubic: Cardano's solution revealed*, The Mathematical Gazette **77** (1993), 354–359.

[75] S. P. Novikov, *The Hamiltonian formalism and a many-valued analogue of Morse theory*, Russian Math. Surveys **37** (1982), 1–56.

[76] P. J. Olver, *Applications of Lie Groups to Differential Equations*, 2$^{\text{nd}}$ ed., Graduate Texts in Mathematics, no. 107, Springer Verlag, New York, 1993.

[77] K. J. Palmer, *Exponential dicotomies and transversal homoclinic points*, J. Differential Equations **55** (1984), 225–256.

[78] V. M. Rothos and T. C. Bountis, *The second order Mel'nikov vector*, Regul. Chaotic Dyn. **2** (1997), 26–35.

[79] B. Sandstede, *Instability of localized buckling modes in a one-dimensional strut model*, Proc. R. Soc. London A **355** (1997), 2083–2097.

[80] T. Schlick, *Modeling superhelical DNA: recent analytical and dynamic approaches*, Curr. Opin. Struct. Biol **5** (1995), 245–262.

[81] T. I. Seidman and P. Wolfe, *Equilibrium states of an elastic conducting rod in a magnetic field*, Arch. Ration. Mech. Anal. **102** (1988), 307–329.

[82] R. Seydel, *Practical Bifurcation and Stability Analysis: From Equilibrium to Chaos*, Interdisciplinary Applied Mathematics, no. 5, Springer-Verlag, New York, NY, 1994.

[83] J-C. Simo, J. E. Marsden, and P. S. Krishnaprasad, *The Hamiltonian structure of nonlinear elasticity: the material and convective representation of solids, rods, and plates*, Arch. Ration. Mech. Anal. **104** (1988), 125–183.

[84] J-C. Simo, T. A. Posbergh, and J. E. Marsden, *Stability of coupled rigid body and geometrically exact rods: block diagonization and the energy-momentum method*, Phys. Rep. **193** (1990), 279–360.

[85] D. Sinden and G. H. M. van der Heijden, *Integrability of a conducting elastic rod in a magnetic field*, J. Phys. A: Math. Theor. **41** (2008), 045207.

[86] P. Smale, *Differentiable dynamical systems*, Bull. Amer. Math. Soc. **73** (1988), 747–817.

[87] T. R. Smith, H. Hanßmann, and N. E. Leonard, *Orientation control of multiple underwater vehicles with symmetry-breaking potentials*, Proc. of the 40th IEEE Conference on Decision and Control, Orlando, FL, December 2001, 2001, pp. 4598–4603.

[88] D. M. Stump, *The hockling of cables: a problem in shearable and extensible rods*, Internat. J. Solids Structures **37** (2000), 515–533.

[89] J-L. Thiffeault and P. J. Morrison, *Classification and Casimir invariants of Lie-Poisson brackets*, Phys. D **136** (2000), 205–244.

[90] ———, *The twisted top*, Phys. Lett. A **283** (2001), 335–341.

[91] J. M. T. Thompson and A. R. Champneys, *From helix to localized writhing in the torsional post-buckling of elastic rods*, Proc. R. Soc. London A **452** (1996), 117–138.

[92] J. M. T Thompson and L. N. Virgin, *Spatial chaos and localisation phenomena in nonlinear elasticity*, Phys. Lett. A **126** (1988), 491–496.

[93] J. Valverde, J. L. Escalona, J. Mayo, and J. Domínguez, *Dynamic analysis of a light structure in outer space: short electrodynamic tether*, Multibody System Dynam. **10** (2003), 125–146.

[94] G. H. M. van der Heijden, *Static deformation of a twisted elastic rod constrained to lie on a cylinder*, Proc. R. Soc. London A **457** (2001), 695–715.

[95] G. H. M. van der Heijden, A. R. Champneys, and J. M. T. Thompson, *The spatial complexity of localized buckling in rods with noncircular cross section*, SIAM J. Appl. Math. **59** (1998), 198–221.

[96] ———, *Spatially complex localisation in twisted elastic rods constrained to lie in the plane*, Mech. Phys. Solids **47** (1999), 59–79.

[97] ———, *Spatially complex localisation in twisted elastic rods constrained to a cylinder*, Internat. J. Solids Structures **39** (2002), 1863–1883.

[98] G. H. M. van der Heijden and J. M. T. Thompson, *Lock-on to tape-like behaviour in the torsional buckling of anisotropic rods*, Phys. D **112** (1998), 201–224.

[99] ———, *Helical and localised buckling in twisted rods: a unified analysis of the symmetric case*, Nonlinear Dynam. **21** (2000), 71–99.

[100] G. H. M. van der Heijden and J. Valverde, *Instability of a whirling conducting rod in the presence of a magnetic field*, Proc. of the 5th EUROMECH Nonlinear Dynamics Conference (ENOC 2005), Eindhoven, Netherlands, 7-12 August 2005 (D. H. van Campen, M. D. Lazurko, and W. P. J. M. van den Oever, eds.), (CD), 2005, pp. 2624–2633.

[101] J-C. van der Meer, *Hamiltonian-Hopf bifurcation with symmetry*, Nonlinearity **3** (1990), 1041–1056.

[102] O. Vivolo, *The monodromy of the Lagrange top and the Picard-Lefschetz formula*, J. Geom. Phys. **46** (2003), 99–124.

[103] L-S. Wang, P. S. Krishnaprasad, and J. H. Maddocks, *Hamiltonian dynamics of a rigid body in a central gravitational field*, Celestial Mech. Dynam. Astronom. **50** (1991), 349–386.

[104] P. Wolfe, *Equilibrium states of an elastic conductor in a magnetic field: a paradigm of bifurcation theory*, Trans. Amer. Math. Soc. **278** (1983), 377–387.

[105] ———, *Rotating states of an elastic conductor*, Phyical Mathematics amd Nonlinear Partial Differential Equations (New York, NY) (J. Lightborne and S. Rankin, eds.), Lecture Notes in Pure and Applied Mathematics, no. 102, Marcel Dekker, 1985, pp. 213–222.

[106] ———, *Bifurcation theory of an elastic conducting rod in a magnetic field*, Quart. J. Appl. Math. **41** (1988), 265–279.

[107] ———, *Bifurcation theory of a conducting rod subject to magnetic forces*, Internat. J. Nonlinear Mech. **25** (1990), 597–604.

[108] ———, *Bifurcation theory of an elastic conducting wire subject to magnetic forces*, J. Elasticity **23** (1990), 201–217.

[109] ———, *Global bifurcation of an elastic conducting rod in a magnetic field*, SIAM J. Math. Anal. **27** (1996), 528–542.

[110] H. H. Woodson and J. R. Melcher, *Electromechanical dynamics 2. Fields, forces, and motion*, Wiley, 1968.